

**1-D Hydraulic and Sediment Transport Model
Final Hydraulic Modeling Technical Memorandum**

Prepared for

Platte River Recovery Implementation Program



March, 2011

Prepared by

HDR Engineering, Inc.

In association with

Tetra Tech, Inc. and The Flatwater Group, Inc.





Table of Contents

1		
2		
3	1.	Introduction and Background 1
4		Project Introduction 1
5		Statement of Work 1
6		Site Description 1
7		Model Extents 1
8		River System Characteristics 1
9		Hydrologic Inputs and Outputs 2
10		Significant Landmarks and Structures in Modeled Reach 3
11	2.	Steady State Hydraulic Model 4
12		Model Development 4
13		Stationline and Secondary Channels 4
14		Cross-Section Alignment, Spacing, and Orientation 4
15		Topography 5
16		Hydraulic Structures 5
17		Overbank Flood Flow Paths 7
18		Hydraulic Roughness 7
19		Phragmites 8
20		Ineffective Flow Areas, Blocked Obstructions, and Levees 8
21		Boundary Conditions 9
22		Model Calibration 9
23		Calibration Data 9
24		Calibration Methods 10
25		Calibration Results 10
26	3.	Unsteady Model 38
27		Steady-State Model Conversion 38
28		Model Calibration 40
29		Calibration and Validation Events and Data 40
30		Historical Reach Gains and Losses 41
31		Ungaged Inputs and Outputs 41
32		Bank Storage Approach 42
33		Calibration Methods 43
34		Calibration Results 44
35		Segment: Lexington to Overton (RM 254 – RM 240) 45
36		Segment: Overton to Kearney (RM 240 – RM 215) 45
37		Segment: Kearney to Chapman (RM 215 – RM 154) 47
38		General Note on Model Stability 48
39		Sensitivity Analyses 48
40		Bank Storage Prediction Tool 51
41		Hydrograph Routing Prediction 51
42		Bank Storage Hydrograph Prediction Tool 52
43		Empirical Relationship Adjustment 52
44		Pulse Magnitude Sensitivity 53
45		Antecedent Condition Sensitivity 53
46	4.	Sediment-Transport Model 116
47		HEC-RAS and HEC-6T Model Limitations 116



1	Model Development	116
2	Model Structure and Geometry.....	116
3	Bed-material Data and the Bed Sediment Reservoir.....	119
4	Hydrologic Data	119
5	Boundary Conditions	120
6	Sediment-transport Function	121
7	Computational Time Steps.....	121
8	Model Calibration	121
9	Lexington to Chapman Models.....	122
10	North Platte Model.....	122
11	Upstream Sediment Supply Sensitivity Analyses	123
12	Model Application and Use.....	124
13	5. Summary and Conclusions.....	124
14	Steady-State Model	124
15	Unsteady Model.....	124
16	Sediment-Transport Model.....	125
17	Overall.....	125
18	6. References	147
19		

20 **List of Tables**

21	Table 1.1: Summary of Canals and Tributaries, RM 310 to RM 156.....	2
22	Table 1.2: Summary of Average Monthly Long-Term Reach Gains/Losses, WY 1985-2008.....	3
23	Table 2.1: Bridges Included in Steady State Model	6
24	Table 2.2: HEC-RAS Model Roughness Values	8
25	Table 2.3: Rating Curves Available for Steady-State Model Calibration.....	10
26	Table 2.4: Calculated Flow splits At Maxwell (RM301).....	12
27	Table 2.5: Flow splits Upstream of Brady (third channel activated at high flow), approx RM 295.	12
28	Table 2.6: Calculated Flow Splits At Gothenburg (RM 278).....	12
29	Table 2.7: Flow Split at Cozad (RM 267)	13
30	Table 3.1: Reached the were Merged and location after Merger	40
31	Table 3.2: Daily Regional Rainfall Totals for Regional Weather Stations (High Plains Regional Climate Center)	42
32	Table 3.3: Summary of Global Manning’s Roughness Coefficient sensitivity.....	50
33	Table 3.4: Bank storage parameter values that best matched the observed behavior of the 2009 hydrograph in each reach.*	52
34	Table 4.1: Summary of computational time steps used in the HEC-6T models.....	121
35		
36		
37		

38 **List of Appendices**

39	Appendix A	Map of Modeled Platte River System
40	Appendix B	Memorandum from Tetra Tech to Steve Smith (PRRIP) dated Sept. 20, 2010, entitled “Proposal to use HEC-6T to perform the sediment-transport modeling for the Platte River, Lexington to Chapman Reach (based on HEC-RAS sediment-transport model limitations)”
41		
42		
43		
44	Appendix C	Input Files for the HEC-6T Sediment-transport Models



- 1 Appendix D Memorandum from Tetra Tech to Steve Smith (PRRIP) dated January 7, 2011, entitled
- 2 "HEC-6T Sediment Transport Model: DRAFT Use and Application Guide"



Platte River Recovery Implementation Program 1-D Hydraulic and Sediment Transport Model Modeling Technical Report

Tri-County Diversion to Chapman (River Mile 310 – River Mile 156) January 28, 2011

1. Introduction and Background

Project Introduction

The Platte River Recovery Implementation Program (Program) was initiated on January 1, 2007 between Nebraska, Wyoming, and Colorado and the Department of the Interior to address endangered species issues in the central and lower Platte River basin. The species considered in the Program, referred to as “target species”, are the whooping crane, piping plover, interior least tern, and pallid sturgeon. The Program would like to investigate the physical processes and how altering flow and sediment load might impact these processes. A hydraulic and sediment-transport model of the Central Platte River provides Program participants a tool to evaluate the relationship between streamflow, sediment transport, and habitat of Program target bird species.

Statement of Work

The purpose of this project is to develop and calibrate a one-dimensional (1D) integrated hydraulic and sediment transport model that will be used to estimate the attenuation of Platte River flows, and predict the influence of various flow levels and sediment-transport and river morphology. To accomplish this, a 1D steady state and unsteady model was developed from the Tri-County Diversion (North Platte) to Chapman. In addition to steady state and unsteady hydraulic model development, a sediment transport model was developed from Odessa to Chapman.

Site Description

Model Extents

The headwaters of the North and South Platte Rivers originate in Colorado. The North Platte flows through Colorado, Wyoming and Nebraska and the South Platte through Colorado and Nebraska. The confluence of the North Platte and South Platte Rivers is located near North Platte, Nebraska. The confluence occurs immediately upstream from the Tri-County Diversion. The Tri-County Diversion was constructed by Central Nebraska Public Power and Irrigation District (CNPPID) to allow for diversion of Platte River water into their canal system. Due to the consistent measured flow record at this location and its location downstream from the confluence with the North and South Platte Rivers, it was a logical upstream boundary condition. Therefore, the Tri-County Diversion, located approximately at River Mile (RM) 310 was designated as the upstream extent of the model. The downstream extent of the model is located at RM 156, near Chapman, Nebraska. In addition to the main channel of the Platte River, the modeled domain also contains numerous side channels of the Platte River. A separate model of the North Platte River “Choke Point” reach, located in the vicinity of the City of North Platte, was also developed and extends from about 5.5 miles upstream from the U.S. Highway 83 Bridge to the Tri-County Diversion.

River System Characteristics

In the period from 1900 through 1938, the central Platte River channel maintained a predominantly braided form, although the width of the river decreased significantly. Braided river forms are



1 characterized by a series of shallow, interconnected low flow channels within the overall channel. This
 2 form provides desirable riverine habitat (i.e., habitat occurring along a river) for whooping crane,
 3 interior least tern, and piping plover because there are wide areas of water with unobstructed sight
 4 distances and bare sandbars for roosting, nesting, and security from predators (BOR and USFWS, 2006).
 5 Over time, reductions in flow volumes, peak flows, and sediment supply have shifted the river's form
 6 from a wide, braided channel to a channel consisting of multiple narrow and deep channels separated
 7 by vegetated islands (anastomosed). These changes have led to a decrease in desirable habitat for the
 8 target species (BOR and USFWS, 2006).

9 **Hydrologic Inputs and Outputs**

10 In addition to numerous channel splits, there are several tributaries as well as irrigation and power canal
 11 diversions, returns located within the modeled reach. Since these gains and losses can impact hydraulic
 12 and sediment-transport, they were considered in the modeling effort. The location of these canals and
 13 diversions are summarized in Table 1.1, and are shown in Appendix A.

14 Table 1.1: Summary of Canals and Tributaries, RM 310 to RM 156.

Canal or Tributary Name	Approximate River Mile	Gage Number
Whitehorse Creek	310	Ungaged
Jeffrey Power Return	288	NDNR 143000
Gothenburg Canal Diversion	288	NDNR 57000
Thirty Mile Canal Diversion	288	NDNR 141000
Six Mile Canal Diversion	282	NDNR 134000
Cozad Canal Diversion	277	NDNR 33000
Six Mile Canal Return	277	NDNR 134000
Orchard-Alfalfa Canal Diversion	271	NDNR 117000
Dawson County Canal Diversion	267	NDNR 37000
Orchard-Alfalfa Canal Return	261	NDNR 117000
Thirty Mile Canal Return	258	NDNR 141000
Johnson (J-2) Power Return	247	NDNR 144000
Phelps County Canal Diversion	247	NDNR 122000
Spring Creek	237	USGS 6768020
Elm Creek	229	USGS 6769525
Buffalo Creek	229	USGS 6769000
Kearney Canal Diversion	229	NDNR73000
Whisky Slough	219	USGS 6770175*
North Dry Creek	216	USGS 6770195*
Ft. Kearney Slough	210	USGS 6770240*
Kearney Canal Return	210	NDNR73000
Downstream Drain	206	USGS 6770255*

15 *Gage is no longer recording data

16
 17 In addition to tributaries and canals, long-term reach gain/loss (RGL) affects streamflow. Long-term
 18 average monthly gains and losses were computed for gaged reaches between North Platte and Grand
 19 Island, based on mean daily flow data from water years 1985-2008. Positive values indicate a long-term
 20 reach gain and negative values indicate a long-term reach loss. These calculations are summarized in
 21 Table 1.2.

22



1 Table 1.2: Summary of Average Monthly Long-Term Reach Gains/Losses, WY 1985-2008
2 (Positive values indicate gain, negative values indicate loss)

	Reach Gain/Loss (acre-ft)				
	North Platte - Brady	Brady - Cozad	Cozad - Overton	Overton - Odessa	Odessa - Grand Island
January	408	139	352	88	-79
February	580	176	361	160	60
March	548	245	465	208	403
April	631	220	332	246	247
May	566	297	427	436	424
June	766	-38	946	370	467
July	439	72	436	376	116
August	427	208	373	398	-105
September	398	109	382	157	-305
October	189	204	367	100	-140
November	258	183	442	-17	62
December	78	224	558	5	-81

3 ***Significant Landmarks and Structures in Modeled Reach***

4 As stated previously, the Tri-County Diversion (located at RM 310) was designated as an appropriate
5 upstream boundary for the Central Platte. Two channels of the Platte River flow from this location. The
6 flow in the main channel, immediately downstream from the diversion structure, is controlled by gates
7 at the diversion structure. Flow in the secondary channel is controlled by a culvert approximately 3000
8 ft south of the Tri-County diversion structure. The river maintains this split-channel for approximately
9 22 miles. See Appendix A, Sheet 2.

10

11 Immediately downstream of the Tri-County Diversion in the main channel, flow measurements were
12 taken at the Nebraska Department of Natural Resources (NDNR) gage number 229000 (Platte River
13 Below Tri-County Diversion) from 1994 to 1999. The first active gaging station is located approximately
14 nine miles below the Tri-County Diversion, near Maxwell (NDNR 228500). Data at this gage have been
15 recorded since 1999, and is only recorded in the main (north) channel. The next downstream gaging
16 station is located near Brady (RM 292, NDNR 06766000). Gage measurements at Brady are taken at
17 both the main (north - 06765980) and secondary (south- NDNR 06765990) channels. See Appendix A,
18 Sheets 2-6.

19

20 The main and secondary channels of the Platte River converge with the Jeffery Power return near RM
21 288, immediately upstream of the 30 Mile Diversion structure. At this structure, the 30 Mile Diversion
22 Canal and the Gothenburg Canal divert flow from the Platte River. Remaining flow is passed through the
23 Gothenburg sluiceway into the main Platte River channel. Below this structure, the Platte River returns
24 to a multi-channeled planform, with the main channel to the north and a secondary channel with
25 numerous of additional side channels to the south. The Six-Mile Canal diversion and return, the Cozad
26 Canal diversion, the Orchard-Alfalfa Diversion, and the Dawson County Diversion are all located between
27 the 30 Mile Diversion and the next stream gage station, at Cozad RM 266.5 (NDNR 06766500). Flow is
28 recorded in both the north (NDNR 06766499) and south (NDNR 06766498) channels at Cozad. See
29 Appendix A, Sheets 6-10.



1 Approximately one mile downstream of Cozad, the river converges into a main channel with several
2 small and poorly-defined flow channels and braids. The Orchard-Alfalfa and Thirty-Mile Canal returns
3 are located in this region, between Cozad and Lexington. The next streamgage on the Platte River is
4 NDNR 228400 - RM 251. Downstream of Lexington, the Johnson 2 (J-2) Canal Return provides significant
5 inflow to the Platte at RM 247. The Platte River resumes a multi-channel planform below the J-2 Canal.
6 The next gage station is located near Overton (RM 240, USGS 06768000). Elm Creek and Buffalo Creek
7 flow into the Platte near RM 229. The Kearney Canal diversion is located just downstream of the Elm
8 Creek and Buffalo Creek confluence. The Odessa gage is located near RM 224(USGS 06770000). See
9 Appendix A, Sheets 10-18.

10

11 Between the Odessa and the next downstream gage station at Kearney (RM 215- NDNR73000), there
12 are only two gaged hydrologic inputs, the Whisky Slough and North Dry Creek (both at RM 216).
13 Downstream of Kearney, the Platte River flows northeast for the remainder of the study area.
14 Significant inputs exist at RM 210 (Ft. Kearney Slough/ Kearney Canal Return) and 206 (Downstream
15 Drain). The last gage station in the project reach is located near Grand Island (RM 175- USGS 06770500).
16 The downstream twenty miles of the model do not contain any gaged inflows. The downstream extent
17 of the model is located at RM 154, just above the confluence with the Wood River. See Appendix A,
18 Sheets 18-30.

19 **2. Steady State Hydraulic Model**

20 **Model Development**

21 *Stationline and Secondary Channels*

22 The main channel stationline was delineated for the approximately 154-mile continuous path of the
23 river that is expected to transport the majority of the flow over the range of modeled discharges, and
24 was based on aerial photography, LiDAR topography and field observations. Thirty-five hydraulically
25 distinct, secondary flow paths ranging in length from about 0.5 to 16.3 miles that transport a significant
26 amount of flow at higher discharges were also identified. The locations of several significant tributaries
27 that primarily represent diversion return channels were also identified as point source inflows along the
28 stationline. The entire model between the Tri-County Diversion and Chapman, NE, including the
29 secondary flow paths, represents approximately 330 miles of river channel. At the request of the
30 Program, a separate stationline was developed for the approximately 10-mile reach of the North Platte
31 in the vicinity of the “Choke Point” subsequent to development of the initial line for the downstream
32 model. This stationline extends from the Tri-County Diversion Structure to a location about 5.5 miles
33 upstream from the U.S. Highway 83 Bridge, and was tied into the next downstream stationline.

34 *Cross-Section Alignment, Spacing, and Orientation*

35 Model cross sections were laid out to extend across the active channel and floodplain and remain
36 perpendicular to the direction of flow. The cross sections were spaced at 1,500- to 2,000-foot intervals,
37 based on target criteria of three to four channel widths for the approximately 500-foot-wide main
38 channel. Additional cross sections were placed at hydraulic structures (e.g., bridges and diversions) near
39 reach junctions and in areas where ground survey data were available. In total, the primary model from
40 the Tri-County Diversion to Chapman contains 1,547 cross sections to characterize the main and
41 secondary channels and modeled tributaries.

42



1 ***Topography***

2 Topography for the model was developed primarily from LiDAR data provided by the Program. LiDAR
3 data covering the entire project reach were collected March 17-19, 2009, and referenced the North
4 American Datum of 1983 (NAD83) and North American Vertical Datum of 1988 (NAVD88). Horizontal
5 accuracy was reported to be 1.88 feet, with a vertical accuracy of 0.28 feet. A limited amount of
6 bathymetric survey data were also available and incorporated into the model. These data were
7 collected between 1998 and 2009, and included the Program's Anchor Point and longitudinal profile
8 surveys that were conducted for the Geomorphology Monitoring Program in 2009, surveys specifically
9 for this project by The Flatwater Group (TFG), and surveys by the U.S. Geological Survey (USGS) and
10 Bureau of Reclamation (BOR).

11 ***Hydraulic Structures***

12 The model includes 45 bridge structures, the data for which were taken from as-built bridge plans
13 obtained from the Nebraska Department of Roads (Table 2.1). Expansion and contraction coefficients in
14 the bounding cross sections to each bridge were set to 0.5 and 0.3, respectively. Information on the
15 dimensions of the Kearney Diversion structure (RM 229) was obtained from a November 2009 survey
16 conducted by TFG (Figure 2.1). The flow patterns in the vicinity of this structure are multi-dimensional,
17 with the primary component flowing parallel to the weir toward the Kearney Canal Headworks, and a
18 secondary component that overtops roughly perpendicular to the weir; thus, the conventional HEC-RAS
19 inline structure feature was not used to represent this structure in the model. Instead, a series of cross
20 sections was laid out upstream from the structure, oriented along the primary flow path with the right
21 end point at the top of the structure (Figure 2.2). The HEC-RAS lateral weir feature, which computes the
22 conveyance across the weir based on the available head, was then used to represent the weir geometry.
23 A total of six cross sections were used to represent the structure, including the downstream section that
24 contains the gate-and-sill geometry. Ineffective flow areas were used at the downstream gate/weir
25 section to eliminate conveyance across the top of the weir, since this conveyance is accounted for in the
26 lateral weir calculations.



1 Table 2.1: Bridges Included in Steady State Model

Bridge	Reach	Station
Interstate 80	RM308-288	124300
Nebraska 56A Spur (North Channel) South Pine Street near Maxwell	RM310-300	72,400
Nebraska 56A Spur (South Channel) Fort McPherson Road near Maxwell	RM308-288	80,000
Highway 56 D Link (North Channel) Banner Road	RM 300-292	19,200
Highway 56 D Link (North Split) Banner Road	RM 300-292	800
Highway 56 D Link (South Channel) South Banner Road	RM308-288	15,300
Interstate 80 (North Channel) Near Brady	RM 292-288	1,750
Interstate 80 (North Channel) Near Gothenburg	283-269	138,000
Highway 47 - Lake Avenue (North Channel) Near Gothenburg	283-269	133,900
Highway 47 - Lake Avenue (South Channel) Near Gothenburg	RM 286-275	59,000
Interstate 80 (North Channel) Near Willow Island	RM 283-269	107,500
Highway 21 (Meridian Avenue) Near Cozad	RM 268-266	70,800
Highway 21 (Meridian Avenue) Near Cozad	RM 268-266	8,000
Road 755 - Road 428 - Thirty Mile - Near Lexington	RM 259-255	20,500
Road 755 - Road 428 - Thirty Mile - Near Lexington	RM 259-255	25,200
U.S. Highway 283	RM255-248	3,298,701
State Highway 24	RM240	3,234,085
U.S. Highway 183	RM233-231_S	1,520
U.S. Highway 183	RM232-231	400,263
State Highway 6	RM231-220	363,475
State Highway 44	RM215-214	314,100
Lowell Road	RM213-200	245,400
Lowell Road	RM209-200_S	11,800
State Highway 10	RM213-200	275,900
State Highway 10	RM209-200_S	42,400
Shelton Rd	RM200-195	211,700
S Alda Rd	RM190-181	137,400
S Alda Rd	RM182-177_S	23,800
West Platte Rd	RM182-177_S	54,500
West Platte Rd	RM190-181	165,800
Tom Osbourne Expy	RM178-171_S	20,900
Tom Osbourne Expy	RM177-168_S	32,400
Tom Osbourne Expy	RM175-171_S	19,000
Tom Osbourne Expy	RM180-169	101,900
Interstate 80	RM178-175_S	1,100
Interstate 80	RM178-171_S	12,000
Interstate 80	RM177-175_S	1,600
Interstate 80	RM177-168_S	38,300
Interstate 80	RM180-169	86,600
S Locust St	RM180-169	88,800
S Locust St	RM178-171_S	8,400
S Locust St	RM177-168_S	18,900
S Locust St	RM175-171_S	7,500
U.S. Highway 34	RM168-162	63,200
8th Rd	RM158-156	6,000

2
3



1 **Overbank Flood Flow Paths**

2 Because certain overbank flow paths only convey an appreciable amount of flow at the most extreme
3 flood events, these flow paths were not included in the step-backwater portion of the model. Instead,
4 the flow loss associated with these paths, and the subsequent return flows, were modeled using the
5 HEC-RAS lateral weir feature. The geometry across the top of the flow breakout zone was coded into
6 the lateral weir input editor based on the LiDAR survey data, and the downstream return location was
7 specified at the appropriate location. While the lateral weir feature does not provide specific hydraulic
8 information for the overbank flow channels, it does remove an appropriate amount of flow from the
9 main channel along the flow breakout zone based on the available head to drive the overbank flow, and
10 returns that flow at the appropriate location. Lateral weir features were used to model the high-flow
11 overbank flow paths along the left overbank of the North Channel of Jeffrey Island at Sta 32491+28
12 (approximate RM 242.5), along the left overbank of the north split-flow channel below Cottonwood
13 Ranch at Sta 31042+10 (approximate RM 233), and along the right overbank upstream from the Kearney
14 Diversion Structure between Station 395426 and Station 392235 (approximate RM 229.5).

15 **Hydraulic Roughness**

16 Hydraulic roughness was incorporated into the model using Manning's roughness coefficients that vary
17 horizontally along the cross section. Vegetation and land-use information from the Program's
18 Vegetation Monitoring Program was used to develop polygons that represent different roughness zones
19 (Figure 2.3). The original land-use polygons include a very dense delineation of vegetation types that
20 would result in more than the maximum number (20) of roughness zones allowed by HEC-RAS at many
21 locations. To reduce the number of roughness zones, the land-use polygons were simplified by
22 combining them into larger zones that represent the dominant roughness characteristics of the
23 delineated area. HEC-GeoRAS was then used to determine the stationing of the roughness zones along
24 the cross section (USACE, 2009). These roughness zones were then assigned a Manning's roughness
25 coefficient based on the vegetation description, field observations, bed-material characteristics, past
26 experience with similar streams, and published values for similar streams (Barnes, 1967; Hicks and
27 Mason, 1991; Arcement and Schneider, 1989) (Table 2.2). Roughness values in the overbanks ranged
28 from 0.020 for flat surfaces with no vegetation to 0.12 for densely vegetated areas with irregular
29 topography. Roughness values for the vegetated area within the channel were then assigned by
30 evaluating the aerial photography, topography and vegetation-type polygons. Main channel *roughness*
31 *coefficients* ranged from 0.028 for the active, non-vegetated portion of the channel to 0.10 for densely
32 vegetated mid-channel bars and islands. Because the estimated roughness value for phragmites of 0.10
33 is the same as that for other types of vegetation, a unique roughness value of 0.101 was used for the
34 phragmites to facilitate changing the value in future model runs to assess the effects of phragmites-
35 control efforts. Because the resulting composite roughness values in the channel vary with depth, and
36 because the assigned roughness values appear to result in good model calibration (discussed below),
37 vertical variation in roughness was not used.

1 Table 2.2: HEC-RAS Model Roughness Values

Vegetation Type/ Land Use	Manning's Roughness Coefficient
Agricultural	0.035
Bare ground/Sparse Veg	0.03
Canal/Drainage	0.02
Irrigation Reuse Pit	0.3
Mesic Wet Meadow	0.03
Phragmites	0.101
Riparian Shrubland	0.07
Riparian Woodland	0.11
River Channel	0.028
River Early Successional	0.1
River Shrubland	0.07
Roads	0.02
Rural Developed	0.02
Sand Pit	0.02
Unvegetated Sandbar	0.035
Upland Woodland	0.12
Warm-water Slough	0.08
Xeric Wet Meadow	0.03

2

3 ***Phragmites***

4 The location of phragmites in the modeled reach was identified using a GIS-based land use information
 5 provided by the Program in ArcGIS shapefile format (Figure 2.3). Areas of dense vegetation were given a
 6 Manning’s roughness coefficient of 0.10, however, in order to distinguish phragmites from other dense
 7 vegetation, phragmites were given a unique roughness coefficient of 0.101. This will allow for relatively
 8 easy and systematic modification of the Manning’s roughness coefficient to model varying stages of
 9 phragmites growth and removal.

10 ***Ineffective Flow Areas, Blocked Obstructions, and Levees***

11 Ineffective flow areas, blocked obstructions, and levees were used at each cross section to prevent the
 12 model from computing flow to areas that are either hydraulically disconnected from the river channel
 13 (i.e. sandpits, roadway ditches) or would not contribute to the area through which flow is passing.
 14 Blocked obstructions were used in areas that permanently are not considered as flow area. Levees were
 15 used in a similar fashion to eliminate conveyance behind permanent and contiguous features such as
 16 the Interstate 80 roadway along areas of the left overbank. Permanent ineffective flow areas were used
 17 to describe areas that may be connected to river flow, but will not contribute to the conveyance area
 18 over the range of modeled flows, while non-permanent ineffective flow areas were used to limit
 19 conveyance at low flows while allowing conveyance at higher flows.



1 **Boundary Conditions**

2 **Reach Flow**

3 As previously mentioned, the Platte River bifurcates at several locations within the modeled reaches.
4 The flow split optimization feature in HEC-RAS was used to determine the amount of flow that is split
5 into each of the two channels by balancing the hydraulic energy at the distributary location (referred to
6 as the upstream junction). The initial allocation of flow among parallel channels prior to flow
7 optimization was estimated based on the size of the two split flow channels, and preserved the total
8 river system flow at the upstream junction. Downstream Boundary Conditions

9 A rating curve, calculated from the in the Sediment Augmentation Feasibility Study was used as the
10 downstream boundary condition for the Tri-County Diversion to Lexington reach. A common cross
11 section between the two models was used to facilitate this boundary condition. The downstream
12 boundary condition for the Odessa to Chapman reach was based on the normal depth using a (slope of
13 0.00125 ft/ft, consistent with the average bed slope in the vicinity of the downstream cross section.

14 **Gate Openings at Inline Structures**

15 There were several in-line gated structures mentioned in Landmarks and Structures. Each structure was
16 modeled in HEC-RAS. For purposes of the steady-state model, all gates were assumed to be fully open,
17 such that the impact of these structures was reduced. This condition best represents a scenario in
18 which no flow is diverted at these structures.

19 **Model Calibration**

20 **Calibration Data**

21 In general, the calibration objective for the steady-state model was to minimize the differences between
22 measured and predicted water-surface elevations, with average differences of less than a few tenths of
23 a foot, no consistent trend of over- or under-predicting along the length of the project reach, and
24 maximum differences of less than 1 foot. The available calibration information included rating curves at
25 the stream gages, water-surface elevations collected in conjunction with local cross-section surveys, and
26 inferred water-surface elevations from the LiDAR data. Rating curves were available at 11 gages
27 operated by either the USGS or NDNR in the reach between the Tri-County Diversion and Chapman, and
28 the North Platte gage was used for this portion of the model (Table 2.3). Ground surveys conducted by
29 Ayres Associates at the Geomorphology Monitoring Program Anchor Points and by TFG in 2009 provided
30 a number of locations where a water-surface elevation and approximate channel discharge could be
31 correlated. A water-surface elevation profile was inferred from LiDAR data survey by assuming the
32 survey did not penetrate the water surface, and was therefore, represented by the lowest measured
33 elevation within the channel. The LiDAR data were collected between March 17-19, 2009, during which
34 time the discharge in the river ranged from 60 to 270 cfs in the upper reaches (RM 310 – RM 255) and
35 380 to 400 cfs in the lower reaches (RM 255 – RM 156). The discharge in the North Platte reach was
36 about 340 cfs at the time of the LiDAR survey.

37
38



1 Table 2.3: Rating Curves Available for Steady-State Model Calibration

Gage Identification	River Mile	Station
Platte River near Maxwell, North Channel (NDNR Gage No. 229000)	301	72457
Platte River at Brady, North Channel (NDNR Gage No. 06765980)	292.5	19297
Platte River at Brady, South Channel (NDNR Gage No. 06765990)	292.5	15360
Platte River near Cozad, North Channel (NDNR Gage No. 06766499)	267	70835
Platte River near Cozad, South Channel (NDNR Gage No. 06766498)	267	8093
Platte River at Overton (USGS Gage No. 06768000)	239.5	446012
Platte River South Channel gage at Cottonwood Ranch (USGS Gage No. 06768025)	237	32613
Platte River Middle Channel gage at Cottonwood Ranch (USGS Gage No. 06768035)	234	417827
Platte River near Kearney, NE (USGS Gage No. 06770200)	215	313947
Platte River near Shelton Road, NE (NDNR Gage No. 229300)	196	211604
Platte River near Grand Island, NE (USGS Gage No. 06770500)	168	63117

2
3

4 Additionally, color-infrared and low-altitude photography was available for some sections of the project
5 reach at several different high flows. These photos were qualitatively compared with predicted results
6 to validate effective and ineffective flow areas specified in the model.

7 *Calibration Methods*

8 Calibration of the model was achieved by refining the cross-section roughness parameters and low-flow
9 channel geometry. As discussed previously, the general horizontal distribution of the Manning's
10 roughness coefficients was originally assigned using information from the Program's Vegetation
11 Monitoring Program. The limits of these roughness zones were initially adjusted to better match the
12 channel geometry and aerial photography. The zones along the banks were then slightly adjusted (up or
13 down the bank) to improve calibration. In areas where no survey data were available, the channel
14 bottom was adjusted to account for the area below the water surface in the LiDAR survey (Figures 2.4
15 and 2.5).

16 *Calibration Results*

17 *Tri-County Diversion to Lexington*

18 Model calibration for the Tri-County diversion to Lexington Reach was performed using LiDAR data,
19 flown on March 19, 2010 and current gage rating curves supplied by the NDNR.

20

21 The initial calibration involved iteratively adjusting subaqueous river channel bathymetry utilizing LiDAR
22 data. Adjustments were made to achieve agreement between the modeled water surface and observed
23 water surface. Calibration was performed so that computed and observed WSELs had agreement at
24 most cross sections within 0.5 feet. Among main channel cross sections, an average error of -0.07ft and
25 standard deviation of 0.28 ft was achieved. Figure 2.6 depicts these results.

26



1 Calibration was also preformed at five NDNR gage locations through the modeled reach at the following
2 locations:

3

- 4 • Platte River near Maxwell- North Channel (NDNR Gage No. 229000),
- 5 • Platte River at Brady- North Channel (NDNR Gage No. 06765980),
- 6 • Platte River at Brady- South Channel (NDNR Gage No. 06765990),
- 7 • Platte River near Cozad- North Channel (NDNR Gage No. 06766499), and
- 8 • Platte River near Cozad- South Channel (NDNR Gage No. 06766498).

9

10 Rating curves for these gages were provided by the NDNR. Model runs for flows ranging from 100 to
11 10,000 cfs were conducted to develop a modeled rating curve. Bank stations, ineffective flow areas, and
12 bridge hydraulics were adjusted to calibrate the modeled rating curve to the NDNR published rating
13 curve. These changes were then reflected in the remainder of the model, to insure that consistent
14 ineffective flow area, bank station assignment, and bridge hydraulic parameters were employed
15 throughout the model.

16

17 Gage calibration efforts were primarily focused on the gages located in main channel locations: Maxwell,
18 Brady- north channel and Cozad-north channel. At the Maxwell gage, water surface elevations (WSELs)
19 for flows ranging from 50 to 6000 cfs were within 0.5 feet of the NDNR rating curve WSEL, with the
20 greatest deviation from the rated discharge occurring near 2,000 cfs (Figure 2.7). Predicted WSELs at
21 the Brady- north channel gage calibrated within 0.5 feet between approximately 100 cfs and 5,000 cfs,
22 predicting within 0.5 ft below the rating at 100 cfs and approximately 0.5 ft above the rating at 5,000 cfs
23 (Figure 2.8). The Cozad-north channel gage calibrates within 0.5 feet from approximately 100 cfs to
24 3,000 cfs, overpredicting the WSEL for flows in excess of 5,000 cfs by less than 1 foot (Figure 2.9).
25 Generally, the modeled trends match observed trends for rating curves at these three gages.
26 Less attention was given to the Brady-south channel and Cozad-south channel gages, since these gages
27 carry significantly less flow than the other three gages considered. Based on modeled results, the
28 amount of flow in the south channel is approximately 5% and 20% for the Brady and Cozad gages,
29 respectively. Calibration results for the Brady-south channel gage demonstrate a consistent
30 underprediction of WSELs of 0.75 to 1 foot for all flows evaluated (Figure 2.10). Despite
31 underprediction, the shape of the modeled rating curve is similar to the NDNR observed rating at this
32 location.

33

34 Modeled WSELs for the Cozad-south channel gage match the NDNR rating most closely at lower flows,
35 but overpredict WSEL by over two feet at flows above 1,000 cfs (Figure 2.11). The differences in
36 modeled WSEL and the rating curve at the Cozad – south channel location is attributed to the south
37 channel being choked with vegetation, beaver dams, and a sand dam. Additionally, in the modeled
38 range, the rating curve is based on only one measurement in the modeled range. NDNR staff has
39 indicated that the gage no longer produces reliable rating measurements. Due to the uncertainty of
40 calibration data, the calibration at this site was not given similar weight as that of other gage locations.

41

42 Tables 2.4 through 2.7 shows how the modeled flow splits (between 1,000 and 5,000) compare with
43 NDNR measurements during the June 2010 event. Measured flow splits were not available at Maxwell
44 and at Gothenburg. Figures 2.12-2.13 provide a qualitative verification by comparing 6/18/2010 flyover
45 photos (Approximately 6,000 cfs) with the modeled 5,000 cfs water surface at a particular cross section
46 in the modeled reach. This validation was carried out at several locations to provide a measure of
47 reasonableness for the model.



1 Table 2.4: Calculated Flow splits At Maxwell (RM301)

Total Flow (cfs)	Flow in North Channel	% of Total	Flow in South Channel	% of Total
1000	950	95.0	50	5.0
2000	1925	96.3	75	3.8
3000	2900	96.7	100	3.3
4000	3850	96.3	150	3.8
5000	4800	96.0	200	4.0

2
3

4 Table 2.5: Flow splits Upstream of Brady (third channel activated at high flow), approx RM 295.

5 *Table 2.5a. Calculated Flow Splits*

Total Flow (cfs)	Flow in North Channel, Main*	% of Total	Flow in N Channel, Split *	% of Total	% of Flow predicted in N Channel *	Flow in South Channel	% of Total
1,000	949	94.9	1	0.1	94.9	50	5.0
2,000	1,877	93.9	48	2.4	96.2	75	3.8
3,000	2,680	89.3	220	7.3	96.4	100	3.3
4,000	3,438	85.9	412	10.3	95.8	150	3.8
5,000	4,171	83.4	629	12.6	95.4	200	4.0

Table 2.5b. Measured Flow Splits

Measured Total Flow (cfs)	Measured Flow in North Channel, Main*	% of Total	Measured Flow in South Channel, Split	% of Total
1,050	1,000	95.2	50	4.8
4,350	4,200	96.6	150	3.4
6,340	6,200	97.8	140	2.2

6 *Note: The Brady north channel gage measurement contains only the main north channel and does not
7 contain the split flow from the north channel. For this reason, the percentage of flow in measured
8 channels is shown for appropriate comparison with the field measurements. This percentage does not
9 take into account any flow in the upstream flow split

10

11 Table 2.6: Calculated Flow Splits At Gothenburg (RM 278)

Total Flow (cfs)	Flow in North Channel	% of Total	Flow in South Channel	% of Total
1,000	962	96.2	38	3.8
2,000	1,890	94.5	110	5.5
3,000	2,759	92.0	241	8.0
4,000	3,537	88.4	463	11.6
5,000	4,247	84.9	753	15.1

12
13



1 Table 2.7: Flow Split at Cozad (RM 267)
 2 *Table 2.7a: Calculated Flow Split at Cozad*

Total Flow (cfs)	Flow in North Channel	% of Total	Flow in South Channel	% of Total
1,000	832	83.2	168	16.8
2,000	1,424	71.2	576	28.8
3,000	1,972	65.7	1,028	34.3
4,000	2,505	62.6	1,495	37.4
5,000	2,993	59.9	2,007	40.1

Table 2.7b: Measure Flow Split at Cozad

Measured Total Flow (cfs)	Measured Flow in North Channel	% of Total	Measured Flow in South Channel	% of Total
1,400	1,000	71.4	400	28.6
5,400	3,400	63.0	2,000	37.0
7,600	3,200	42.1	4,400	57.9

3

4 **Lexington to Chapman**

5 At the six gages downstream from Lexington, correlation between published gage-rating curves and
 6 predicted results is very good over the full range of modeled flows, with differences of less than a few
 7 tenths of feet at all locations (Figures 2.14- through 2.19). The comparison with the LiDAR-based WSELs
 8 at estimated discharges between 70 to 230 cfs also indicate very good agreement, with an average
 9 difference of about 0.04 feet, and 90 percent of the points falling between -0.7 and +0.9 feet (Figure
 10 2.20). The differences are distributed nearly evenly between over- and under-prediction with no
 11 systematic trend along the reach. These differences are considered to be acceptable because there are
 12 several potential sources of error in these comparisons that are not related to the quality of the model
 13 calibration, including uncertainty in the local discharge at the time the LiDAR data were collected and
 14 uncertainty in the mapped WSEL.

15

16 The modeled discharge used for the comparison with the LiDAR WSELs was estimated from the mean
 17 daily flows reported at the DNR and USGS gages; thus, it was necessary to estimate the local discharge
 18 by interpolating between the gages. As noted above, the reported vertical accuracy of the LiDAR data
 19 are ± 0.28 feet. While the true error associated with the individual LiDAR-based water-surface points is
 20 unknown, it is probably considerably larger than ± 0.28 , due to variability in the water surface across the
 21 channel and additional uncertainty in how well the LiDAR sensor actually detects the water surface.
 22 Investigation of the location with errors larger than ± 0.5 feet indicates that they generally fall into one
 23 of three categories:

24

- 25 1. The model predicted critical flow, and as a result, the WSEL at the next upstream cross section is
 26 over-predicted due to the steep energy gradient associated with critical depth. This accounts for
 27 many of the locations where the predicted WSELs were high (positive), and is a relatively localized
 28 effect.

29

30



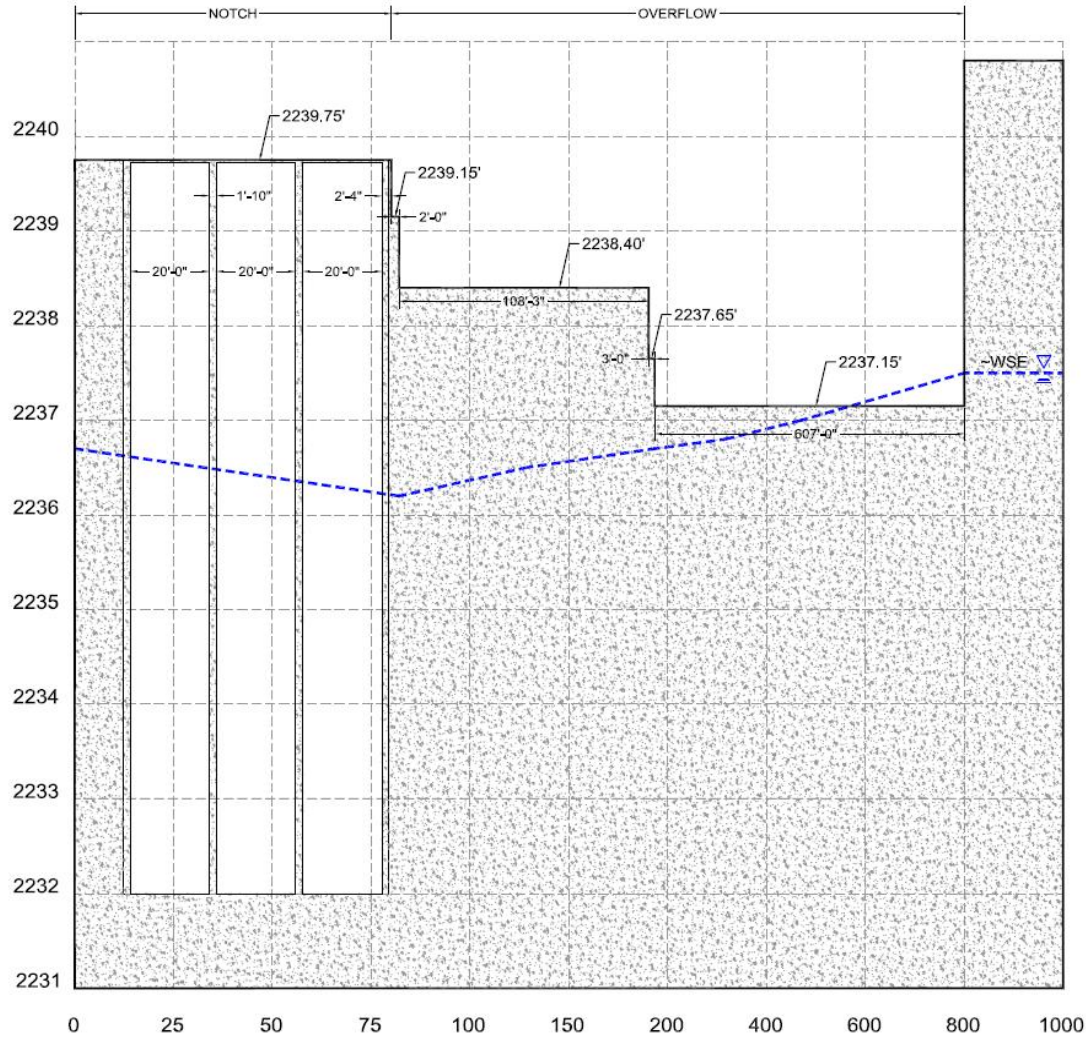
1 2. The LiDAR water surface increased abruptly and may not be realistic based on the local topography
2 and aerial photography, resulting in predicted WSELs that were lower than the LiDAR water surface.
3 The abrupt rises in LiDAR WSEL were commonly followed by a surface that was unreasonably flat
4 compared to the general channel gradient in this area.

5
6 3. In some locations, there were long stretches where survey data from several collection efforts were
7 incorporated into the model. In these areas, it was assumed that these data were accurate and
8 relevant, and the cross-section bathymetry was not modified to refine the calibration because the
9 surrounding cross sections validated the other model parameters at these cross sections (i.e.,
10 roughness distribution, ineffective flow areas, etc.).

11
12 Agreement between the Anchor Point data and modeled water surface was also very reasonable
13 (Figures 2.21 through 2.23). The individual points on the calibration plots are the reported WSELs from
14 the survey notes. In some cases, these elevations varied by as much as 1 foot across a single cross
15 section. The mean daily flows at the USGS gages at Overton, Kearney and Grand Island were reviewed
16 to determine the most appropriate discharge level for the calibration runs at each Anchor Point. Due to
17 system operations, flow fluctuated significantly between 200 and 600 cfs during the day and from day-
18 to-day at these gages. As a result, possible high and low flows during the time of the surveys were
19 identified and modeled, and the resulting elevations are shown on each plot for a single cross section.
20 At 61 of the 102 cross sections, the predicted results are in the middle of the observed points (Figure
21 2.21), at 25 of the cross sections, the predicted results are on the low side (Figure 2.22), and at 14 cross
22 sections, the predicted results were high (Figure 2.23). Based on the uncertainty in the local discharge
23 at the time each water-surface point was measured, this level of agreement is considered to be
24 acceptable.

25
26 A final test of the calibration was conducted by comparing the horizontal location of the modeled water
27 surface with the inundation boundaries shown on aerial photographs taken on June 8, 2010, when the
28 discharge was approximately 6,000 cfs (Figures 2.24 and 2.25) This comparison also indicates
29 reasonable agreement between the observed and modeled water surfaces.

30
31 Predicted results from the North Platte model also match the measured information reasonably well
32 (Figures 2.26 and 2.27). Although the most weight was given to the surveyed and gaged water surfaces,
33 the calibration required optimizing the match between the predicted and various measured WSELs
34 (Figure 2.26). For example, at the Highway 83 gage, the rating-curve comparison indicates the model
35 over-predicts the water surface by about 0.2 feet at 1,200 cfs, but the model under-predicts the
36 surveyed WSEL at survey section 861265 (located a short distance upstream) by about 0.5 feet. The
37 model appears to calibrate reasonably well, since the predicted WSELs are generally within a few tenths
38 of the WSEL inferred from the LiDAR data, with maximum differences of +0.5 and -0.8 feet, and no
39 consistent over- or under-prediction. The predicted results also match the surveyed WSELs reasonably
40 well. The model also appears to match the gage-rating curve fairly well, especially considering the
41 scatter in the measured data and the associated gage measurement shift values (Figure 2.27).

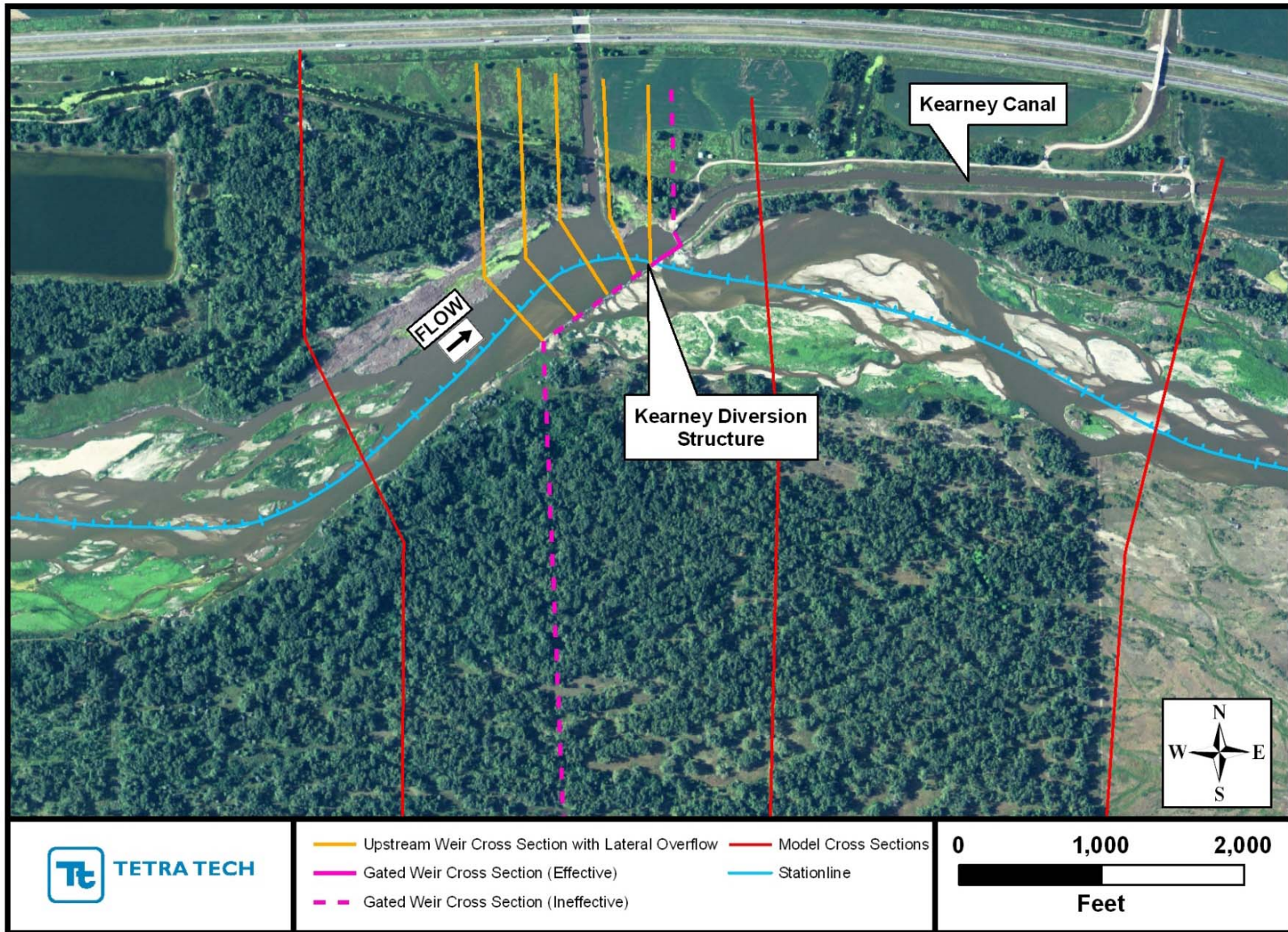


PROVISIONAL FLOW-RATES OF 1,760 AND 1,800 CFS WERE RECORDED DURING THE SURVEY TIME PERIOD AT THE USGS STREAM GAGE STATION NEAR OVERTON, NE (SITE# 06768000).

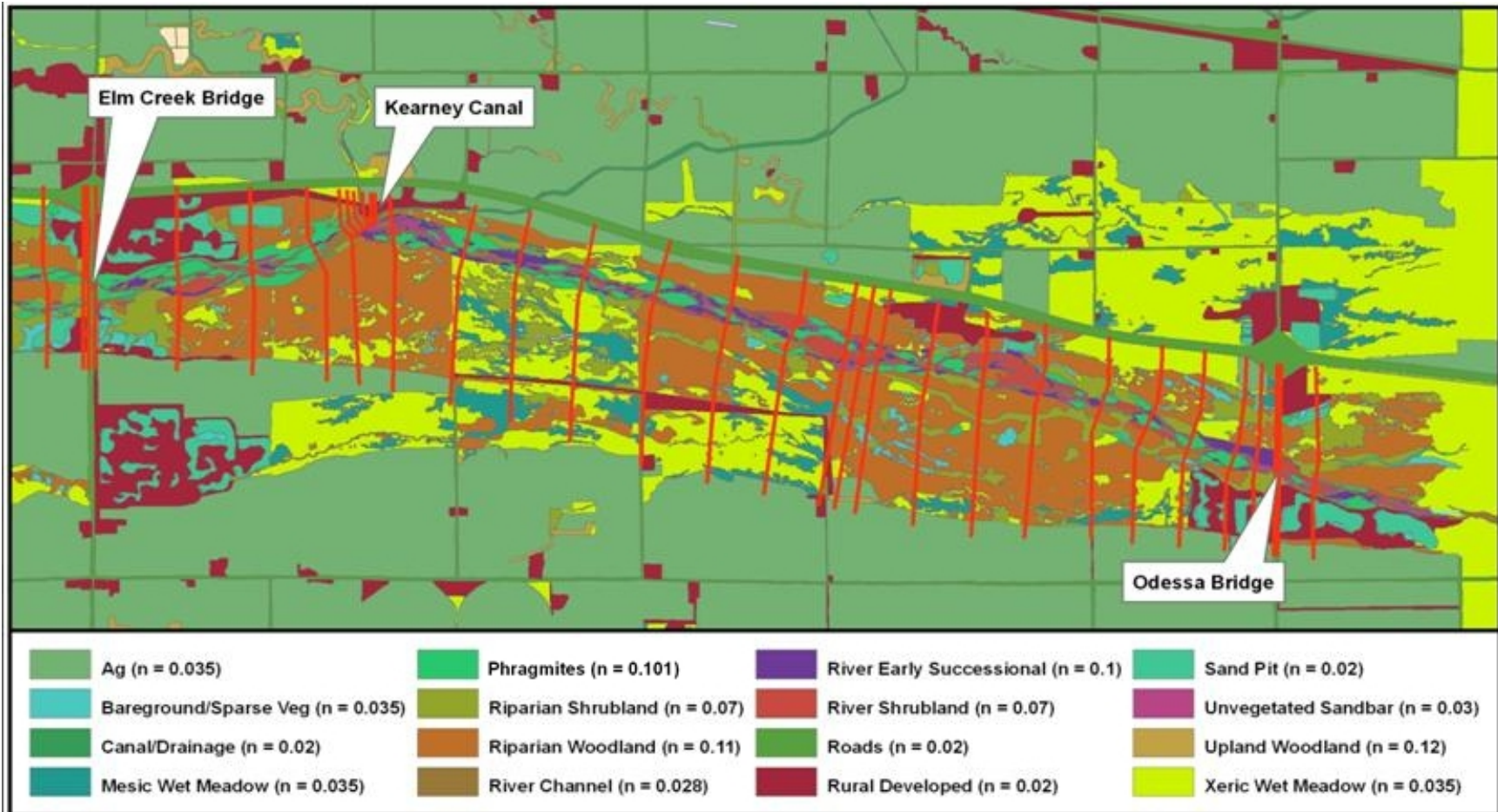
BASE ELEVATION OF NOTCH IN DAM COULD NOT BE SURVEYED DUE TO OVERFLOW. BASE OF CANAL DIVERSION HAD AN ELEVATION OF 2234.3'. HYDRAULIC FLOW CALCULATIONS WERE USED TO ESTIMATE NOTCH BASE ELEVATION BETWEEN ROUGHLY 2231.5' AND 2232.1'. THIS ELEVATION RANGE IS BASED ON AN ASSUMED WATER SURFACE ELEVATION OF 2236.5' AND THE PROVISIONAL FLOW-RATE DATA.

Kearney Canal - Weir Diversion (Surveyed: 12:00 - 12:30, 10 November 2009)

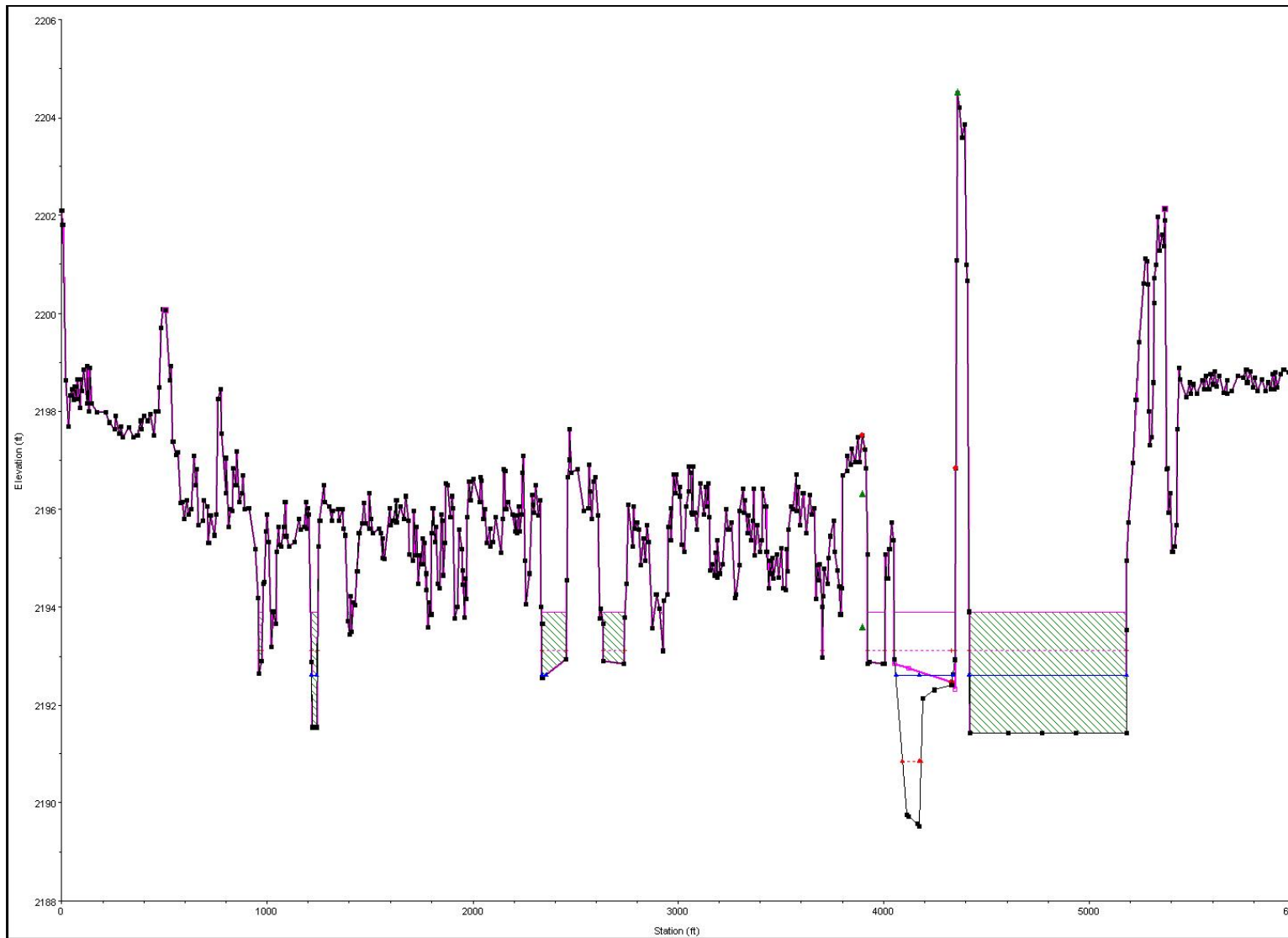
- 1
- 2 Figure 2.1: Dimensions of the Kearney Diversion Structure Weir , surveyed by TFG on November 10, 2009
- 3



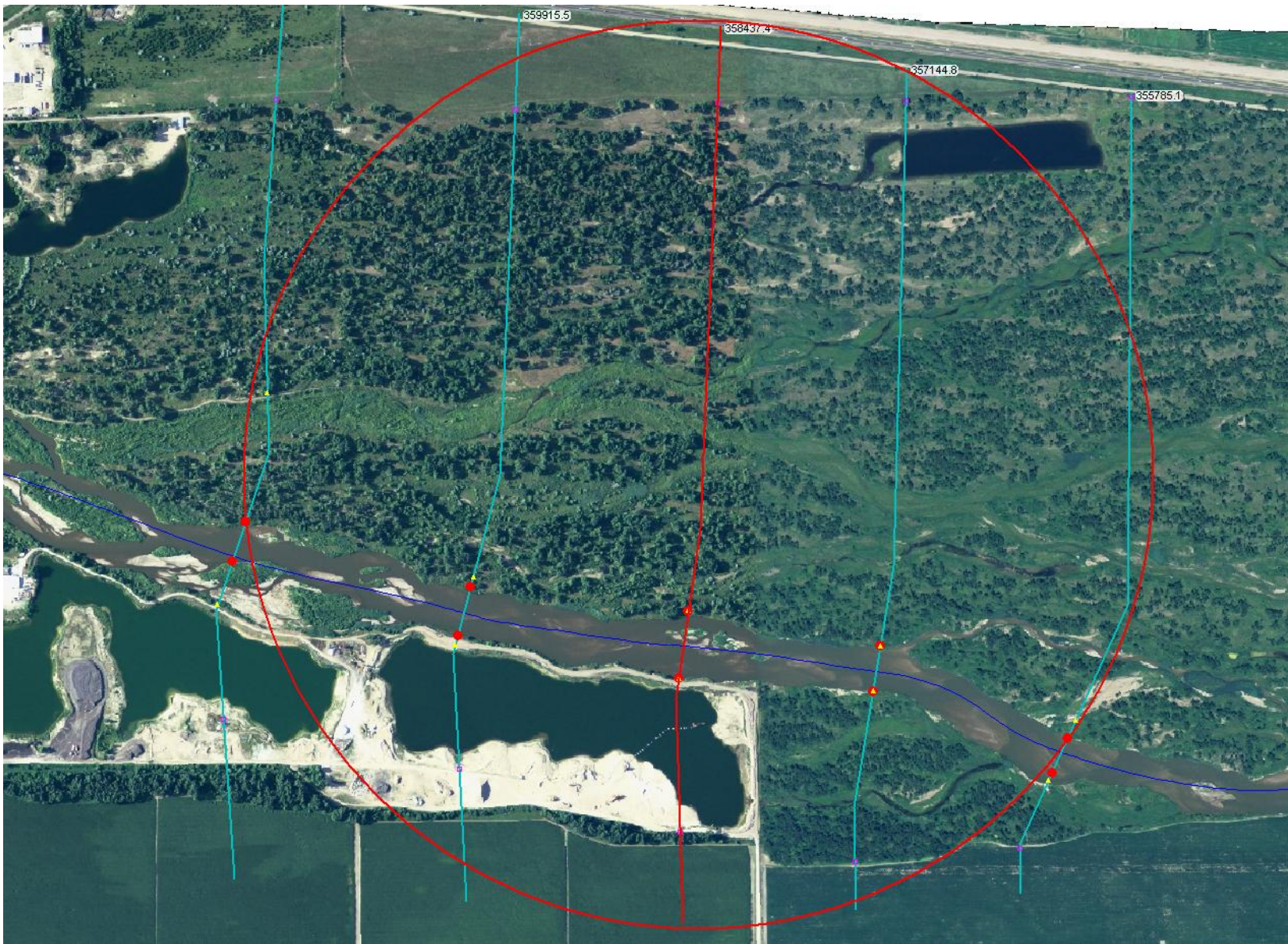
1
2 Figure 2.2: Aerial photograph showing the location and orientation of cross sections used to model the Kearney Diversion
3



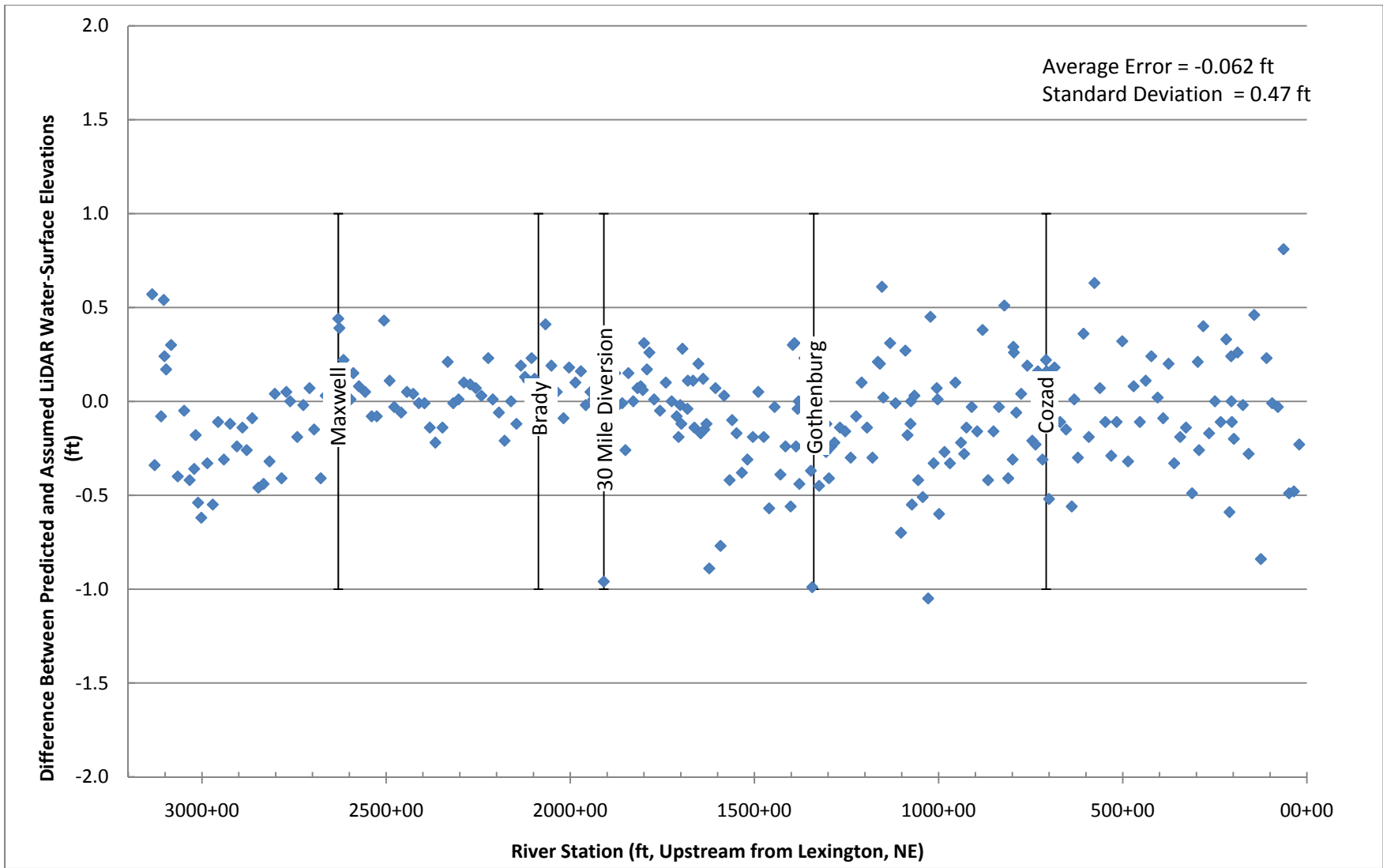
1
2 Figure 2.3: Typical land-cover polygons in the reach between the Elm Creek and Odessa Bridges (provided by the Program via TFG) and the
3 assigned roughness values
4



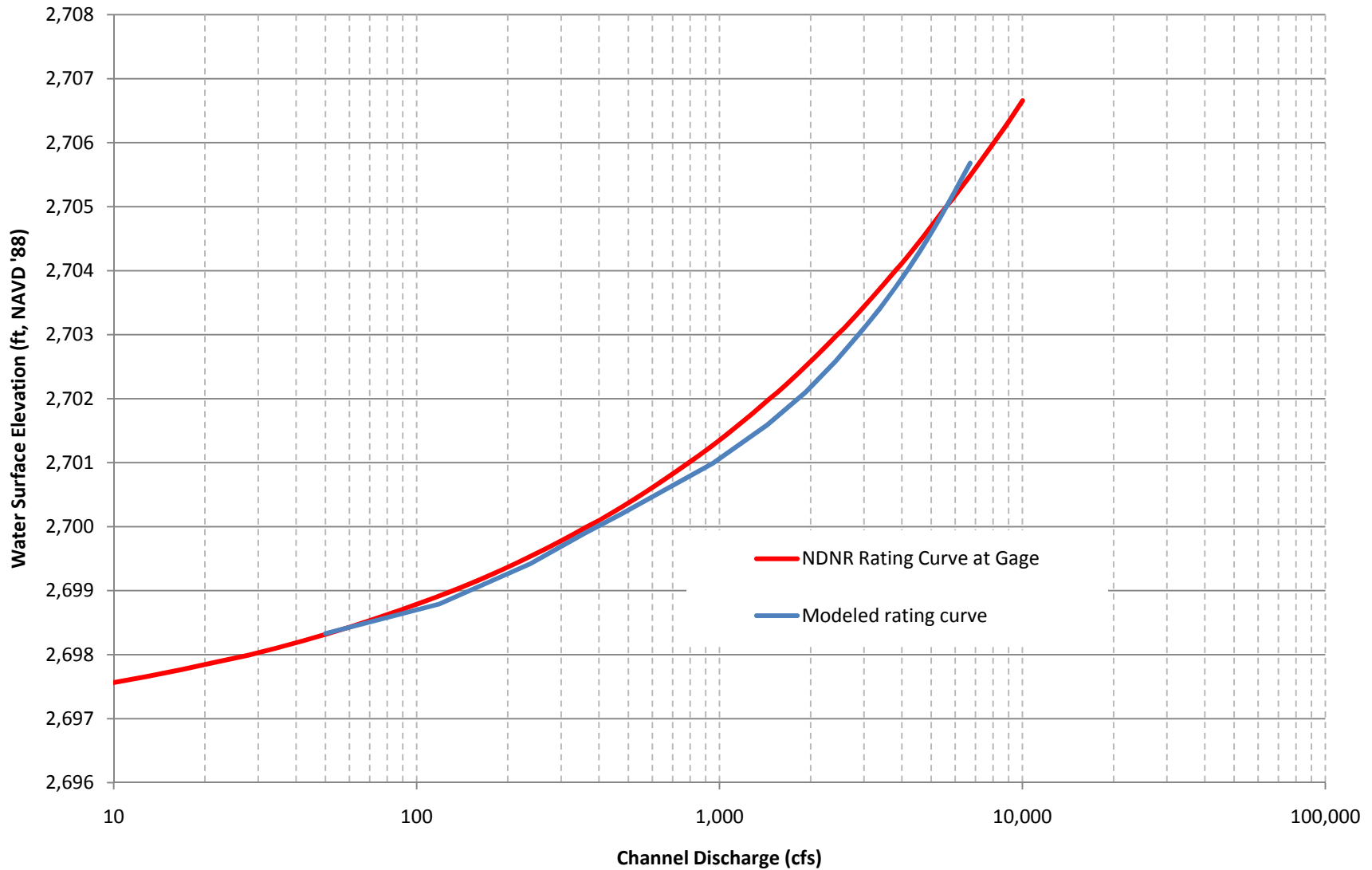
1
 2 Figure 2.4: XS 358437.4 (RM222.8) showing typical channel adjustment of the original LIDAR surface. The channel thalweg was determined from
 3 longitudinal survey.
 4



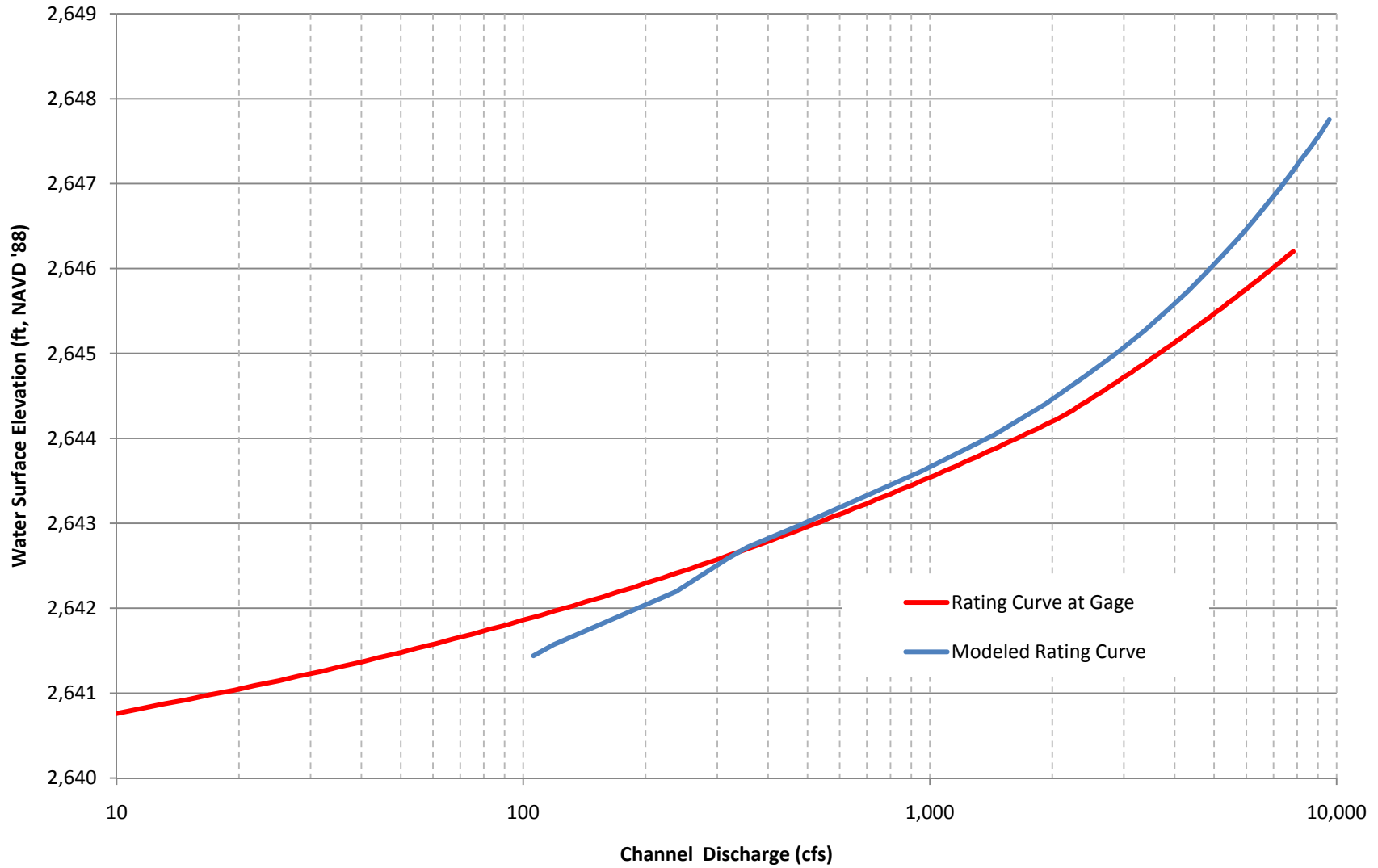
1
2 Figure 2.5: Aerial photograph showing the location of XS 358437.4 (RM 222.8)



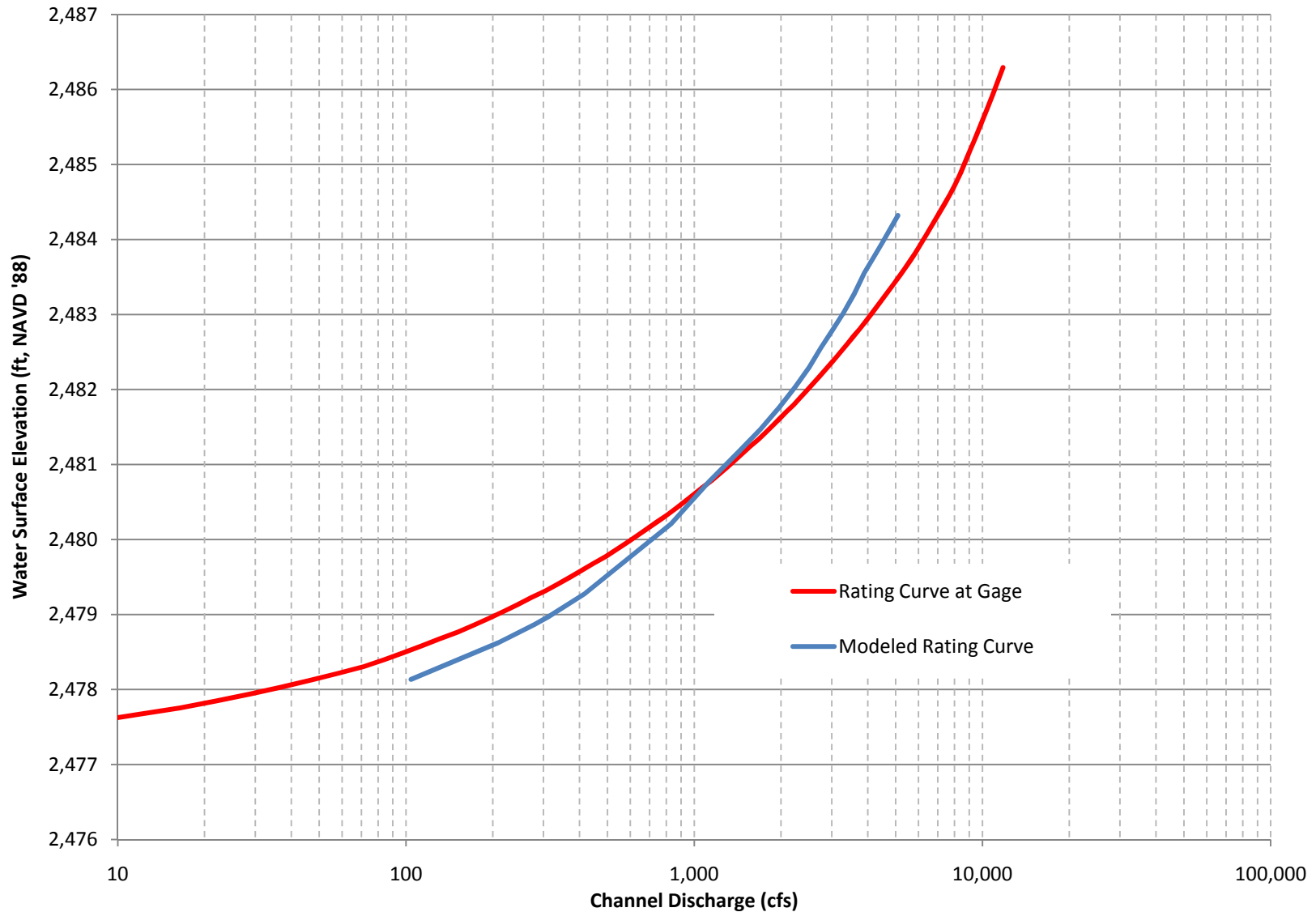
1
2 Figure 2.6: Differences between predicted and assumed LiDAR WSEL in the main channel. (Positive values indicate the predicted result is higher
3 than the LiDAR surface).
4



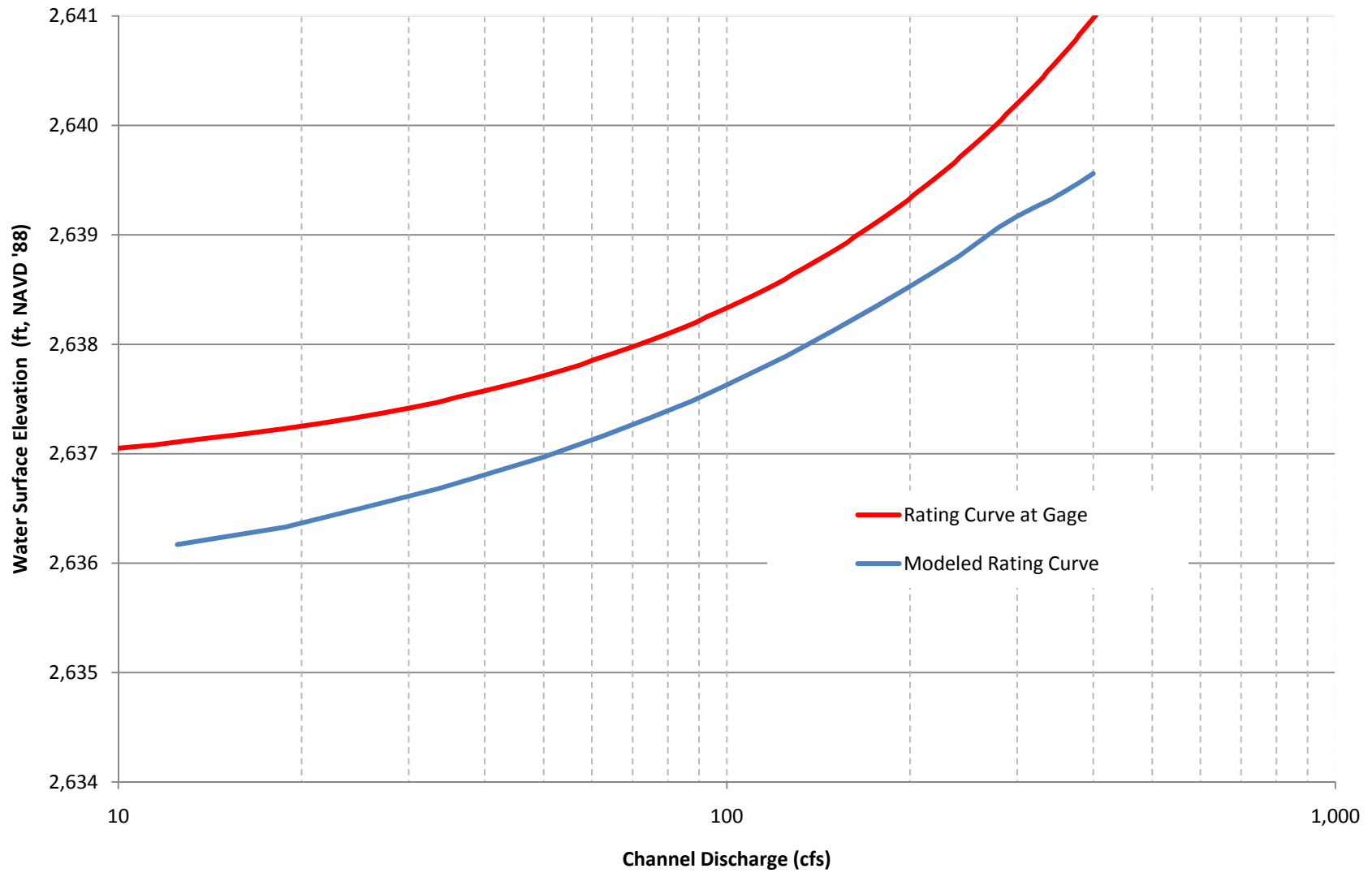
1
 2 Figure 2.7: Comparison of WSELs predicted by HEC-RAS and the published rating curve for the Platte River near Maxwell gage (NDNR Gage No.
 3 229000)



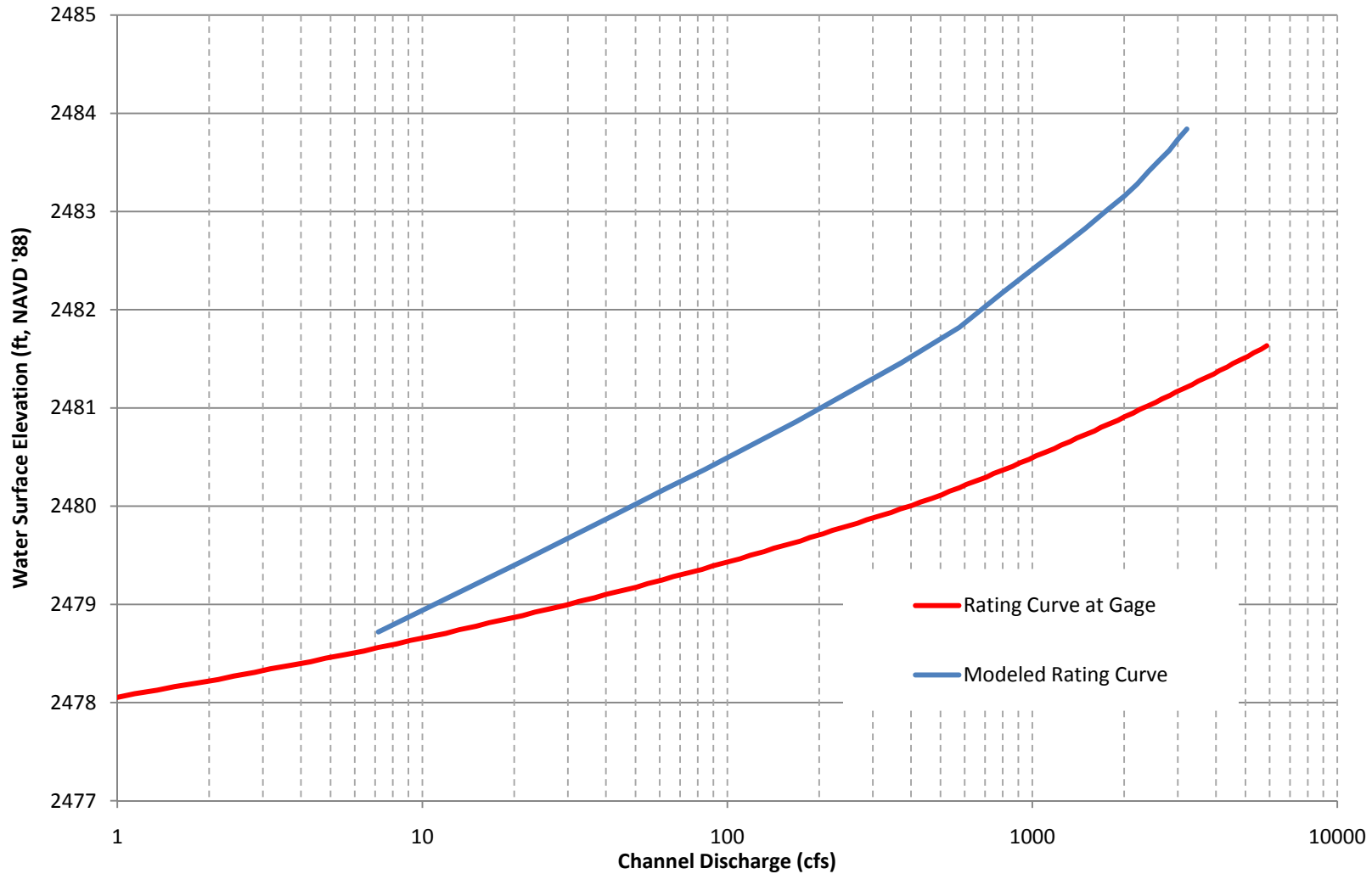
1
 2 Figure 2.8: Comparison of WSELs predicted by HEC-RAS and the published rating curve for the Platte River near Brady, North Channel (NDNR
 3 Gage No. 06765980)
 4



1
 2 Figure 2.9: Comparison of WSELs predicted by HEC-RAS and the published rating curve for the Platte River near Cozad, North Channel (NDNR
 3 Gage No. 06766499)



1
 2 Figure 2.10: Comparison of WSELs predicted by HEC-RAS and the published rating curve for the Platte River near Brady, South Channel (NDNR
 3 Gage No. 06765990)



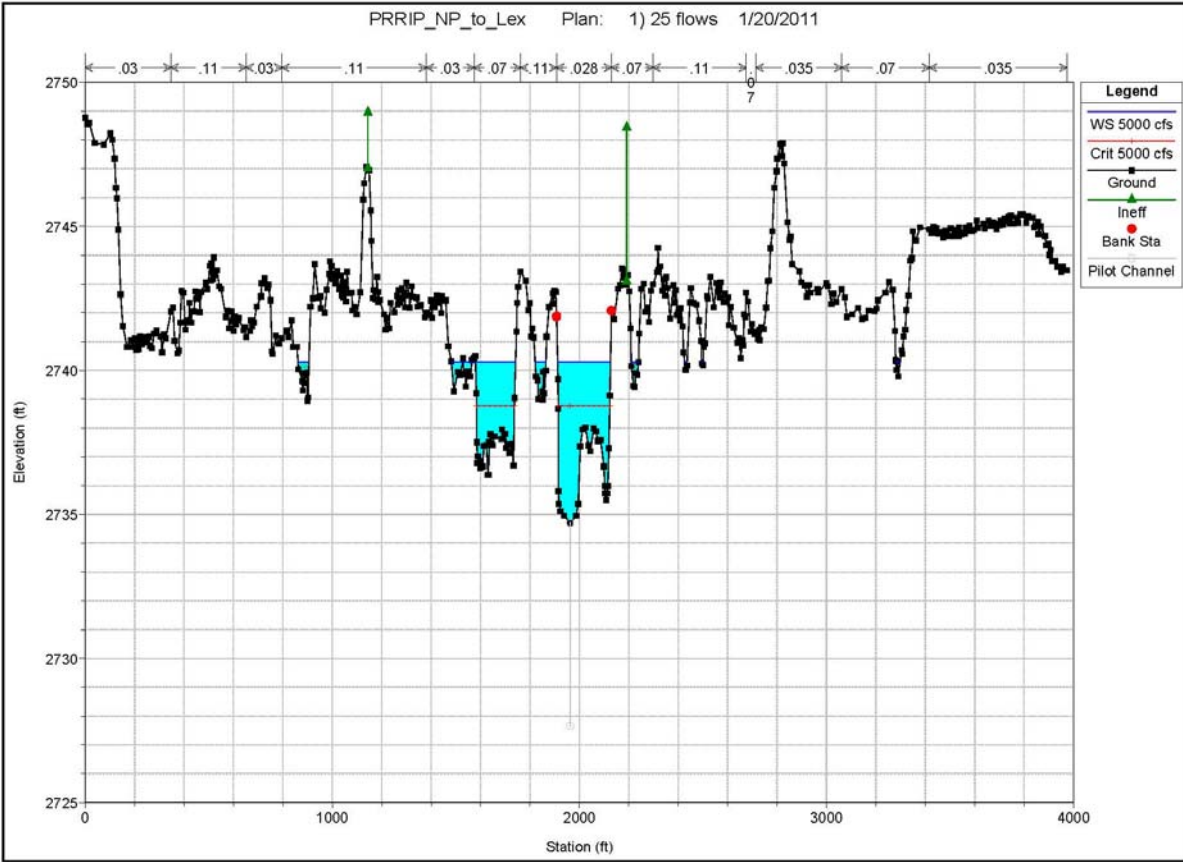
1
2 Figure 2.11: Comparison of WSELs predicted by HEC-RAS and the published rating curve for the Platte River near Cozad, South Channel (NDNR
3 Gage No. 06766498)
4



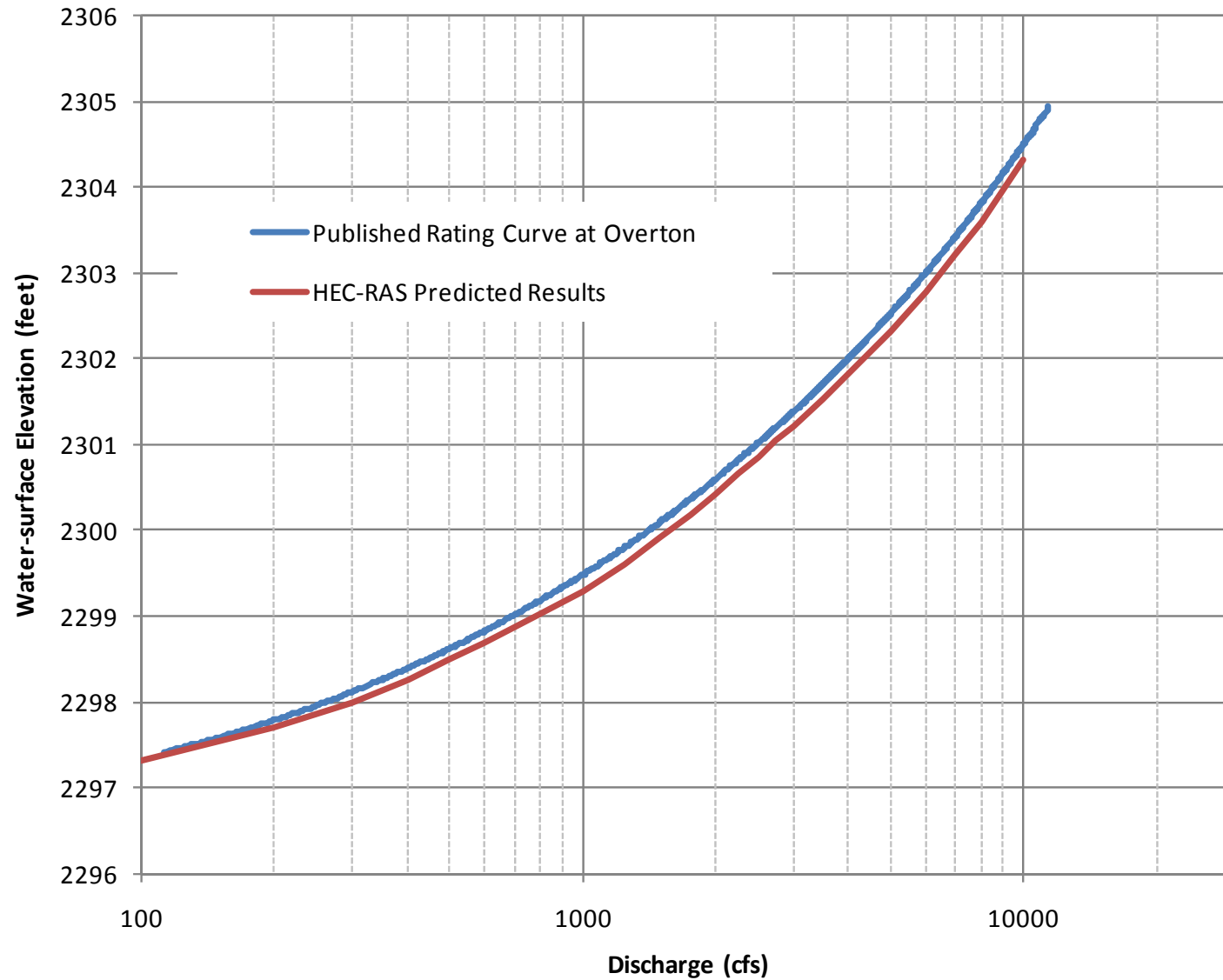
1
2 Figure 2.12a: Flyover Photo, (RM 306.5), from NW, Channel and LOB flow – Water Flowing from Right to
3 Left
4
5



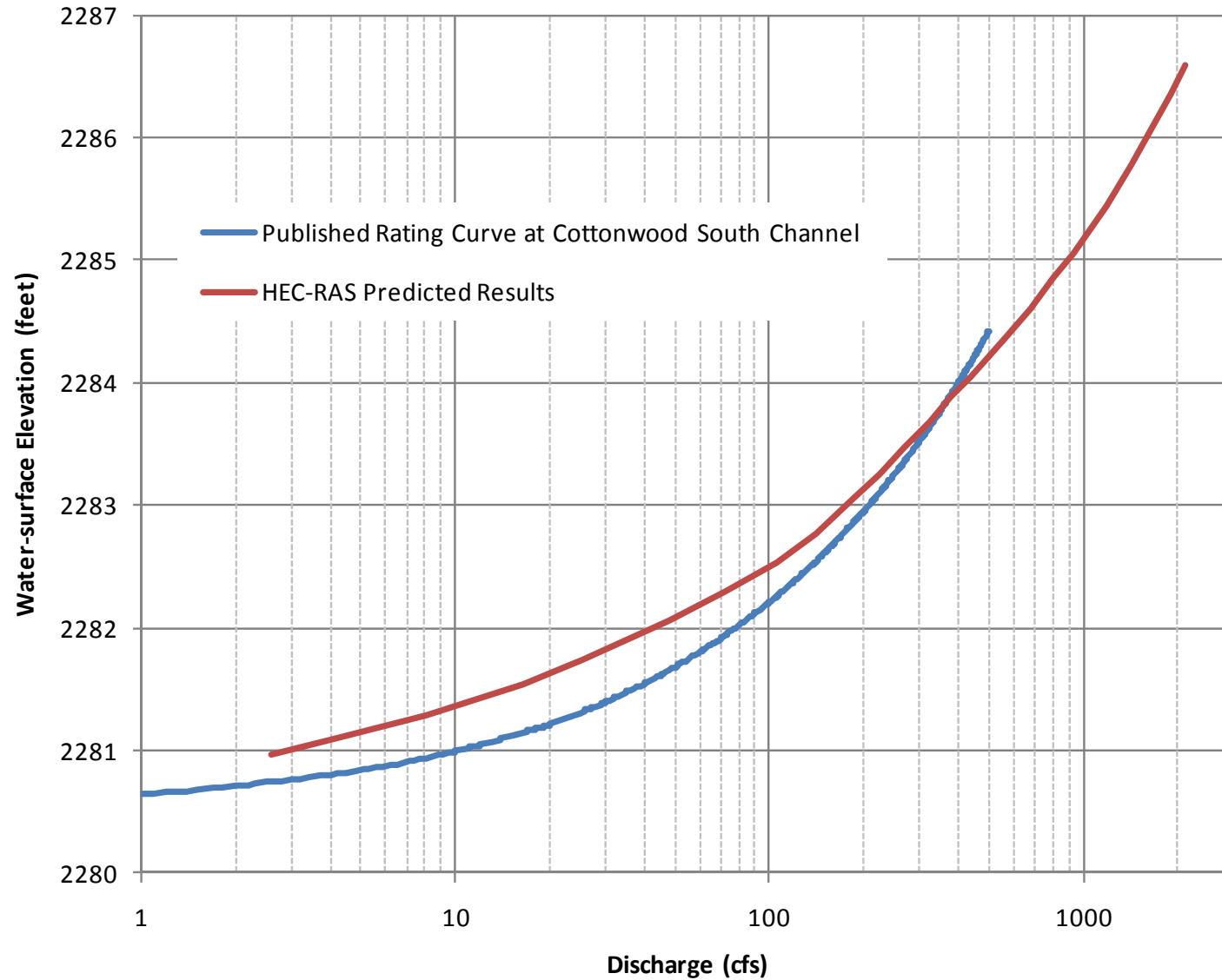
6
7 Figure 2.12b: (RM 306.5), XS Location (center) – Water flowing from Left to Right



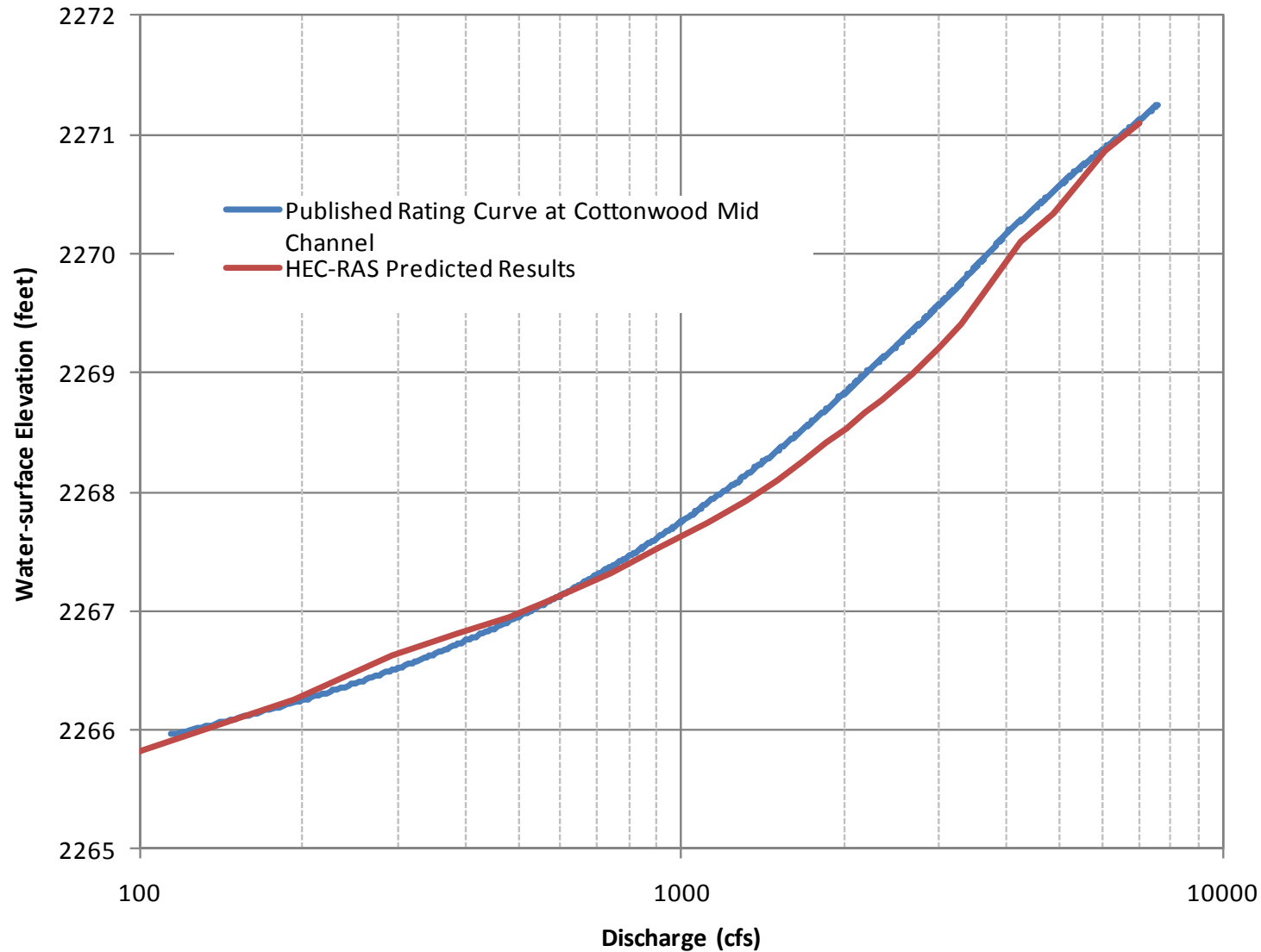
1
 2 Figure 2.13: Hydraulic Model Cross Section (RM 306.5). Platte_N, RM 310-300, 103122 (Oriented Left
 3 Bank to Right Bank looking downstream).
 4



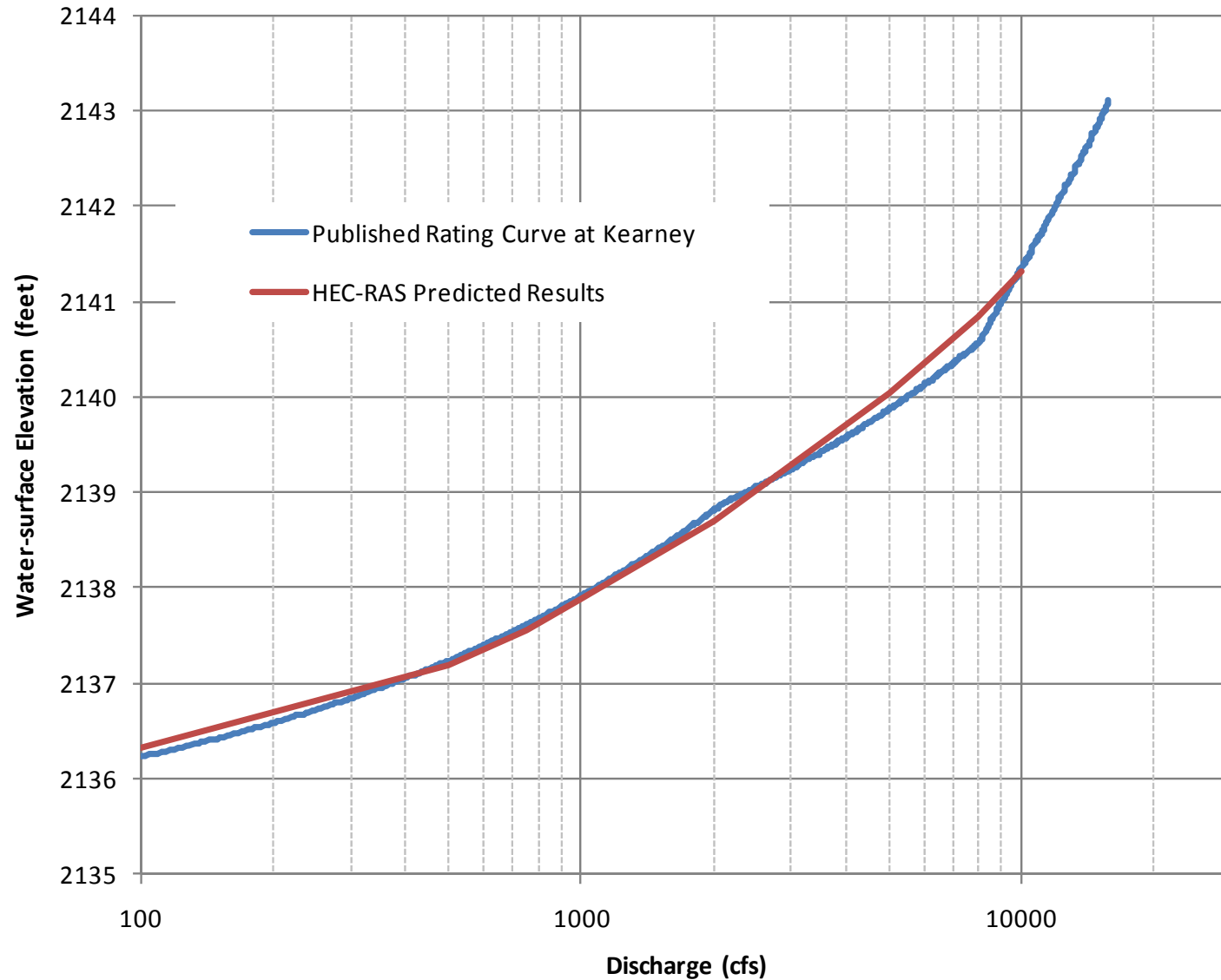
1
 2 Figure 2.14: Comparison of WSELs predicted by HEC-RAS and the published rating curve for the Platte River at Overton gage (USGS Gage No.
 3 06768000).



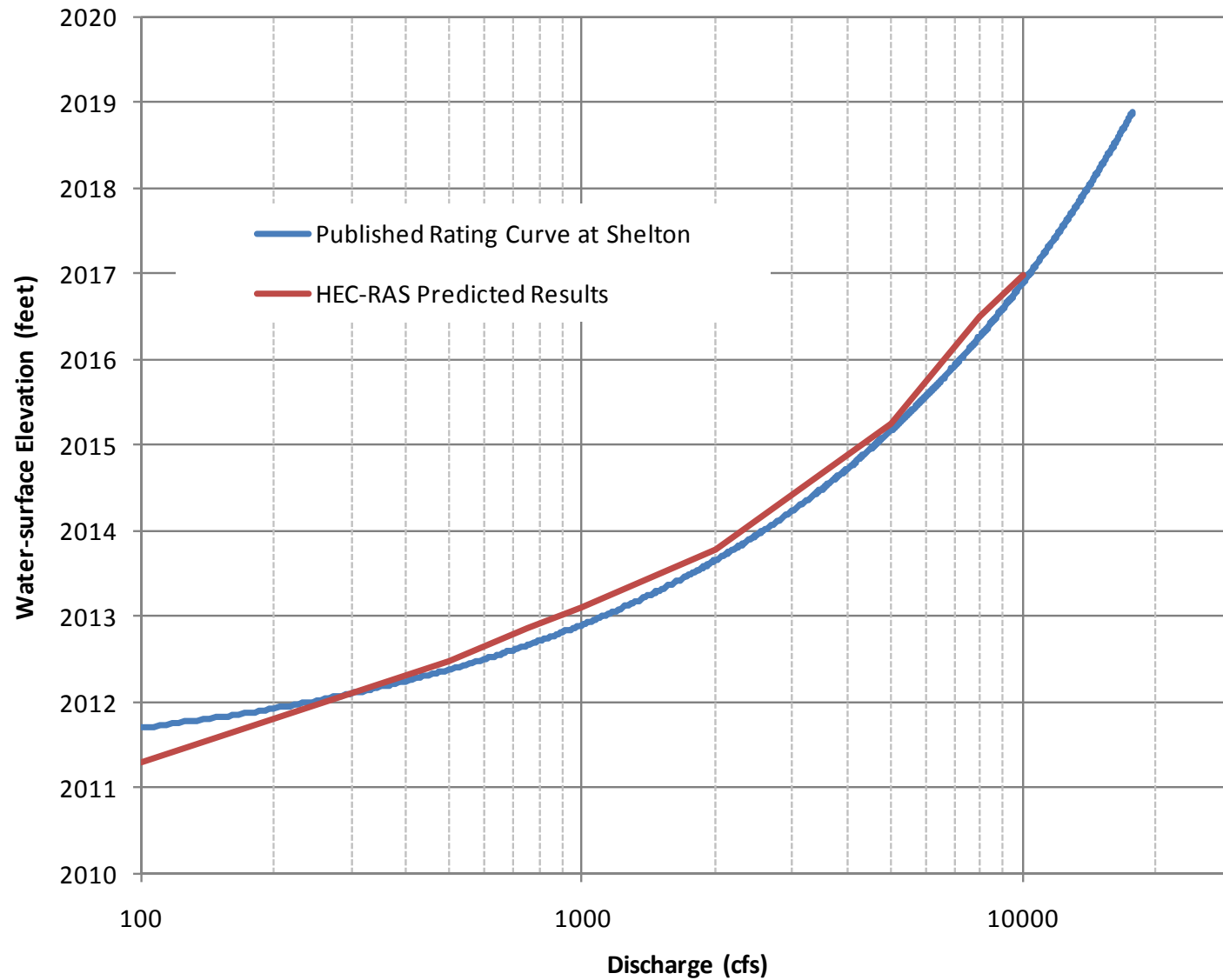
1
 2 Figure 2.15: Comparison of WSELs predicted by HEC-RAS and the published rating curve for the Platte River South Channel gage at Cottonwood
 3 Ranch (USGS Gage No. 06768025).



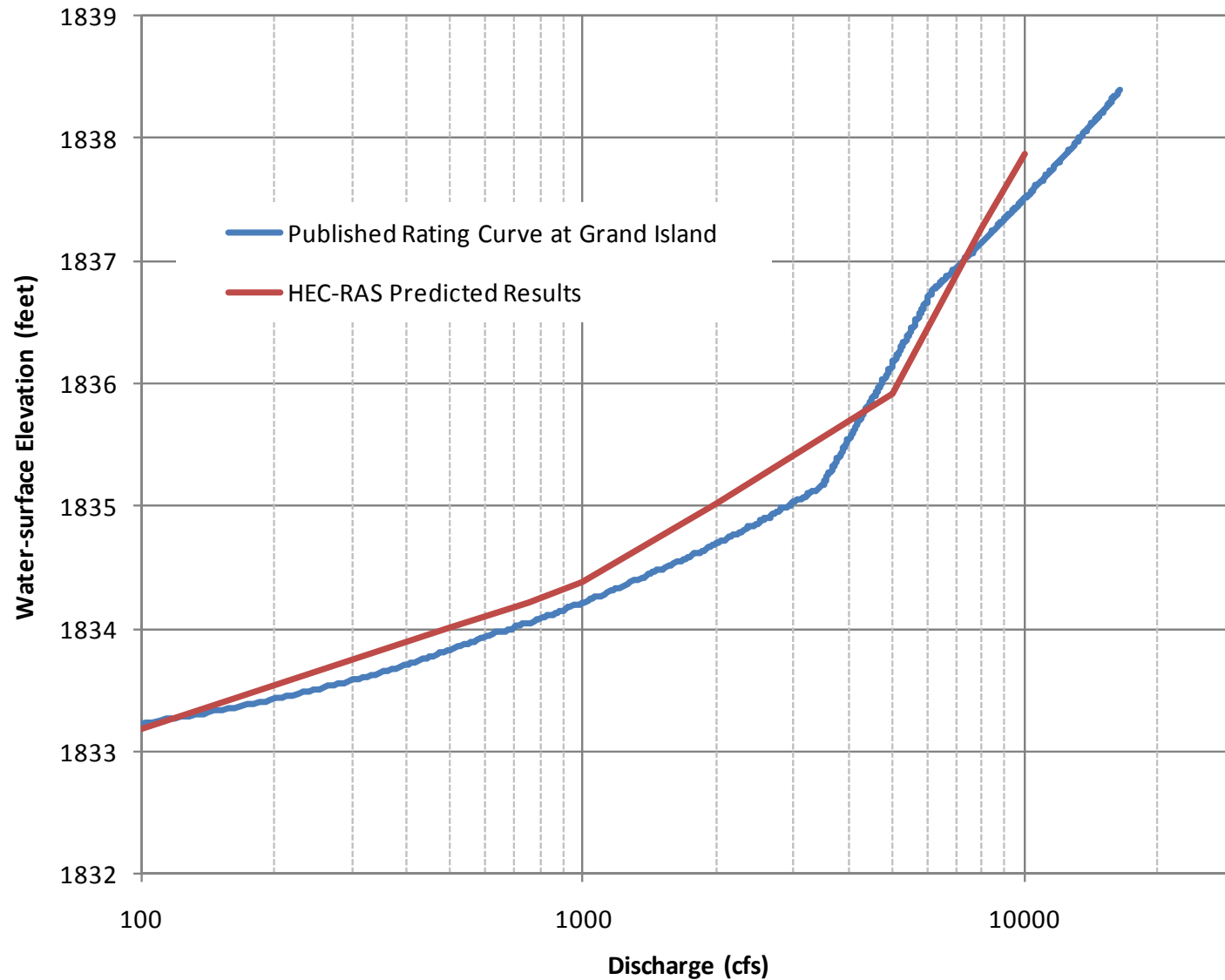
1
 2 Figure 2.16: Comparison of HEC WSELs predicted by HEC-RAS and the published rating curve for the Platte River Middle Channel gage at
 3 Cottonwood Ranch (USGS Gage No. 06768035).
 4



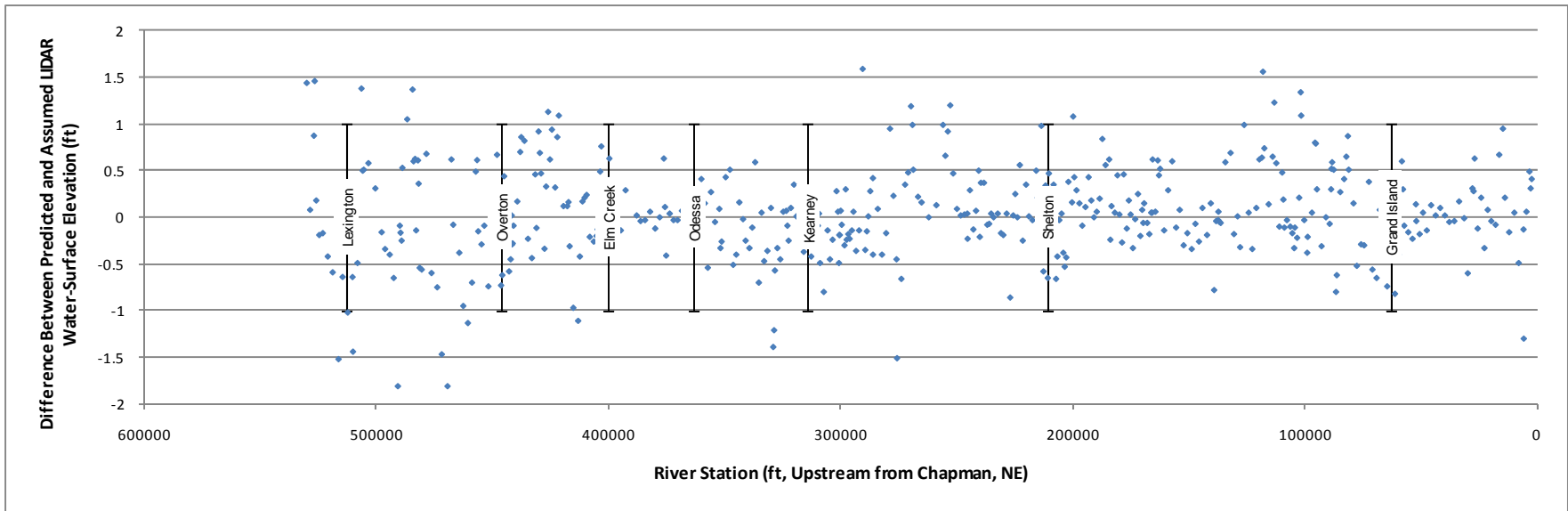
1
 2 Figure 2.17: Comparison of WSELs predicted by HEC-RAS and the published rating curve for the Platte River near Kearney gage (USGS Gage No.
 3 06770200).



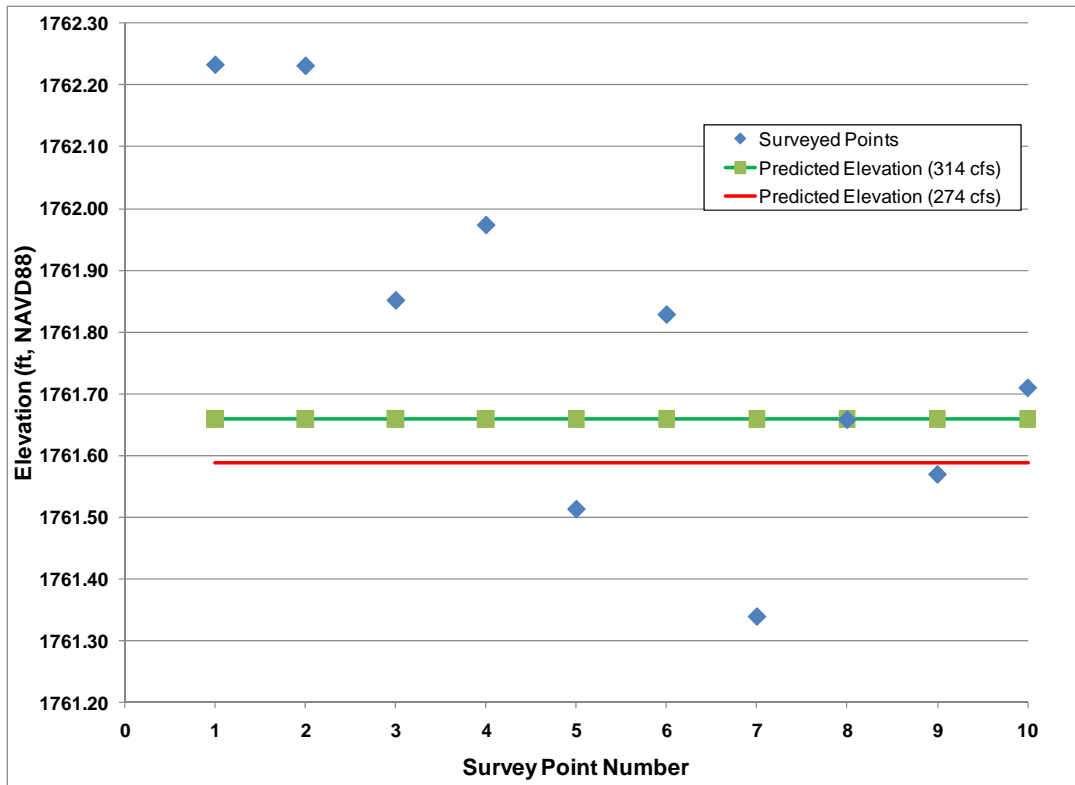
1
 2 Figure 2.18: Comparison of HEC WSELs predicted by HEC-RAS and the published rating curve for the Platte River near Shelton Road gage (NeDNR
 3 Gage No. 229300).



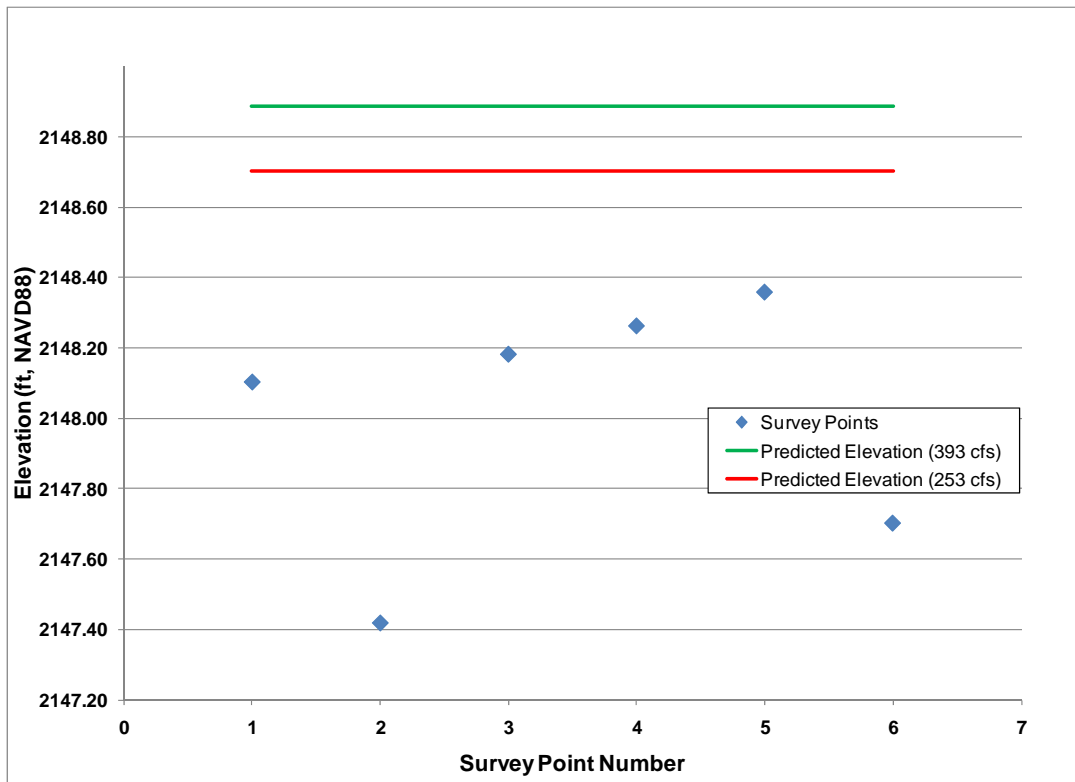
1
 2 Figure 2.19: Comparison of WSELs predicted by HEC-RAS and the published rating curve for the Platte River near Grand Island, NE gage (USGS
 3 Gage No. 06770500).



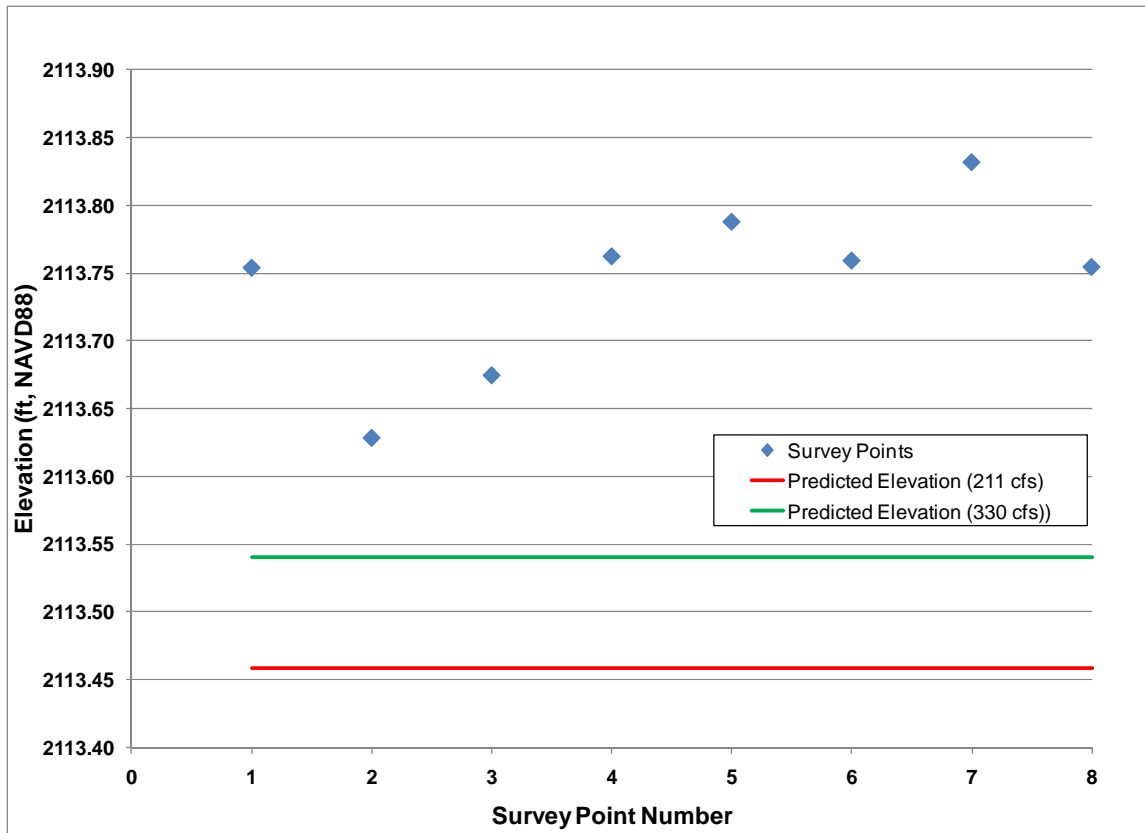
1
 2 Figure 2.20: Difference between the WSEL predicted by the HEC-RAS model and the inferred WSEL from the LiDAR-based mapping
 3



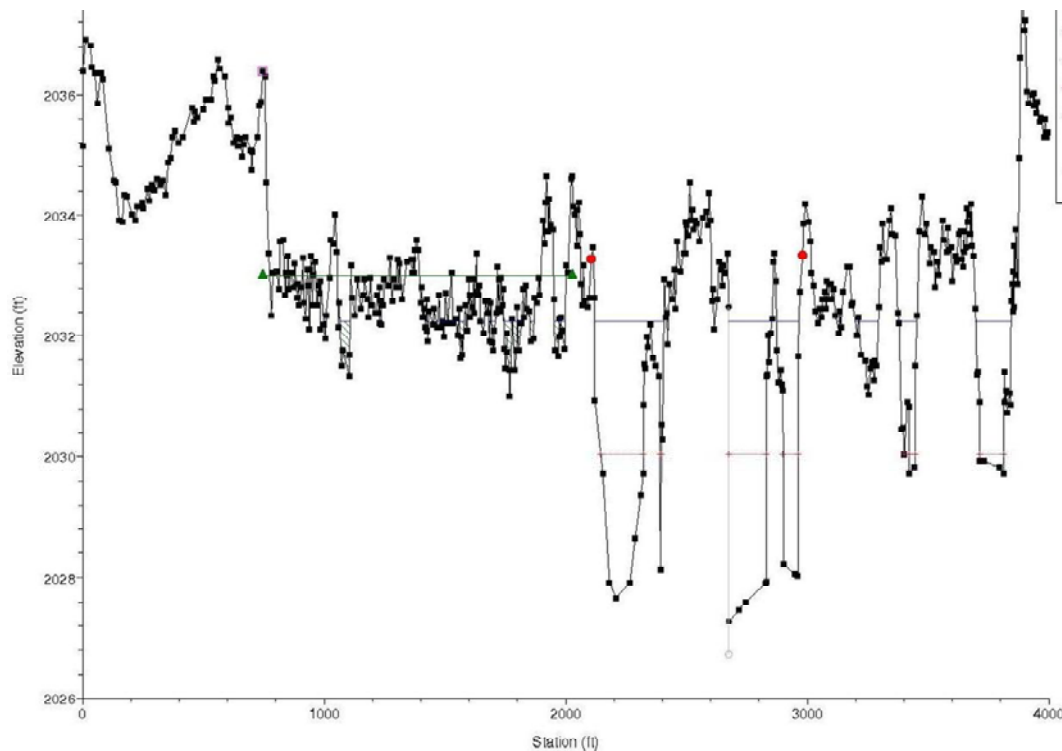
1
2 Figure 2.21: Surveyed WSEL at Anchor Point 1 (RM 156.5, Sta 24+77) and predicted model results for the
3 range of flows at the time of the survey (August 22, 2009).
4



5
6 Figure 2.22: Surveyed WSEL at Anchor Point 25 (RM 216.5, Sta 3233+62) and predicted model results for
7 the range of flows at the time of the survey (August 2, 2009).



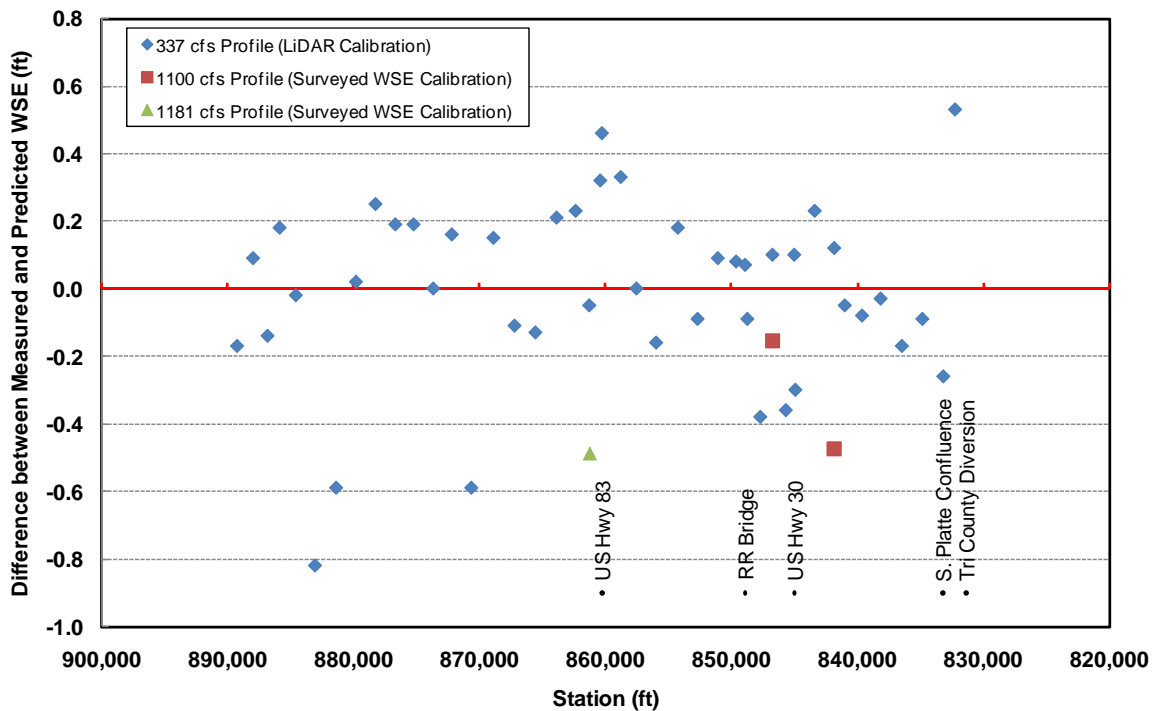
1
2 Figure 2.23: Surveyed WSEL at Anchor Point 23 (RM 216.5, Sta 3233+62) and predicted model results for
3 the range of flows at the time of the survey (August 2, 2009).
4



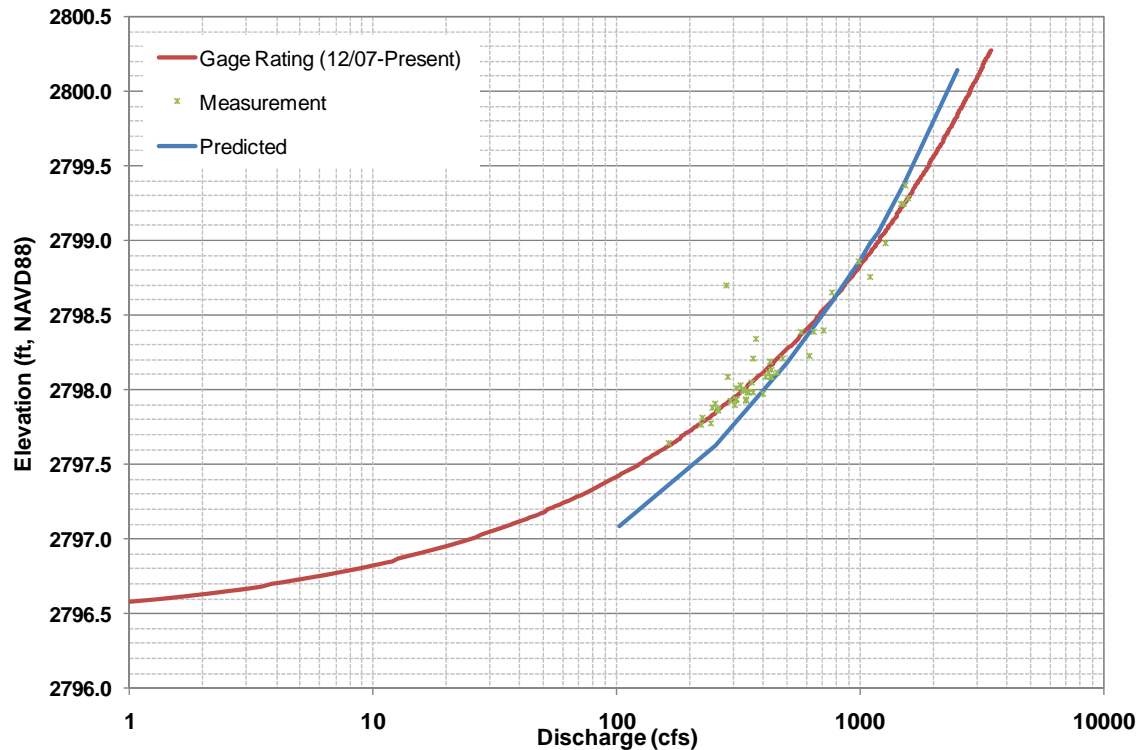
5
6 Figure 2.24: RM 198.5, XS 225677.7 showing the effective (non-hatched) and ineffective (hatched) flow
7 areas at 6,000 cfs.



1
2 Figure 2.25: CIR aerial corresponding to XS 225677.7 where flow is approximately 6,000 cfs.
3



4
5 Figure 2.26: Comparison of WSELs predicted by the steady-state HEC-RAS model of the North Platte
6 “Choke Point” reach and the observed (surveyed and LiDAR-inferred) WSELs.
7



1
2

3 Figure 2.27: Comparison of the predicted WSEL and the DNR gage rating curve and associated
4 measurements.

5 3. Unsteady Model

6 Steady-State Model Conversion

7 The calibrated steady-state model, including cross-section geometry, roughness parameters, hydraulic
8 structures and ineffective flow areas, was used as the basis for the unsteady model. A variety of
9 modifications were made to the model geometry and other parameters to achieve and maintain
10 computational stability, typically the greatest challenge in creating a useable unsteady model. Unlike
11 the standard-step backwater algorithm used in the steady- state model, unsteady modeling algorithms
12 are very sensitive to certain physical parameters (USACE, 2010). As a result, it is commonly necessary to
13 modify the original geometry and other data parameters, with the objective of increasing model stability
14 while maintaining model reliability. Causes of instability include channel network complexity, cross-
15 section spacing and critical-flow conditions at low-flow areas that cause numerical instabilities that
16 prevent the model from finding a valid solution.

17

18 Below Lexington, the number of secondary channels increases significantly compared to the upstream
19 reach. Since the HEC-RAS unsteady algorithm allows a specified maximum number iterations to
20 converge on a solution before moving on to the next time step, reducing the number of stream
21 junctions was effective in increasing the likelihood of a solution before this maximum is reached. To
22 simplify this process, the portion of the project reach below Lexington was separated into three
23 different geometry files [Lexington to Overton (RM 254 – RM 239), Overton to Kearney (RM 239 – RM
24 215) and Kearney to Chapman (RM 215 – RM 156)]. The stage-discharge rating curves at Overton,
25 Kearney and Chapman from the steady-state model were used for the downstream boundary conditions
26 for each model segment (Figures 3.1 and 3.2). In applying these models, the predicted hydrograph at
27 the downstream boundary of each model is used as the upstream boundary conditions for the next



1 downstream model. While this procedure may introduce some limited uncertainty into the model
2 results, repeated testing of various combinations of combined reaches failed to produce a model that
3 was sufficiently robust for future use.

4
5 Model instability caused by cross-section spacing was to be resolved by either removing cross sections in
6 areas of high density or adding cross sections to reduce the distance across junctions. In developing the
7 model, eight cross sections were removed to increase spacing, and a total of 86 cross sections were
8 added to reduce the distance across split-flow junctions. The added cross sections were generally
9 copied from the nearest cross section, and with the floodplain and bathymetric elevations adjusted to
10 match the local slope.

11
12 Critical-flow conditions most frequently occur at low flows and can result from a relatively steep slope
13 between cross sections or flow that is split between two channels. As suggested by the Program's peer
14 reviewer of the draft model, use of an in-line weir modeling can be an effective method of eliminating
15 issues associated with calculated critical-flow conditions in cases with locally steep gradients. These in-
16 line weirs can, however, introduce other unexpected instabilities, and the technique is best applied
17 when there are a small number of locations that are persistently problematic over a range of flows.
18 Thorough review of the model geometry and performance using inline weirs indicated that
19 unanticipated problems with this method when applied to the large and complex Platte River model far
20 out-weighed the benefits.

21
22 Some secondary channels are not active at all flows in the modeled hydrograph; however, the HEC-RAS
23 unsteady algorithm requires that all channels that are incorporated into the model carry at least some
24 flow. The HEC-RAS pilot channel functionality was used to designate small slots in secondary flow
25 channels that allow them to carry a very small amount of flow that permits numerical stability, but does
26 not significantly affect conditions in the primary flow paths. These pilot channels are ignored once flow
27 levels rise to the point where the channels can flow normally. In some cases, this transition can lead to
28 additional critical-flow conditions in the secondary channels, even when discharge in the main channel is
29 high. In these cases, the most effective method is to re-combine the primary and secondary channel
30 geometry, in which case the model assumes that the WSEL is the same in both branches, with the flow
31 area in the secondary channel designated as permanently ineffective to account for the storage and
32 attendant routing effects (Figures 3.3 through 3.6).

33
34 In general, low flows are the most problematic in achieving model stability. Based on the anticipated
35 use of the model to route Short-duration High Flow (SDHF) releases and other hydrographs, the model
36 was refined to permit routing of a target minimum flow of 500 cfs over the entire reach. To achieve this
37 goal, a total of 17 flow splits that were incorporated into the steady-state model were merged back into
38 a single cross section for the unsteady model (Table 3.1). The 500-cfs threshold was achieved in all
39 models sections using this approach, with the exception of reach between Overton and Kearney, where
40 a minimum channel discharge of 650 cfs was found to be necessary.



1 Table 3.1: Reached the were Merged and location after Merger

River	Merged Reach	Location of Reach After Merger	Number of Cross Sections
Platte_S2	RM273-272	RM286-275	5
Platte_S2	RM275-273	RM286-275	6
Platte_S2_a	RM275-273	Platte_S2, RM286-275	6
Platte	RM238-237_S	RM238-236_S	5
Platte	RM177-168_S	178-175_S	49
Platte	RM236_S	RM238-236_S	3
Platte	RM220-217_S	220-218	12
Platte	RM182-177_S	RM190-181	58
Platte	RM177-175_S	178-175_S	16
Platte	RM-175-171_S	178-175_S	25

2

3 Model Calibration

4 *Calibration and Validation Events and Data*

5 The Program designated several events as calibration events for the unsteady modeling effort. The
 6 criteria used to identify calibration events were: similar peak as planned short-duration high flows
 7 (1,000cfs to 5,000 cfs upstream of Lexington, 1,000cfs-8,000cfs downstream of Lexington), similar
 8 phragmites condition as after successful control efforts, and data availability. Initially, the Program
 9 designated the April 2009, June and July 2010, and March and April 1998 events as the basis for model
 10 calibration. The 2010 NDNR data were not made available until near the time of writing the report, and
 11 the 1998 data were limited to one main channel gage (Cozad, North Channel, NDNR gage no.
 12 06766499);the remaining gage data were found to be corrupt by NDNR. The Program then identified
 13 events from 1996 and 1997 for use in calibrating the unsteady model between the Tri-County Diversion
 14 and Cozad. The events discussed in the following sections were used as calibration events for this
 15 model. Figures 3.7 through 3.14 show the gaged flow data from these events. Plots have been divided
 16 into modeled sub-reaches: Tri-County Diversion to Lexington and Lexington to Grand Island.

17 April 2009 Flow Routing Test

18 In April 2009, a test-pulse was routed from Lake McConaughy. At the upstream end of the modeled
 19 reach, CNPPID recorded this pulse having peak of 1,700cfs, which lasted approximately 3 days and 9
 20 hours, beginning on April 14th, 2009. Gage data show this pulse translation from the Tri-County
 21 Diversion at North Platte to Lexington (Figure 3.7). Just downstream of Lexington, the J-2 Return
 22 released four pulses, ranging in 1,800 cfs to 3400 cfs, the third coinciding with the arrival of the pulse in
 23 the main channel (Figure 3.8). Downstream from the confluence with the South Channel of Jeffrey
 24 Island (i.e., the inflow from the J-2 Return), the Overton gage data show four distinct pulses, with the
 25 augmented main channel pulse having a peak discharge between 3,000 and 3,600. Phragmites in 2009
 26 is slightly higher than what the Program is expecting in the future. Data from this event were used in
 27 calibrating the model from the Tri-County Diversion to Chapman.

28 2010 Natural High Flow Event

29 A natural high flow event occurred in June and July 2010. This system experienced peak flows of 7,500
 30 cfs to 9,000 cfs during this event. A flow of approximately 3,000 cfs above Overton and 5,000 cfs below
 31 Overton was maintained over a three week period. Flows in this event are within the discharge range



1 of the Program’s anticipated short duration high flows. With respect to channel vegetation, phragmites
2 control had been enacted by the summer of 2010. The spatial extents of phragmites observed during
3 future short duration high flow events are expected to be similar to that seen in this event. Data for this
4 event were processed expeditiously by NDNR for the Tri-County Diversion to Lexington reach and
5 provided to the team in January of 2011. Limited calibration of the model has been performed to date.
6 However, the initial results are provided, and are reasonable, especially as they relate to flow
7 attenuation. The data from this event are shown in Figures 3.9 and 3.10 and were used in calibrating
8 the model from the Tri-County Diversion to Cozad, and Overton to Grand Island.

9 1998 Natural High Flow Event

10 In April 1998, a natural high flow event occurred. This event lasted from late March through mid-April.
11 The gage data shows peaks varying from 2,500 to 7,500 cfs throughout the reach. Some irregularities
12 exist between gages, showing large ungaged RGLs between gages. Inability to reconcile these
13 differences led to some data being disregarded in calibration. Phragmites had not fully flourished in the
14 Central Platte River. Gage data from this event are shown in Figures 3.11 and 3.12. Data from this event
15 were used in calibrating the model from the Tri-County Diversion to Cozad, and Overton to Grand Island.

16 1997 Natural High Flow Event

17 As per the Program’s request, the 1997 event was included in calibration for the model segment from
18 the Tri-County Diversion to Lexington. This event had gaged peak flows below the Tri-County Diversion
19 of approximately 8,000 cfs. A large ungaged gain is shown between the Tri-County Diversion and Brady,
20 and a large loss of similar magnitude occurred between Brady and Cozad. Anomalies at the Brady,
21 North Channel Gage (NDNR Gage no. 06765980) resulted in this gage not being used for calibration
22 purposes. Gaps in available data at the other gages limited the extent to which calibration could be
23 carried out. Gage data for this event are shown in Figure 3.13.

24 1996 Natural High Flow Event

25 As per the Program’s request, the 1996 event was included in calibration for the model segment from
26 the Tri-County Diversion to Lexington. This event had gaged peak flows below the Tri-County Diversion
27 of approximately 4,500 cfs, and maintained flow above 2,500 cfs for roughly two weeks. Data gaps in
28 the south channel at Cozad limited the extent to which calibration could be evaluated at this gage. Gage
29 data for this event are shown in Figure 3.14.

30 *Historical Reach Gains and Losses*

31 In addition to gaged inflows and diversions, incorporating historical reach gains and losses aided in the
32 prediction of streamflow in many of the modeled reaches. Reach gains and losses (Table 1.2) were
33 incorporated utilizing a uniform lateral inflow boundary condition. The calculated gain/loss rate was
34 distributed, based on the fraction of distance between gages each model reach represented. For
35 lengths where multiple channels exist, equal gain or loss was distributed among the two channels. In
36 certain exceptions, the long-term historical gain or loss was not supported by event specific data. For
37 this case, an event-specific gain/loss was specified based on the available gage data.

38 *Ungaged Inputs and Outputs*

39 Gage data demonstrate, on an event and reach- specific basis, some discrepancies between upstream
40 and downstream gaged volumes that are not easily reconciled by incorporating historical reach gain or
41 loss. Such discrepancies can either be attributed to variability in gaged measurements, or an ungaged
42 input or output. Ungaged inputs may be a result of significant contributions from ungaged tributaries
43 (point input) or runoff from a local high-intensity storm event. In cases where ungaged inflows or
44 outflows exist, calibration efforts were focused on matching timing and trends or gage data were
45 disregarded.



1 An example of ungedged inflow occurred during the 2009 event. During this short duration high flow
 2 test, a significant rainfall event occurred in western and central Nebraska. Daily rainfall totals at eight
 3 regional rainfall measurement stations in western and central Nebraska during this event are shown
 4 below in Table 3.2 (High Plains Regional Climate Center).

6 Table 3.2: Daily Regional Rainfall Totals for Regional Weather Stations (High Plains Regional Climate
 7 Center)

Date	Rainfall in Inches							
	Hershey	North Platte	Gothenburg	Cozad	Lexington	Kearney	Wood River	Grand Island
April 11, 2009	0	0	0	0	0	0	0	0
April 12, 2009	0	0	0.1	0	0	0.2	0.06	0.09
April 13, 2009	0.17	0.13	0.07	0	0	0.16	0.08	0.02
April 14, 2009	0	0	0	0.08	0	0	0	0
April 15, 2009	0	0	0	0	0	0	0.04	0.04
April 16, 2009	0	0	0.14	0	0	0	0.03	0.01
April 17, 2009	0.61	0.37	0.45	0.06	0.706	0	0	0
April 18, 2009	1.04	0.9	0.61	0.84	0	0.45	0.36	0.29
April 19, 2009	0.01	0	0	0	0	0.02	0	0
April 20, 2009	0	0	0	0	0	0	0	0
April 21, 2009	0	0	0	0	0	0	0	0

8
 9 Based on the gage data, an ungedged gain of approximately 4,800 acre-ft occurs between the Tri-County
 10 Diversion and the Cozad gage between April 16 and April 21. The difference in contributing drainage
 11 area between these two gages is about 1,100 square miles (according to published gage information).
 12 Assuming a rough average of one inch of precipitation fell in the additional 1,100 square mile watershed
 13 area contributing to the Cozad gage, the observed gain would correspond to a runoff percentage of 8%.
 14 This runoff rate is within a reasonable range. This confirms that the ungedged inflow may be due to local
 15 runoff and increased tributary contribution from this rainfall event. In the in instance of ungedged gains,
 16 it is recommended that the Program evaluate runoff as a potential source of the gain.

17 **Bank Storage Approach**

18 One study modeling high flow events in the central Platte River determined that the inclusion of bank
 19 storage effects is necessary to accurately predict the hydrograph peak and shape of short duration high
 20 flows (Randle and Samad, 2008). The conceptual model developed by Randle and Samad approximates
 21 the bank storage response as a function of the hydrograph (Figure 3.15). Based on their conceptual
 22 model, a qualitatively similar approach was implemented in estimating bank storage effects in this
 23 model. The approach assumes a rapid linear increase of water entering the bank on the rising limb of
 24 the hydrograph. Once the hydrograph reached it peak, that rate decreases exponentially. Similarly, on
 25 the falling limb of the hydrograph, a volume of water is returned to the channel with a rate that
 26 decreased again over time. Based on this response, a conceptual bank storage hydrograph was
 27 developed, shown in Figure 3.16. In this conceptual hydrograph, water is removed from the channel
 28 flow beginning at t_b . The rate of flow removed from the channel increases linearly from zero to its
 29 “peak” (Q_a) at t_a . After t_a , the flow removed decreases as an exponential decay function. The removal
 30 of flow from the river channel begins with the rising limb of the hydrograph, with t_a occurring during the
 31 rising limb. As the hydrograph reaches its falling limb, flow is then returned to the channel, starting at
 32 t_b . Flow is returned to the channel in a like manner- increasing linearly from zero to a “peak” (Q_c) at t_c ,





1 then decreasing as an exponential decay function. The April 2009 event is the only event modeled in
2 which bank storage effects are considered and is most representative of a short duration high flow
3 event. This event had steep rising and falling limbs. The model predicted relatively fast downstream
4 translation and little change in hydrograph shape in comparison to gaged data.

5
6 A limitation of this approach is that flow is removed uniformly throughout the reach. In cases where
7 there is a different discharge at the upstream and downstream ends of a reach (beginning of a sudden
8 pulse), flow into bank storage would vary significantly. Modeling this as a uniform lateral flow can result
9 in a brief period of spatial misrepresentation of flow into bank storage. This effect manifests as an
10 occasional oscillation in the modeled discharge (see Figure 3.17 for an example). During the calibration,
11 the timing of bank storage hydrographs was adjusted to minimize the presence of these oscillations.

12
13 The general concept of a bank storage hydrograph, used to represent the volume of water lost on the
14 rising limb of the hydrograph and returned to the river channel after the falling limb was adopted as the
15 a calibration tool for the April 2009 short-duration high flow event. Bank storage hydrographs were
16 developed as part of the calibration and implemented to produce similar pulse celerity and peak
17 attenuation as that observed in gage data. Bank storage relationships were developed for the gaged
18 reaches, and distributed among the corresponding model reaches. The uniform lateral inflow
19 hydrograph boundary condition was utilized to apply the bank storage hydrograph throughout the
20 model at the scale of individual model reaches.

21
22 It should be noted that initial model runs for natural high flow events predicted reasonable hydrograph
23 translation and attenuation without accounting for bank storage when compared to gaged reaches (see
24 Figures 3.17 through 3.30). Bank storage effects were likely masked by the gradual nature of the rising
25 and falling limbs and duration of the event. For this reason, bank storage was not considered during
26 calibration of the long duration natural high flow events (2010, 1998, 1997, and 1996). This observation
27 is consistent with other unsteady modeling efforts on the central Platte River (Randle and Samad, 2008).

28 29 *Calibration Methods*

30 The unsteady hydraulic model was calibrated and validated by routing five events, using hydrologic
31 inputs and outputs as the flow boundary conditions and making bank storage adjustments based on
32 comparison to gage data and overall model performance. In the calibration of the model, some isolated
33 adjustments were made to improve model performance. Such adjustments included slight changes to
34 subaqueous channel bathymetry, additional or eliminated cross sections, and appropriate adjustments
35 to ineffective flow areas. These adjustments often improved model stability and minimized error
36 associated with HEC-RAS hydraulic calculations. As previously stated natural high flow events did not
37 require adjustment to account for bank storage.

38
39 For the 2009 event, a short-duration high flow pulse release, bank storage hydrographs were adjusted
40 to achieve improved calibration at main-channel gage stations. Calibration involved adjusting the bank
41 storage hydrograph timing parameters (t_o , t_a , t_b , t_c) and magnitude parameters (Q_a , Q_c , k_1 , k_2) (Figure
42 3.16) to replicate pulse magnitude, timing, and attenuation throughout the modeled river system. One
43 bank storage hydrograph was developed per river section between gages, and was distributed
44 throughout the length of river between the two gages.

45
46 Calibration was performed by comparing predicted hydrographs with measured discharge data provided
47 by the NDNR and USGS. The model was considered to be adequately calibrated when computed
48 hydrographs resulted in similar shapes, peaks, and temporal trends as measured hydrographs at the



1 gages, considering the unaged gains and losses. This was initially qualitatively assessed and later
2 quantified using a Nash-Sutcliffe efficiency coefficient.

3 4 *Calibration Results*

5 6 *Segment: North Platte to near Lexington (RM 310 to RM 254)*

7 Bank storage calibration efforts were based on the April 2009 event. This event featured a single pulse
8 flow with a peak discharge of 1,700 cfs at the Tri-County Diversion. This flow rate remained constant for
9 approximately three and a half days. The Tri-County diversion release flow (upstream boundary
10 condition, recorded by CNPPID), was assigned to the north channel. The south channel below the Tri-
11 County Diversion is not hydraulically connected to this section of river. Therefore, the south channel
12 was assigned a constant base flow of 70 cfs, based on the south channel at Brady gage. Only three canal
13 diversions in the reach were active during the simulation, which all began diverting after the receding
14 limb of the pulse.

15
16 Using the bank storage approach to account for water lost on the rising limb of the hydrograph and
17 returned on the falling limb improved agreement in hydrograph timing and shape (see Figures 3.17
18 through 3.21). Inclusion of cumulative bank storage effects became more important in the downstream
19 reaches for predicting both pulse timing and attenuation, as can be seen in the figures depicting the
20 2009 calibration event in this reach. The predicted hydrograph at Lexington did not match as well as at
21 upstream locations. The Program has noted that this gage was newly installed before the 2009 test
22 pulse, and the rating curve used to determine the “gaged” flow may not be accurate since it is based on
23 only a few rating points. Note that the Lexington gage record has been shifted three hours ahead in the
24 figure in order to account for the approximate lag time between the downstream cross section of this
25 model segment (RM 254) and the Lexington Gage (RM 251).

26
27 Calibration efforts for the 2010 event were limited since 30-minute stream gage data from the NDNR
28 were not received until January 2011. The upstream inflow boundary condition (release from the Tri-
29 county Diversion) was calculated based on half-hourly gage data for the South Platte at North Platte
30 (06765500) and North Platte at North Platte (06693000) gages, and hourly data for the Sutherland
31 Return (138000), and Tri-County Diversion flows (Provided by CNPPID). Gage data indicate that the
32 hydrograph reaches two peaks. However, this gain is most likely due to an unaged inflow that was not
33 included in the upstream hydrograph. Still, the model predicts hydrograph timing and peak fairly
34 consistently throughout the entire modeled domain, as is demonstrated favorably by Nash-Sutcliffe
35 Coefficients. Figures 3.22 through 3.26 compare gaged and modeled results for the 2010 event. Again,
36 bank storage was not applied for this natural high flow event.

37
38 Calibration efforts for the 1998 event were limited by the amount of reliable data. The upstream inflow
39 boundary condition (release from the Tri-county diversion) was calculated based on half-hourly gage
40 data for the South Platte at North Platte (06765500), the North Platte at North Platte (06693000),
41 average daily data from the Sutherland Return (138000), and Tri-County Diversion flows (Provided by
42 CNPPID). According to the NDNR, data from the Platte River below Tri-County Diversion gage (142000)
43 were corrupt and unable to be retrieved properly. As discussed above, the Brady gage indicates very
44 large unaged inflows between the Tri-County Diversion and Brady, as there are no major tributaries or
45 canal returns between these two gages. Furthermore, the reach between Brady and Cozad indicates a
46 loss of similar magnitude (Figure 3.11). Due to these irregularities (or inexplicable unaged inflow and
47 outflow), measurements at the Brady north channel gage were disregarded in calibration of the 1998
48 event. The Cozad gage was used to evaluate calibration for this event. Overall, the timing and trends
49 from the predicted 1998 model match the gage data (see Figure 3.27 for comparison). At peak flows,



1 the modeled discharge is consistently 200-300 below the gaged discharge. This difference cannot be
2 reconciled with any of the gaged canal returns or tributaries. At the 2,500 to 3,000 cfs range, the
3 difference in river stage at the Cozad gage is approximately 0.2 ft for 300 cfs. This difference could be
4 attributed to increased local gains, stemming from the natural high-flow event, or standard error
5 associated with the rating used in 1998.

6
7 Like the 1998 event, calibration to the 1996 and 1997 events were limited due to questionable reliability
8 and record gaps in the 30 minute data supplied by the NDNR. The upstream boundary condition for the
9 1996 and 1997 events was developed using data from the Platte River below Tri-County Diversion gage
10 (NDNR Gage no. 229000) data. There is a gap in the 1997 gage record from June 27 to July 12. The
11 flows during this period were estimated based on half-hourly gage data for the South Platte at North
12 Platte (06765500), North Platte at North Platte (06693000), average daily data from the Sutherland
13 Return (138000), and Tri-County Diversion flows (Provided by CNPPID). Like in the 1998 event, the
14 Brady gage indicates very large ungaged inflows between the Tri-County Diversion and Brady that are
15 not explained by tributary inflow or storm event. Furthermore, the reach between Brady and Cozad
16 indicates a loss of similar magnitude. Due to these irregularities (or inexplicable ungaged inflow and
17 outflow), measurements at the Brady north channel gage were disregarded in calibration of the 1997
18 event also. Calibration was only evaluated at the Cozad Gage. This gage demonstrates good calibration
19 overall, with the exception of the time when the gap in upstream flow data was estimated. See Figure
20 3.28 for this comparison. The 1996 event had a complete and reasonable gage record at the Brady gage,
21 and the predicted hydrograph calibrated to the gaged hydrograph well. An incomplete gage record
22 limited comparison to the period after September 24th. From September 24th through October 15th, the
23 total flow gaged at Cozad compares favorably to the flow predicted by the model. See Figures 3.29 and
24 3.30 for the comparison of the 1996 event.

25 *Segment: Lexington to Overton (RM 254 – RM 240)*

26 Input hydrographs were available for the 2009 event in the main channel at Lexington and for the J-2
27 Return and Plum Creek inflows to the South Channel of Jeffreys Island (Figure 3.8). Corresponding data
28 downstream of the confluence were available at Overton. The event features a single pulse in the main
29 channel starting from a baseflow of approximately 300 cfs rising to a peak of about 1,900 cfs and then
30 receding to around 150 cfs. Stability limitations in this portion of the reach prevent modeling of flows
31 less than 400 cfs. The secondary channel carried four pulses originating from the J-2 Return that start
32 from zero flow and rise to peaks between about 1,800 and 3,400 cfs. with essentially no flow in between
33 peaks. Plum Creek contributes a baseflow of about 12 cfs and a peak discharge of approximately 32 cfs.
34 Stability limitations in the secondary channel require a minimum flow of 20 cfs in the channel. The
35 downstream gage at Overton represents the response of the combined upstream inputs.

36
37 Routing of the 2009 input hydrographs through the unsteady model produced hydrographs at Overton
38 gage with a similar translation speed and hydrograph shape (Figure 3.31). Differences between
39 observed and predicted peak discharges for the initial model runs that did not incorporate bank storage
40 were attributed to the effects of bank storage. To improve agreement between the observed and
41 routed hydrographs, a gain/loss hydrograph was developed relating bank storage flow to flow in the
42 channel based on the general form of the relationship outlined by Randle and Samad (2008). When
43 applied independently at each pulse, this method of accounting for the effects of bank storage improved
44 the calibration.

45 *Segment: Overton to Kearney (RM 240 – RM 215)*

46 For the 2009 event, input hydrographs were available at Overton, Spring Creek, Buffalo Creek and Elm
47 Creek. No data were available for flow input from Whiskey Slough and North Dry Creek. A flow



1 diversion hydrograph was also available for the Kearney Diversion. Data from the Odessa and Kearney
2 gages were available for calibration within the model segment. At Overton, four pulses were recorded,
3 starting from a baseflow of approximately 400 cfs and rising to peak discharges between about 2,000
4 and 3,600 cfs. Spring Creek contributed a baseflow of about 20 cfs with a peak discharge of 45 cfs.
5 Buffalo and Elm Creeks enter the system at the same location just upstream from the Kearney Diversion,
6 and added a baseflow of 7 cfs with a peak discharge of 86 cfs. The Kearney Diversion was mostly
7 inactive during the event, but diverted flow between April 22 and 29, 2009, with a peak diversion rate of
8 approximately 300 cfs.

9

10 Similar to the modeled results between Lexington and Overton, predicted translation speeds and
11 general hydrograph shapes for the 2009 event at Odessa matched well with observed data (Figure 3.32).
12 For three of the four pulses, the gage data indicate a reduction in peak discharge in the downstream
13 direction, and these were correctly predicted by the model that included a bank storage hydrograph
14 developed in the manner previously discussed. In the largest pulse, however, the observed data
15 indicate an increase in peak discharge from 3,600 to 4,000 cfs between Overton and Odessa. None of
16 the available data indicate the source of this increase in flow; thus, it is assumed to result from ungaged
17 tributaries or overland flow. A rain event with a total of 0.45 inches of precipitation was recorded in
18 Kearney on April 18, 2009. Between Odessa and Kearney, no reduction in peak discharge is seen for
19 three of the four peaks (Figure 3.33). This is the opposite behavior that was observed upstream
20 between Overton and Odessa (Figure 3.32). A modified version of the bank storage hydrograph was
21 developed to account for the reduction of peak discharge observed in the third peak.

22

23 For the 1998 event, input hydrographs were available at Overton, Spring Creek, Buffalo Creek, Elm
24 Creek, Whiskey Slough and North Dry Creek. Additionally, an outflow hydrograph at Kearney Diversion
25 was also available. The 1998 event was an extended high-flow event with a single large pulse starting at
26 a baseflow of about 1,000 cfs and increasing to approximately 5,800 cfs over the course of about 16
27 days, followed by a very gradual recession to about 2,000 cfs over about two months. No gain/loss
28 adjustments were made based on the assumption that the large magnitude and extended duration of
29 the event would fill near-river groundwater storage, limiting the tendency for net loss or gain in the
30 main channel flow.

31

32 Model runs show only a general correlation between predicted and gaged data at Odessa (Figure 3.34).
33 Inspection of the gaged data shows multiple increases in discharge at Odessa before a rise in the
34 upstream hydrograph at Overton. This implies that additional flow that is not accounted for in the
35 available data must have entered the system between Overton and Odessa. Precipitation data show
36 two large rain events on March 27 and May 21-22, 1998, during the two events. The very long
37 translation time of the observed flood peak (8 days) over the relatively short 15-mile distance (0.1 ft/s)
38 also appears to be anomalous. By comparison, the 2009 event, which had a peak flow of 4,000 cfs,
39 traveled at a speed of approximately 2 ft/s. Between April 15 and 22, 1998, the rate of decrease in
40 discharge at Odessa is much faster than the measured rate in the next upstream reach above Overton
41 that is not explained by the available data. The relatively short length of this reach (15 miles) and
42 confined nature of the channel makes it is unlikely that flow was naturally stored and returned into the
43 system at the indicated rate. In the next downstream reach (Odessa to Kearney), the gage data indicate
44 a large drop in discharge at Kearney while the inflow is increasing (Figure 3.35). Overall, approximately
45 315 cfs is lost during the period between March 16 and May 28, 1998. Given this anomalous behavior in
46 the observed hydrographs, calibration of the model to the observed flows is not possible.

47



1 The 2010 data for this segment were limited to gage data at Overton and Kearney. No data were
2 available for Spring Creek, Buffalo Creek, Elm Creek, Kearney Diversion, Whiskey Slough or North Dry
3 Creek. The event has a single pulse starting from a baseflow of approximately 2,000 cfs and rising to
4 7,000 cfs. After approximately two weeks, the discharge recedes back to about 2,500 cfs. Model
5 results show general agreement with observed timing and translation speed of the pulse (Figure 3.36).
6 No bank storage adjustment was made due to the large magnitude and extended duration of this event.
7 Gage data at Kearney indicate a small general loss in flow of about 200 cfs between Overton and
8 Kearney until the pulse begins to rise. For the 2-week period between June 15 and 28, 2010, when the
9 maximum flow occurs, an increase in flow of approximately 1,000 cfs is measured between these two
10 gages. As the pulse recedes, the flow increase is reduced somewhat but maintains at a gain of about
11 500 cfs. Precipitation data show several large events between Lexington and Grand Island, which may
12 be the source of the observed increase. Similar to the results from the 1998 event, ungaged inflows
13 were not incorporated into the model because the specific source of the flow cannot be identified from
14 the available data.

15 ***Segment: Kearney to Chapman (RM 215 – RM 154)***

16 For the 2009 event, input hydrographs were available at the Kearney gage and the Kearney Power
17 Return. No input data were available for the Fort Kearney Slough or Downstream Drain near Newark.
18 Gage records at Grand Island were available for calibration. This event is a continuation of the four
19 upstream pulses that start at a baseflow of approximately 600 cfs and rise to peak discharges between
20 1,700 and 3,400 cfs. Historical analysis indicates a gain of approximately 105 cfs between Kearney and
21 Grand Island. Routing the 2009 event shows behavior similar to the upstream reaches between Overton
22 and Odessa, with peak discharges decreasing for three of the four smaller pulses (Figure 3.37).
23 Accounting for bank storage as before, increases the correlation between measured and predicted
24 discharges for these pulses. In this reach, the bank storage hydrographs incorporated a baseflow of 200
25 cfs, which appears to be consistently gained throughout the entire event. As seen upstream at Odessa,
26 the large pulse increases to a peak discharge that exceeds the modeled inputs by approximately 100 cfs,
27 indicating the presence of unknown contributing sources. Significant inflow may have been delivered by
28 the Fort Kearney Slough and Downstream Drain tributaries or other sources as a result of a rainfall event
29 on April 18, 2009.

30
31 For the 1998 event, input data were available for the Fort Kearney Slough and Downstream Drain, in
32 addition to the gages at Kearney, Grand Island and the Kearney Power Return. The input flood pulse
33 starts at approximately 1,500 cfs and rises to around 4,700 cfs for about 11 days before gradually
34 receding to about 1,600 cfs over a period of about 45 days (Figure 3.38). As with previous segments for
35 this flow event, bank storage effects were assumed to be insignificant due to the long duration. The
36 measured hydrograph at Grand Island had significantly higher flows than were measured upstream,
37 indicating significant flow contribution from unknown sources along the reach. Significant rain events
38 on March 27 and May 21-22, 1998 may explain the increase.

39
40 The 2010 data for this segment were limited to gage data at Kearney and Grand Island. No data were
41 available for Fort Kearney Slough, the Kearney Power Return or Downstream Drain near Newark. The
42 flood pulse for this event starts at a baseflow of approximately 2,000 cfs and peaks at about 8,000 cfs
43 that is generally sustained for about 12 days before receding back to about 2,400 cfs. As before, no
44 bank storage hydrograph was developed for this event due to the long duration. Gage data indicate a
45 general gain of about 400 cfs prior to the rising limb, with no gain after the sustained peak. Unlike
46 observations in the upstream reaches, there does not appear to be significant ungaged inflow during the
47 duration of the peak discharge. Modeled results generally correspond to the timing and shape of the
48 gaged hydrograph at Grand Island (Figure 3.39).



1 *General Note on Model Stability*

2 Model stability was a significant and continual issue in the development of the unsteady model. All
3 calibration runs were successfully executed with a minimal number of computational warnings. As
4 noted in the HEC-RAS User's Manual (USACE, 2010), unsteady-flow results are, by definition,
5 approximations, and accuracy and stability become more difficult to achieve as model complexity
6 increases. The development process detailed above focused primarily on finalizing the geometric
7 parameters that best characterize the routing behavior of the river system for the hydrographs that
8 were available for calibration. Because the routing behavior can change with differing antecedent and
9 vegetation conditions and the magnitude and duration of the flows, it may be necessary to adjust these
10 parameters in future model runs. The hydrologic inputs and computational parameters specified by the
11 user can significantly affect the stability of the model runs. USACE (2010) provides guidance for
12 adjustment of input values, including computational time steps, Theta weighting factor, water-surface
13 calculation tolerances and maximum number of iterations that can improve stability and accuracy for a
14 specific set of hydrologic input conditions.

15 *Sensitivity Analyses*

16 Sensitivity to roughness parameters was examined to determine how adjusting roughness, both globally
17 and for phragmites, would impact hydrograph timing and attenuation. A series of simulations were
18 executed to examine the response of model results to a change in the Manning's roughness coefficients.
19 Globally, Manning's roughness coefficients were increased 20% (high roughness), and decreased 20%
20 (low roughness) from calibrated Manning' roughness coefficients to analyze sensitivity to making a
21 global proportional shift. Next, the Manning's roughness coefficient assigned to phragmites was
22 changed from 0.101 to 0.051 and 0.151 to demonstrate how a change in phragmites growth might
23 impact model results. In each of these sensitivity analysis simulations, a simplified short duration high
24 flow hydrograph was used. The simplified short duration high flow inflow hydrograph at the Tri-County
25 Diversion had the same starting and ending times as the 2009 event, and linear rising and falling limbs.
26 The pulse peaks at 1,700 cfs, a duration that is sustained for 3 days and 9 hours (same peak and duration
27 of the 2009 event). Bank storage effects were neglected for these simulations, to allow for a clear,
28 direct comparison of the impact of roughness on the timing and attenuation of a short duration high-
29 flow event. The use of this idealized hydrograph allows for a direct comparison that is not interfered by
30 any hydrograph irregularities.

31 *Global Roughness Sensitivity*

32 From the Tri-County Diversion to Maxwell, very little change can be seen in the hydrograph, from visual
33 inspection. The simulation with the high Manning's roughness coefficient arrives (2% of the difference
34 between base and max) about a half hour after the base condition, and the low roughness simulation
35 arrives about a half hour earlier. The peak duration of these events are all roughly the same, varying no
36 more than a half an hour. At Brady, the peak of the of the high roughness run arrives 2 hours later than
37 the base condition, and the low roughness coefficient simulation roughly 1.5 hours earlier. The peak
38 durations of the base, high roughness, and low roughness at Brady are 78.5 hours, 79.5 hours, and 77.5
39 hours, respectively. At the Cozad gage, the high roughness hydrograph peak arrives 4 hours later than
40 the base condition, and the reduced roughness hydrograph arrives at its peak 3.5 hours earlier than the
41 base condition. The peak duration of the base, high roughness, and low roughness runs decrease at this
42 point to 72.5 hours, 70.5 hours, and 76.5 hours, respectively. Near Lexington, the spread between the
43 base condition and high roughness has increased to 4.5 hours, and the low roughness simulation now
44 models the hydrograph peak arriving 5 hours before the base roughness condition. The peak duration
45 for the base, high, and low roughness sensitivity simulations at Lexington are 69.5 hours, 67 hours, and
46 75 hours, respectively. Results are shown in Table 3.3 and Figures 3.40-3.43.



1 Predicted results downstream from Lexington continue the trend observed upstream of increasing
2 travel time and decreasing pulse duration with increasing roughness (Table 3.2). The results also
3 indicate very little attenuation of the maximum discharge with increasing roughness for this hydrograph.
4 Although at first counter-intuitive, the reduction in duration of the approximately steady, maximum
5 flows in the pulse appears to result from slowing of the rising limb which tends to shift flow volume from
6 the steady maximum portion of the hydrograph back into the rising limb. At Overton, 15 miles
7 downstream from Lexington, the low roughness hydrograph arrived approximately 6 hours before the
8 base roughness hydrograph and 12 hours before the high roughness hydrograph (Figure 3.44). Peak
9 duration for the low roughness was unchanged at about 3 days, with the base and high roughness
10 results continued to decline to approximately 2.8 and 2.6 days. Fifteen miles downstream at Odessa,
11 the low roughness hydrograph arrived about 9 hours before the base roughness hydrograph and 18
12 hours before the high roughness hydrograph (Figure 3.45). Peak duration for the low roughness
13 scenario declined to 2.9 days and the base and high roughness declined to approximately 2.7 and 2.5
14 days, respectively. Nine miles downstream at Kearney, the low roughness hydrograph arrived about 12
15 hours before the base roughness hydrograph and 24 hours before the high roughness hydrograph
16 (Figure 3.46). Peak duration times were not significantly different from those predicted upstream at
17 Odessa. Forty-seven miles downstream at Grand Island, the low roughness hydrograph arrived about
18 16.5 hours before the base roughness hydrograph and 31 hours before the high roughness hydrograph
19 (Figure 3.47). Peak duration for the low roughness scenario declined to 2.7 days and the base and high
20 roughness declined to approximately 2.4 and 2.2 days, respectively. Twelve miles downstream at
21 Chapman, the low roughness hydrograph arrived about 16.5 hours before the base roughness
22 hydrograph and 31 hours before the high roughness hydrograph (Figure 3.48). Peak duration times
23 were not significantly different from those predicted upstream at Grand Island.

24

25 As expected, lowering the overall roughness values in the model results in faster propagation of the
26 pulse, with less attenuation of the rising and falling limbs and a longer duration of the maximum
27 discharge (Table 3.3). Correspondingly, slower propagation and more attenuation is seen with higher
28 roughness values. No change in peak discharge is seen because the original pulse is sufficiently long to
29 overcome the storage effects of rising stage at higher flows. The celerity (wave speed) through the
30 overall reach from Lexington to Chapman with the base roughness is approximately 2.1 fps, increasing
31 to 2.6 fps for the lower roughness value and decreasing to 1.8 fps for the higher roughness value.

32 Phragmites Sensitivity

33 Above Lexington, land use coverages show limited phragmites near the Platte River, and none above RM
34 283. Changes to the phragmites roughness coefficient had little effect on the timing and attenuation of
35 the pulse through the first 56 miles of the model. The pulse peak (98% of the difference) of the two
36 extremes arrived at Lexington within an hour of the base condition, and had peak durations within a half
37 hour of the base condition. Downstream of Lexington, the model again demonstrated little sensitivity to
38 the roughness values associated with phragmites. The most dramatic change occurred at the most
39 downstream location, where the arrival time of the hydrographs at Chapman are offset about 3 hours
40 before and 3 hours after the base hydrographs for the low and high roughness values, respectively, and
41 approximately 2 percent change in travel time. Unlike the response to the changes in generalized
42 roughness described in the previous section, varying the roughness value used for the phragmites
43 resulted in an insignificant change in the predicted hydrographs. Results at Lexington are shown in
44 Figure 3.49.



1 Table 3.3: Summary of Global Manning's Roughness Coefficient sensitivity

Location	River Mile	Pulse Travel Time		Pulse Celerity (fps)			Duration at Peak (days)		
		(hours offset from base condition)		Low Roughness	Base Roughness	High Roughness	Low Roughness	Base Roughness	High Roughness
		Low Roughness	High Roughness						
Maxwell	301	-0.5	+0.5	2.9	2.6	2.4	3.4	3.3	3.3
Brady	292	-1.5	+2.0	2.9	2.4	2.1	3.3	3.3	3.2
Cozad	267	-3.5	+4.0	4.1	3.3	2.8	3.2	3.0	2.9
Lexington	254	-5.0	+4.5	4.2	3.5	2.9	3.1	2.9	2.8
Overton	239	-7.0	+6	2.7	2.0	2.1	3.0	3.0	2.8
Odessa	224	-9.0	+10	2.0	1.7	1.3	2.9	2.9	2.7
Kearney	215	-9.5	+9	2.5	1.9	2.2	2.9	2.8	2.7
Grand Island	168	-13.5	+15	2.6	2.2	1.9	2.7	2.7	2.5
Chapman	156	-16.0	+15	4.7	5.0	2.6	2.7	2.9	2.5



1 **Bank Storage Prediction Tool**

2 ***Hydrograph Routing Prediction***

3 The routing characteristics of the reach during short-duration, high-flow releases appear to be strongly
4 affected by the gains and losses in flow associated with bank storage. The HEC-RAS software includes a
5 relatively simple algorithm based on Darcy's Law that is intended to provide a means of accounting for
6 the interaction between the surface and groundwater along the reach. The study team initially believed
7 that this algorithm could be used for this project. Extensive testing early in the model development
8 phase, however, demonstrated that the controlling processes in the study reach of the Platte River
9 cannot be adequately accounted for using this simple algorithm, primarily because the level of the near-
10 river groundwater table varies with time during the passage of the hydrograph, and the HEC-RAS
11 software only allows the user to specify a constant groundwater table. After evaluating a range of
12 potential methods for accounting for the groundwater interaction, it was determined that the most
13 practical approach is to model the process implicitly by applying a boundary condition hydrograph that
14 approximates the flow out of and back into the flows in the river following the general form of the
15 relationship suggested by Randle and Samad (2008). As discussed above, distributed hydrographs
16 representing the flow losses and gains from bank storage that had the same general shape as the Randle
17 and Samad (2008) hydrographs were developed during model calibration for the 2009 event. The
18 hydrographs were then used as the basis to develop an empirical relationship between the input
19 hydrograph and the parameters that define the specific hydrograph shape. The conceptual bank
20 storage hydrographs are defined by four magnitude parameters (Q_a , Q_c , k_1 and k_2) and four timing
21 parameters (T_o , T_a , T_b and T_c) (Figure 3.50). A series of rating curves were developed for the reaches
22 bounded by the available gages, except for the reach between Grand Island and Chapman for which no
23 suitable data were available, that relate channel discharge to the average stage in the reach (Figure
24 3.51). The values of these parameters were selected based on the set of values that best matched the
25 observed behavior of the 2009 hydrograph in each reach (Table 3.4). The selected coefficients reflect
26 the transmissivity of the bank material and are assumed to be constant for a given antecedent
27 condition. The timing parameters were then related to the corresponding points in the input
28 hydrograph (T_{rise} , T_{peak} , T_{fall} and T_{base}) by the following relationships:
29

$$T_o = (A + T_{rise})$$

$$T_a = T_o + B * (T_{peak} - T_{rise})$$

$$T_b = A + T_{fall} + C * (T_{fall} - T_{base})$$

$$T_c = A + T_{fall} + D * (T_{fall} - T_{base})$$

30

31

1 Table 3.4: Bank storage parameter values that best matched the observed behavior of the 2009
2 hydrograph in each reach.*

Reach	k1	k2	A	B	C	D
NP to Maxwell	-6.500	-1.230	0.208	0.021	0.125	0.021
Maxwell to Brady	-6.500	-1.230	0.438	0.718	0.165	0.089
Brady to Cozad	-1.750	-0.870	0.229	1.000	0.065	0.230
Cozad to Lexington	-0.500	-0.080	0.292	0.500	0.082	0.149
Lexington to Overton	-0.158	-1.500	0.240	0.660	0.030	0.090
J-2 Return	-0.158	-1.500	0.100	0.250	0.030	0.100
Overton to Odessa	-0.158	-1.500	0.260	0.820	0.230	0.400
Odessa to Kearney	-0.060	-1.500	0.260	0.710	0.090	0.270
Kearney to Grand Island	-0.267	-0.811	0.750	0.730	0.090	0.200

*See text for explanation.

3

4 *Bank Storage Hydrograph Prediction Tool*

5 A spreadsheet was compiled to apply the above relationships to enable the user to develop the
6 distributed hydrographs necessary to model future scenarios and further refine the empirical
7 relationships as necessary. The Excel file consists of eight spreadsheets corresponding to the segment of
8 the model between successive gages. Each sheet contains a series of color-coded cells that contain the
9 information necessary to calculate an approximate bank storage hydrograph for each reach (Figure
10 3.52). The yellow cells define the averaged stage-discharge relationship for each reach. These cells are
11 fixed geometric characteristics of the reach and should not be changed unless additional bathymetry
12 and steady-state modeling indicates that the relationship should be updated. These cells have been
13 locked in the current version of the tool. Grey cells indicate values determined from empirical analysis
14 of the available calibration data, including the decay coefficients k1 and k2, the hydrograph timing
15 variables To, Ta, Tb and Tc as well as the two rating curves defining the relationships between the
16 magnitudes of Qa and Qc and change in river stage. Though not intended to vary, these values may be
17 refined as more data become available, and are therefore, not locked in the current version of the tool.
18 Additionally, a threshold discharge can be defined below which bank storage does not occur. Orange
19 cells represent user input for the upstream boundary condition hydrograph, as well as the timing
20 parameters Tr, Tp, Tf and Tb. Once the inputs are entered, the user clicks the “Execute” button and the
21 calculated results will be written in the red cells. The hydrograph produced by the Excel file represents
22 an estimation of the total flow of water into and out of the banks within each reach. This hydrograph
23 can be distributed across the various subreaches within the reach by applying a percentage of the total
24 flow into each of the uniform lateral inflow boundary conditions as indicated in the HEC-RAS flow file.

25 *Empirical Relationship Adjustment*

26 At the time this report, calibration data were limited to only the 2009 event. While the empirical
27 parameters developed for this study are believed to be reasonable, the groundwater interaction
28 behavior of the reach will likely vary with the specific hydrograph and antecedent conditions. As
29 additional calibration data become available, particularly in the range of the anticipated SDHF’s, these
30 parameters should be checked and adjusted, as appropriate. The decay coefficients, k1 and k2, are likely
31 affected by antecedent conditions that are wetter or drier than the 2009 event. Under drier conditions,
32 one would expect flow into the bank to decay less quickly because the potential groundwater storage is
33 likely larger.



1 *Pulse Magnitude Sensitivity*

2 A sensitivity analysis was conducted to determine impact the predicted bank storage relationship would
3 have on the pulse shape, timing, and attenuation on pulses of varying flows. Three pulses of the with
4 peak discharges of 1,000 cfs, 1,700 cfs, and 5,000 cfs at the Tri-county diversion were analyzed. At the
5 tri-County Diversion, the respective peak discharge persisted for 3 day and 9 hours.

6
7 From the Tri-County Diversion to Lexington, predicted bank storage effects did not have a great impact
8 on the pulse peak. Considering that a uniform long term gain of over 500 cfs is applied throughout the
9 event, no impact would lead to a peak increase of about 500 cfs from North Platte to Lexington. With
10 this in mind, bank storage limits the pulse magnitude in each case, especially in the 1,700 cfs and 5,000
11 cfs case, but does not greatly diminish the pulse magnitude. Rather, bank storage acts to change the
12 shape of the hydrograph from a trapezoidal shape with defined peak duration, to a hydrograph with
13 more gradual rising and falling limbs. This trend can be expected, since at an abrupt rise in the WSEL,
14 flow into bank storage would be at a high magnitude, removing a volume of water from the rising limb
15 of the hydrograph and returning that most rapidly on a sharp receding limb. Figures 3.53 through 3.55
16 demonstrate pulse magnitude sensitivity to the tool-generated bank storage hydrographs for pulses of
17 1,000 cfs, 1,700 cfs, and 5,000 cfs.

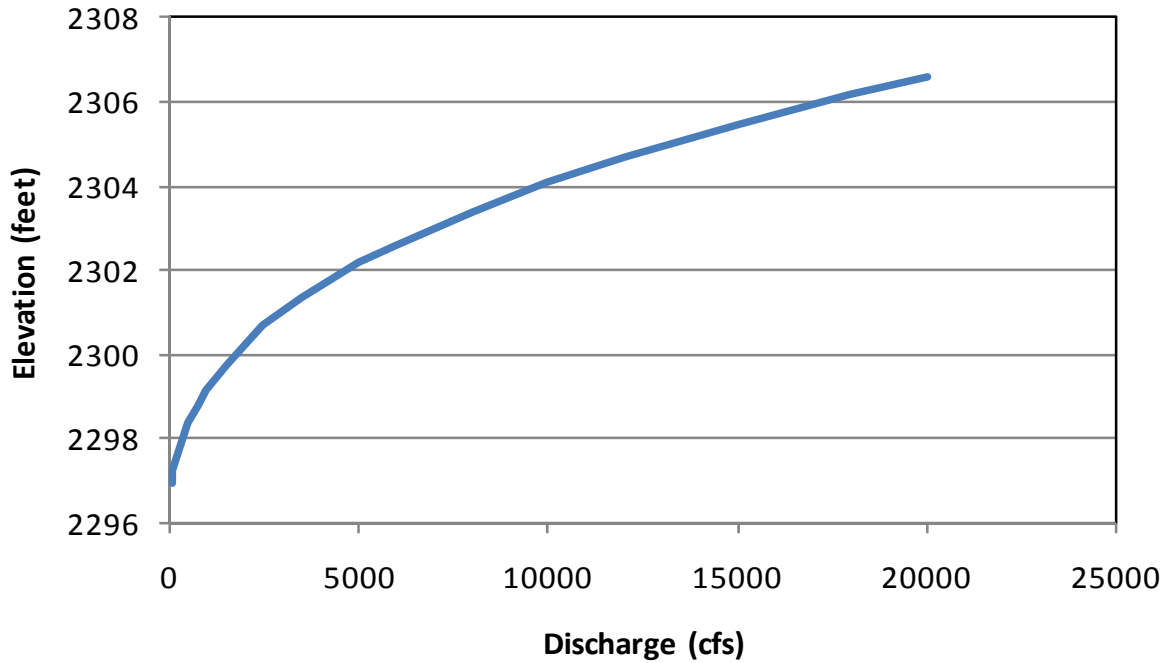
18
19 Figures 3.56 through 3.58 show the continued routing results of the three hydrographs through
20 Lexington, Overton, Odessa and Kearney. As expected, the bank storage hydrographs predicted for the
21 high pulse have the most effect on the peak discharges, decreasing from 5,000 cfs at Overton to about
22 3,400 cfs at Grand Island. Bank storage peak discharge (Q_a) varies between 500 cfs and about 777 cfs.
23 The slope of the rising limb decreases noticeably in the downstream direction, as well. Bank storage
24 hydrographs have less effect on peak discharges for the medium pulse with a total decrease of only
25 about 100 cfs. This is partially due to the 345 cfs total historical gain applied through the system.
26 Additionally, no bank storage hydrograph was applied between Odessa and Kearney because the pulse
27 discharge was below the observed threshold of 2,300 cfs. Interestingly, the small pulse shows
28 effectively no attenuation of peak discharge in the downstream direction, possibly due to the fact that
29 the bank storage hydrograph are essentially countered by the applied historical gain. A noticeable
30 double-hump is seen to build as the pulse passes through Overton and continues downstream. This may
31 be an artifact of the way the bank storage hydrograph is applied, implying that too much water is drawn
32 out on the rising limb. This could be confirmed by measured data from a future release.

33 *Antecedent Condition Sensitivity*

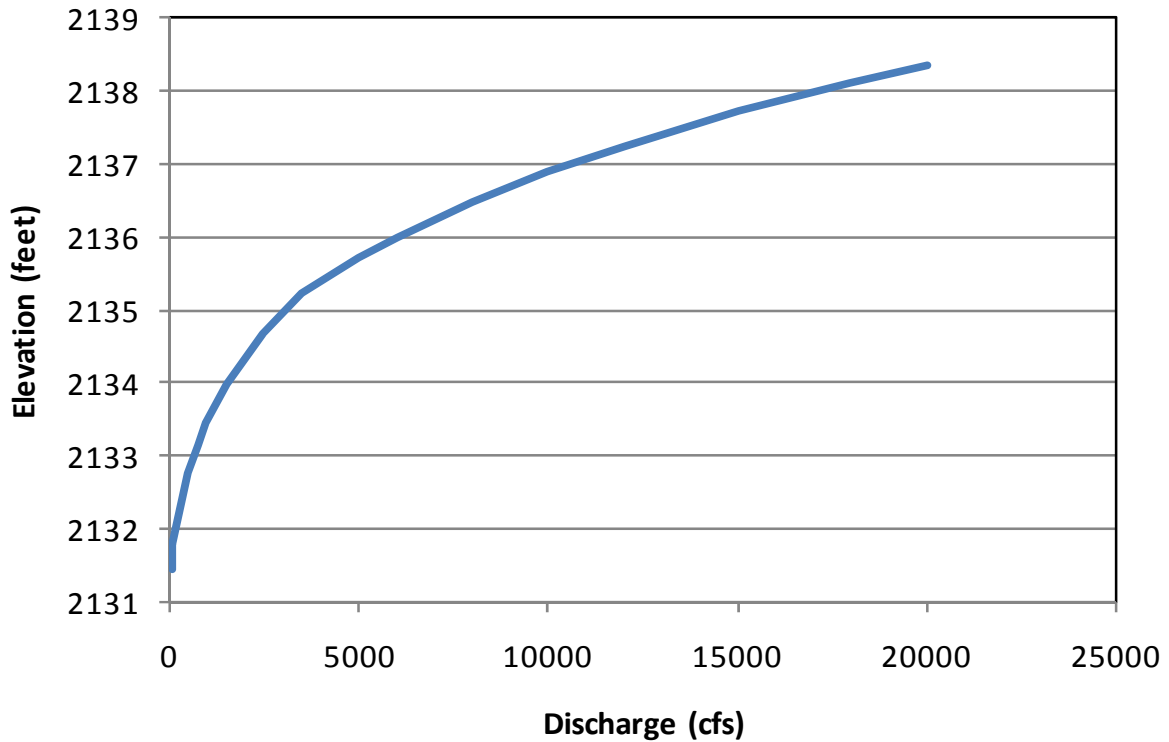
34 Another sensitivity analysis was completed to determine impacts antecedent moisture condition would
35 have on predicted bank storage effects. We expect antecedent moisture conditions affect baseflow
36 levels and the ability for the near bank to store additional water. In terms of the bank storage
37 prediction tool, a change in antecedent moisture condition would change both the head differential
38 (magnitude of the bank storage hydrograph, Q_a and Q_c) and the quickness at which this rate decays (k_1
39 and k_2). To isolate one variable and the sensitivity of predictions to that variable, the decay rates were
40 adjusted to increase and decrease the time between t_a/t_c to the point where this rate decays halfway by
41 50%. This is mathematically equivalent to multiplying the decay constant by 1.5 and 0.67. The higher
42 decay constant represents a wet condition in which flow into the bank is diminishes more quickly than in
43 the 2009 event, and the lower decay constant represents a dry condition in which the bank take a
44 greater volume of water after t_a/t_c than in the 2009 event. This analysis is intended to provide insight as
45 to how adjusting these variables, related to antecedent moisture content, would impact predicted
46 hydrograph attenuation.



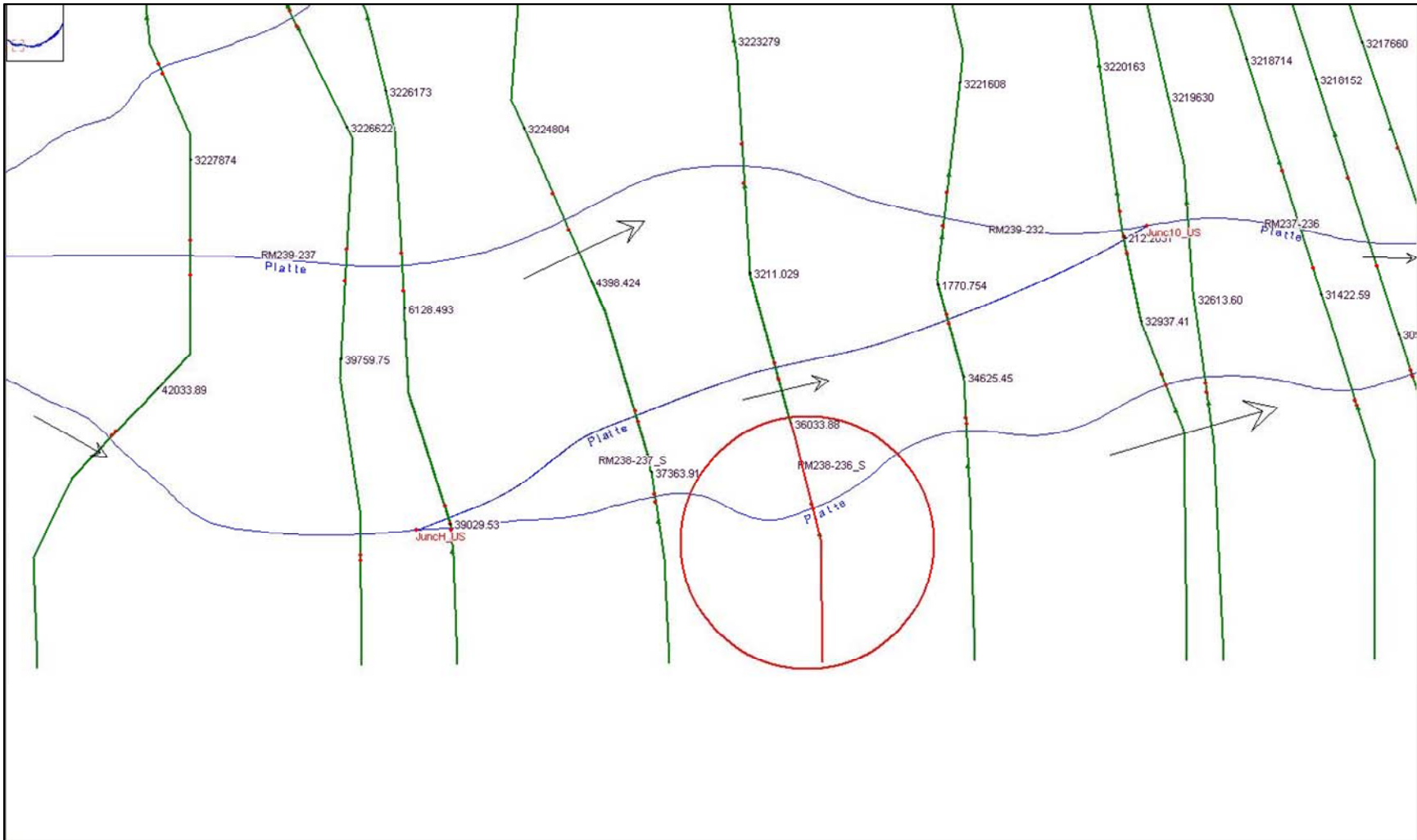
1 Sensitivity to antecedent moisture condition was considered for a short duration high pulse of 1,700 cfs.
2 Antecedent condition, as it is expected to change the bank storage hydrograph, impacts both the change
3 in shape and the peak of the routed hydrograph. The under wet conditions, water lost to bank storage
4 would be limited by the volume capacity of the near bank. Therefore, one can expect less water to
5 enter bank storage, thus impacting the shape and peak of the hydrograph less. Conversely, with dry
6 antecedent conditions, it is expected that more water would enter bank storage, as the capacity would
7 be greater. Since more water would be lost to bank storage, the shape and peak would be dampened.
8 Figures 3.59 through 3.63 depict routed hydrographs under both wet and dry conditions.
9



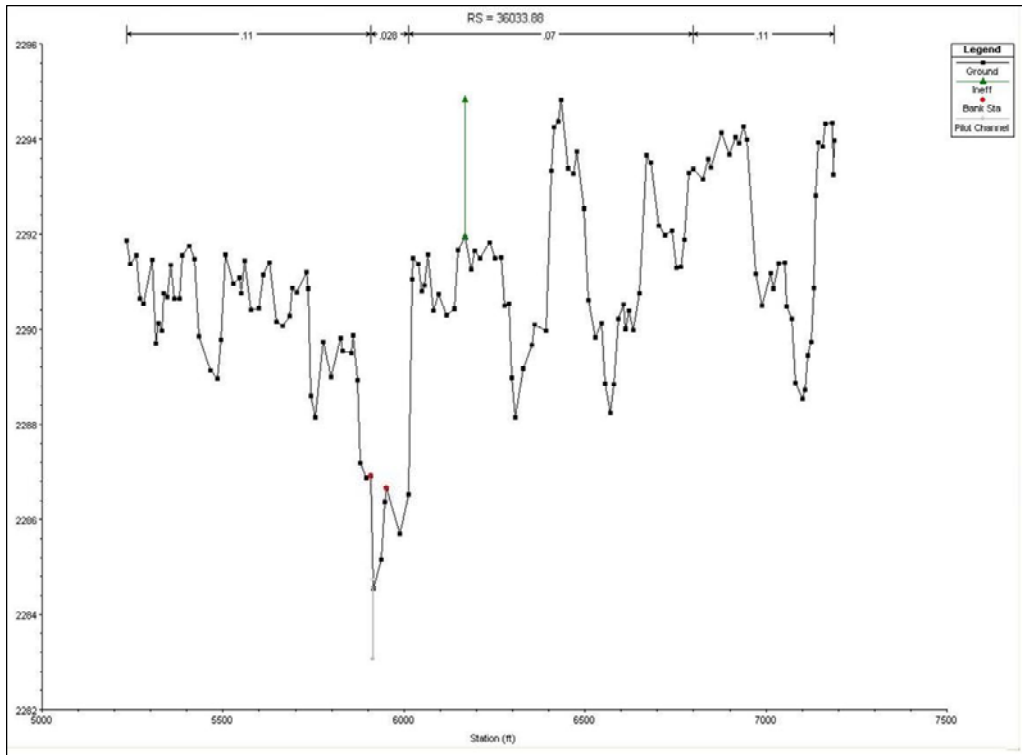
1
2 Figure 3.1: Downstream boundary condition for the Lexington to Overton model.
3



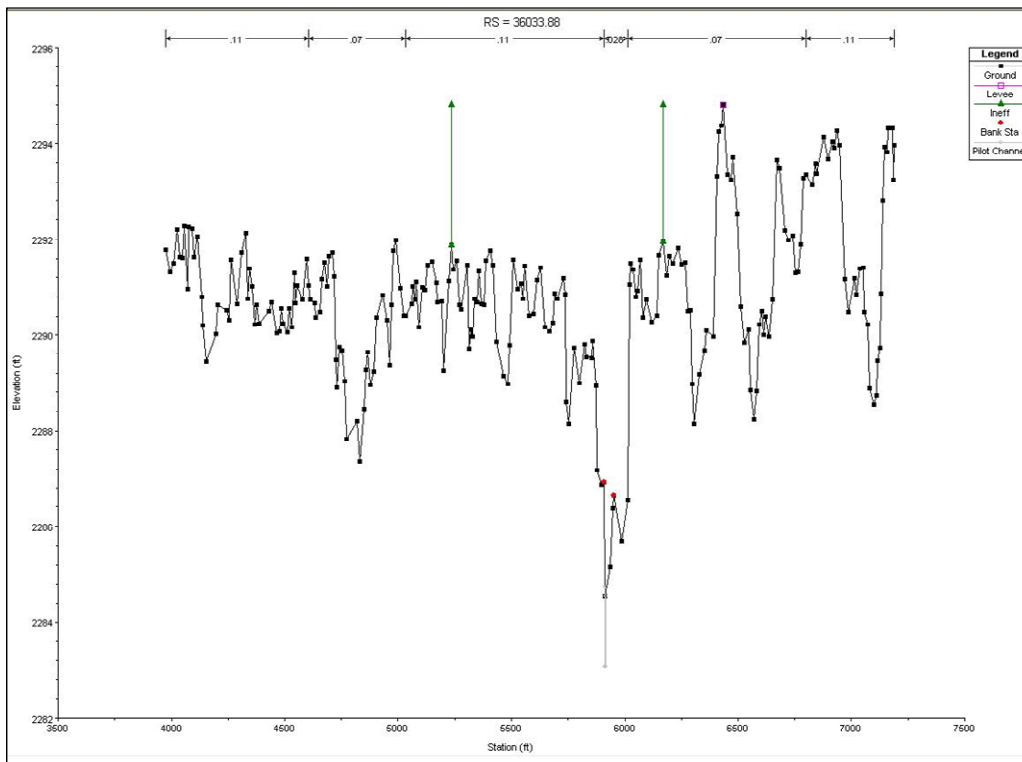
4
5 Figure 3.2: Downstream boundary condition for the Overton to Kearney model



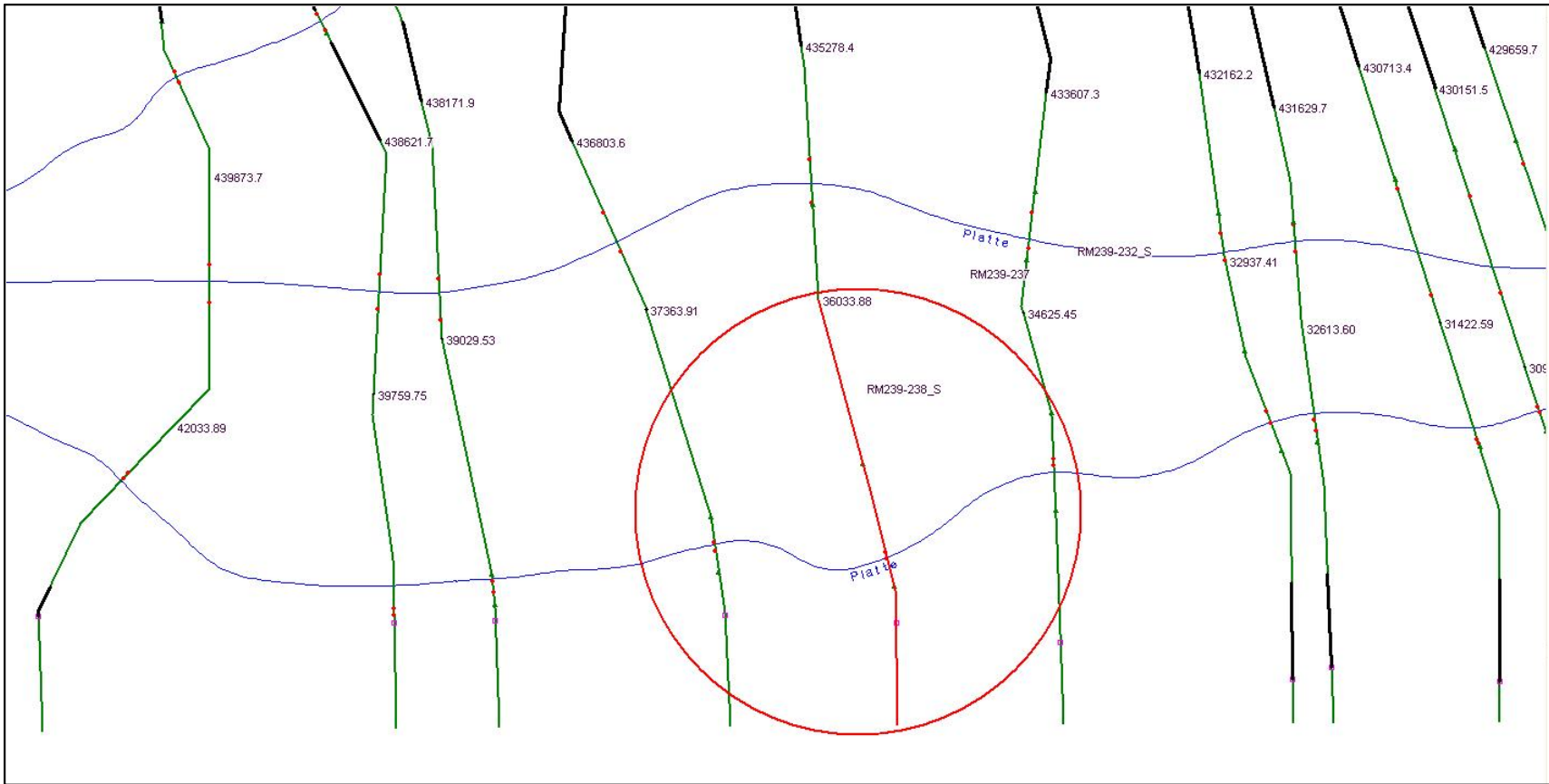
1
2 Figure 3.3: Planview of typical reach with an ineffective secondary channel that acts as a storage area



1
2 Figure 3.4: Plot of primary channel cross-section (highlighted in Figure 3.3) before merge.
3

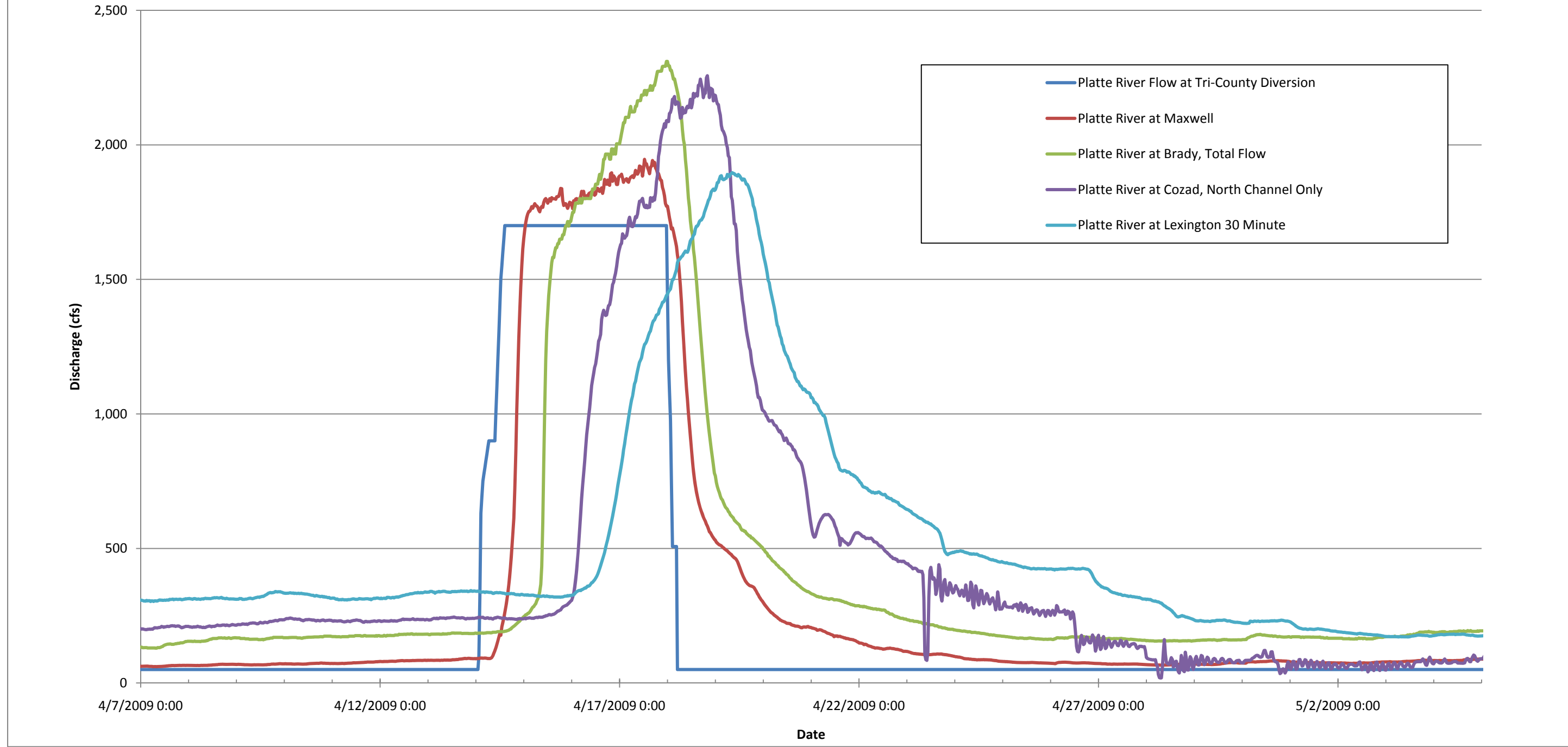


4
5 Figure 3.5: Plot of primary and secondary channel cross section (highlighted in Figure 3.3) after merge.
6 Note, new cross-section information is designated permanently ineffective.



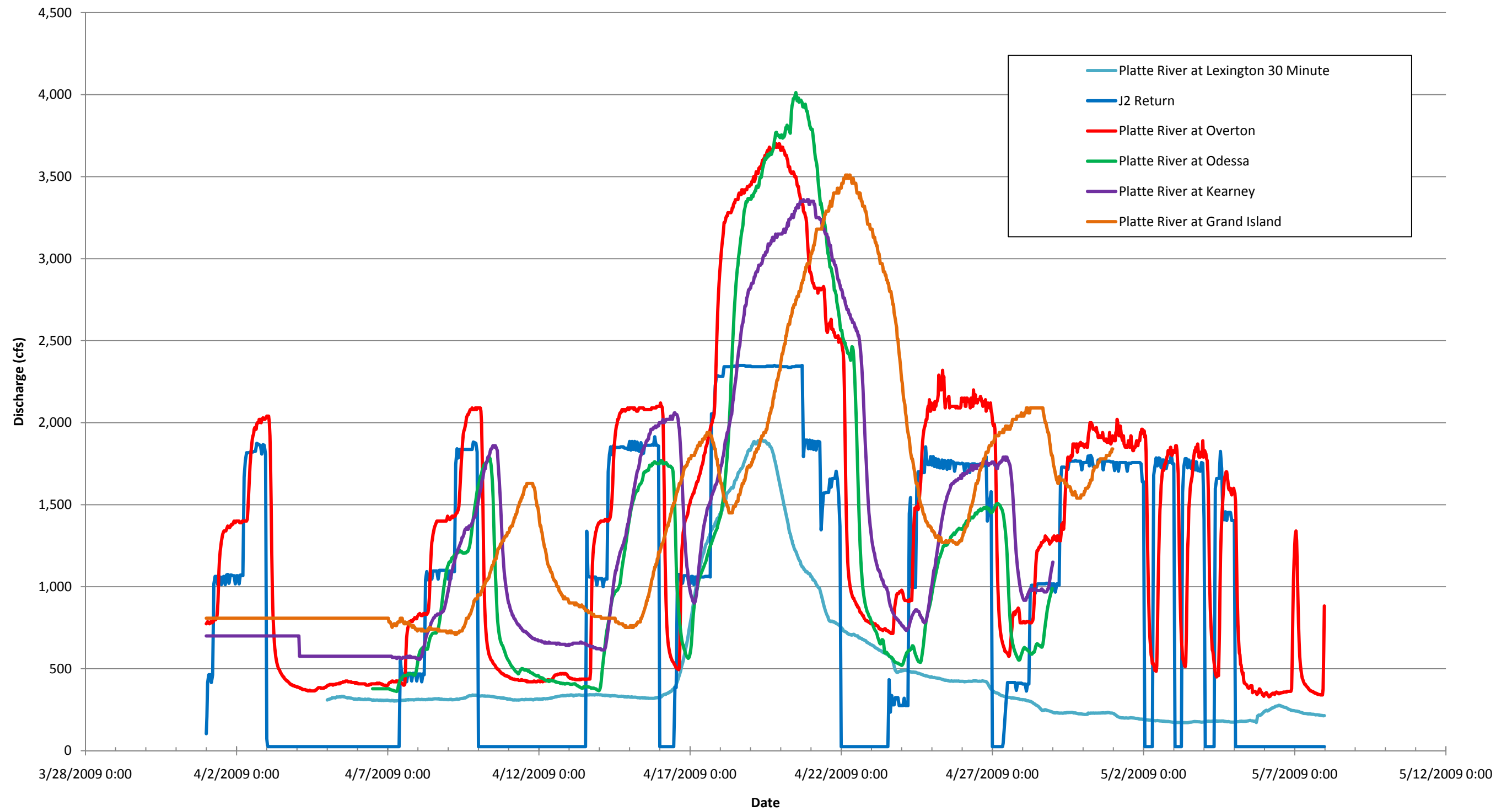
1
2 Figure 3.6: Planview of typical reach with an ineffective secondary channel that acts as a storage area after the merge.
3

April 2009 Event Flow Data- Tri-County Diversion to Lexington

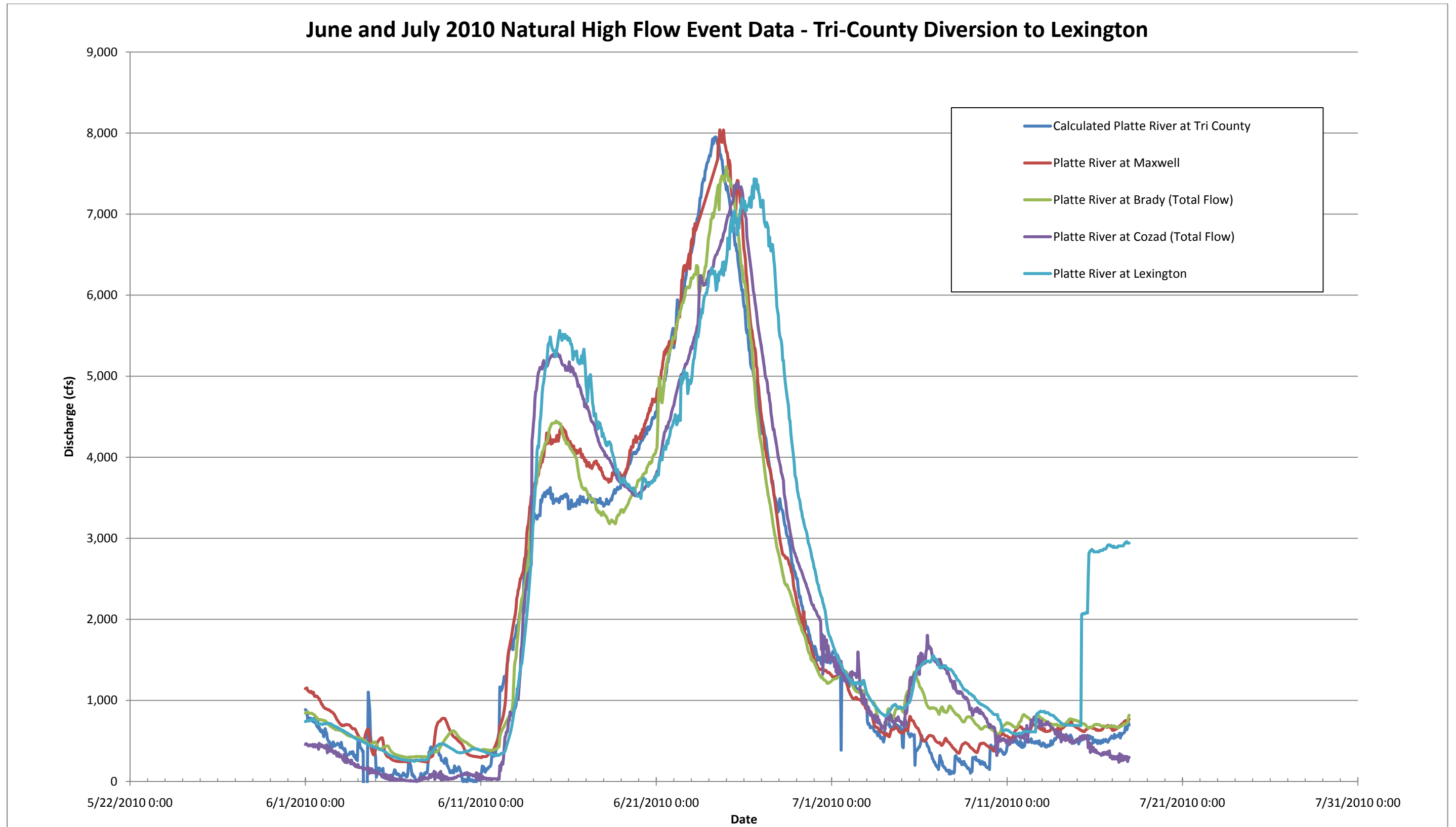


1
2 Figure 3.7: Measured hydrographs from 2009 Event- Tri-County Diversion to Lexington
3

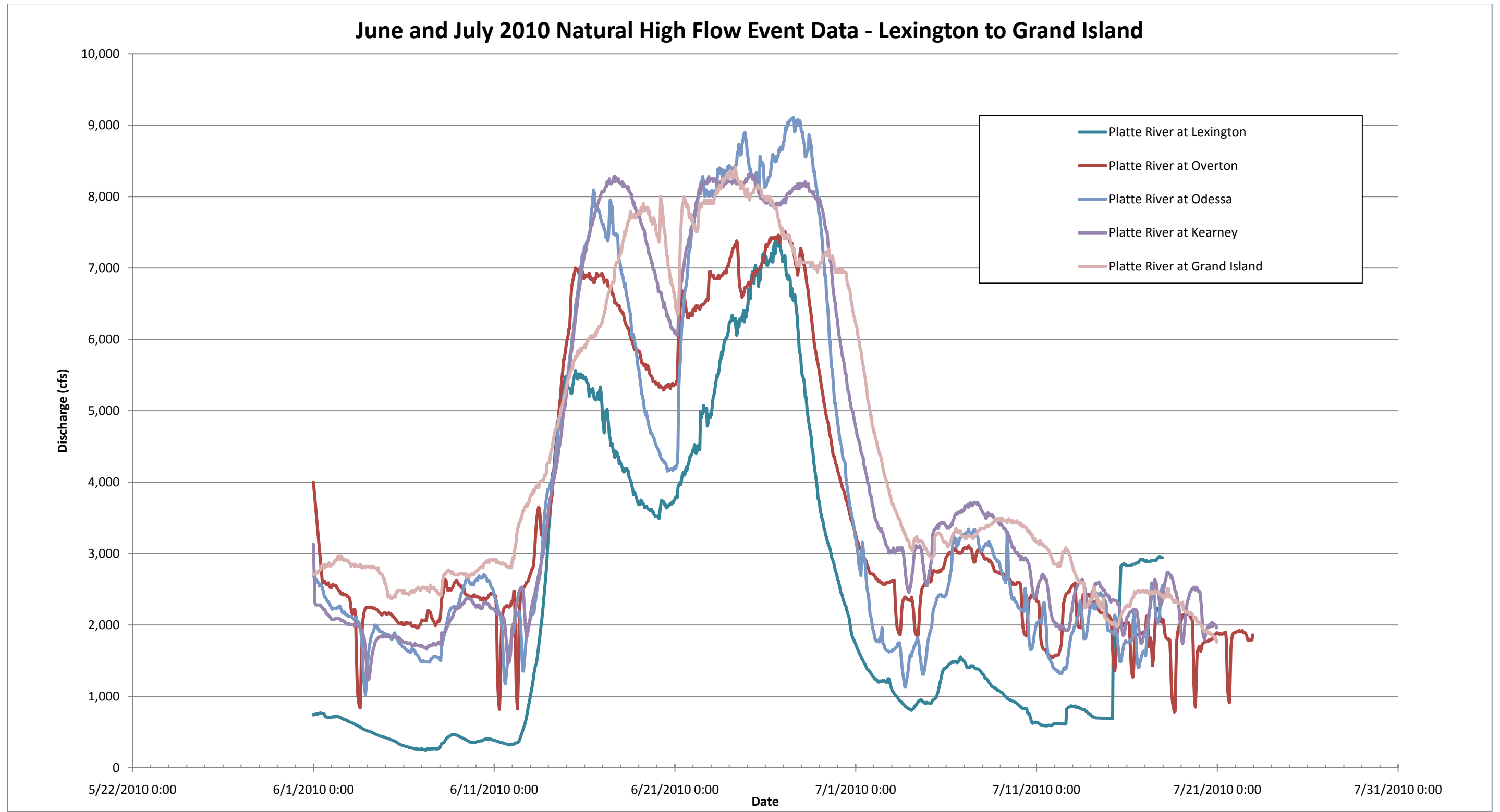
April 2009 Event Flow Data - Lexington to Grand Island



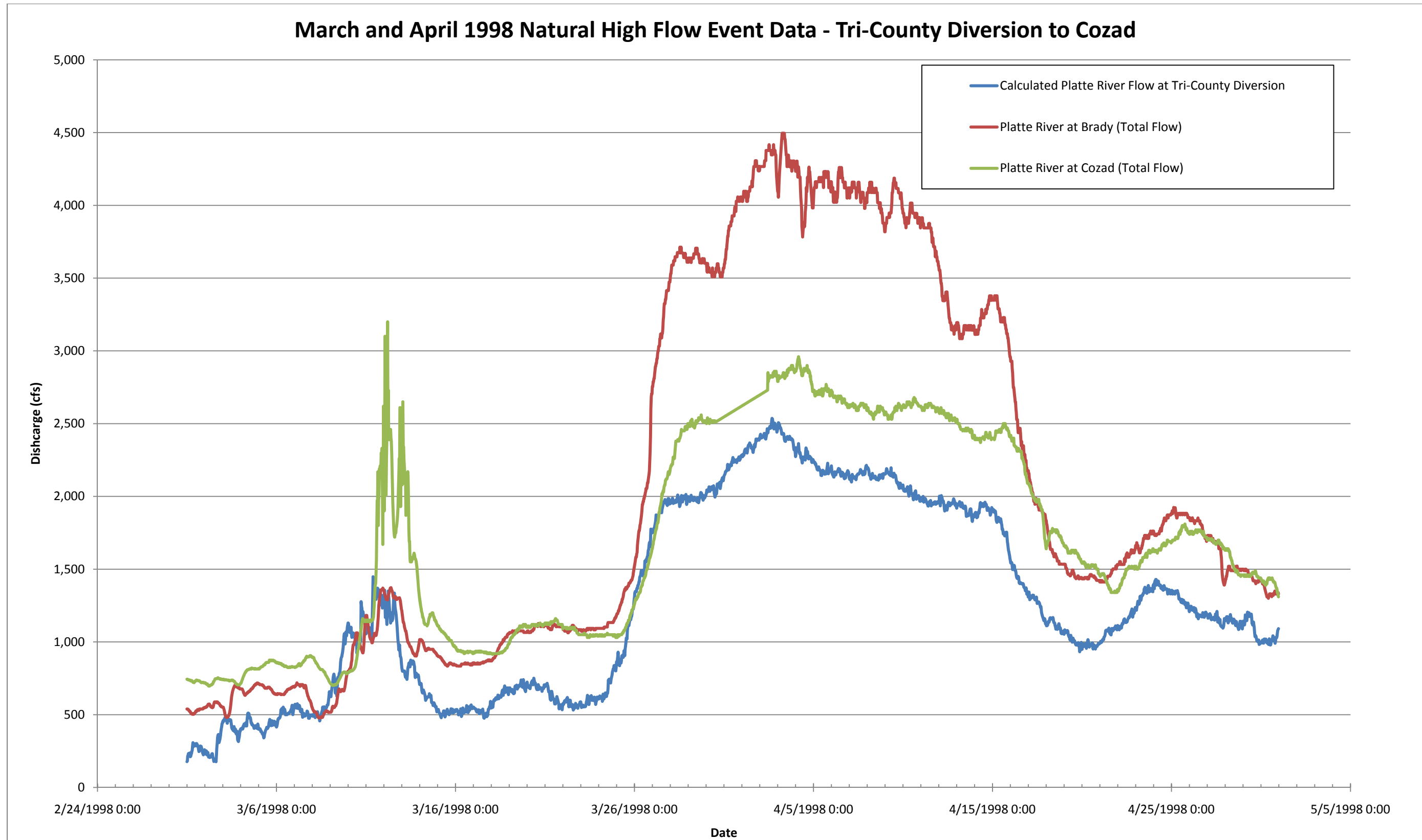
1
2 Figure 3.8: Measured hydrographs from 2009 Event- Lexington to Grand Island
3



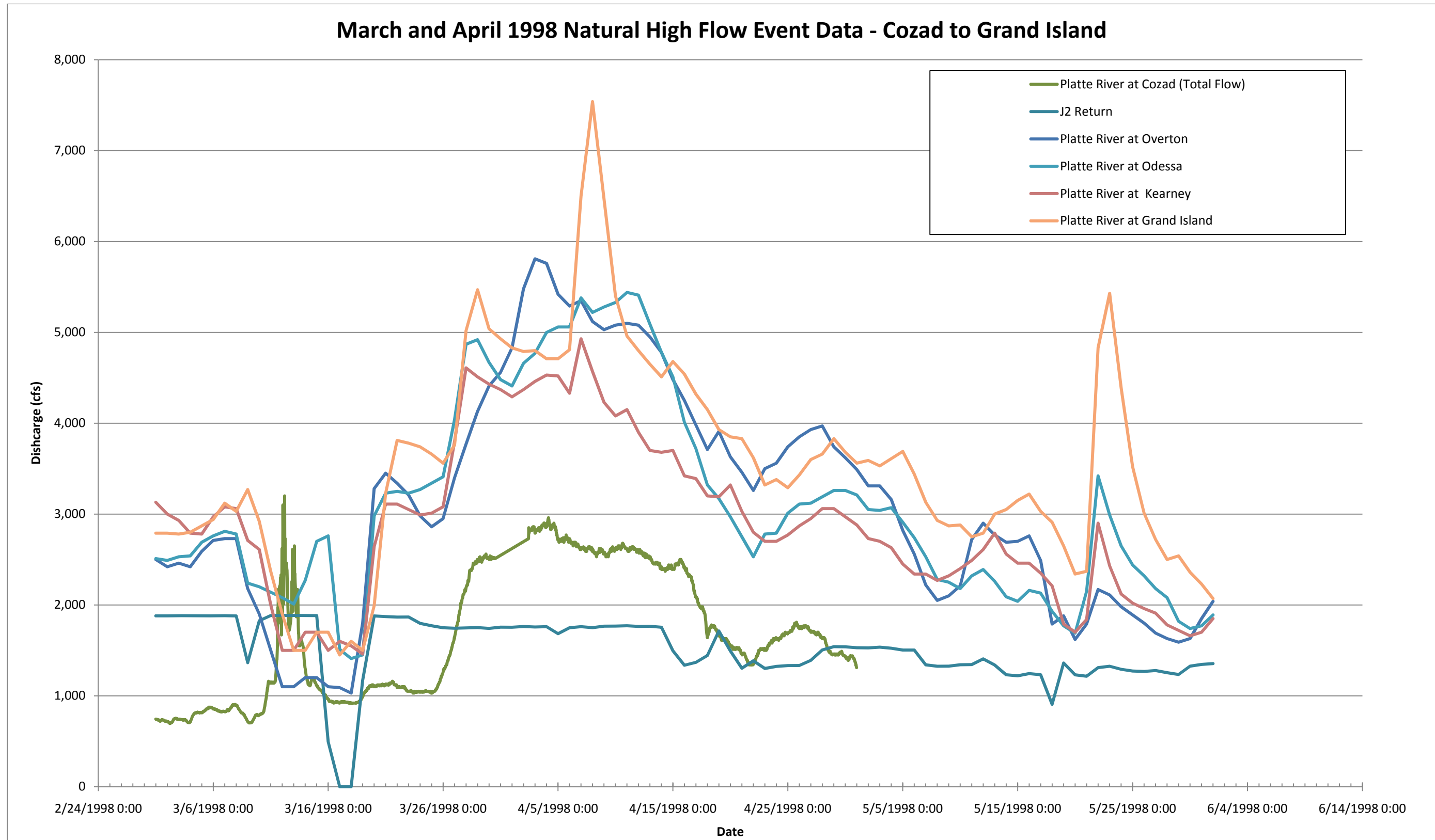
1
2 Figure 3.9: Measured hydrographs from 2010 Event- Tri-County Diversion to Lexington
3



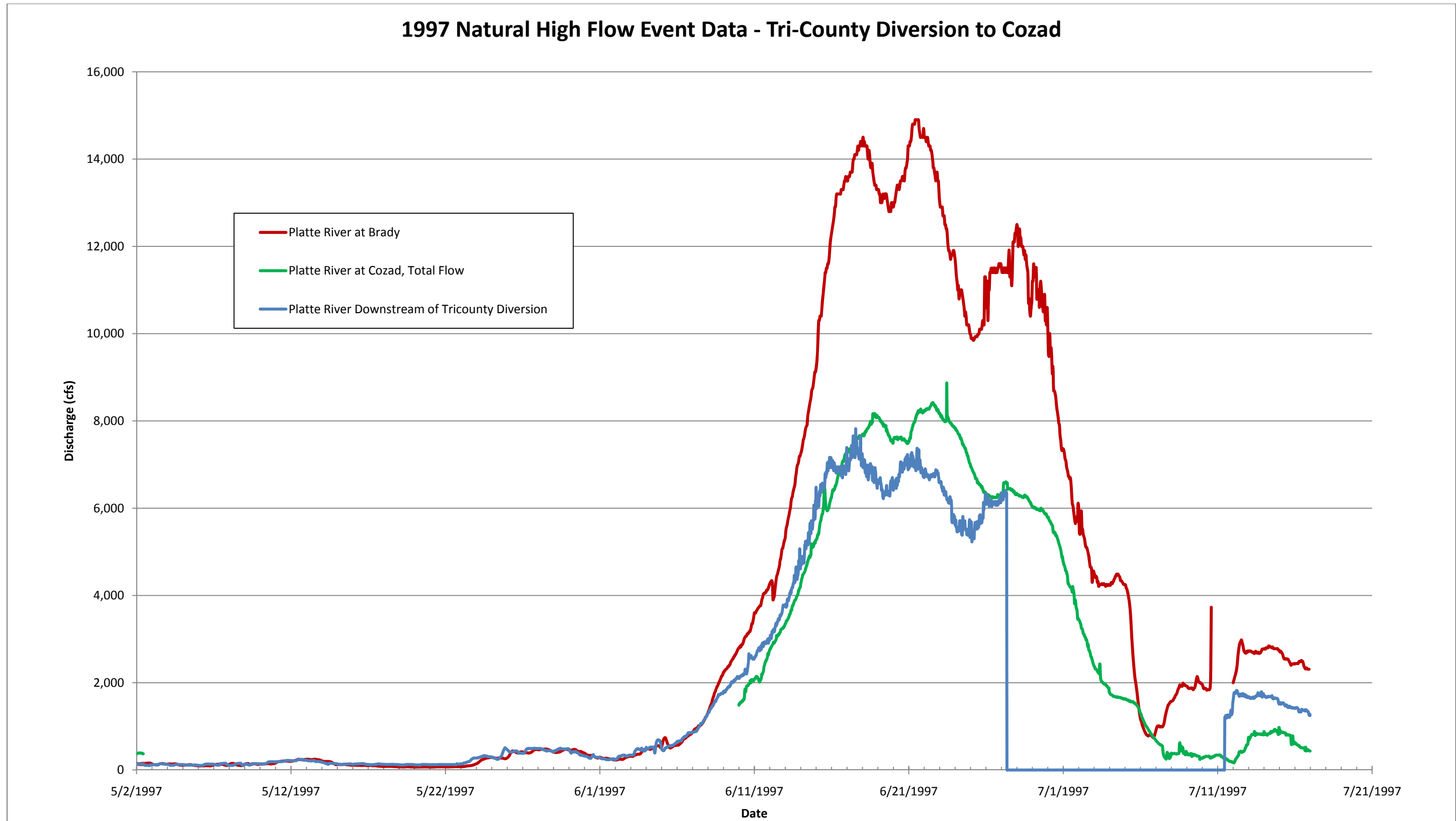
1
2 Figure 3.10: Measured hydrographs from 2010 Event- Lexington to Grand Island
3



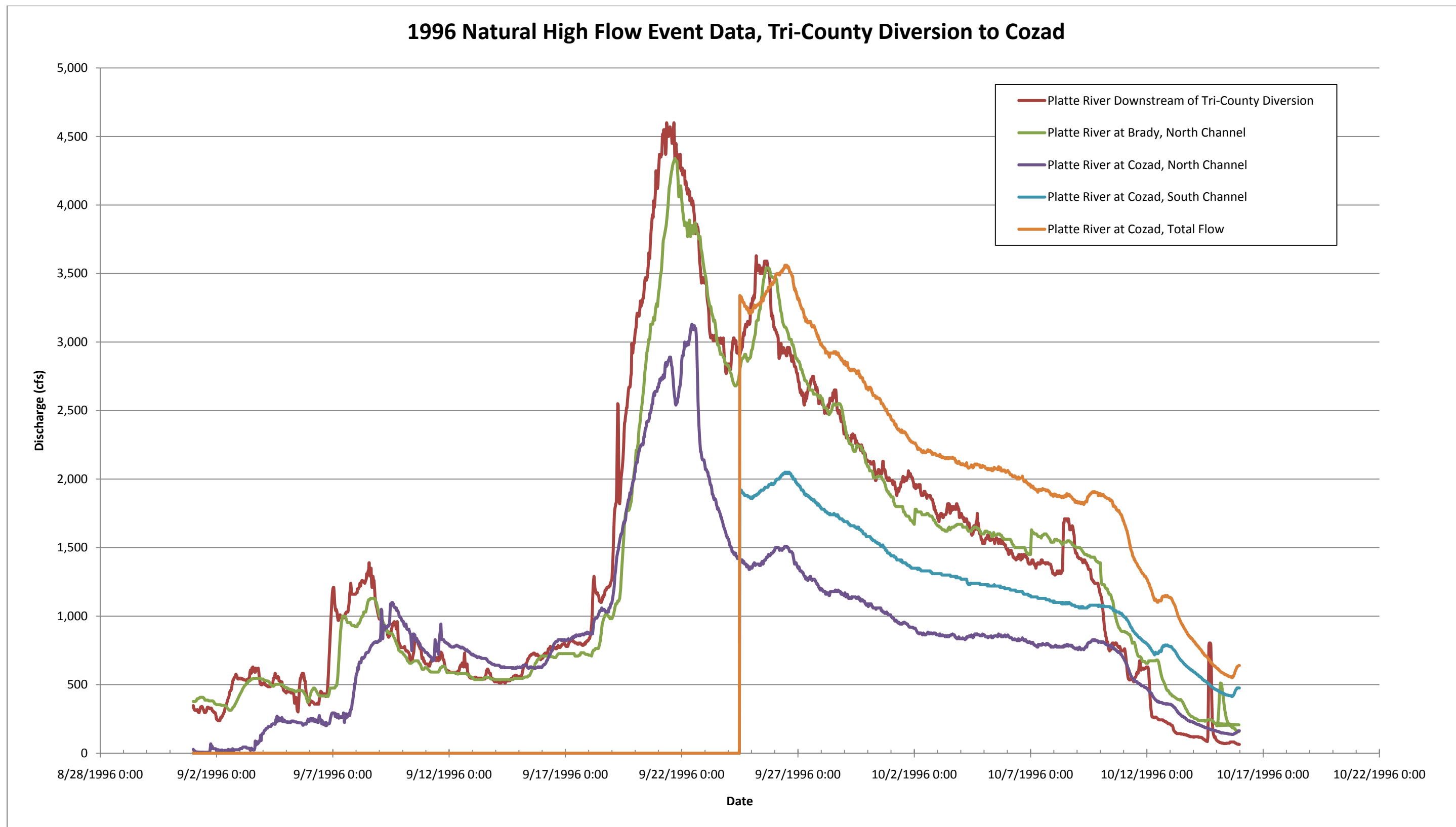
1
2 Figure3.11: Measured hydrographs from 1998 Event- Tri-County Diversion to Cozad
3



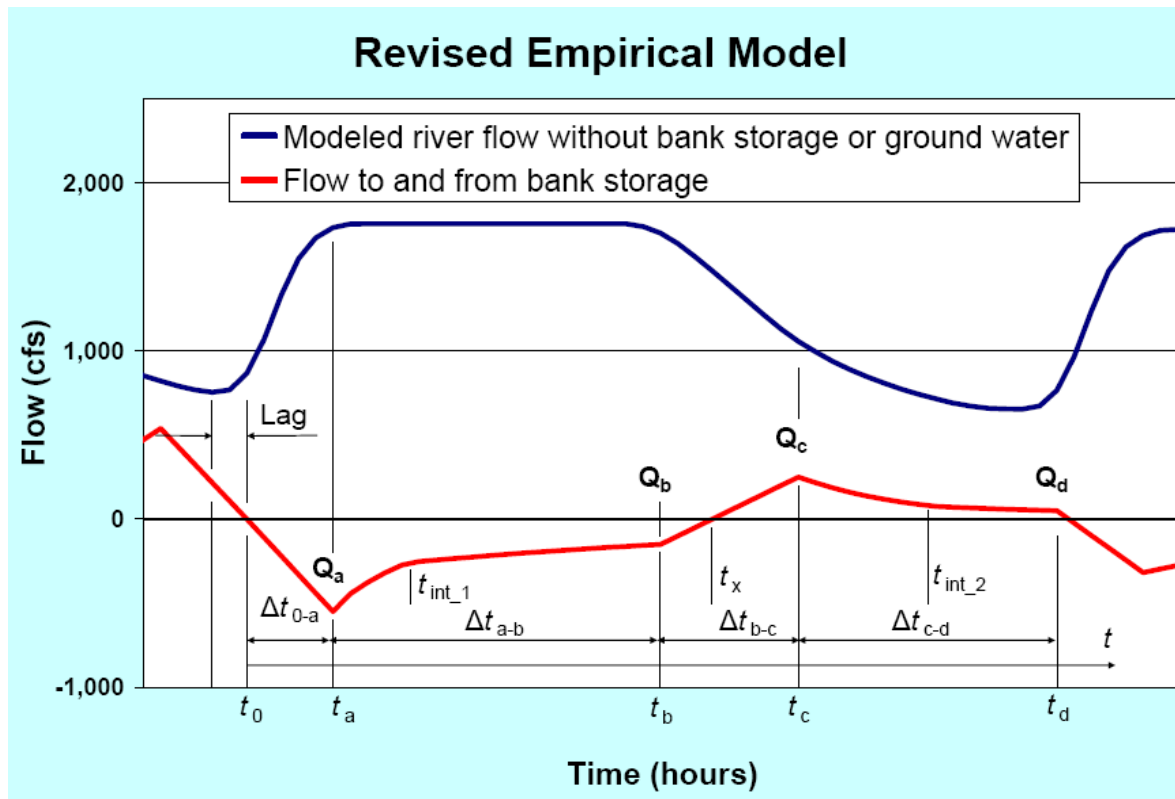
1
2 Figure 3.12: Measured hydrographs from 1998 Event- Cozad to Grand Island
3



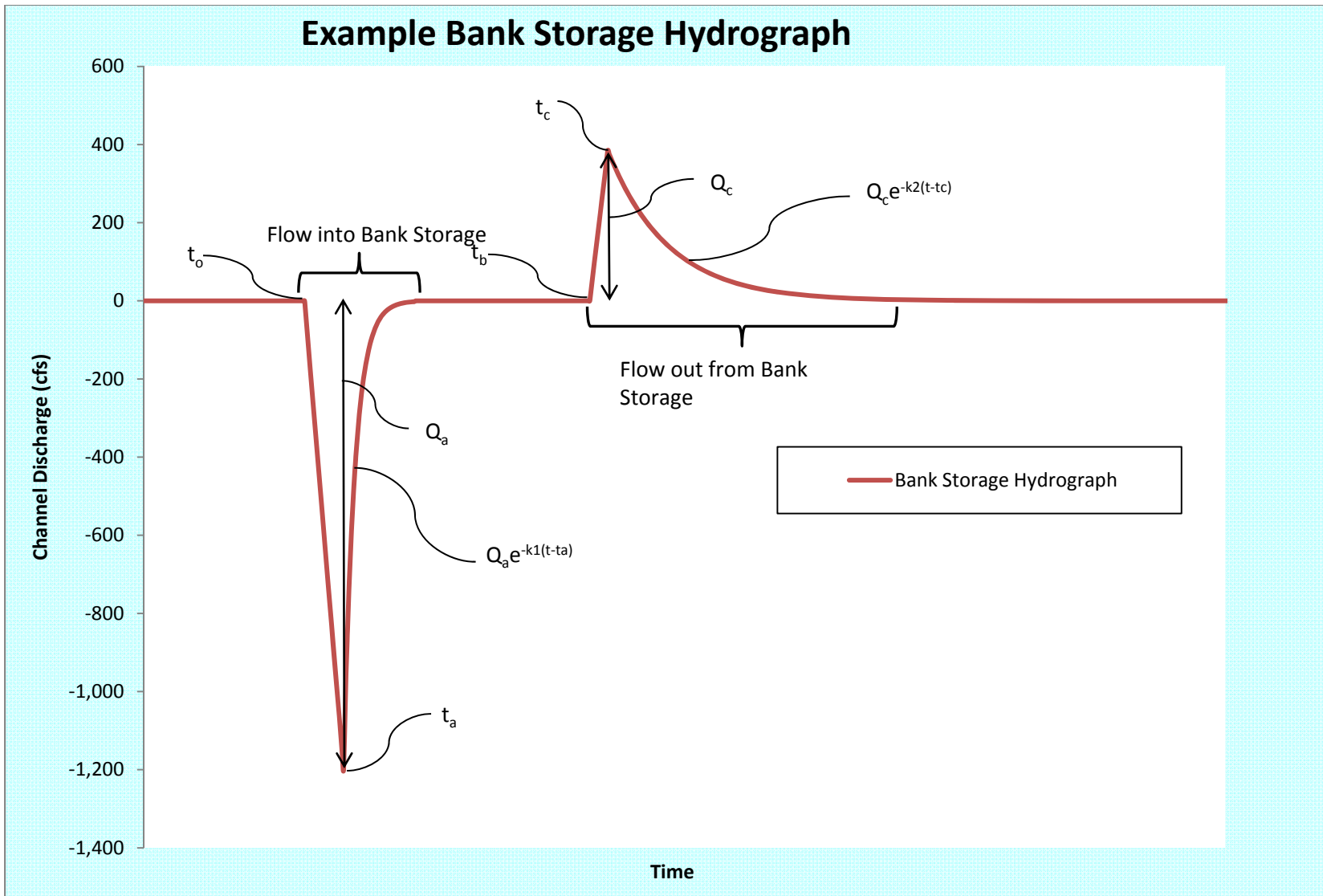
1
2 Figure 3.13: Measured hydrographs from 1997 Event- Tri-County Diversion to Cozad
3



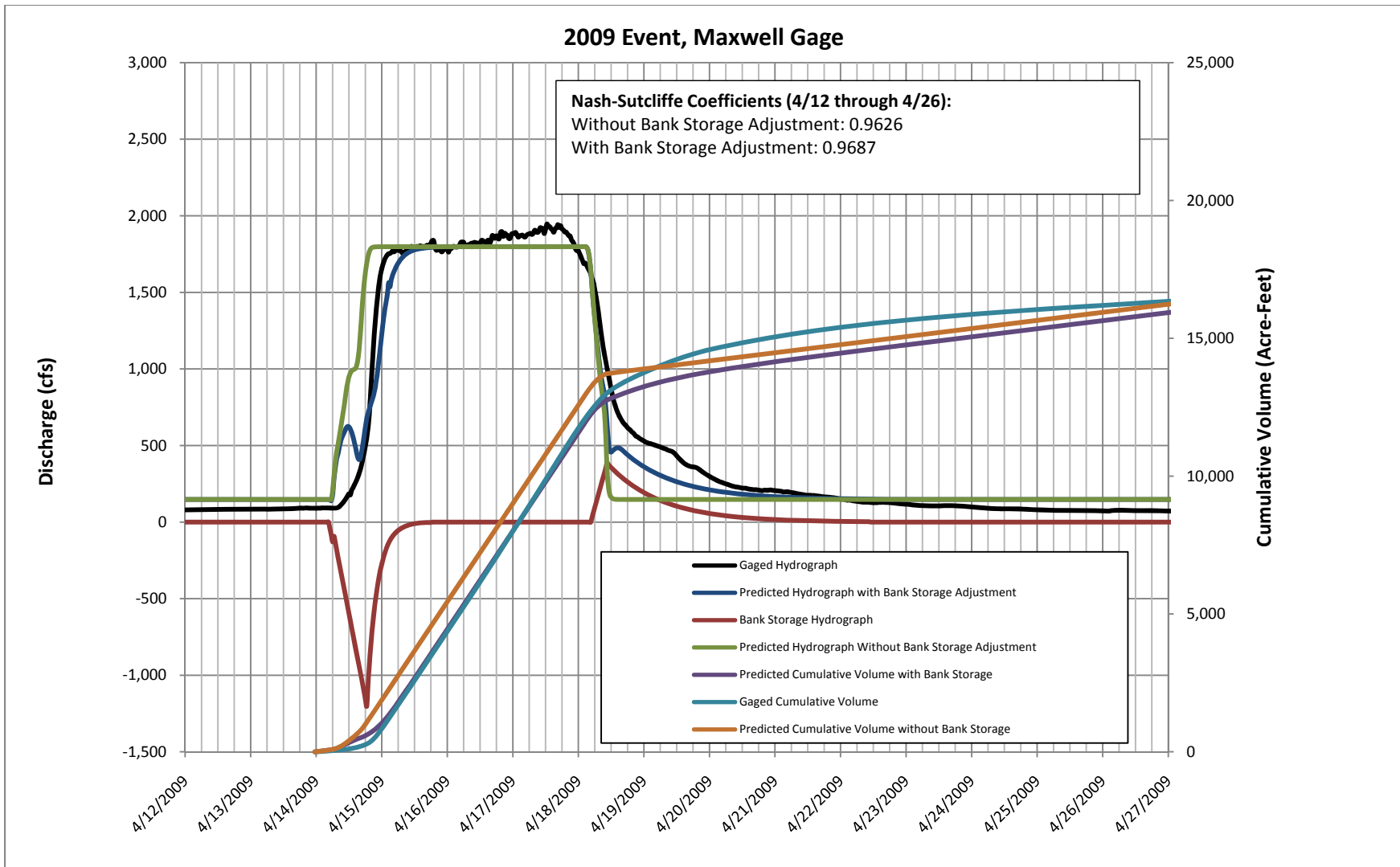
1
2 Figure 3.14: Measured hydrographs from 1996 Event- Tri-County Diversion to Cozad



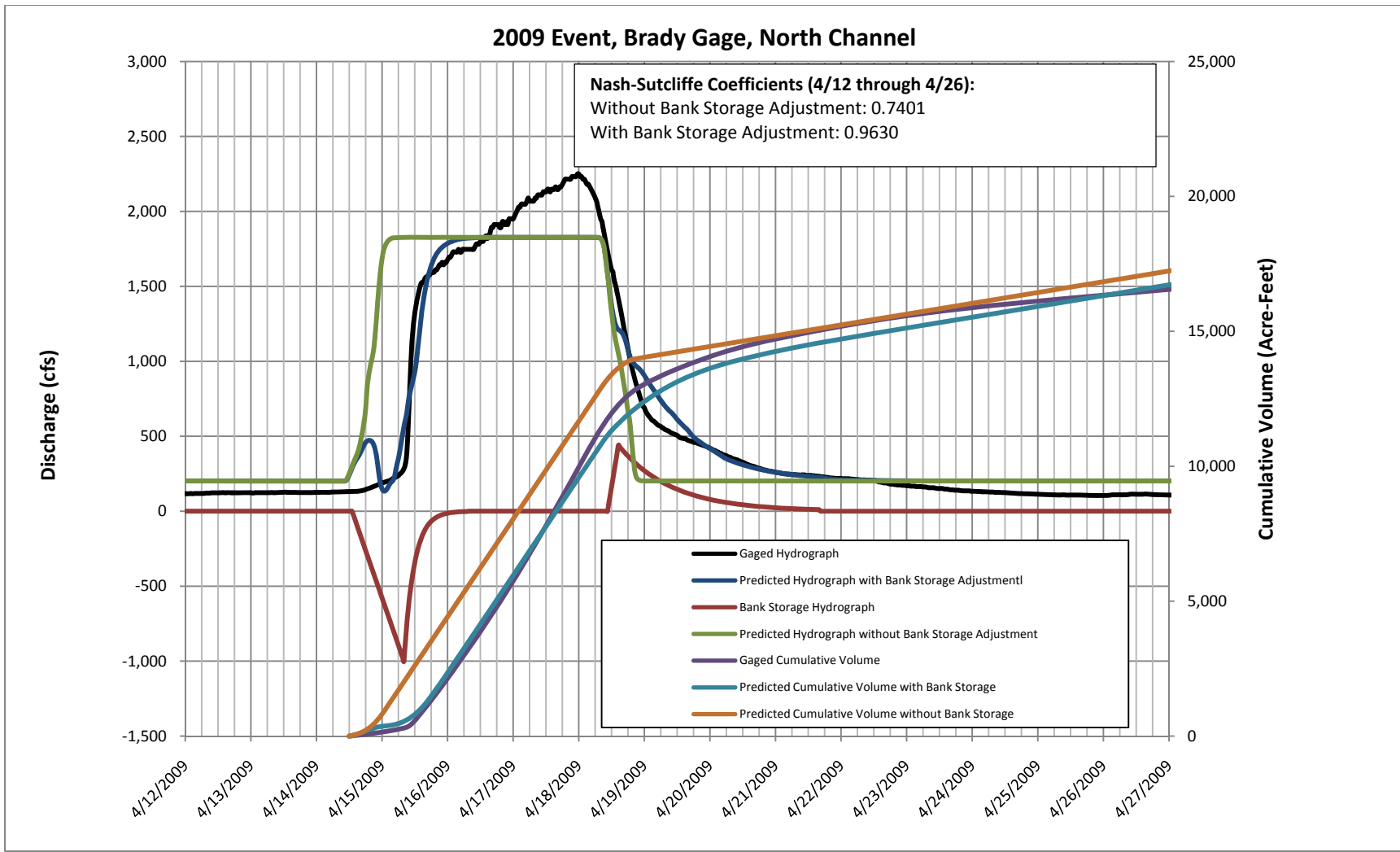
1
2 Figure 3.15: General Figure of Bank Storage relationship developed by Randle and Samad (2008)



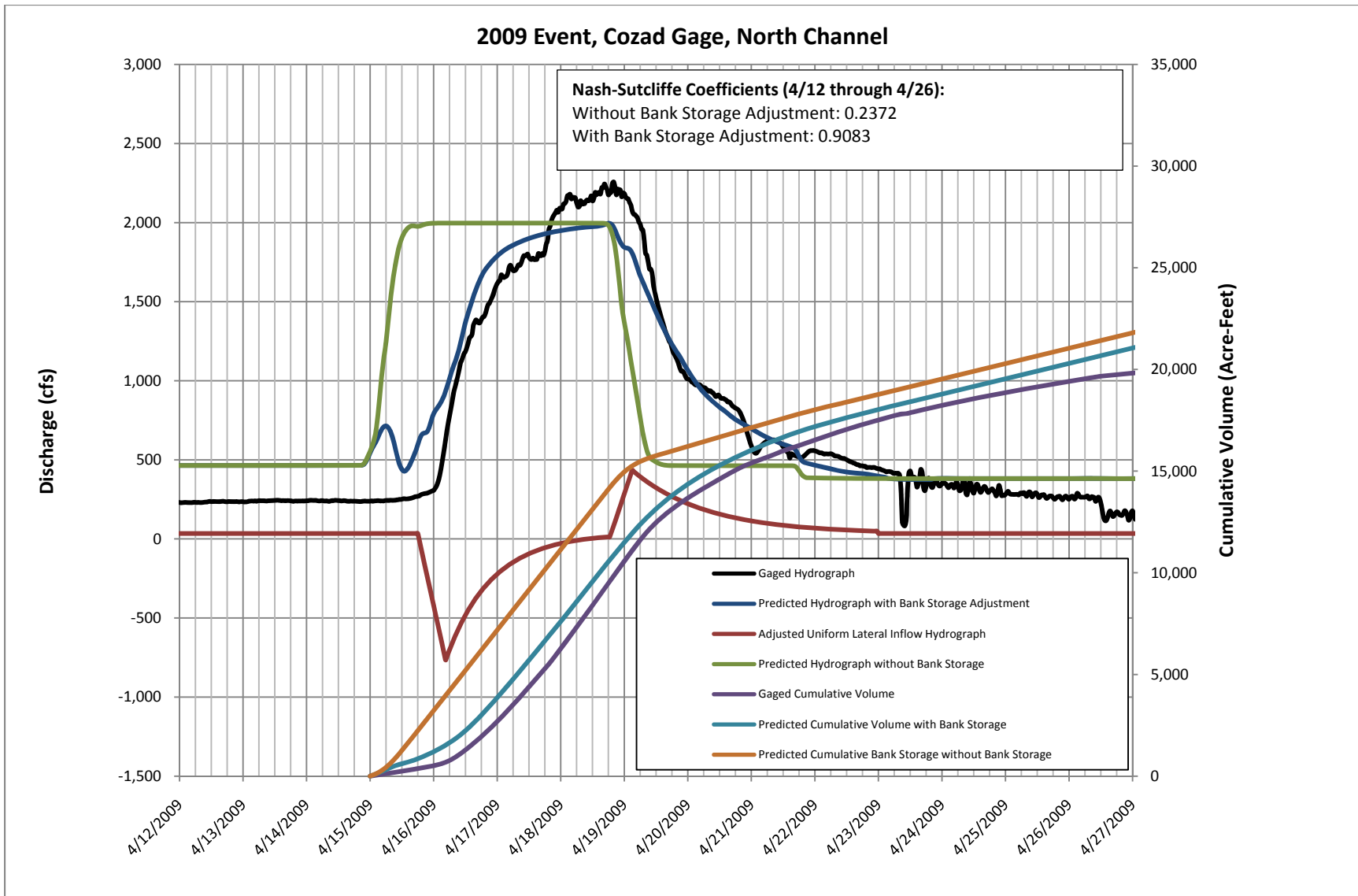
1
2 Figure 3.16: Example of Conceptual Bank Storage Hydrograph
3



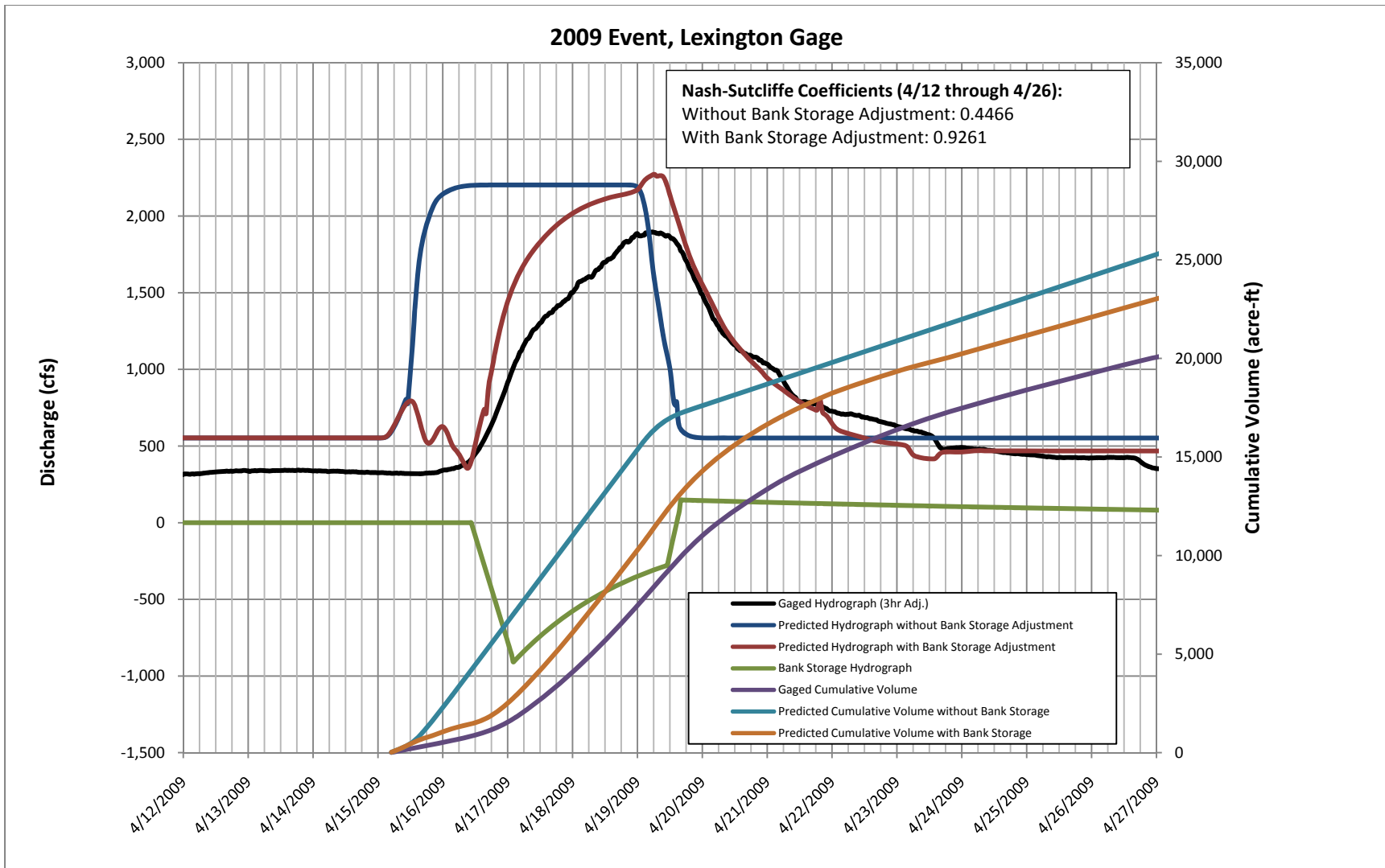
1
 2 Figure 3.17: 2009 Event, Calibration at Maxwell Gage, Predicted vs. Gaged



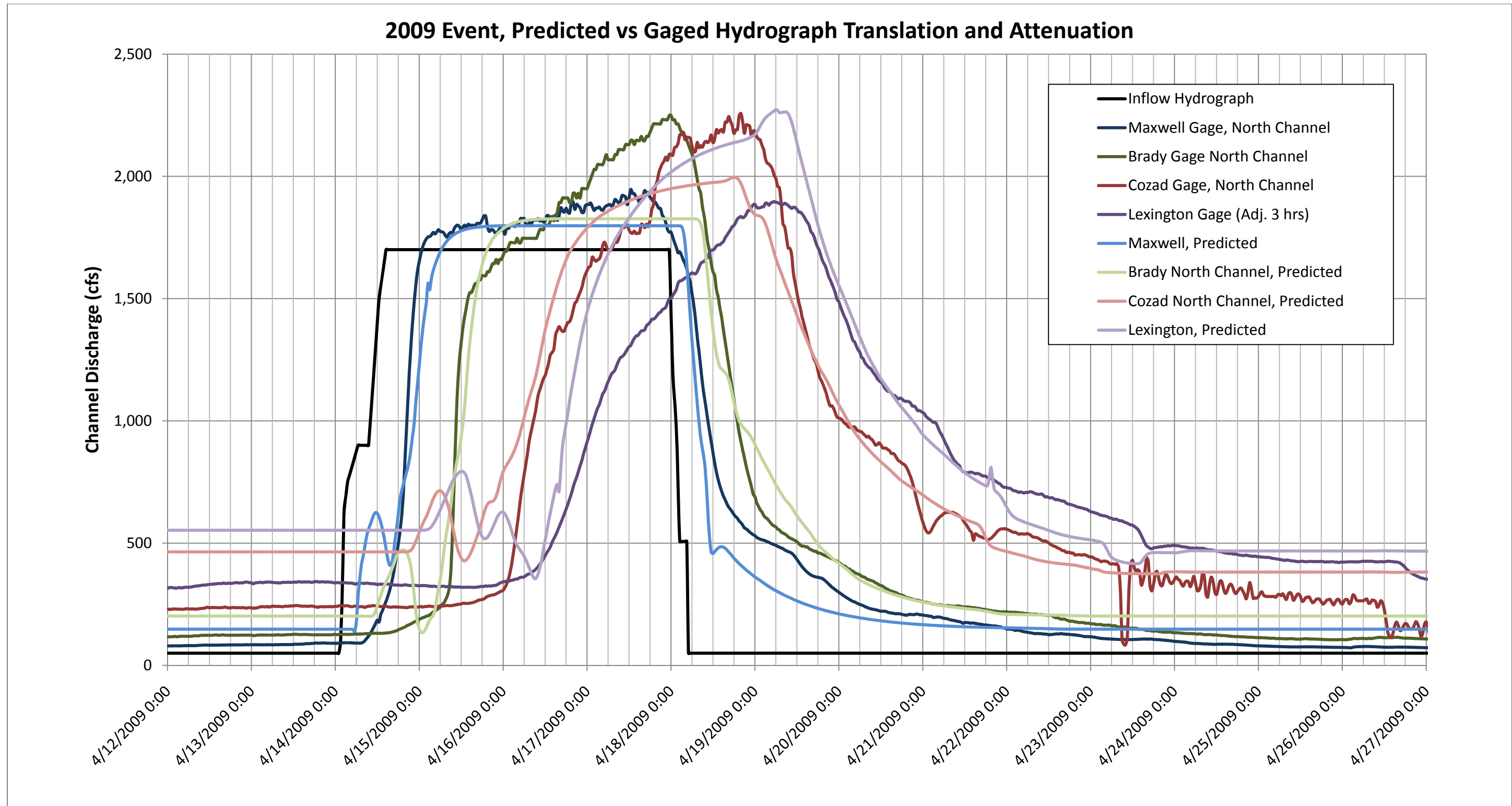
1
2 Figure 3.18: 2009 Event, Calibration at Brady Gage, Predicted vs. Gaged



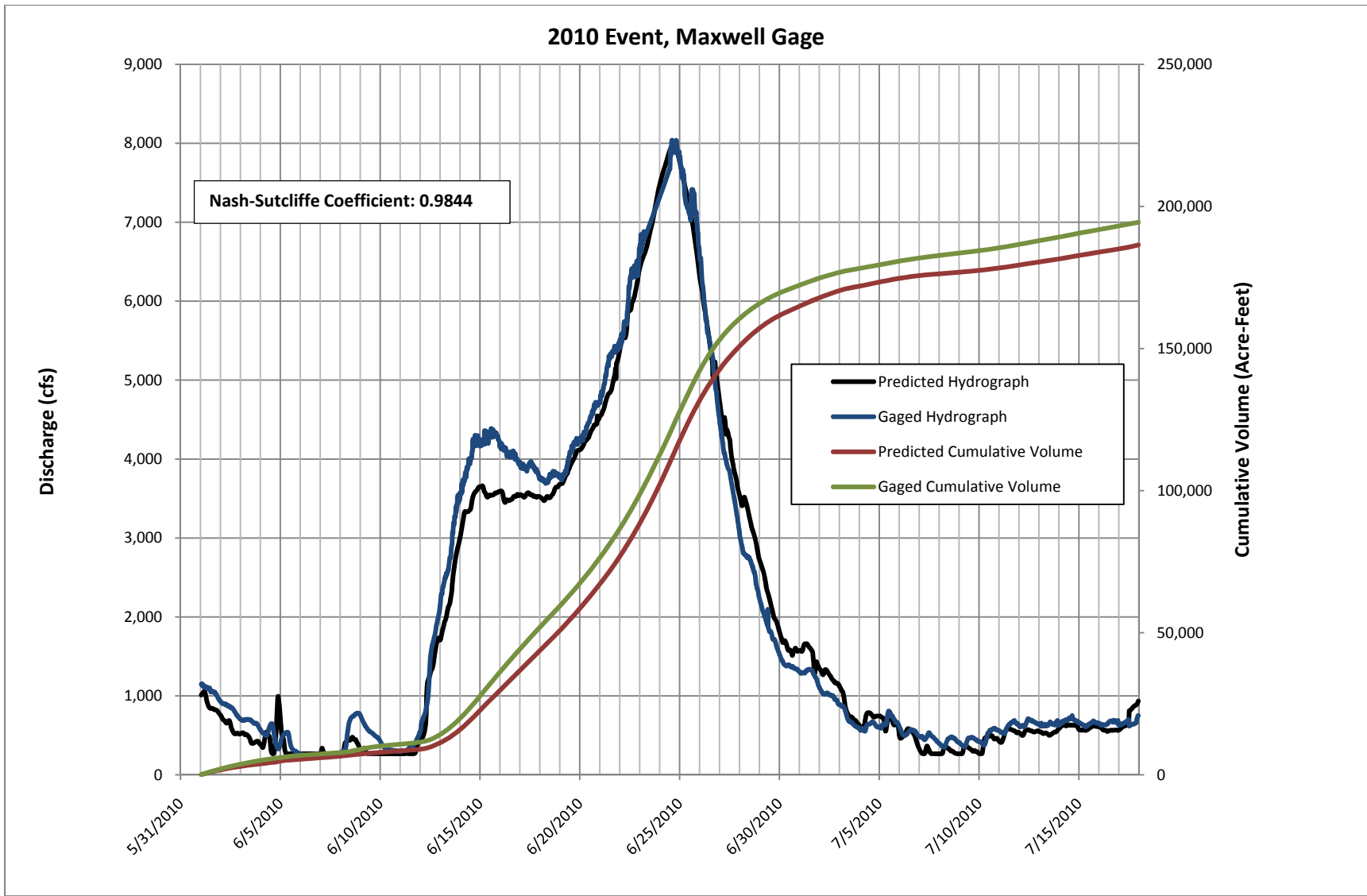
1
2 Figure 3.19: 2009 Event, Calibration at Cozad Gage, Predicted vs. Gaged



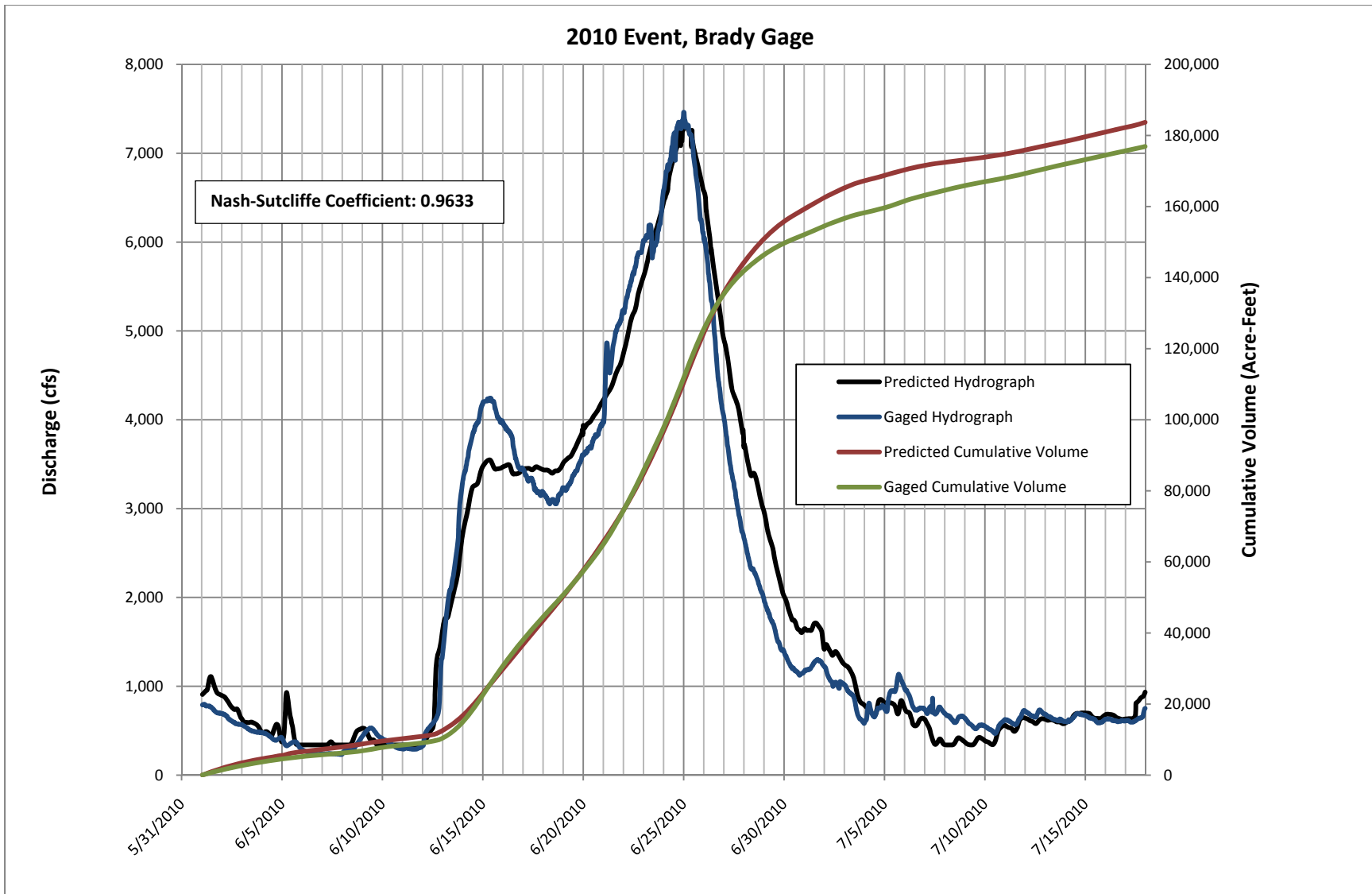
1
 2 Figure 3.20: 2009 Event, Calibration at Lexington Gage, Predicted vs. Gaged (Note: Lexington Gage has been shifted 3 hours to account for lag
 3 between the downstream end of this model segment and the Lexington gage location)



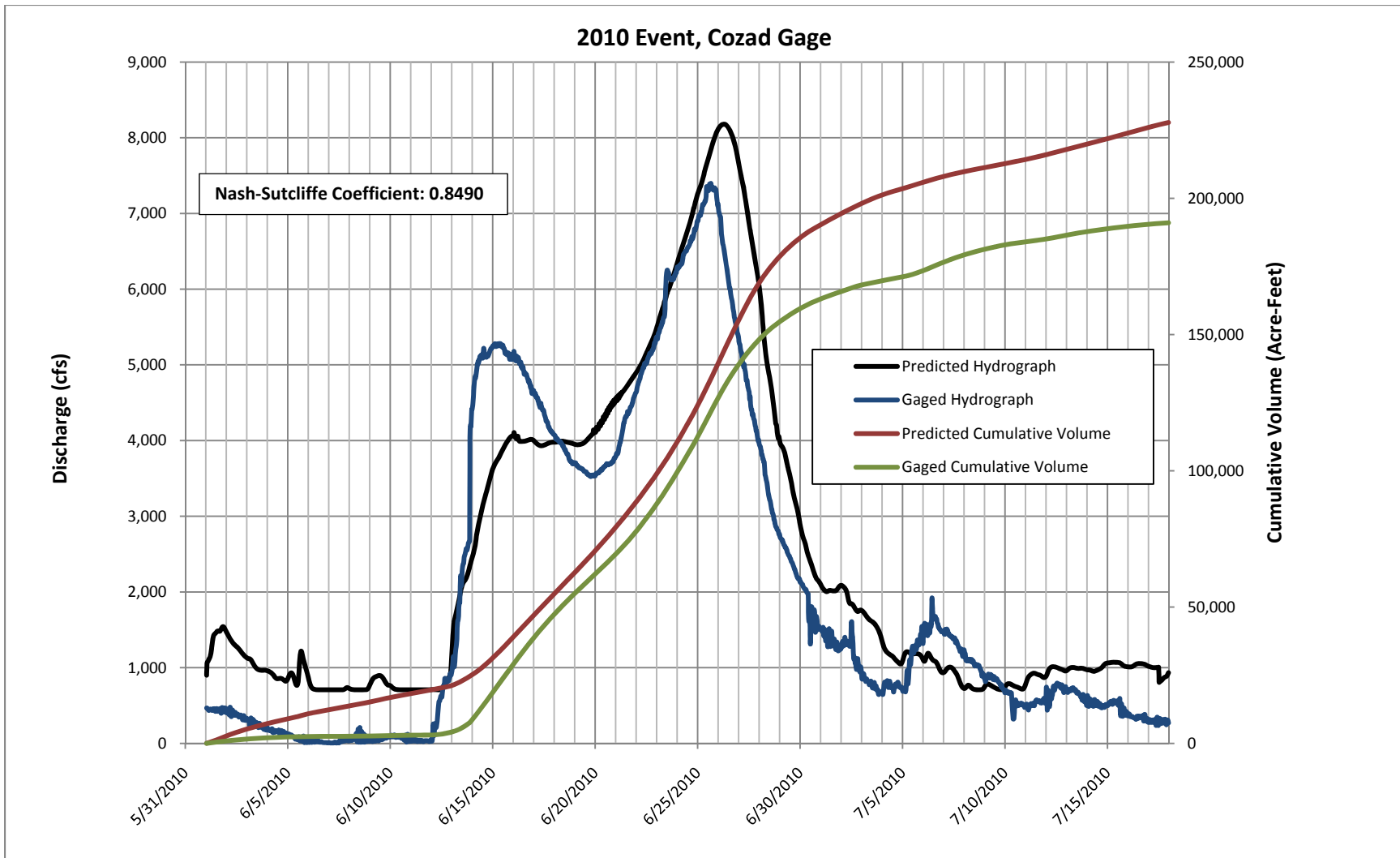
1
2 Figure 3.21: 2009 Event. Observed and Predicted Hydrograph Translation and Attenuation



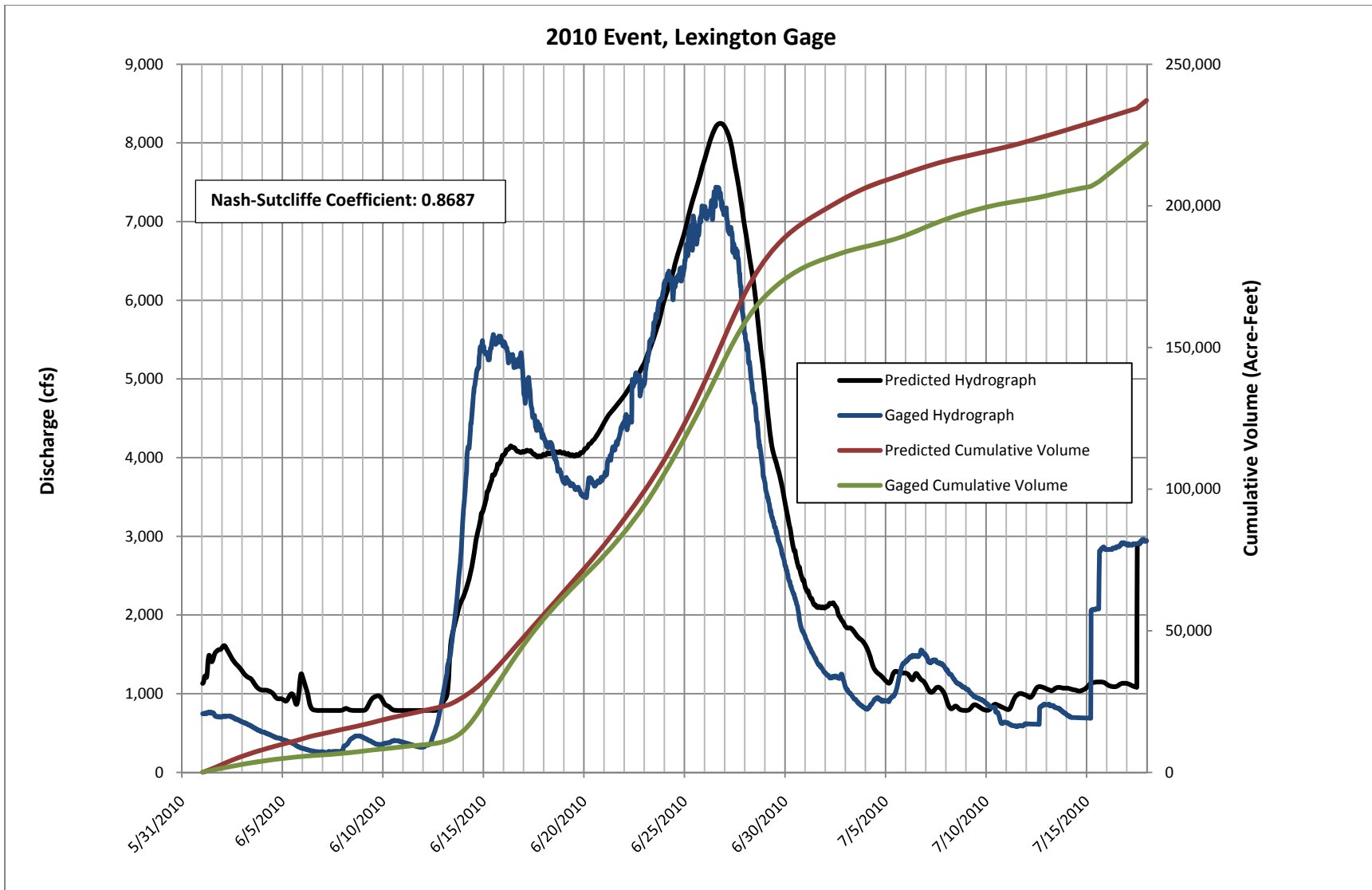
1
2 Figure 3.22: 2010 Event, Calibration at Maxwell Gage, Predicted vs. Gaged
3



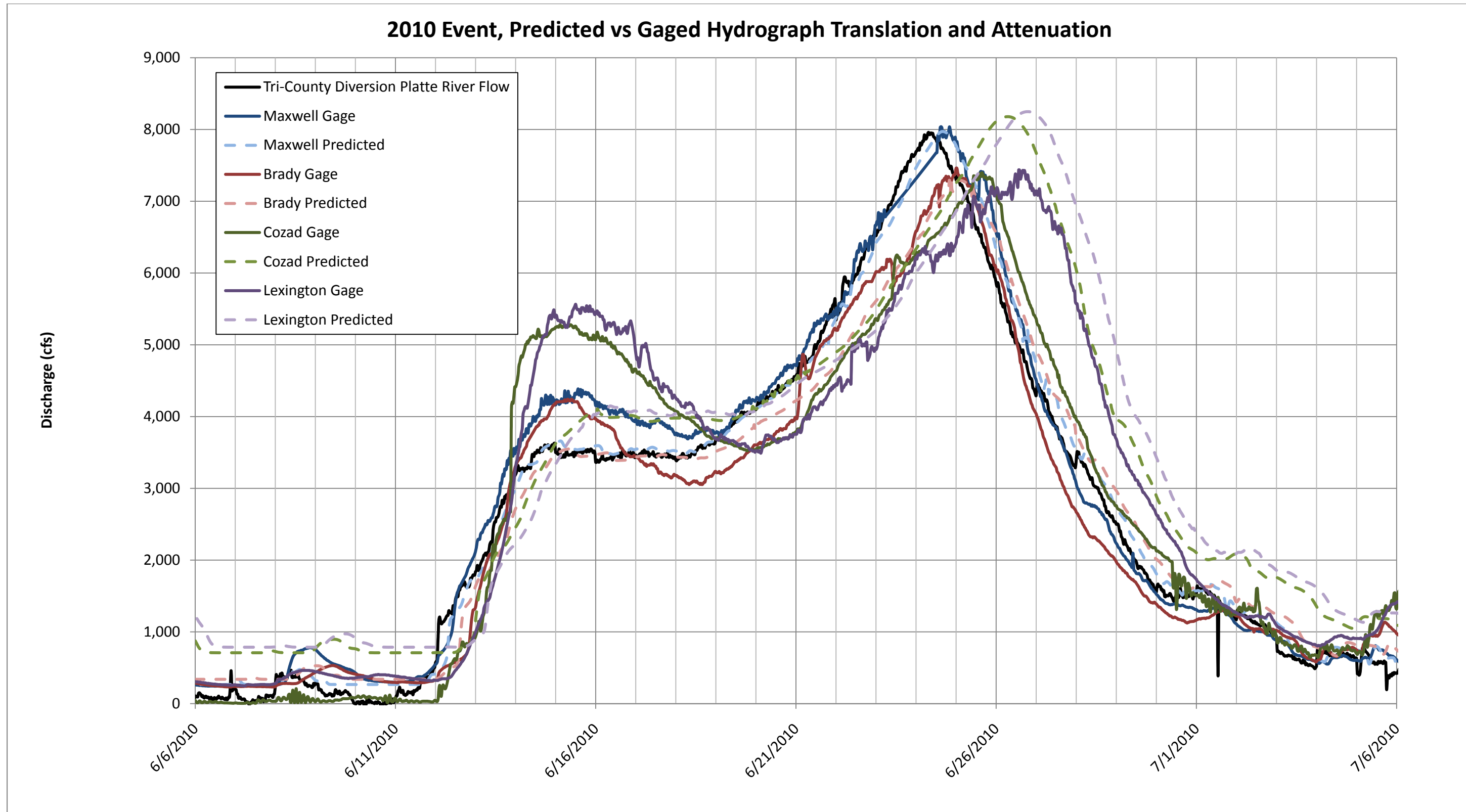
1
2 Figure 3.23: 2010 Event, Calibration at Brady Gage, Predicted vs. Gaged
3



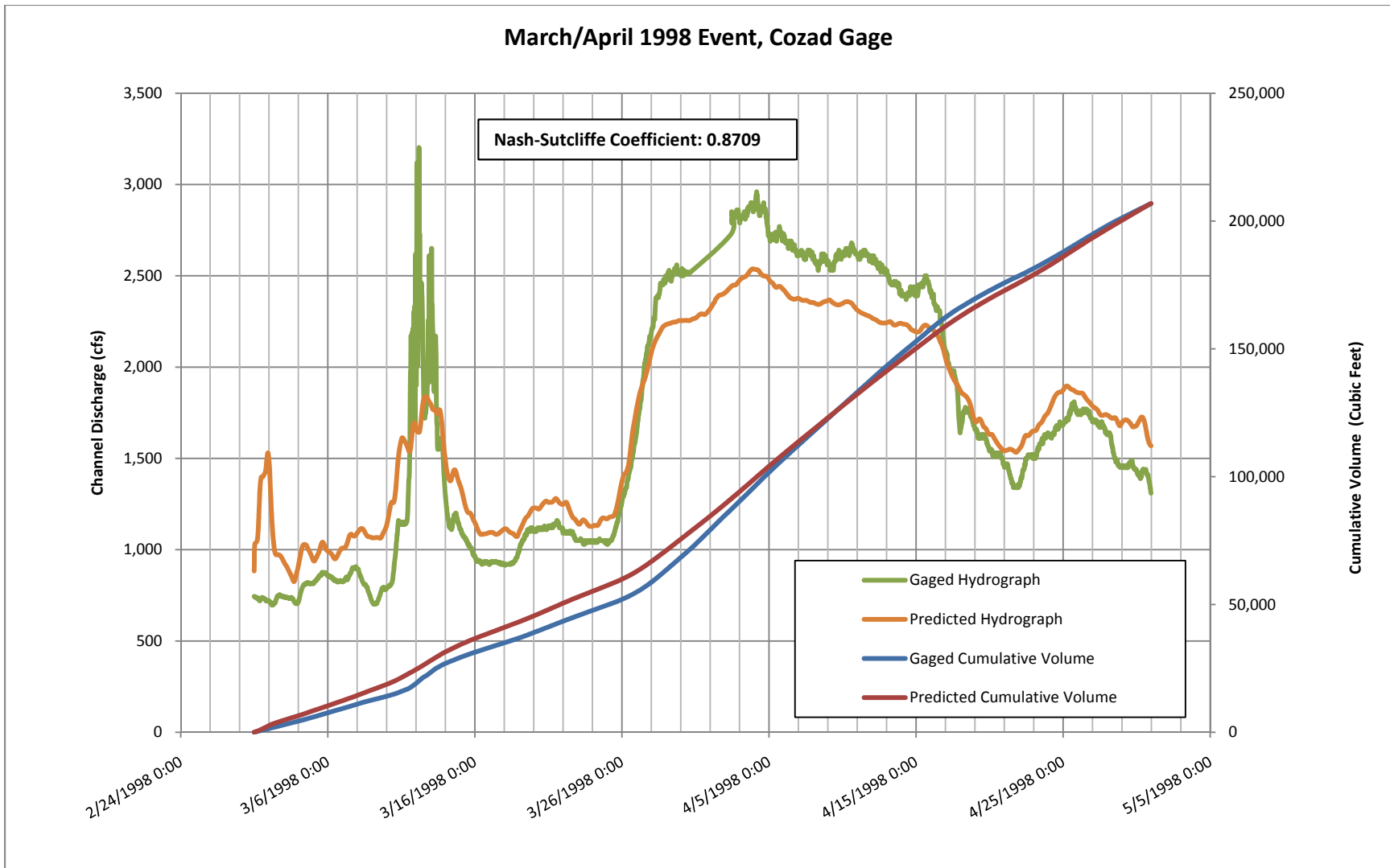
1
2 Figure 3.24: 2010 Event, Calibration at Cozad, Predicted vs. Gaged



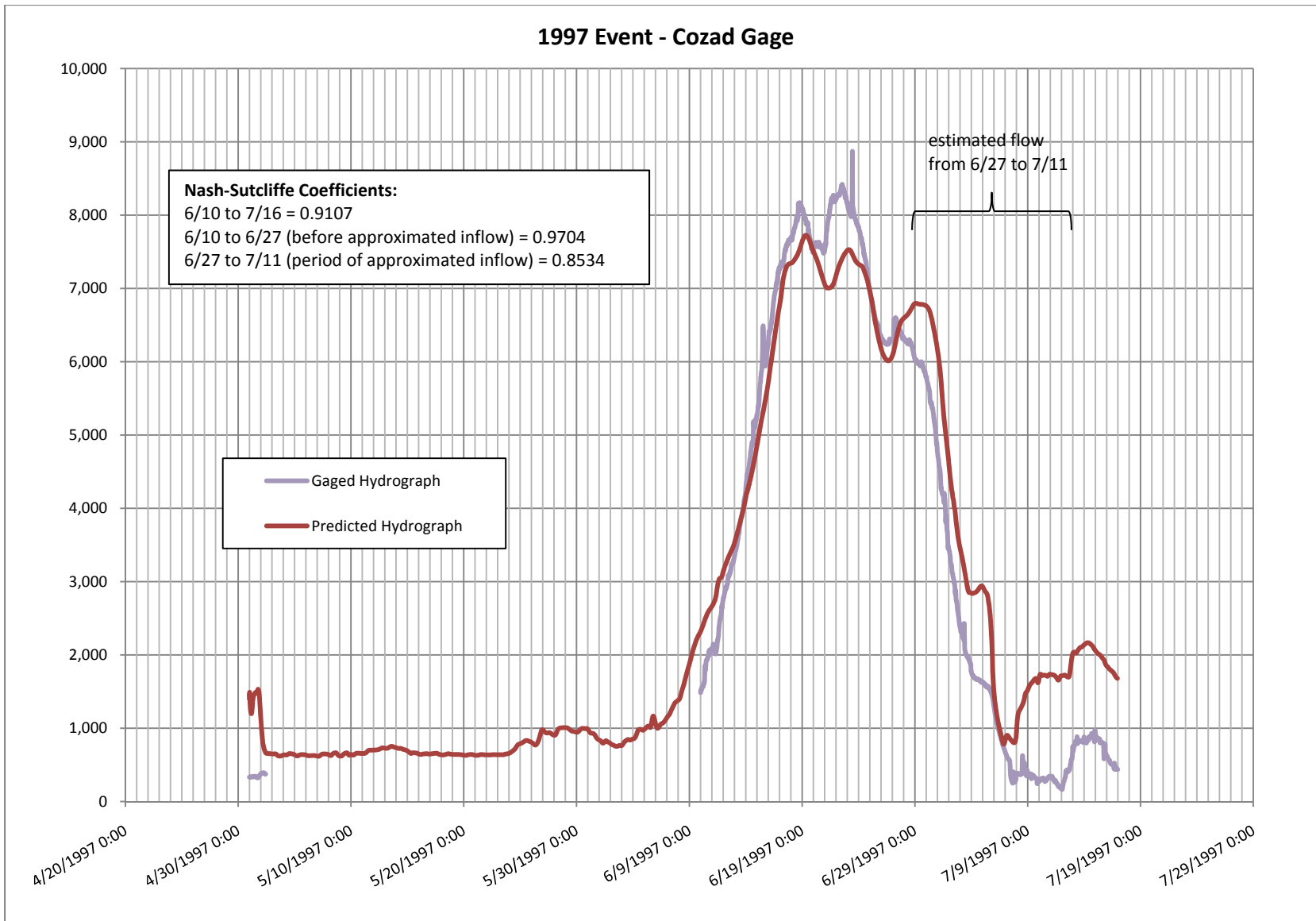
1
2 Figure 3.25: 2010 Event, Calibration at Lexington, Predicted vs. Gaged



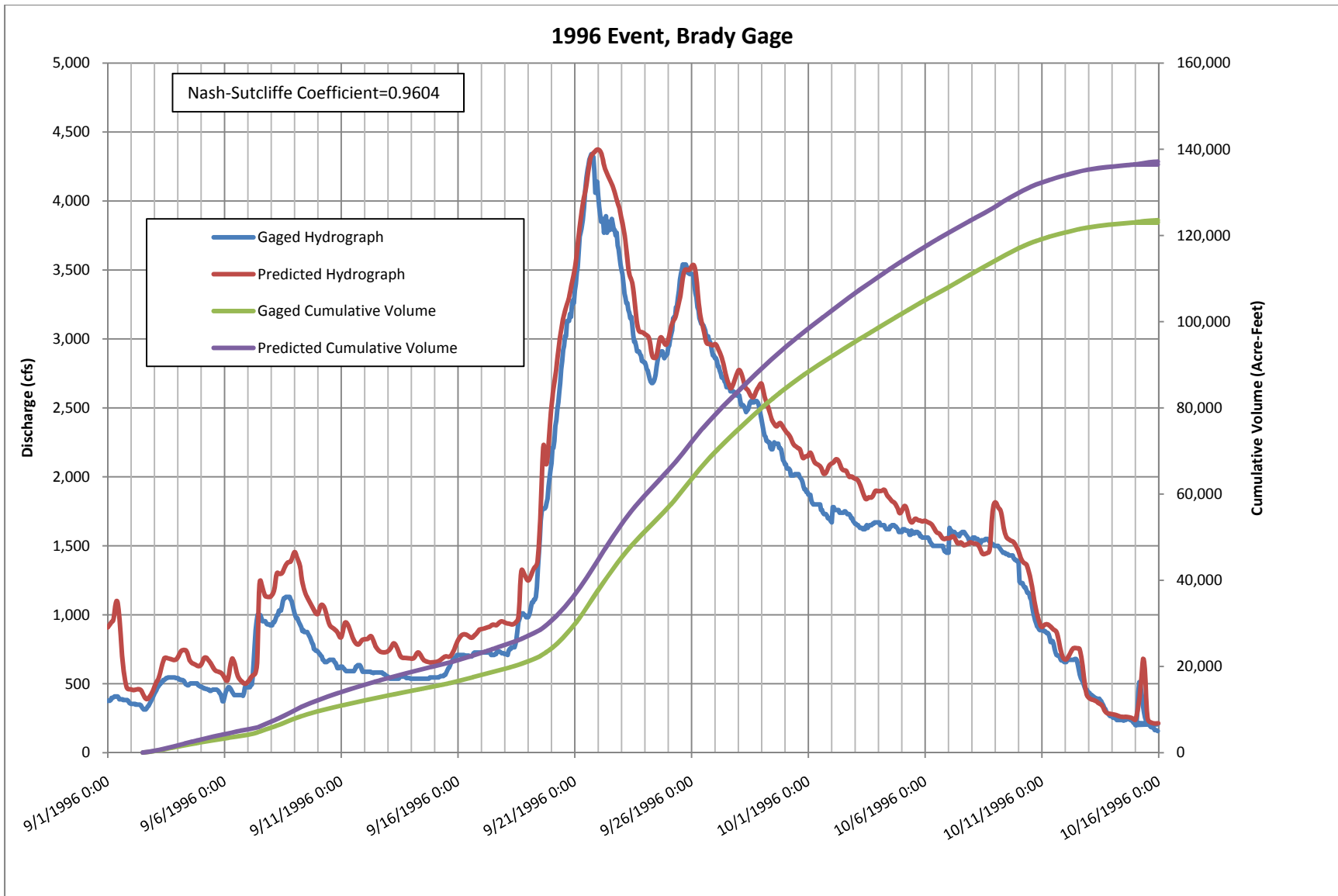
1
2 Figure 3.26: 2009 Event. Observed and Predicted Hydrograph Translation and Attenuation



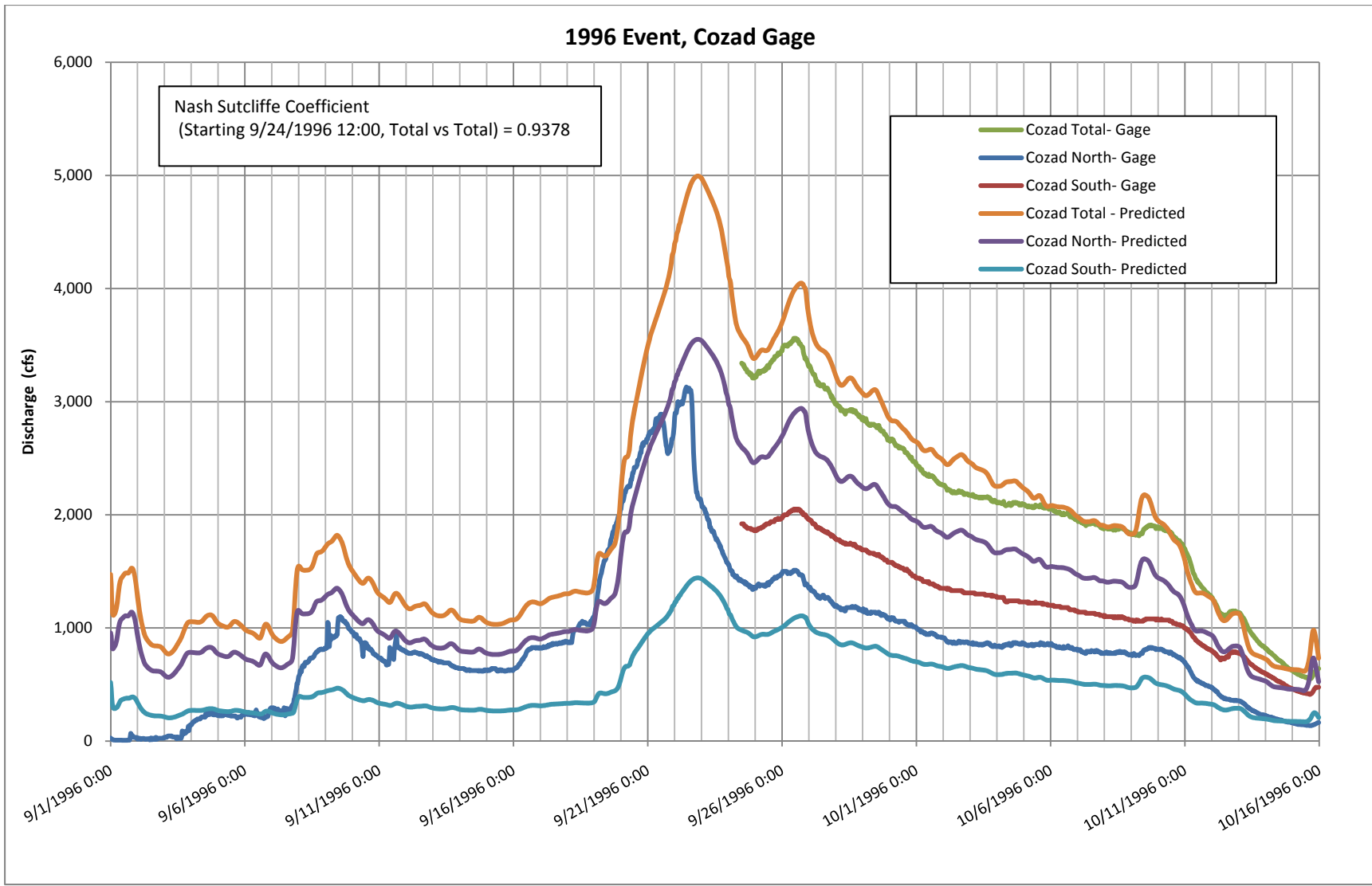
1
2 Figure 3.27: 1998 Event, Calibration at Cozad, Predicted vs. Gaged
3



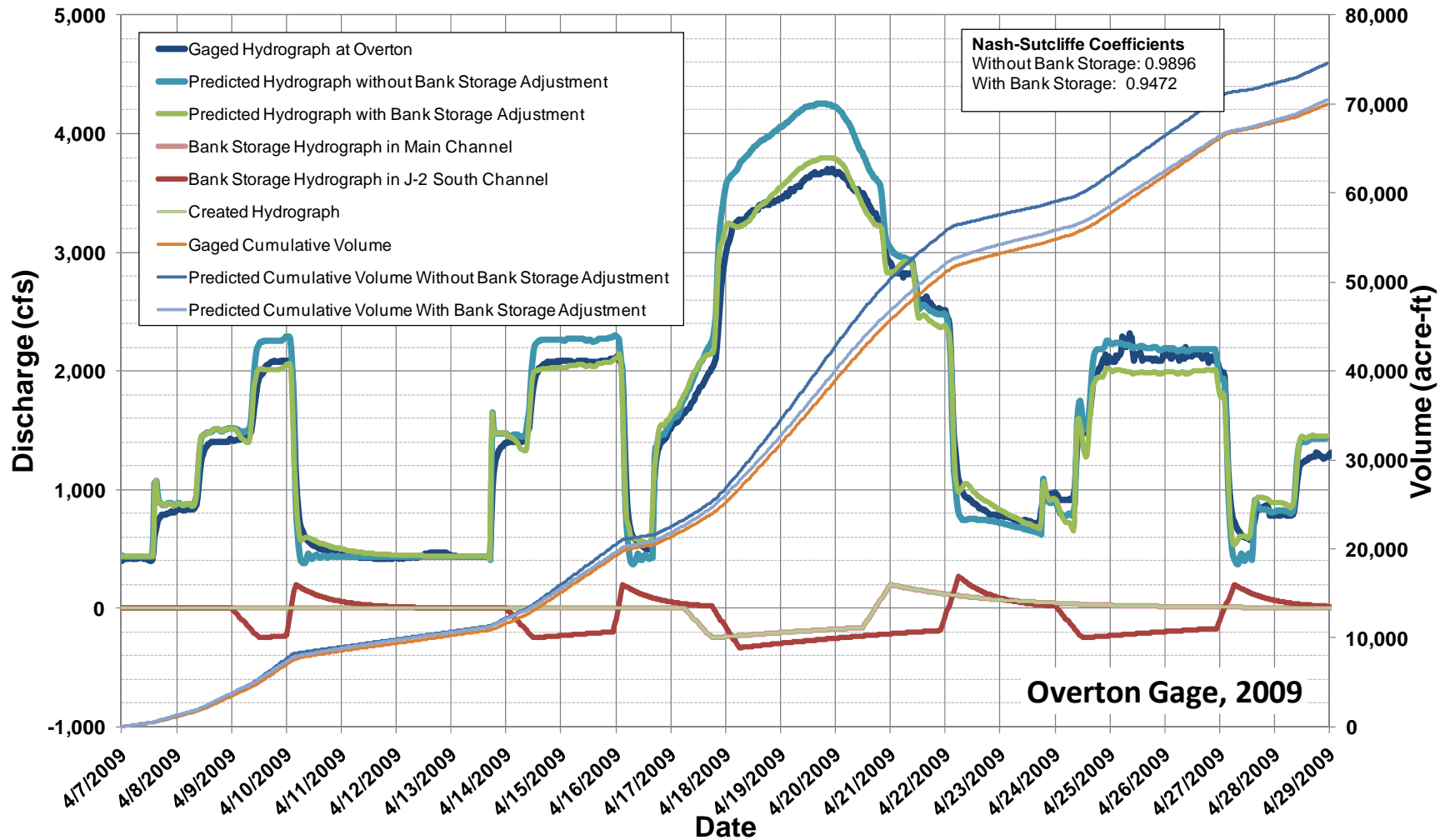
1
 2 Figure 3.28: 1997 Event, Calibration at Cozad, Predicted vs. Gaged (Note: cumulative volumes not shown due to incomplete gage record)



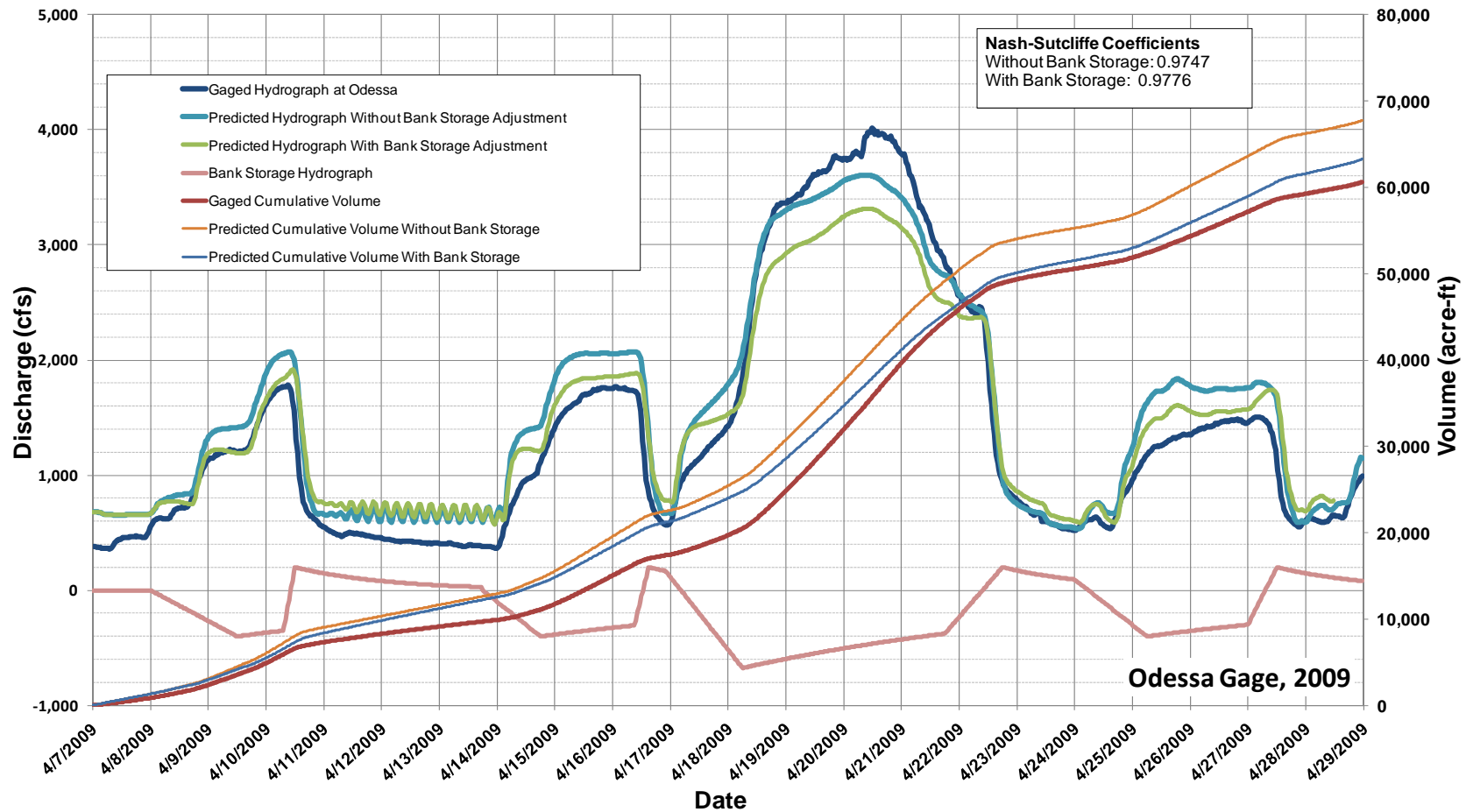
1
2 Figure 3.29: 1996 Event, Calibration at Brady, Predicted vs. Gaged



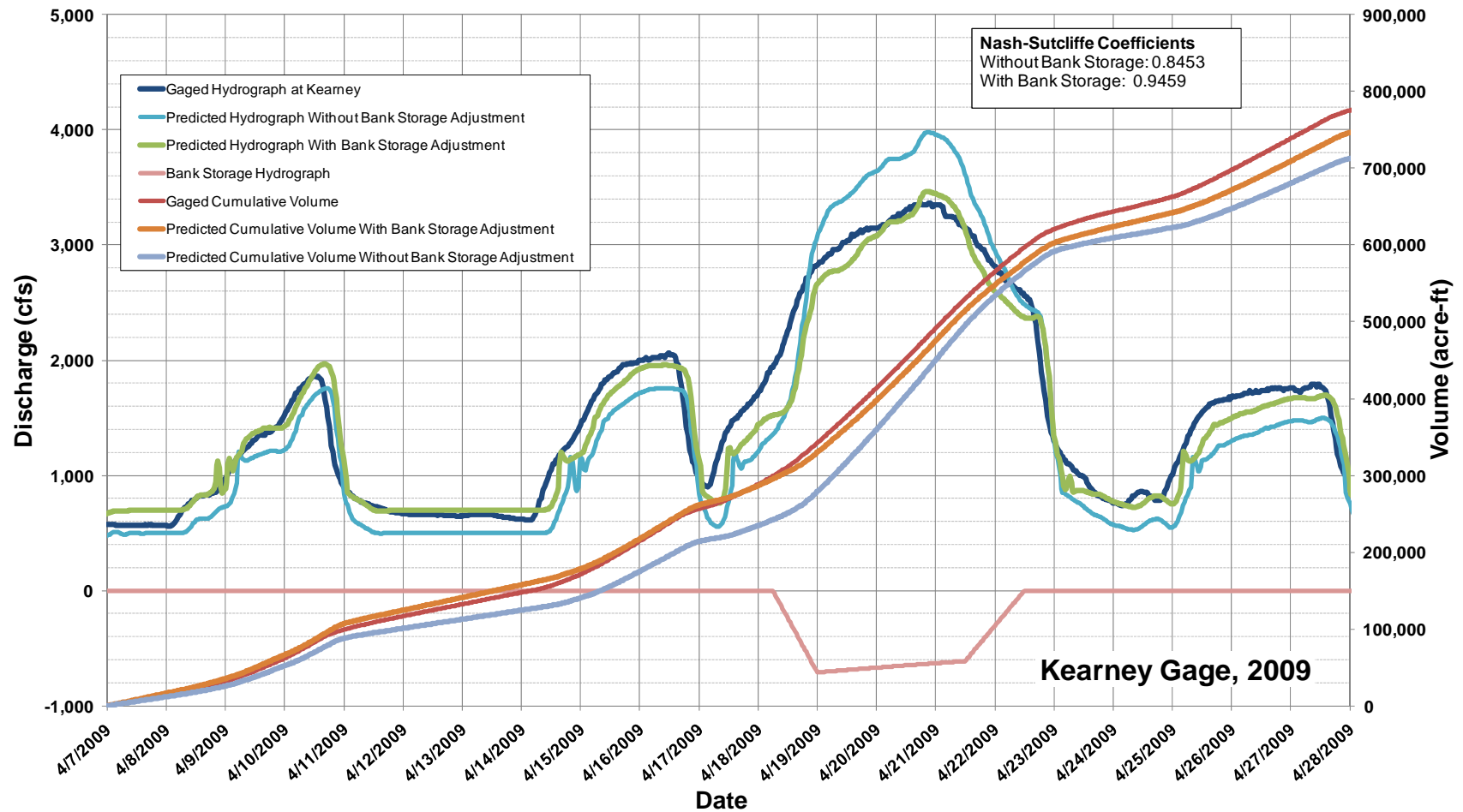
1
 2 Figure 3.30: 1996 Event, Calibration at Brady, Predicted vs. Gaged.
 3 (Note: cumulative volumes not shown due to incomplete gage record)
 4



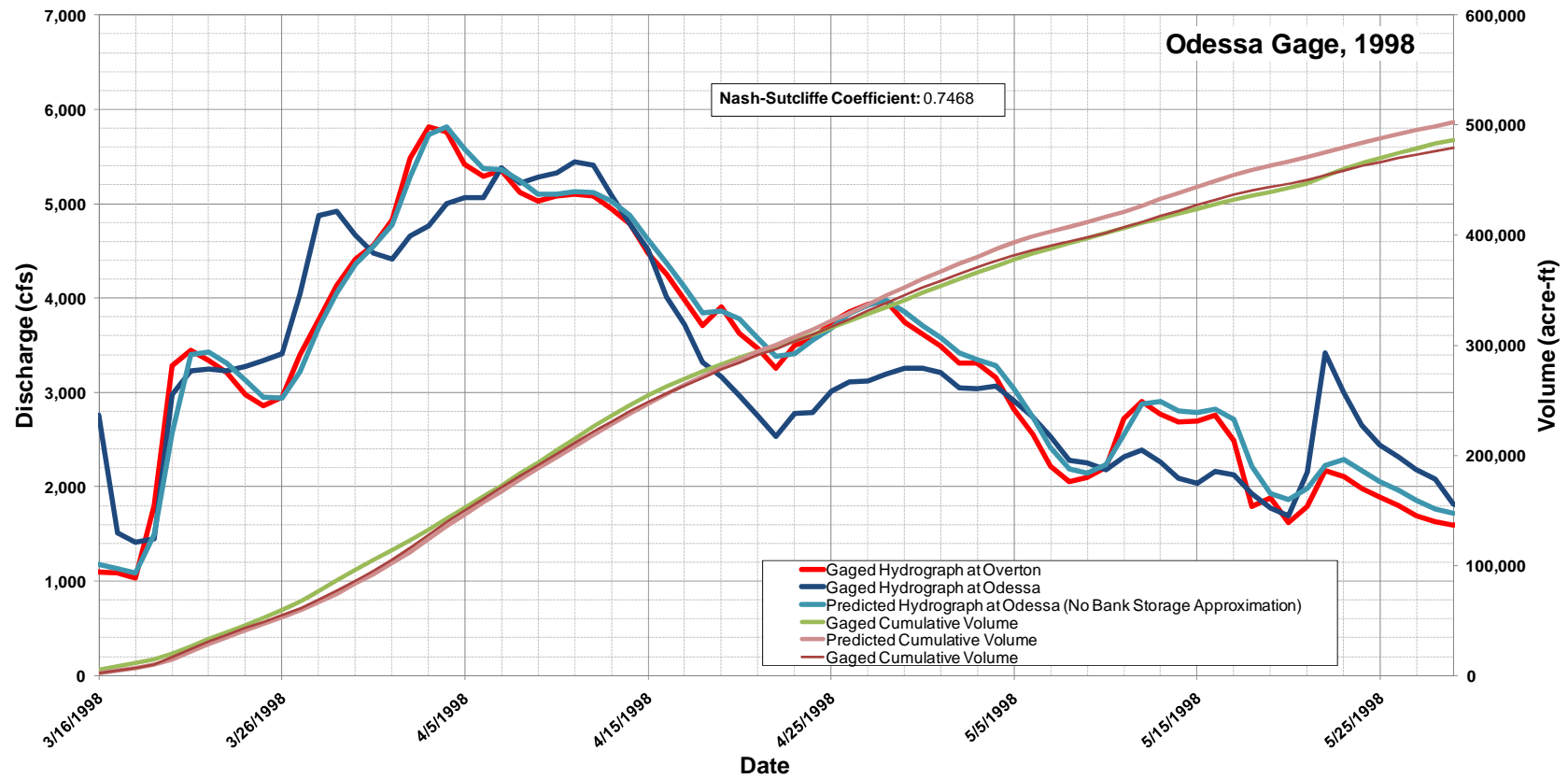
1
 2 Figure 3.31: Comparison of predicted and measured hydrographs at the Overton Gage for the 2009 flow event. Also shown is the cumulative
 3 water volume.



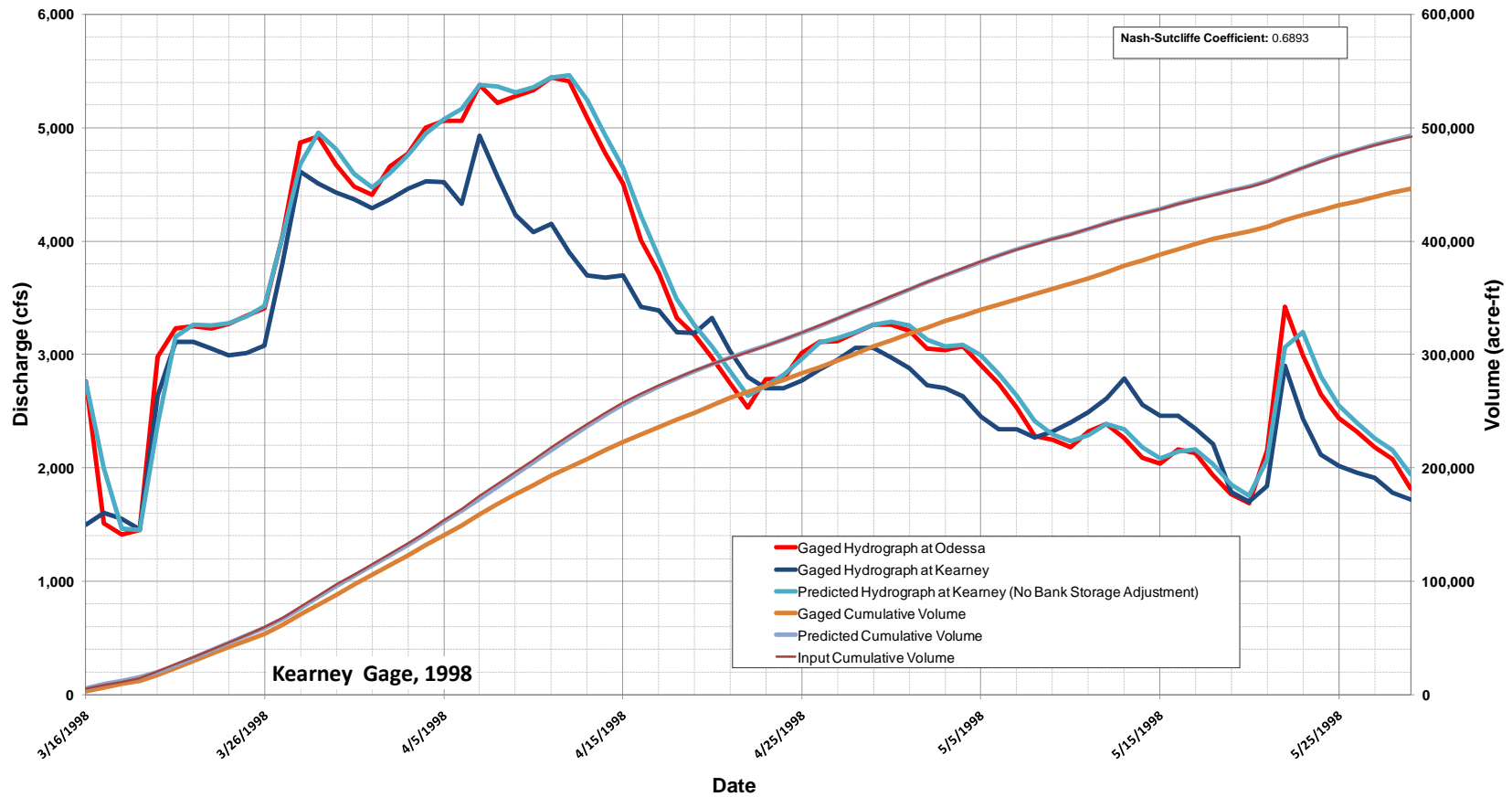
1
 2 Figure 3.32: Comparison of predicted and measured hydrographs at the Odessa Gage for the 2009 flow event. Also shown is the cumulative
 3 water volume.



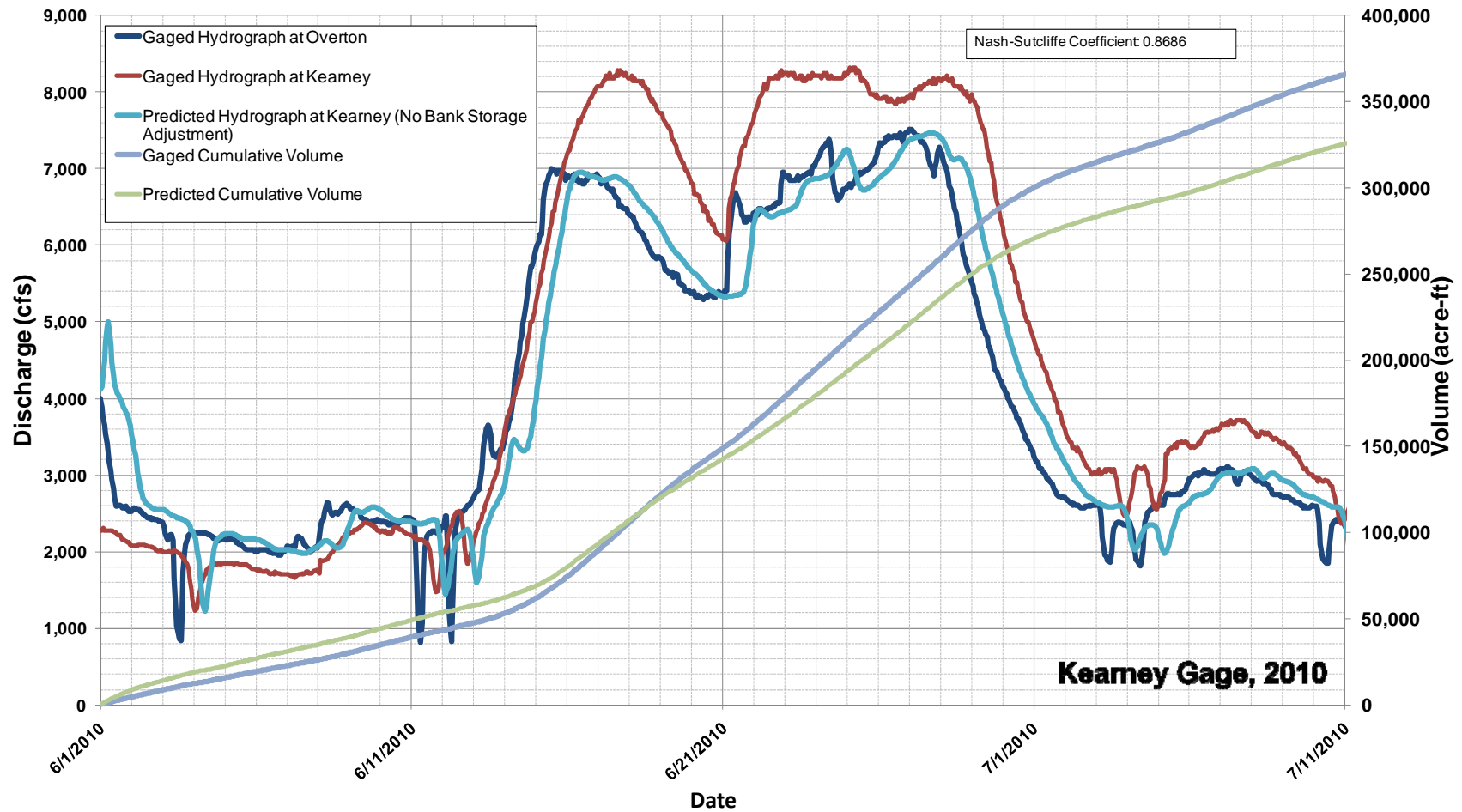
1
 2 Figure 3.33: Comparison of predicted and measured hydrographs at the Kearney Gage for the 2009 flow event. Also shown is the cumulative
 3 water volume.



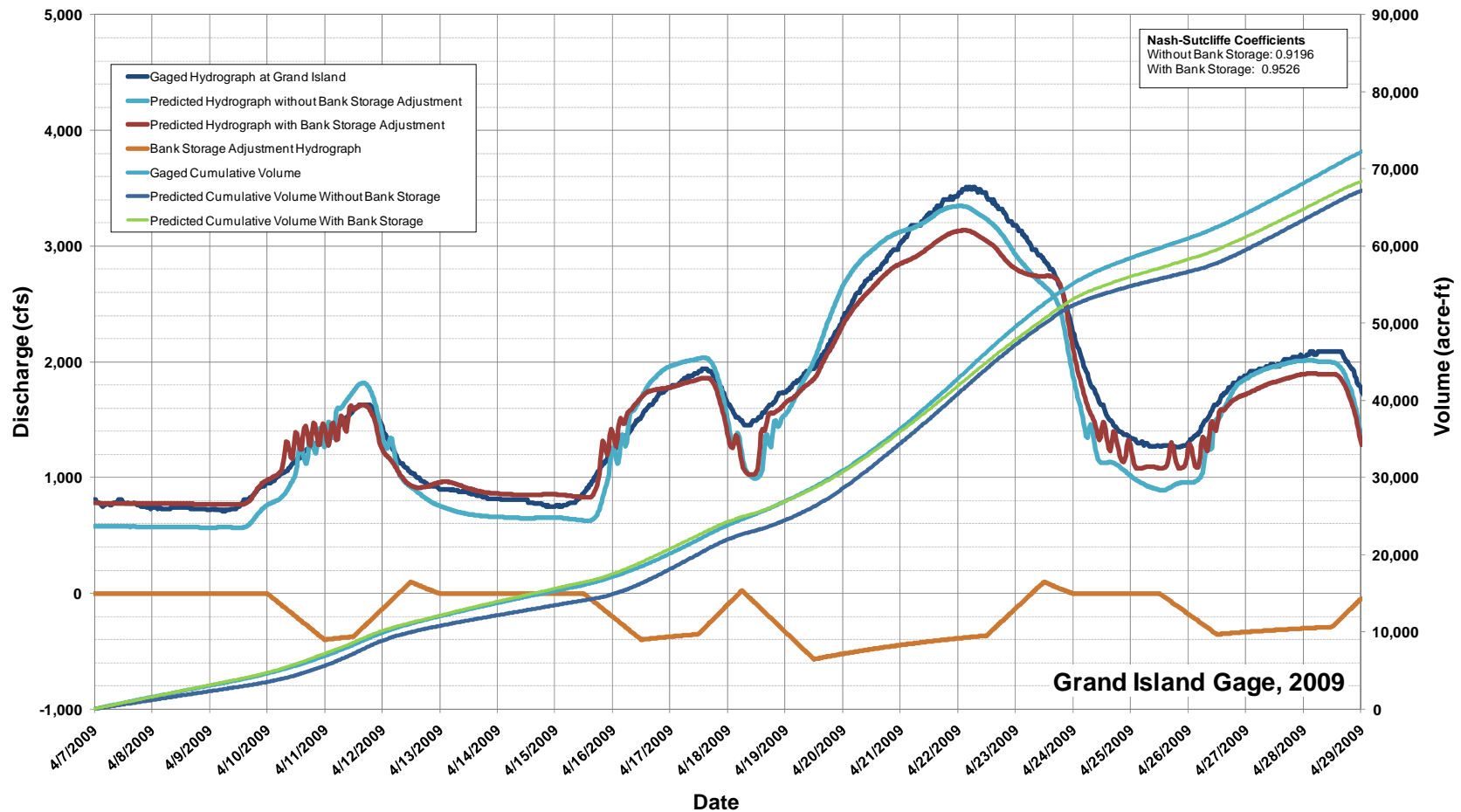
1
 2 Figure 3.34: Comparison of predicted and measured hydrographs at the Odessa gage for the 1998 event. Also shown is the cumulative water
 3 volume.



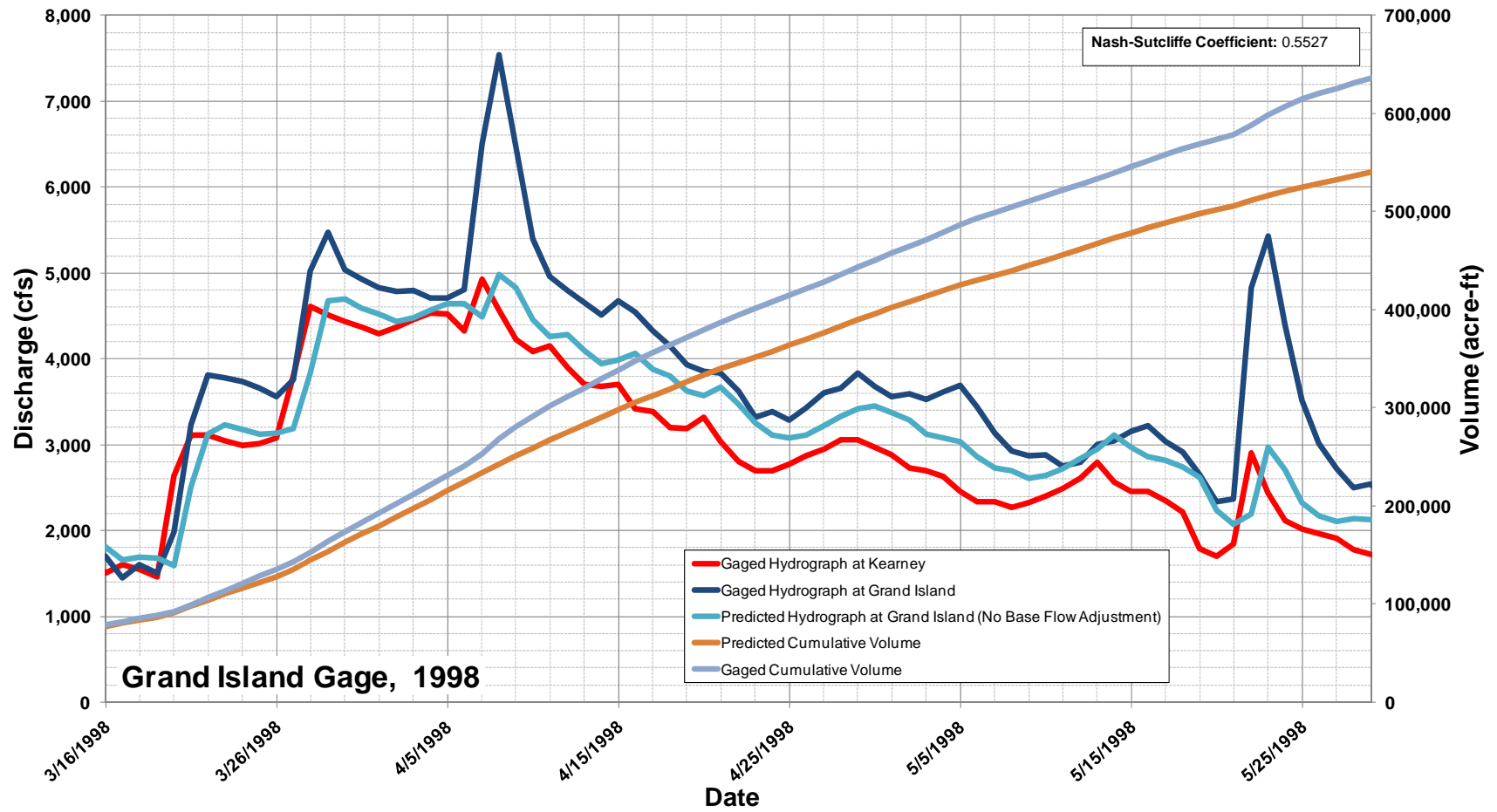
1
2
3 Figure 3.35: Predicted Comparison of predicted and measured hydrographs at the Kearney gage for the 1998 event. Also shown is the
4 cumulative water volume.



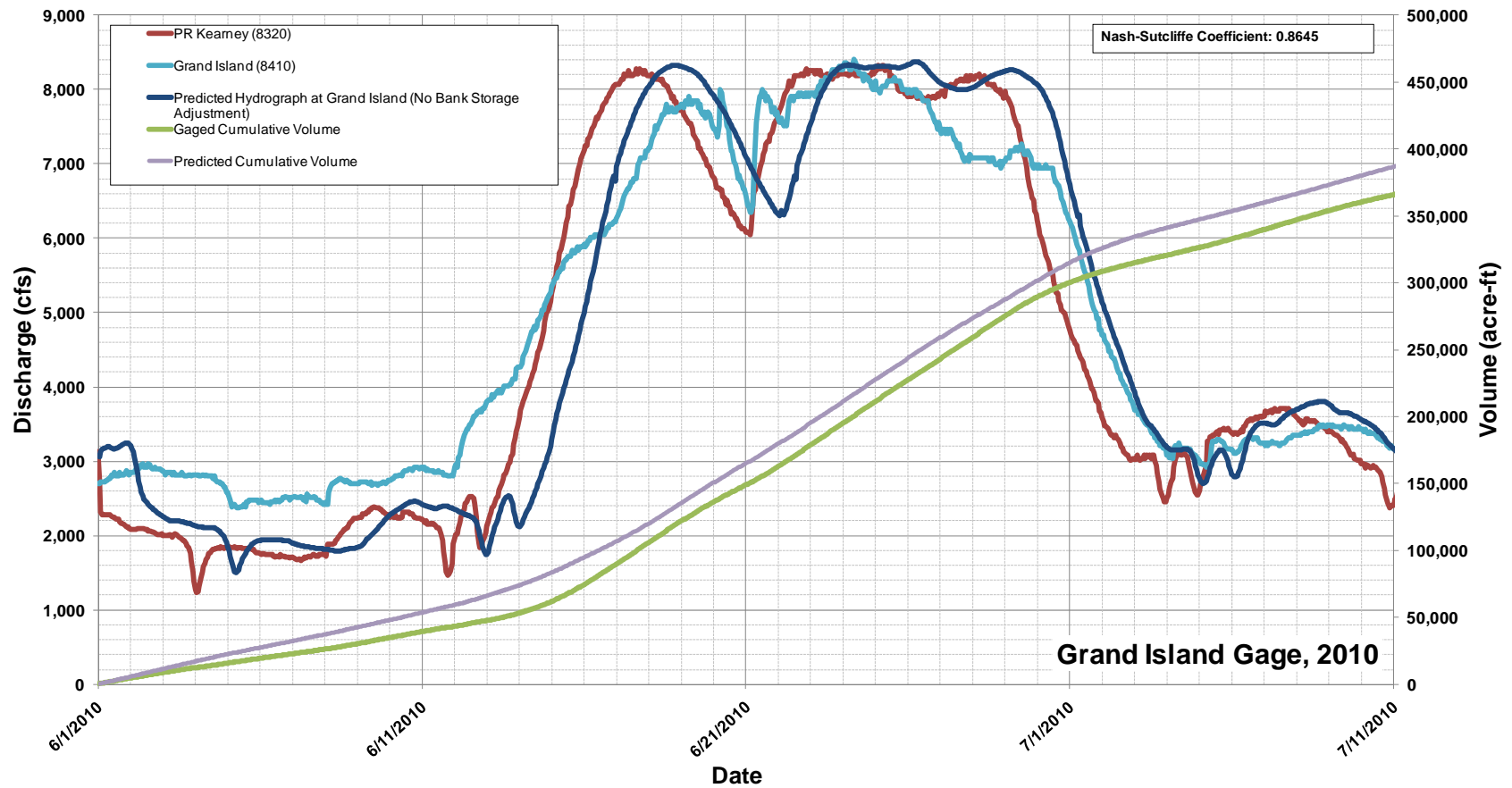
1
 2 Figure 3.36: Comparison of predicted and measured hydrographs at the Kearney gage for the 2010 event. Also shown is the cumulative water
 3 volume.
 4



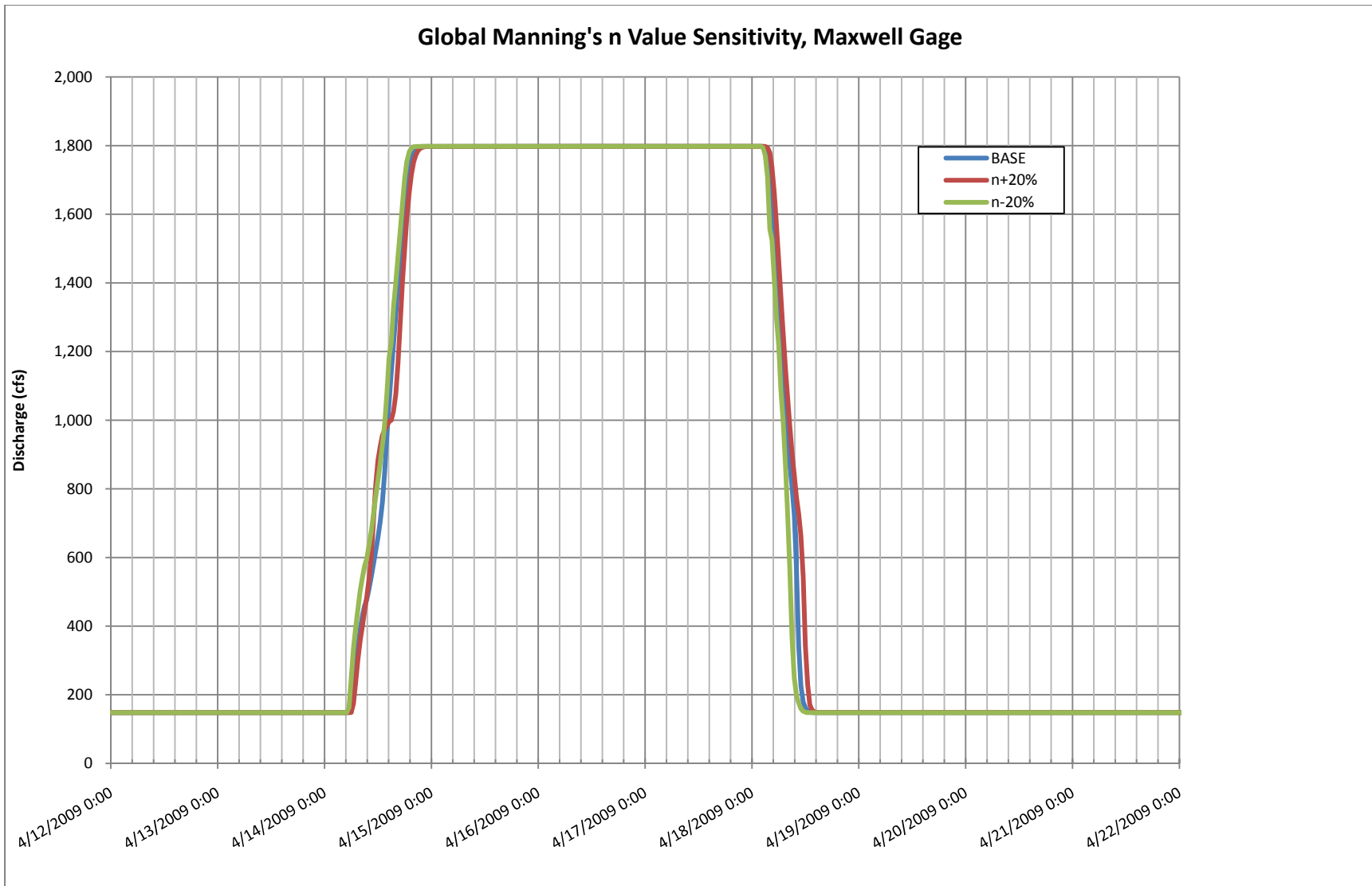
1
 2 Figure 3.37: Comparison of predicted and measured hydrographs at the Grand Island gage for the 2009 event. Also shown is the cumulative
 3 water volume.
 4



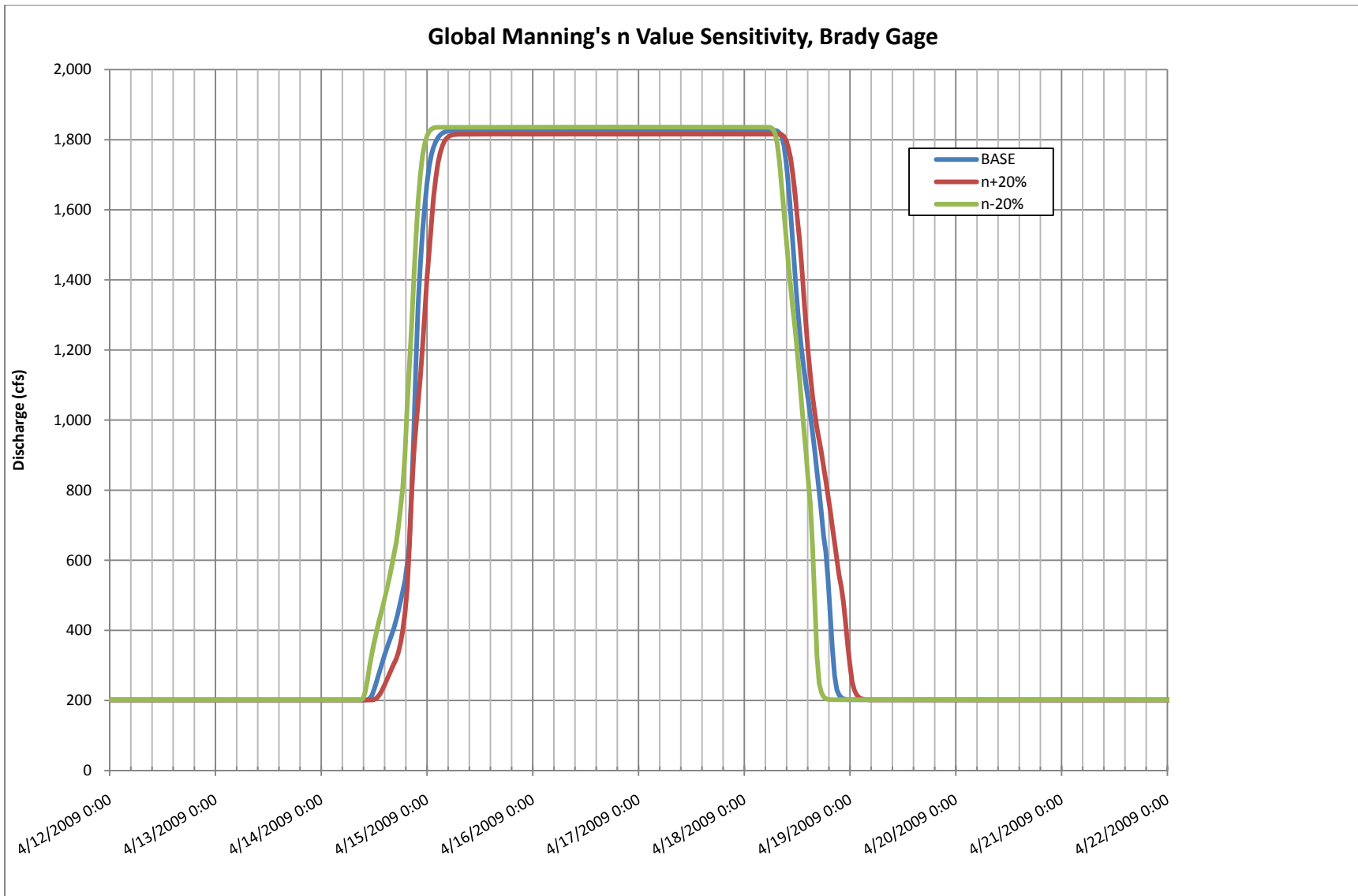
1
 2 Figure 3.38: Predicted Comparison of predicted and measured hydrographs at the Grand Island gage for the 1998 event. Also shown is the
 3 cumulative water volume.
 4



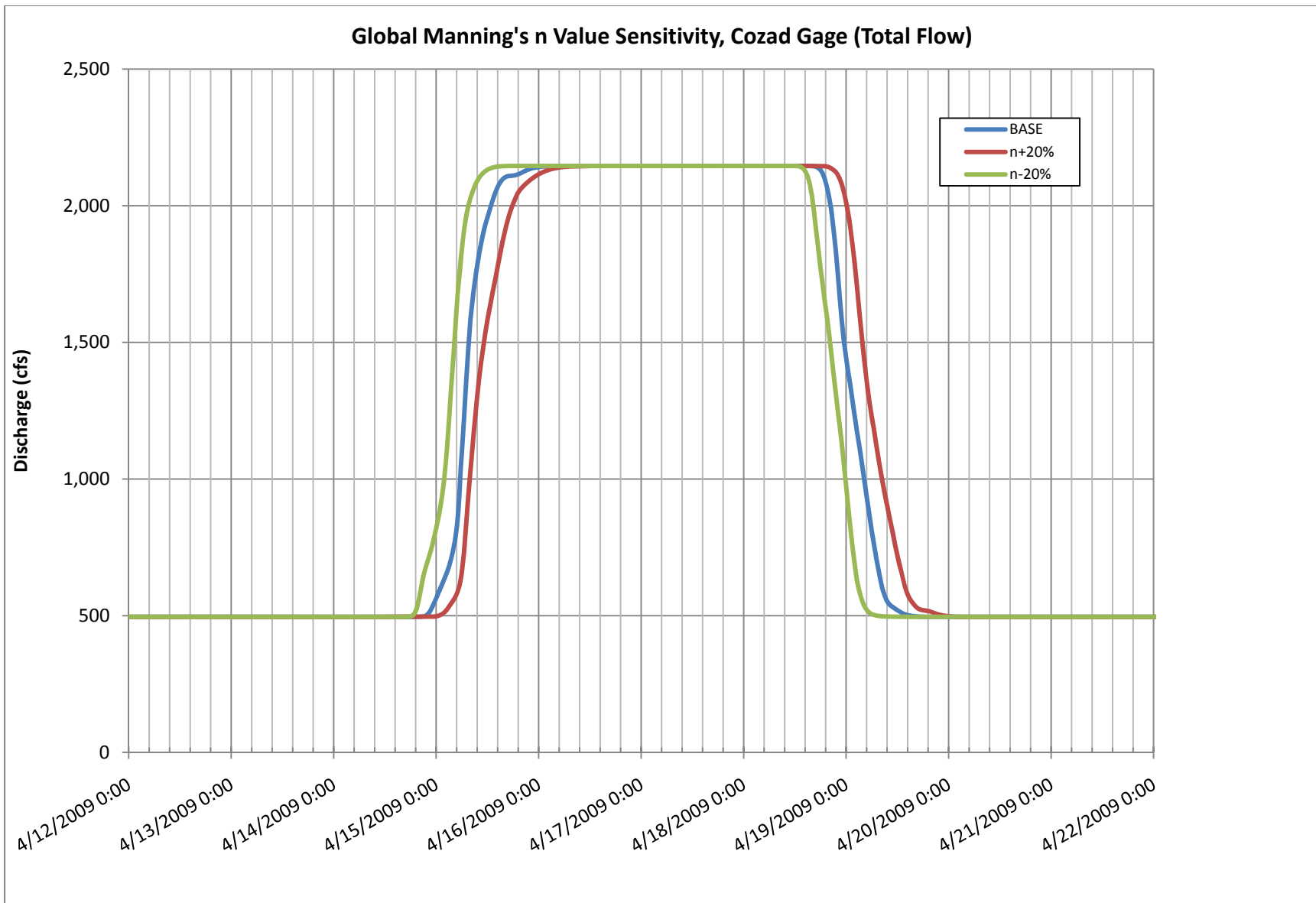
1
 2 Figure 3.39: Comparison of predicted and measured hydrographs at the Grand Island gage for the 2010 event. Also shown is the cumulative
 3 water volume.
 4



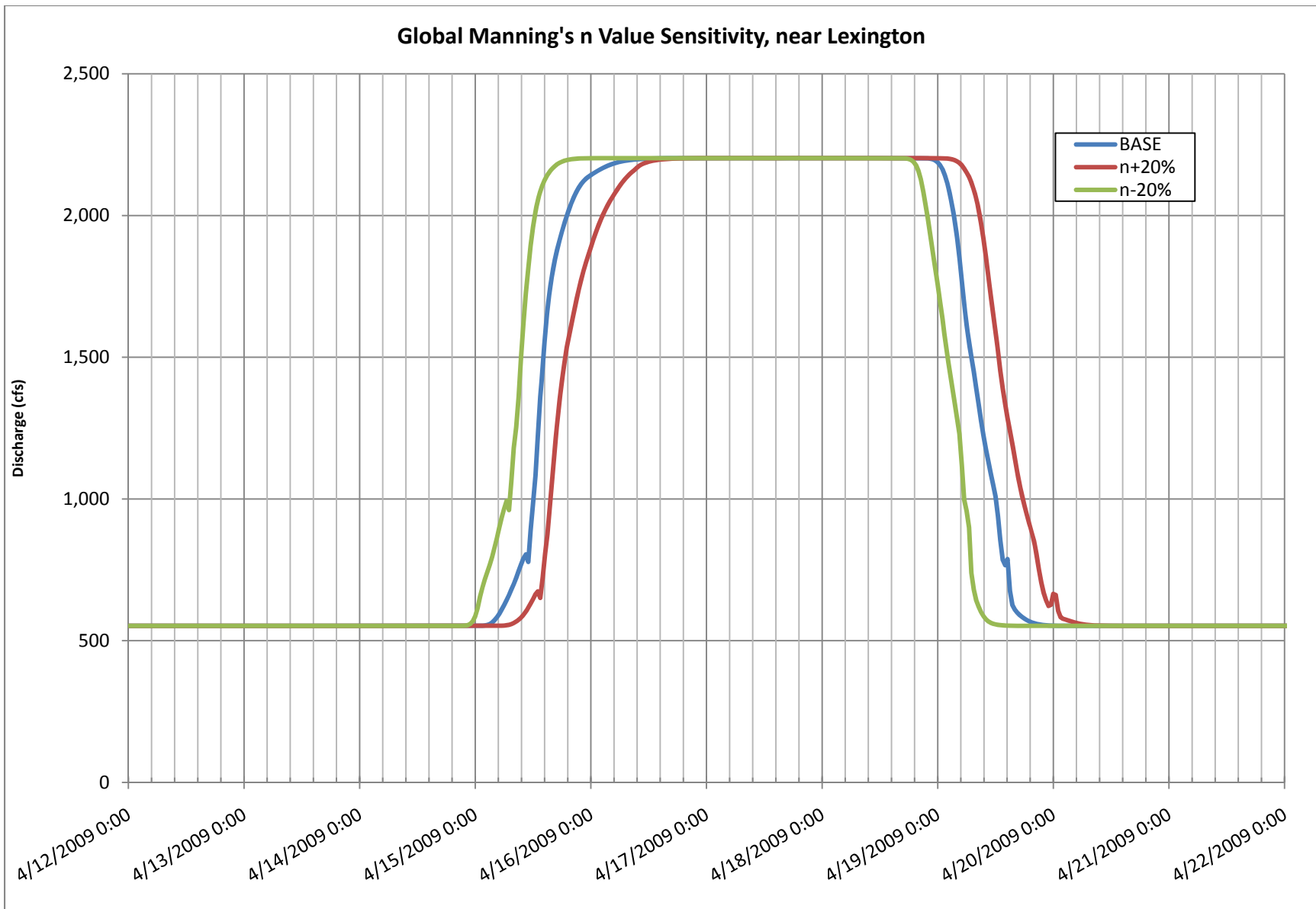
1
2 Figure 3.40: Sensitivity to a global change in Manning's roughness coefficient of 20%, Maxwell Gage



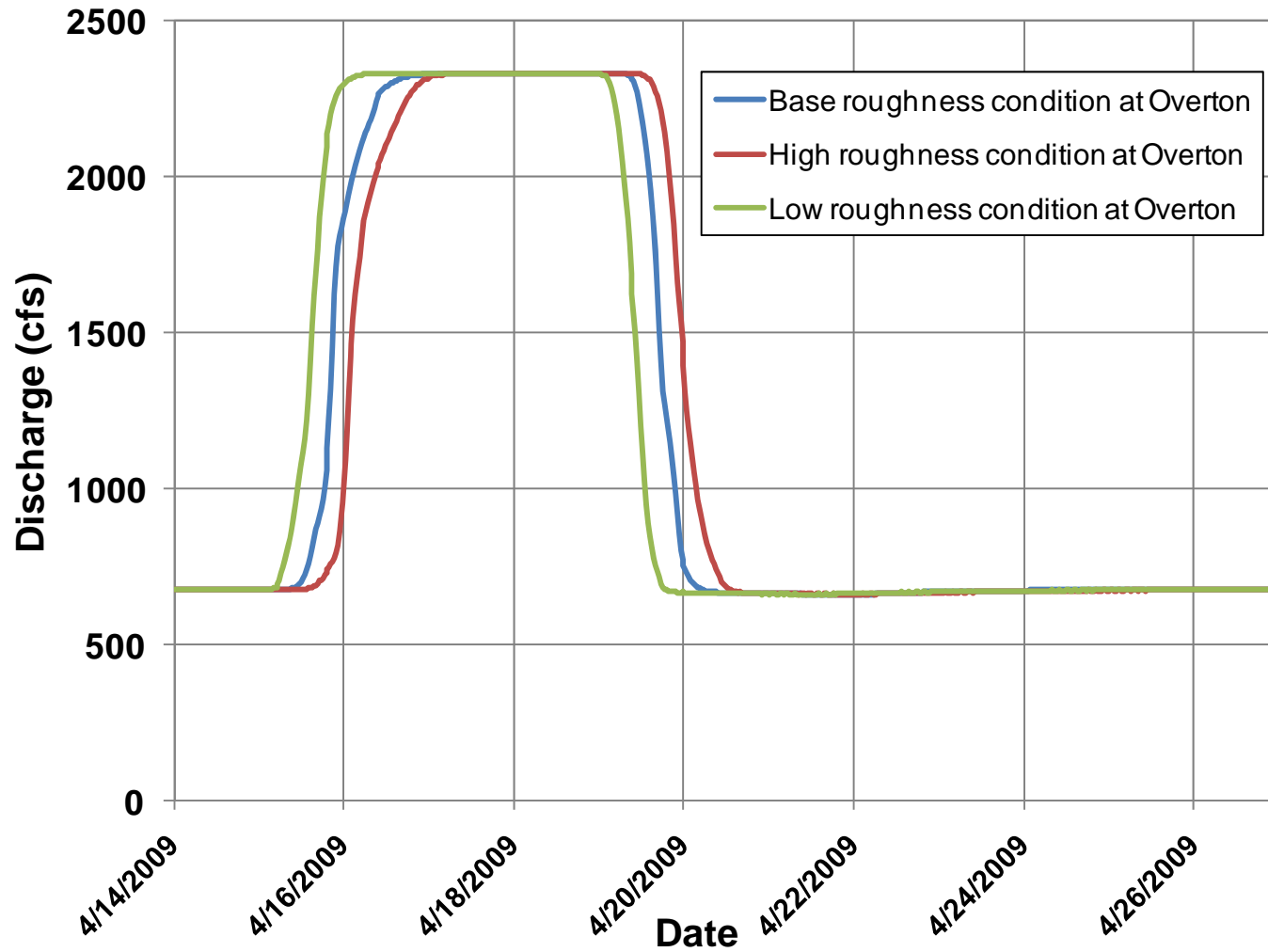
1
2 Figure 3.41: Sensitivity to a global change in Manning's roughness coefficient of 20%, Brady Gage
3



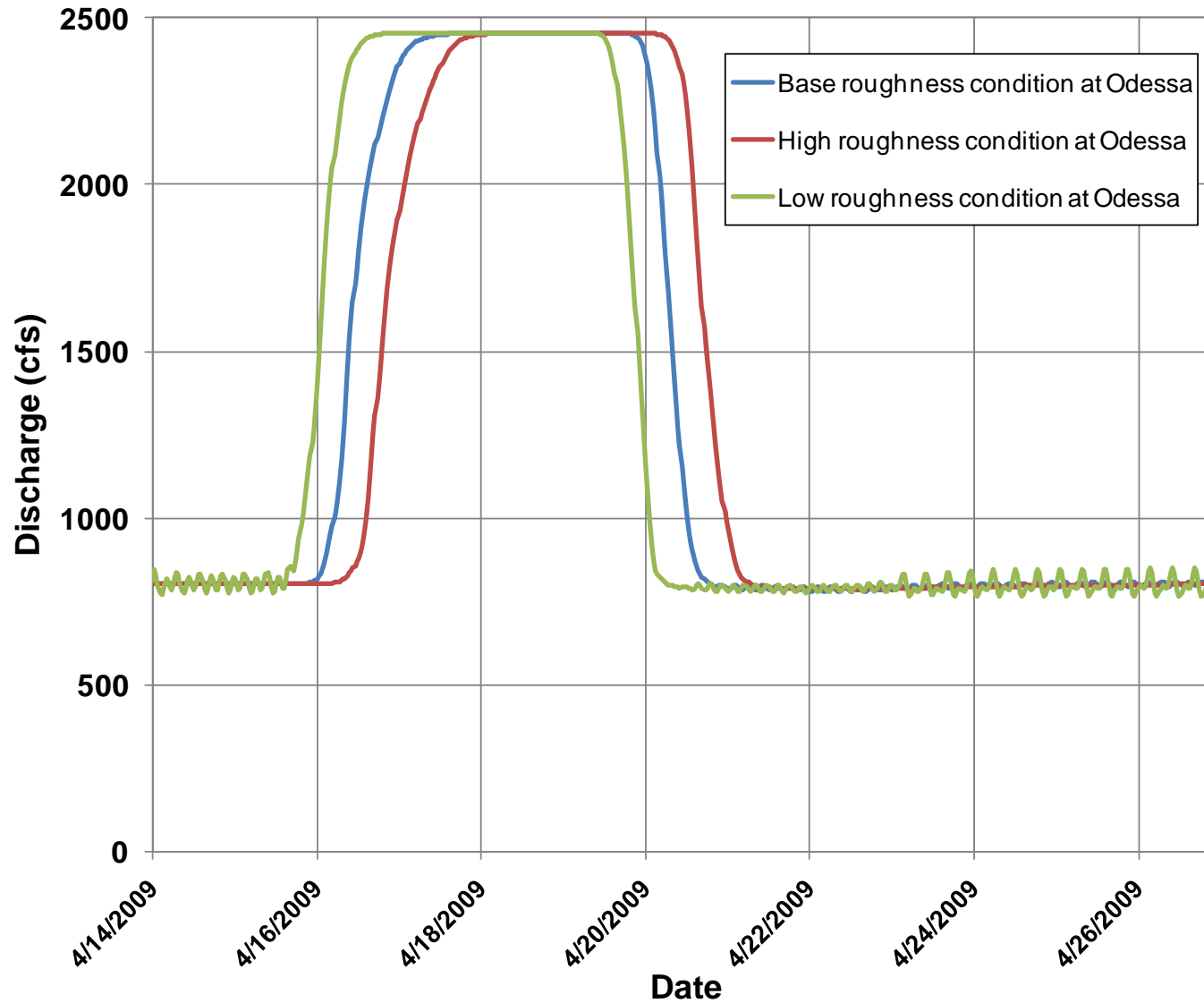
1
2 Figure 3.42: Sensitivity to a global change in Manning's roughness coefficient of 20%, Cozad Gage



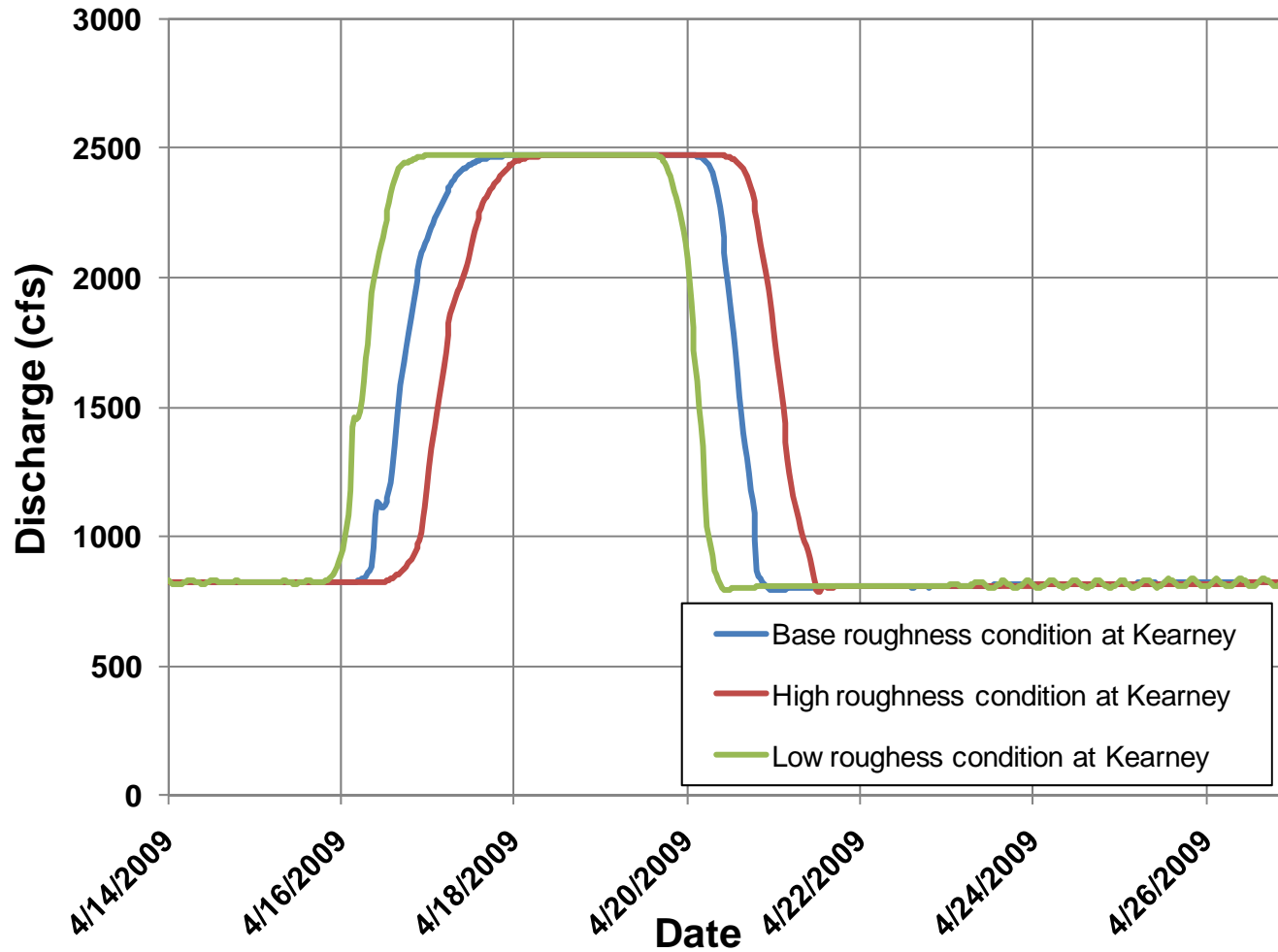
1
2 Figure 3.43: Sensitivity to a global change in Manning's roughness coefficient of 20%, Lexington



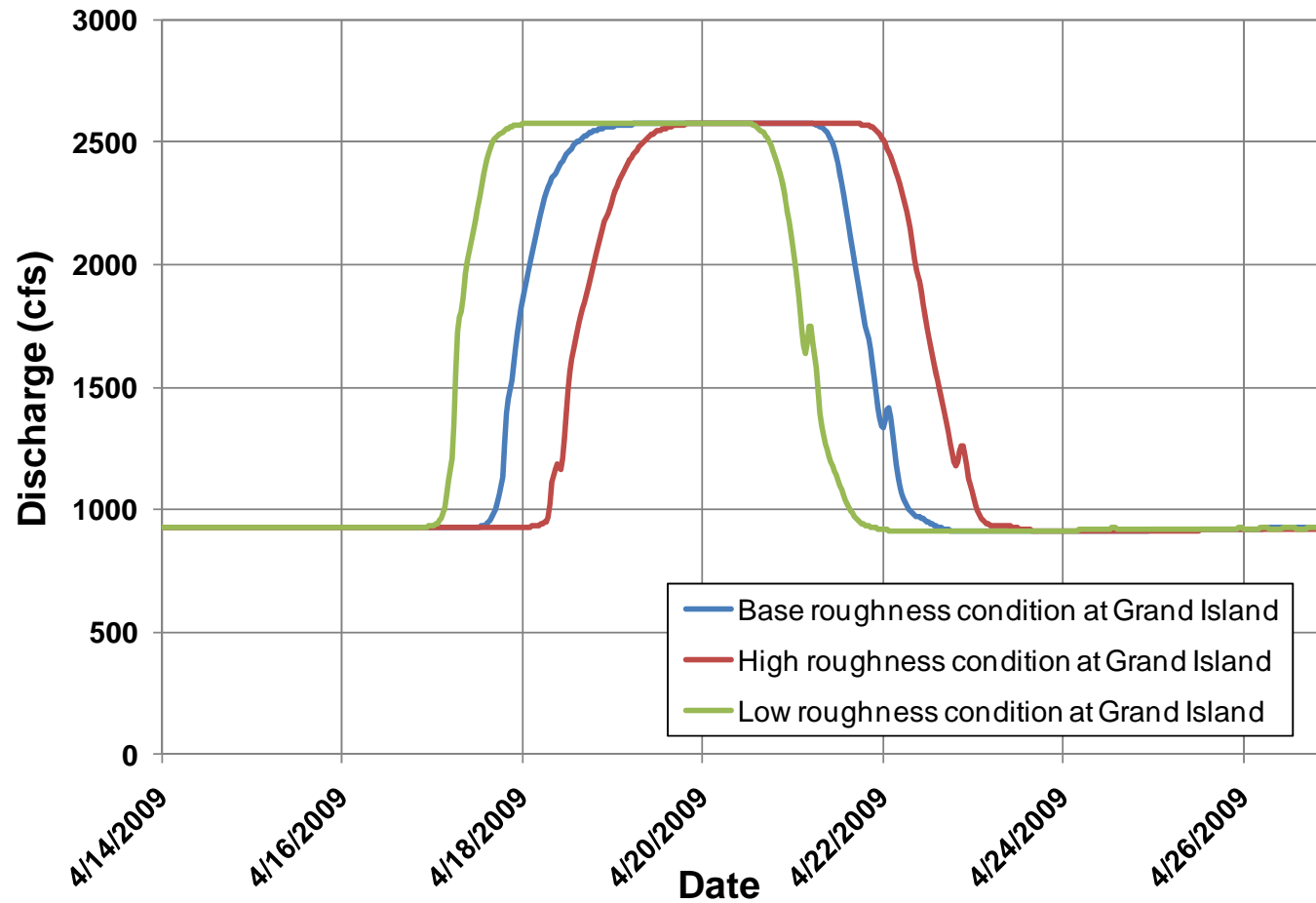
1
2 Figure 3.44: Comparison of hydrographs predicted using base, low and high roughness conditions at the Overton gage.



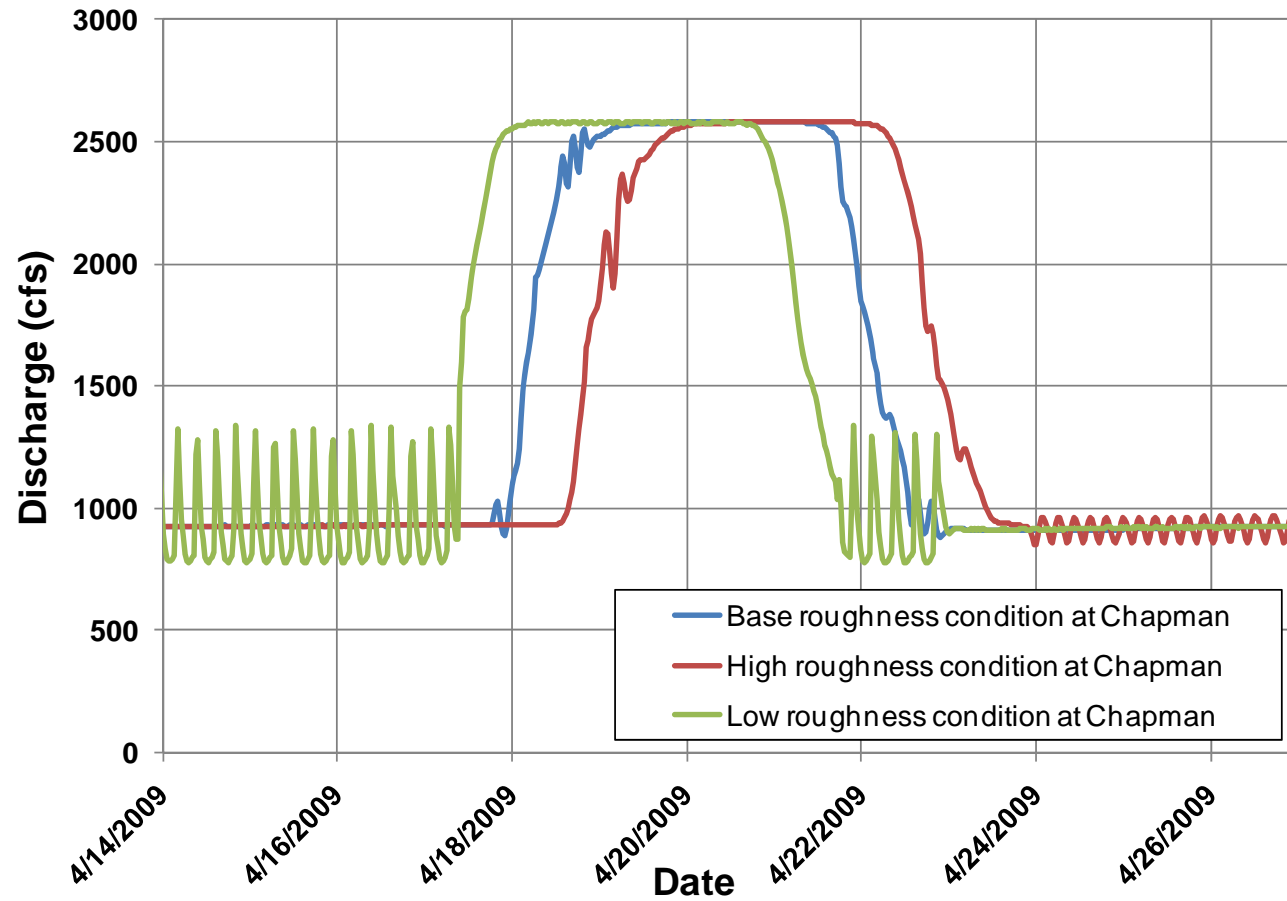
1
 2 Figure 3.45: Comparison of hydrographs predicted using base, low and high roughness conditions at the Odessa gage.
 3



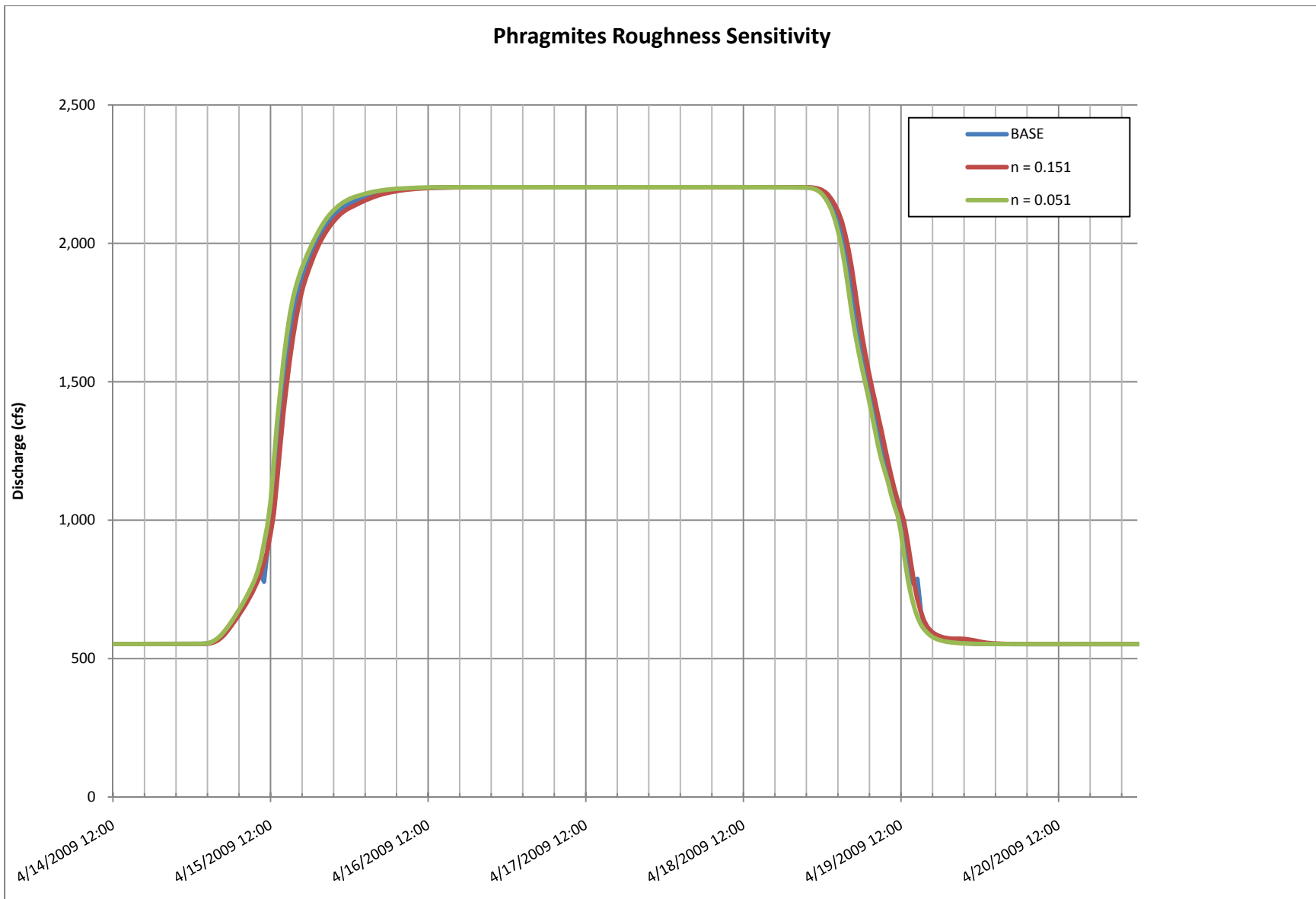
1
2 Figure 3.46: Comparison of hydrographs predicted using base, low and high roughness conditions at the Kearney gage.



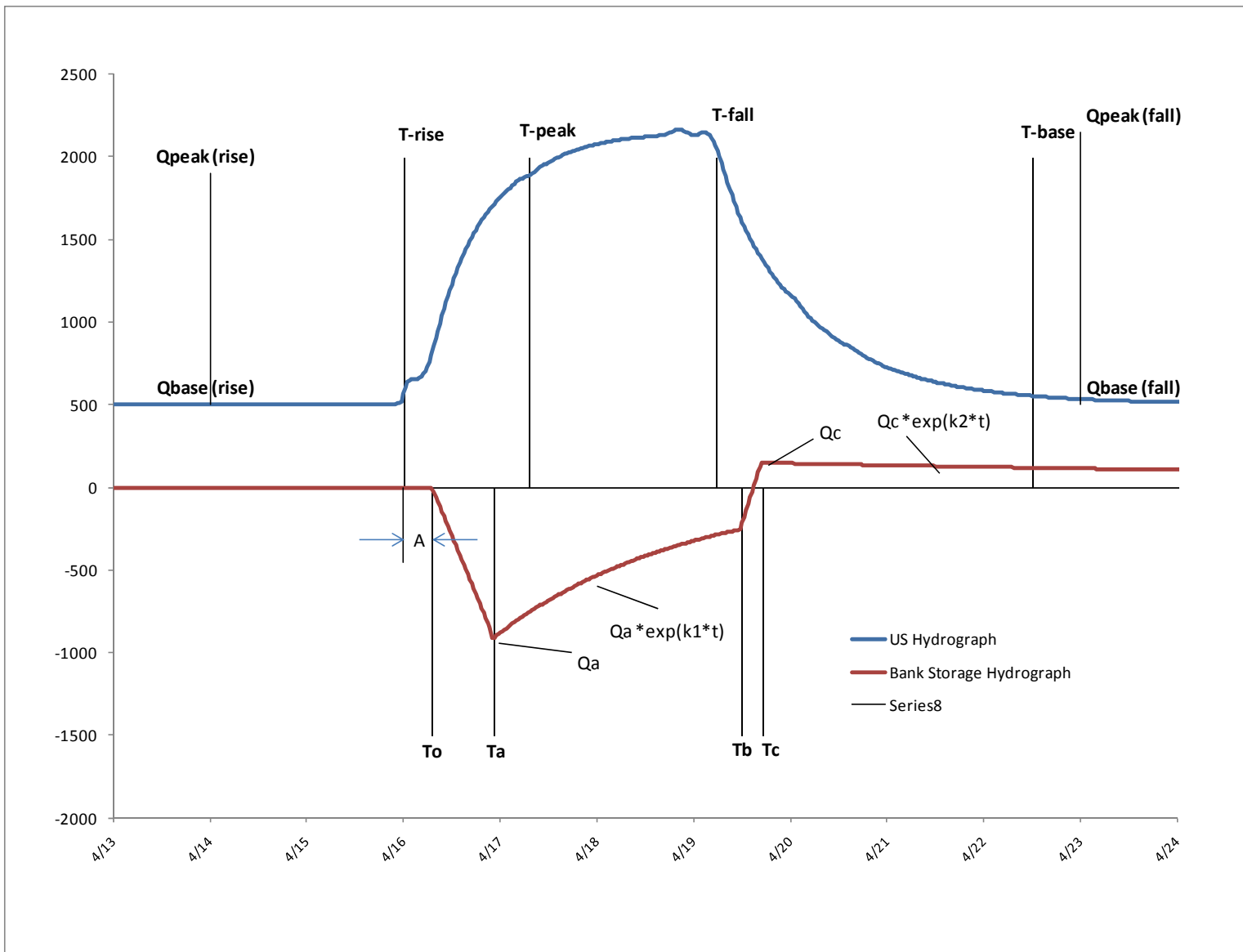
1
2 Figure 3.47: Comparison of hydrographs predicted using base, low and high roughness conditions at the Grand Island gage.
3



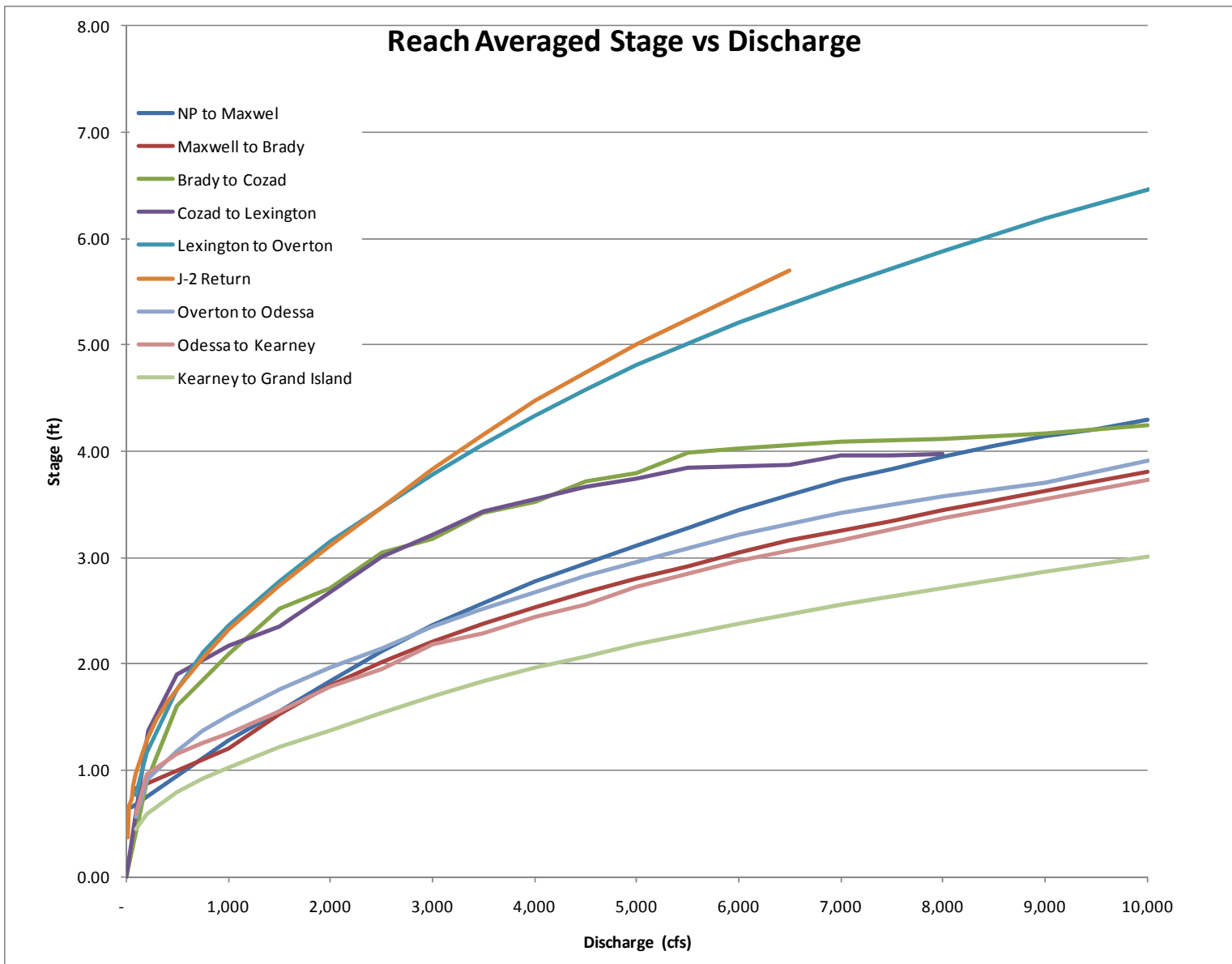
1
2 Figure 3.48: Comparison of hydrographs predicted using base, low and high roughness conditions at the Chapman gage.
3



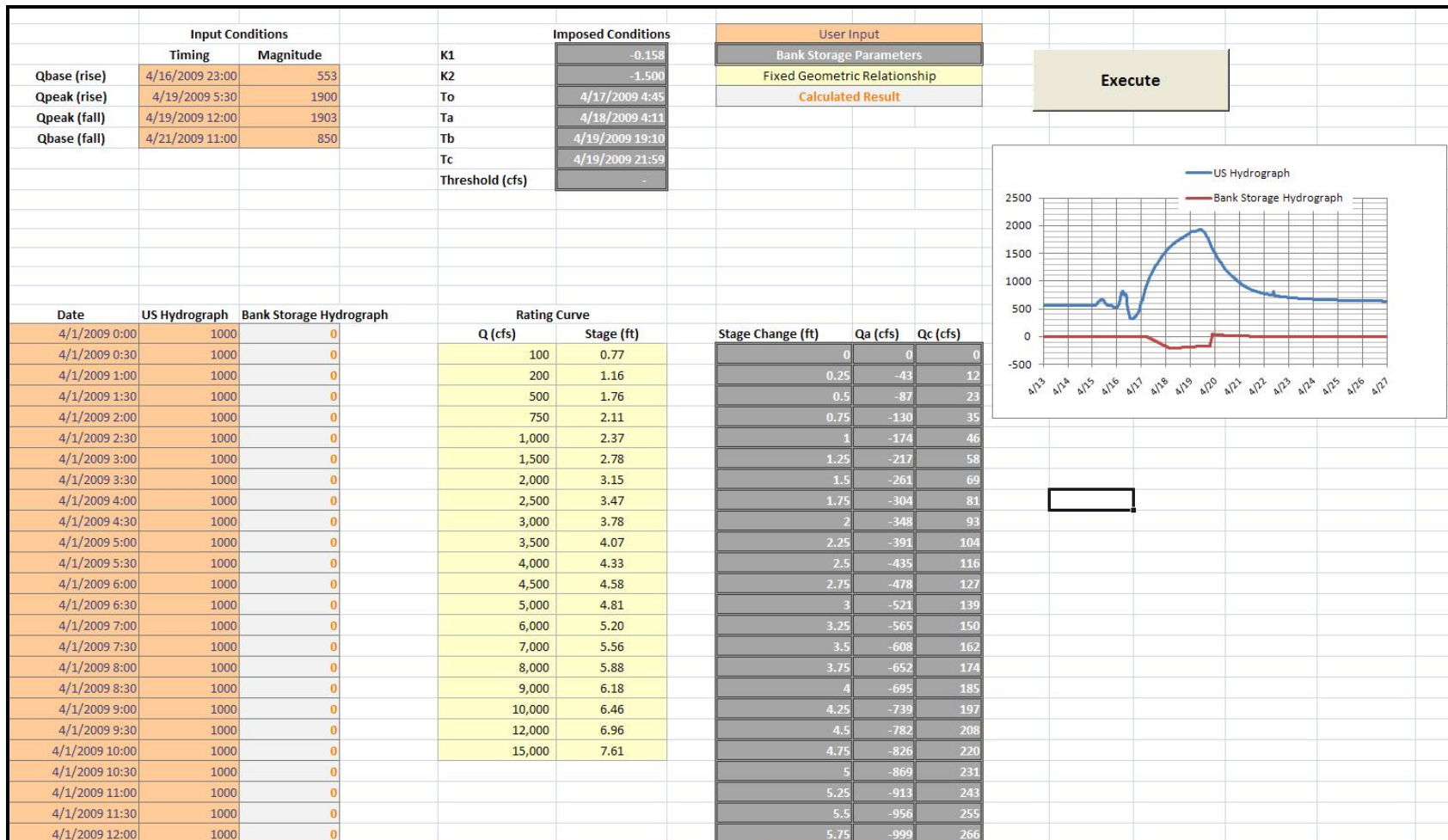
1
2 Figure 3.49: Sensitivity to Phragmites Roughness, at Lexington



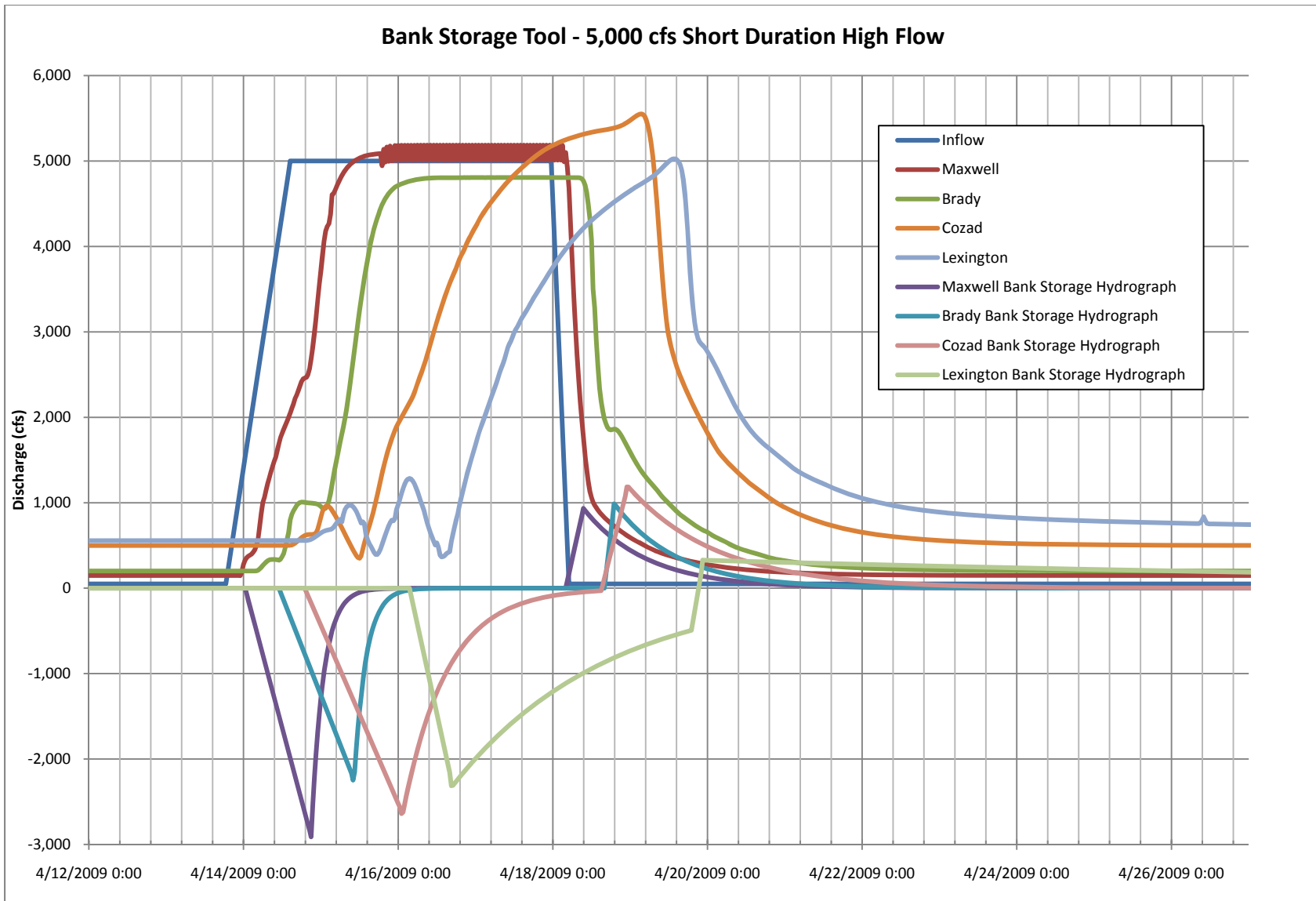
1
 2 Figure 3.50: Example river flow and bank storage hydrographs and the parameters used in to describe bank storage relationship.
 3



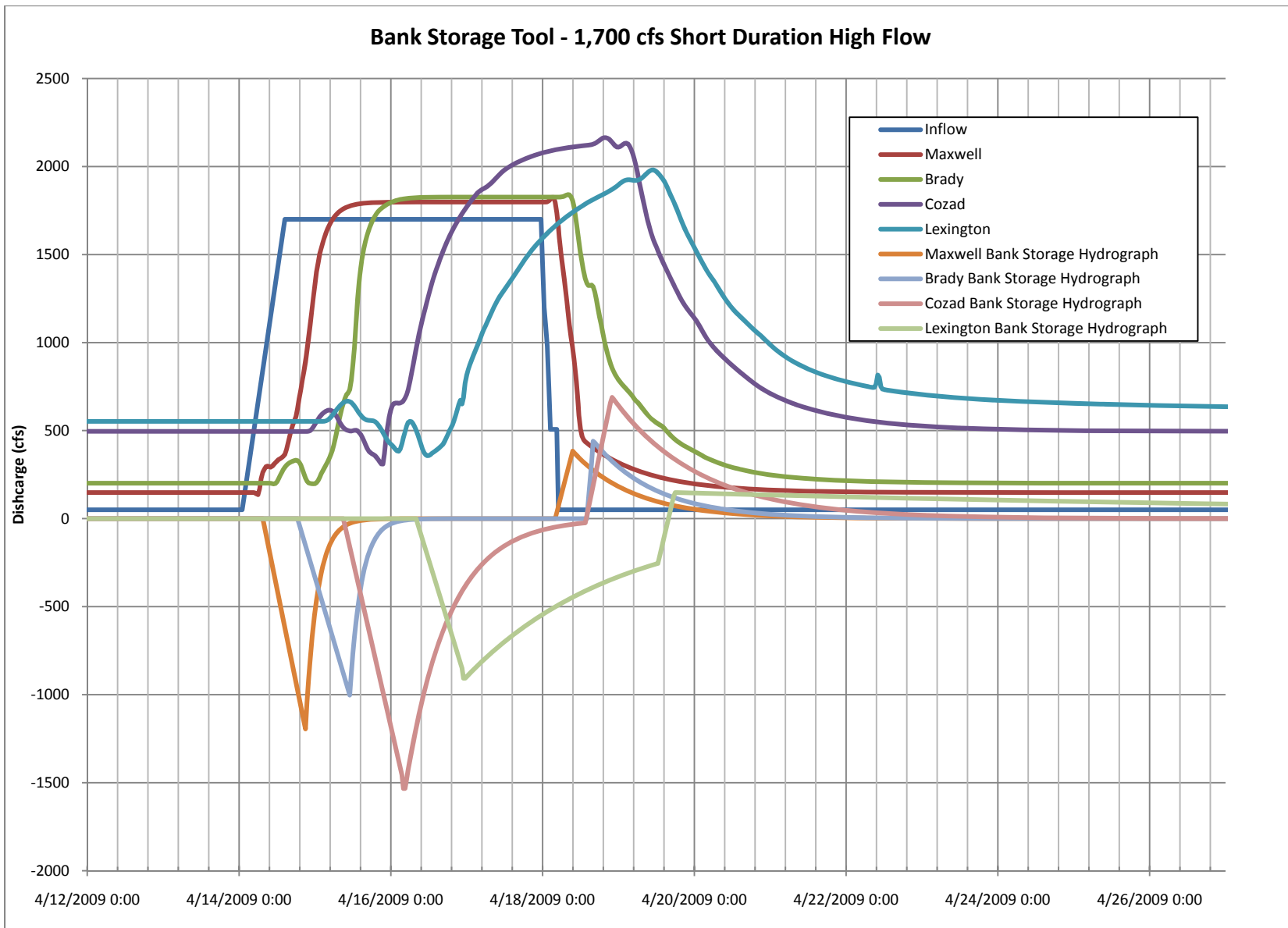
1
2 Figure 3.51: Reach-averaged stage versus discharge rating curves for each of the bank storage reaches



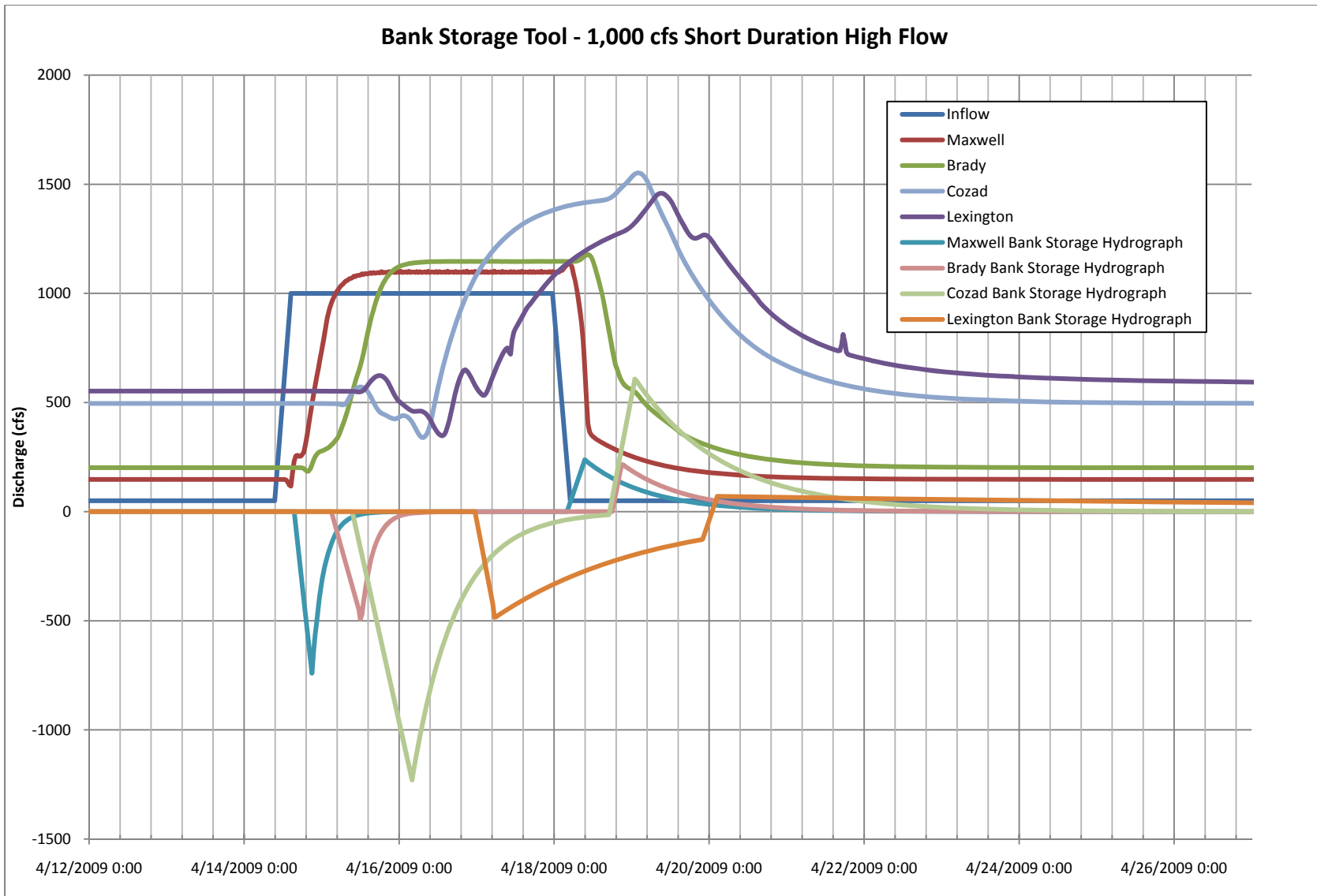
1
2 Figure 3.52: Example of the bank storage tool that was developed to calculate the bank storage hydrograph for each reach.
3



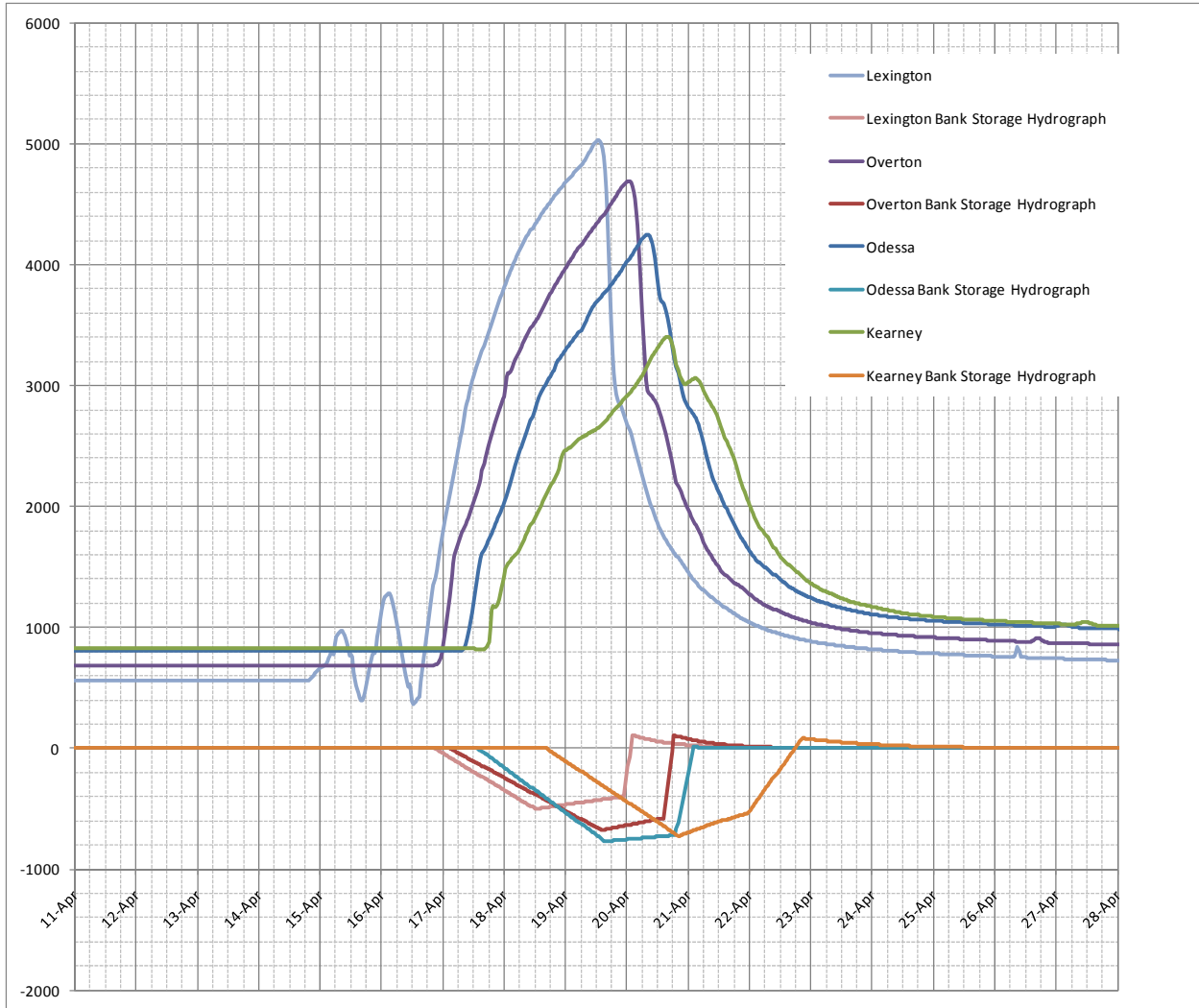
1
2 Figure 3.53: Pulse Magnitude Sensitivity, 5,000 cfs Short Duration High Flow Hydrograph



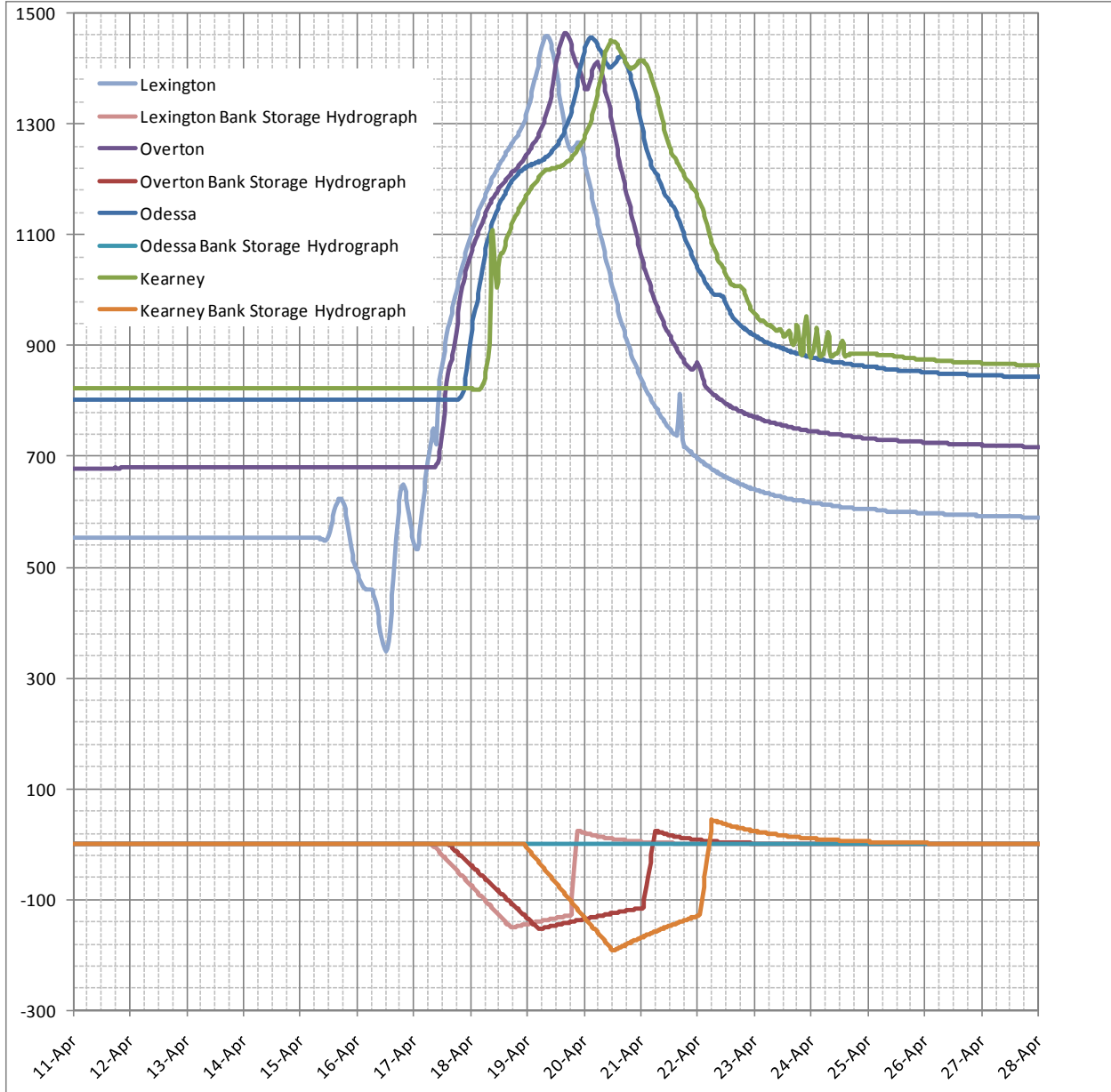
1
2 Figure 3.54: Pulse Magnitude Sensitivity, 1,700 cfs Short Duration High Flow Hydrograph



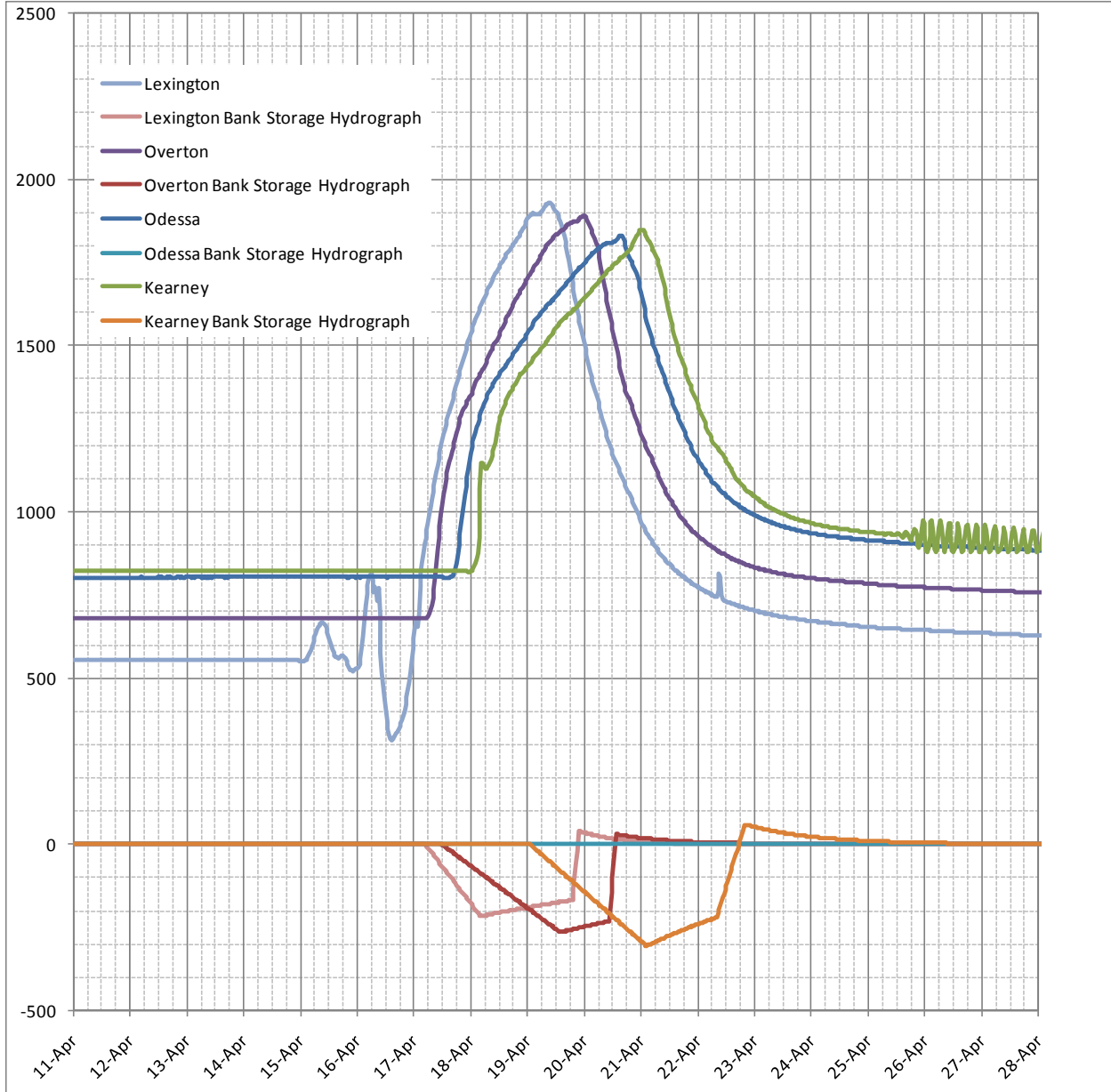
1
2 Figure 3.55: Pulse Magnitude Sensitivity, 1,000 cfs Short Duration High Flow Hydrograph
3



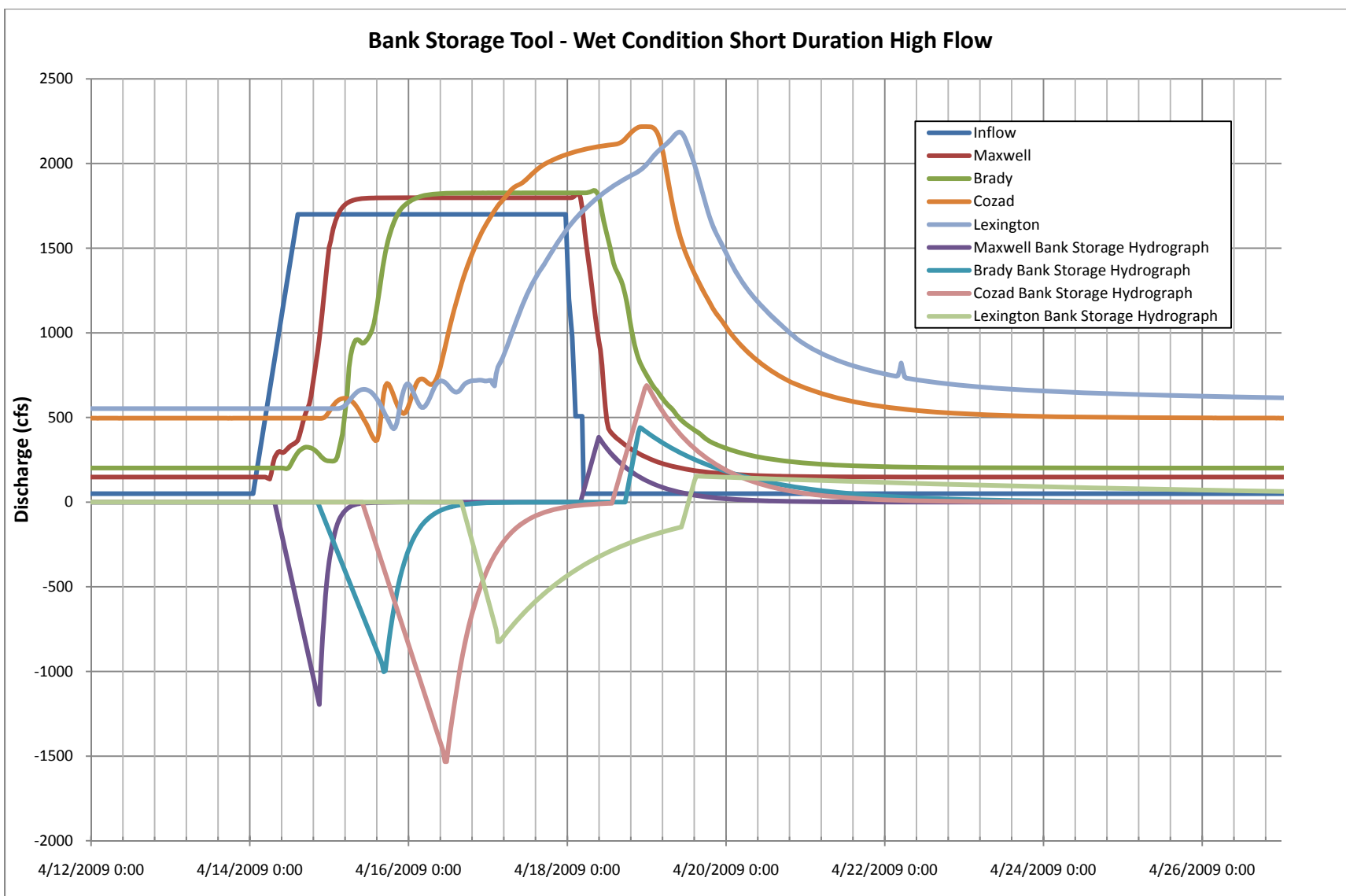
1
2 Figure 3.56: Predicted progression of the 5,000-cfs pulse from Lexington to Kearney.
3



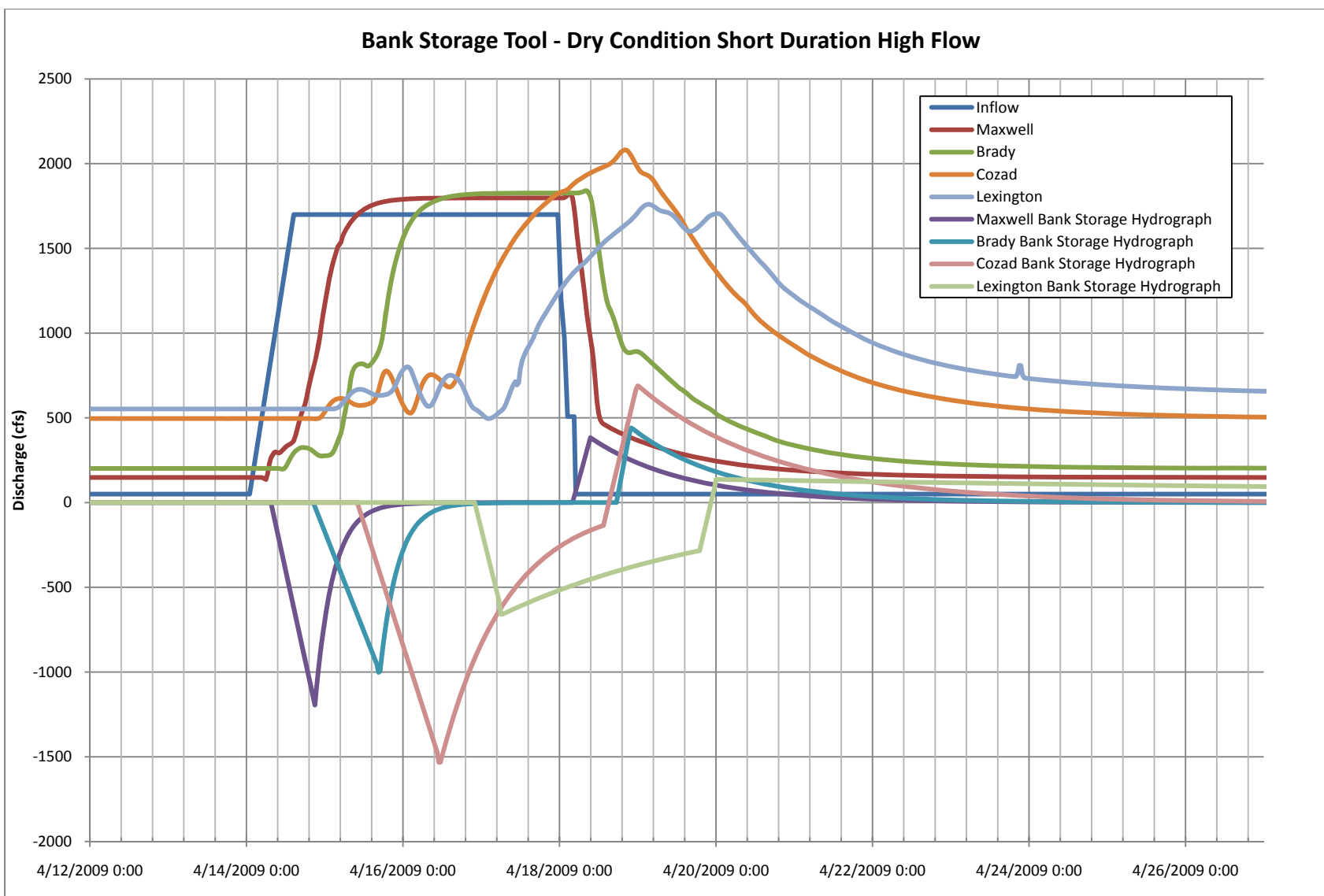
1
2 Figure 3.57: Predicted progression of the 1,000-cfs pulse from Lexington to Kearney.



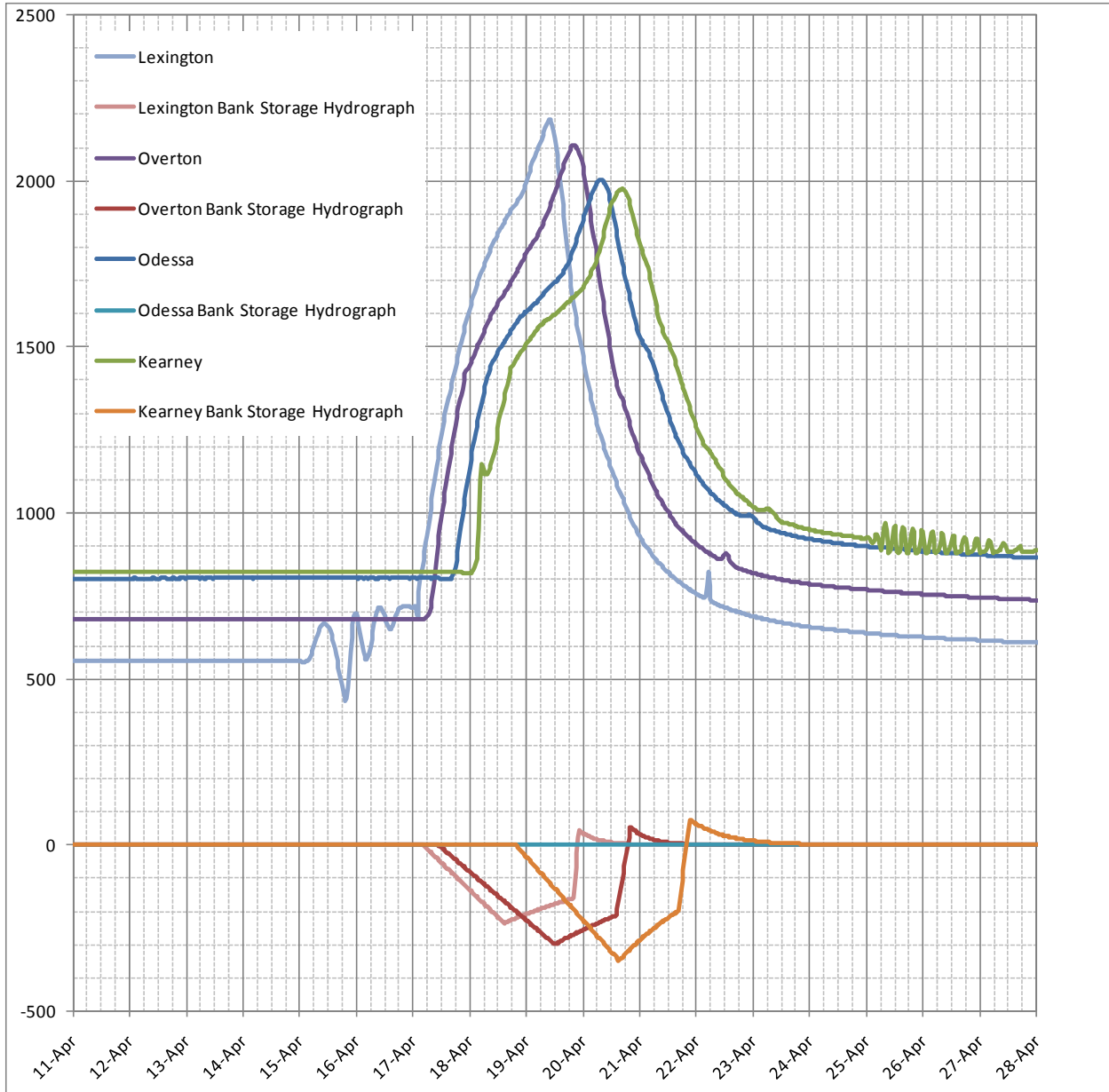
1
2 Figure 3.58: Predicted progression of the 1,700-cfs pulse from Lexington to Kearney



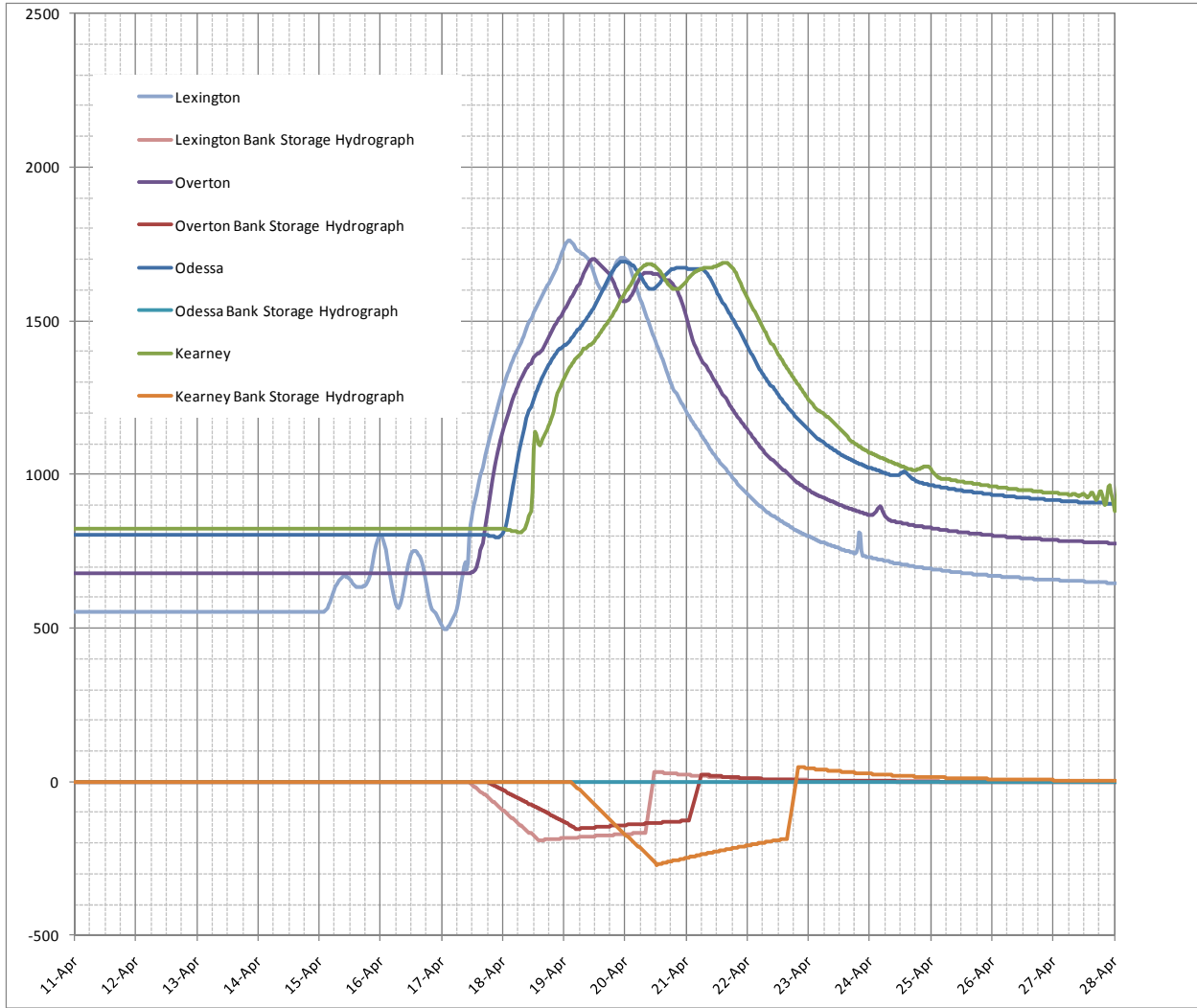
1
2 Figure 3.59: Bank Storage Sensitivity to Wet Antecedent Condition, 1700 cfs Short Duration High Flow Hydrograph



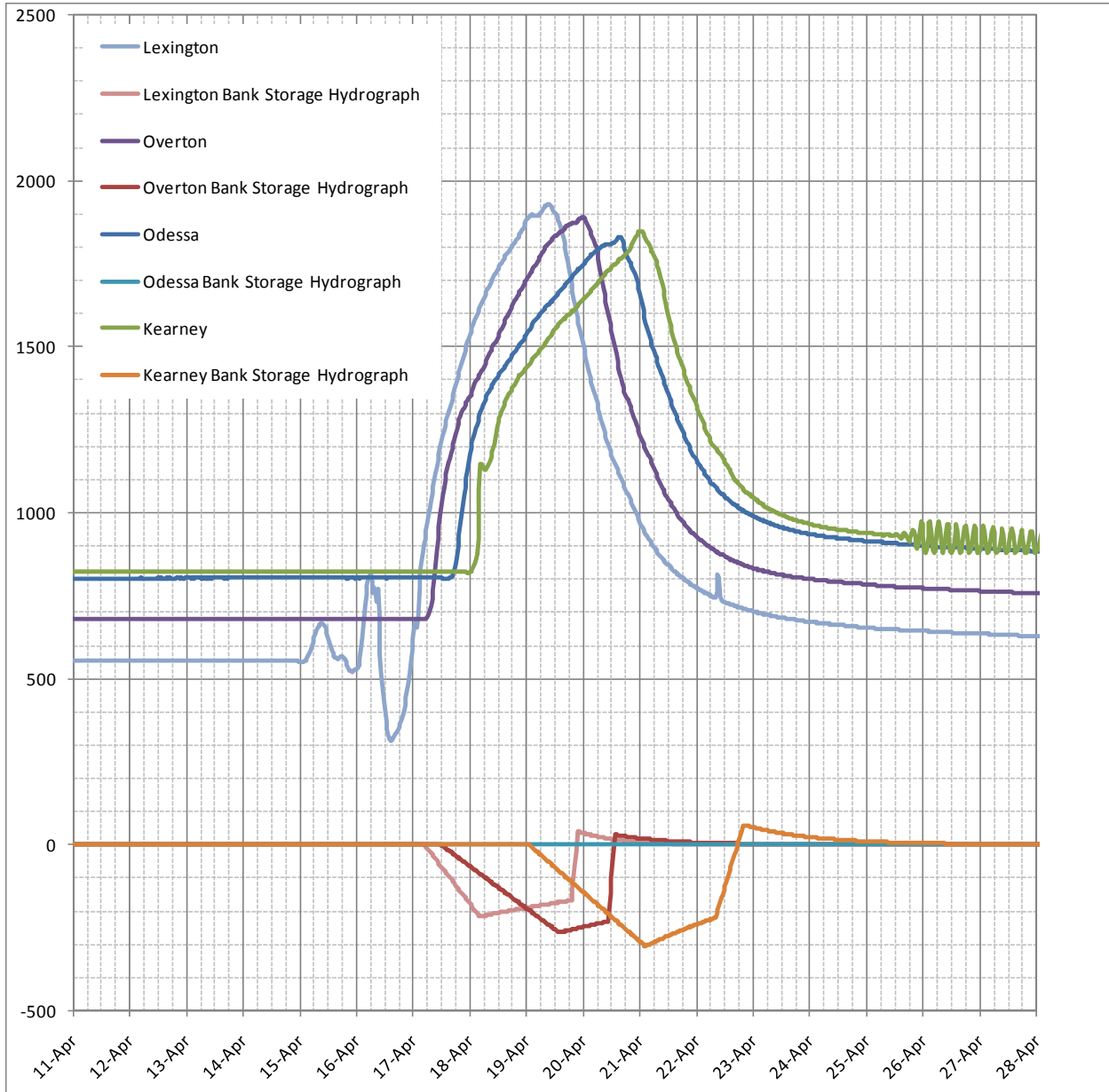
1
2 Figure 3.60: Bank Storage Sensitivity to Dry Antecedent Condition, 1,700 cfs Short Duration High Flow Hydrograph



1
2 Figure 3.61: Predicted progression of the 1,700-cfs pulse from Lexington to Kearney with wet
3 Antecedent conditions.



1
 2 Figure 3.62: Predicted progression of the 1,700-cfs pulse from Lexington to Kearney with dry Antecedent
 3 conditions
 4



1
 2 Figure 3.63: Predicted progression of the 1,700-cfs pulse from Lexington to Kearney with typical
 3 Antecedent conditions.
 4



4. Sediment-Transport Model

A sediment-transport model was developed for the portion of the project reach between Lexington Bridge and Chapman, and a separate model was developed for the approximately 10-mile long “Choke Point” reach of the North Platte River in the vicinity of the City of North Platte. The sediment-transport model was developed using HEC-6T (version 5.13.22 08p; MBH, 2010), a sediment-transport program that uses algorithms similar to the Corps’ HEC-6 and HEC-RAS (Version 4.1.0, USACE, 2010) sediment-transport module. The overall project reach was subdivided into two separate model reaches to reduce the input and output file sizes, improve model stability, and reduce the model run time. The upstream model segment extends from River Mile (RM) 255 to RM 222 and spans the reach between about 4 miles above Lexington Bridge to about 2 miles below Odessa Bridge (Figures 4.1a and 4.1b). This model is similar to the HEC-RAS sediment-transport model that was developed for the Program’s Sediment Augmentation Feasibility Study (Tetra Tech, 2010), but there are a number of important differences that are summarized in the following sections. The downstream model segment extends from RM 222 to RM 156 and extends from the downstream limit of the upstream model segment to just below the 8 Road Bridge near Chapman (Figures 4.1c through 4.1f). The separate North Platte model extends from about 5.5 miles upstream from the U.S. Highway 83 Bridge to the Tri-County Diversion Structure (Figure 4.1g). Figures 4.2a through 4.2c are schematic diagrams of the models showing the model segments, control points, and inflow/outflow locations.

HEC-RAS and HEC-6T Model Limitations

A number of limitations are associated with the HEC-RAS sediment-transport module, as outlined in Appendix B. Of these limitations, perhaps the most significant limitation involves the inability of HEC-RAS to compute flow-sediment distributions in split flow reaches around islands. A recent beta version of HEC-RAS (version 4.2) is currently being developed, and includes the capability of performing the flow and sediment distribution calculations at split flow junctions, but this version is not currently available to the public. The HEC-RAS developers, however, did make this version available for this project to evaluate the potential for using the beta version. To perform this evaluation, simplified HEC-RAS (version 4.2) and HEC-6T models were developed for the reach of the North Channel of Jeffries Island between Lexington and Overton Bridge, which included two separate split flow “island” reaches (as shown in Figure 4.1g). The models were executed over the 12.5 year period between Water Year 1989 (WY89) and April 1, 2002 using the Yang (sand and gravel) equation and identical geometric, bed sediment reservoir, hydrologic, and boundary condition input. The HEC-6T model executed the entire simulation with a run time of about 6 minutes, while the HEC-RAS (beta version 4.2) model encountered a model instability at approximately model year 9, after a model run time of about 18 hours. Because the HEC-RAS model encountered an instability, a direct comparison of the results from the two models is not available. However, a comparison of the results reported at the simulation time associated with the HEC-RAS error indicates the results from the two models are similar (Figure 4.3).

Model Development

Model Structure and Geometry

Cross-sectional Geometry

The cross-sectional geometry was developed using the geometry in the calibrated HEC-RAS steady state models. HEC-RAS allows for a number of options to limit the conveyance along a cross section, including multiple ineffective flow areas, blocked obstructions, and levees. HEC-6T provides only two options, including single ineffective flow areas/encroachments (one ineffective flow area or encroachment in each overbank) and left and right conveyance limits. For the ineffective flow areas, HEC-6T is capable of limiting the effective area to the area between the bank stations, or if ineffective flow



1 areas/encroachments are prescribed it adjusts the overbank geometry to match the extent and
2 elevation of the ineffective flow area. It was therefore necessary to adjust the HEC-RAS geometry prior
3 to importing into the HEC-6T model. The following steps were taken to preserve the HEC-RAS geometry,
4 to the extent possible, in the HEC-6T geometry:

- 5
6 1. A modified version of the HEC-RAS model was developed for making the first phase of
7 adjustments. The geometry for this model was adjusted by removing non-permanent ineffective
8 flow areas that were relatively insignificant. For the more significant non-permanent ineffective
9 flow areas, the bank stations were adjusted to reasonably match the elevation of the ineffective
10 flow areas, since HEC-6T is capable of limiting the conveyance area to the area between the
11 bank stations using the X3 Record, which essentially has the same result.
12
- 13 2. The second phase of the adjustment involved modifying the elevation of the geometric points in
14 the overbank to match the elevation of all permanent ineffective flow areas, blocked
15 obstructions, and levees.
16
- 17 3. The last phase of the adjustment involved coding the geometry into HEC-6T format.
18

19 An example of the original (HEC-RAS) steady-state geometry and the geometry that was modified and
20 incorporated into the HEC-6T model is presented in Figures 4.4a and 4.4b.

21
22 To insure the geometric adjustments did not significantly affect the computed hydraulic conditions,
23 WSELs computed by the HEC-6T model were compared to those computed by the calibrated, steady-
24 state HEC-RAS model. To perform this comparison, the HEC-RAS model was executed for the 90-, 50-,
25 10, and 1-percent mean daily flow exceedance levels, with the HEC-RAS optimization feature used to
26 determine the distribution of flows among the various split flow channels in the network. The results
27 from the optimized HEC-RAS model were then used as input for a rigid boundary HEC-6T simulation that
28 was executed for the same flow rates and flow distributions predicted by the HEC-RAS model. In
29 general, the difference between the WSELs predicted by the HEC-RAS and HEC-6T models is less than 0.2
30 feet (Figures 4.5a through 4.5c). Differences of up to 0.8 feet occur at a limited number of locations
31 such as at bridge crossings and at flow junctions above and below islands, and are a result of the
32 following:

- 33
34 1. As discussed below, the HEC-6T and HEC-RAS models involve different bridge modeling
35 methods and energy loss calculations at bridge structures, and
36
- 37 2. The HEC-6T model computes flow distributions by balancing energy at the upstream cross
38 section in each of the split flow reaches below a distributary junction, while HEC-RAS computes
39 the distribution by balancing energy at the common cross section upstream from the junction.
40

41 Since the most significant differences between the WSELs predicted by the steady-state HEC-RAS model
42 and the rigid boundary HEC-6T model occur at these locations, and because the differences are
43 relatively small throughout the remainder of the reach, the changes to the geometry that were
44 necessary for the HEC-6T model appear to be insignificant.

45 **Roughness Values**

46 The HEC-6T models maintain the horizontal variation in roughness that was used in the steady-state
47 HEC-RAS files using the HEC-6T "NX-Record". HEC-6T is capable of compositing the roughness using a



1 variety of methods, including the default method (conveyance weighting in the overbanks and equal
2 velocity computations in the channel) that was used for these models, which is similar to the HEC-RAS
3 compositing algorithms. The roughness coefficients representing a specific vegetation type (i.e.,
4 Phragmites, $n = 0.101$) can be easily changed to represent vegetation clearing either by segment or for
5 the entire model.

6 Cross Section Spacing

7 The entrainment and deposition algorithms that are built into HEC-6T include computations that limit
8 the rate of entrainment or deposition depending on the reach length between cross sections. The
9 characteristic rate of entrainment was incorporated into the HEC-6T source code using empirical data,
10 while the characteristic rate of deposition is based on the particle settling velocity. The varied cross
11 section spacing used in the steady-state hydraulic model should, therefore, not be a significant
12 limitation to the sediment-transport calculations in the HEC-6T model. However, at locations where the
13 cross section spacing is very small (i.e., up- and downstream from bridge structures and at some of the
14 Anchor Point locations), one of the sections was removed to improve model stability.

15 Split Flow Reaches

16 Each of the primary split-flow reaches were coded into the HEC-6T model. HEC-6T is capable of
17 performing island flow calculations (which HEC-6T refers to as closed loop calculations) that distribute
18 the flow and sediment load to split-flow reaches based on an energy balancing procedure. However,
19 because of the complex nature of the split-flow reach connections along the project reach that include
20 splits within splits and “overlapping” islands with split reaches that connect to separate closed loops, it
21 was necessary to simplify the split-flow geometry. The simplified geometry (Figures 4.1 and 4.2) was
22 developed using the following methods:

- 23
24 1. The flow paths were classified as primary flow paths, secondary flow paths, and tertiary flow
25 paths based on the percentage of the upstream flow that is distributed among each split-flow
26 channel (Figures 4.1). Primary flow paths convey more than 50 percent of the inflowing
27 discharge, secondary flow paths carry between 5 and 50 percent of the inflowing discharge, and
28 tertiary flow paths convey less than 5 percent of the inflowing discharge.
- 29
30 2. The HEC-RAS closed loop feature was used to model island flows that included primary flow
31 paths and the most significant secondary flow paths.
- 32
33 3. The flow distribution to less significant secondary flow paths were modeled using the HEC-6T QP
34 Record that removes a percentage of the inflowing water and sediment load based on a split-
35 flow rating curve. The split-flow rating curves were developed using the results from the
36 calibrated steady state model that includes optimized split flows. HEC-6T QL records were then
37 used to insert the computed outflow of water and sediment into the head of the split-flow
38 reach.
- 39
40 4. To improve the stability or executability of the model, it was necessary to assume that some of
41 the shortest and least significant flow paths were transmissive (i.e., the sediment load entering
42 the upstream limit is passed through the reach and delivered to the connecting reach). Since no
43 aggradation or degradation occurs in these reaches, they were removed from the model
44 geometry; however, continuity of flow and sediment is maintained using a QP record at the
45 head of these reaches and a QL record at the confluence with the connecting reach.



1 5. Since tertiary flow paths will not have a significant effect on the overall sediment balance along
2 the project reach, these flow paths were not included in the model geometry.

3 **Infrastructure**

4 Bridges were coded into the model by incorporating the road surface (in the overbanks) and abutments
5 into the cross sectional geometry of the representative bridge section. The bridge deck and piers were
6 not coded into the model since use of the HEC-6T “S-Method” requires elimination of the horizontally
7 varied roughness coefficients, and these coefficients have a more significant effect on the hydraulic and
8 sediment-transport conditions than the bridge piers and deck.

9 **Bed-material Data and the Bed Sediment Reservoir**

10 The control volume of bed material that is available for entrainment and transport is often referred to as
11 the bed sediment reservoir (BSR). The characteristics of the BSR required as input to the model include
12 the initial gradation of the bed material and the size of the control volume.

13 **Gradation of Bed Material**

14 The gradation of the bed material that makes up the bed sediment reservoir was obtained from the
15 Program’s Geomorphology Monitoring Program, which included a number of sediment samples
16 collected at the Anchor Point cross sections. At each Anchor Point cross section set, a composite bed
17 material sample was developed using selected representative bed material samples; samples that
18 appeared to be anomalously fine or coarse compared to the other samples at that location were not
19 included in the composite gradation. Median grain sizes of the samples in the primary channel ranged
20 from about 0.7 to about 2.1 mm (Figure 4.6). Distance weighted gradations were computed at the up
21 and downstream limit of each model segment, and were coded into the model along with the composite
22 samples at the appropriate cross section.

23
24 Bed material information for the North Platte model was obtained from bed material samples collected
25 by The Flatwater Group in 2010 for this study, and included 3 samples that were located near the U.S.
26 Highway 30 Bridge, near the U.S. Highway 84 Bridge, and near the upstream limit of the project reach
27 (Figure 4.1g). Individual grab samples were taken by along the cross section sampling location. These
28 samples were mixed to develop one composite sample at each location. Median grain sizes for the
29 composite samples ranged from about 0.5 to 0.6 mm and included between 10 and 15 percent gravel
30 (Figure 4.7).

31 **Bed Sediment Reservoir Dimensions**

32 The extent (lateral limits) of the bed sediment reservoir was determined using the results from the
33 steady state model, repeat cross section surveys (BOR, 2006) and available aerial photography to assess
34 the active portions of each cross section. A depth of 30 feet was assigned to the bed sediment reservoir
35 to insure down cutting was not artificially limited.

36 **Hydrologic Data**

37 Hydrologic data used to develop the Central Platte model input files included measured mean daily
38 flows at USGS and NDNR gages, the J-2 Return, the Kearney Canal Diversion, and the Kearney Power
39 Return. The simulation period for the baseline model run extends from October 1, 1989, through April
40 1, 2002. This period was selected to be consistent with the HEC-RAS model simulation that was
41 developed for the Sediment Augmentation Feasibility Study, and because comparative cross-sectional
42 survey data are available over this period. The selected period includes a series of wet and dry water
43 years, with annual volumes at the Overton gage ranging from about 610,000 ac-ft in 1991 to 1,900,000
44 ac-ft in 1998 and mean daily flows at the Overton gage ranging from about 140 to 14,100 cfs. Although



1 there are also active gages in the middle and south channels at Cottonwood Ranch, these gages are
2 relatively new and the periods of record are too short to be of use in this simulation.
3 Since recorded flow data are available only at specific points within the project reach and the gains and
4 losses can be significant, it was necessary to estimate the flow distribution along the reaches between
5 the gages. In the upstream reach between Lexington Bridge and the downstream end of Jeffrey Island
6 that includes the North Channel along Jeffrey Island, the flow was estimated as the difference between
7 the recorded flows at Overton and the inflows from the J-2 Return. In the reach between the Overton
8 and Odessa gages, flows are affected by tributary contributions, the Kearney Diversion, and other gains
9 and losses. Inflows and outflows that were developed for the Sediment Augmentation baseline HEC-
10 RAS model were used as input for the upstream HEC-6T model. In the downstream model (Odessa to
11 Chapman), the Kearney Power Return is the only measured inflow, so the gains and losses between the
12 gages at Odessa, Kearney and Grand Island were computed by subtracting the measured outflows from
13 the measured inflows. The resulting gains and losses for each of the two reaches (Odessa to Kearney
14 and Kearney to Grand Island) were then distributed at 10 locations along each reach. Because these
15 gains and losses are in some cases significant, primary channel reaches that convey the highest
16 percentage of the overall flow were selected for inputting the gains and losses. These reaches included
17 RM222-220 and RM220-218 in the reach between Odessa and Kearney, and RM200-195 in the reach
18 between Kearney and Grand Island.

19
20 As discussed below, the information that is available to calibrate the North Platte model is somewhat
21 limited, and includes measurements at the U.S. Highway 83 gage (DNR Gage no. 6693000) as well as a
22 comparison of the model geometries from the SEH model (SEH, 2008) that represents conditions
23 ranging from 2002 through 2007 conditions and from the 2010 conditions model developed for this
24 study. The North Platte model was, therefore, executed over the available period of record from
25 WY2002 to WY2009 using the measured mean daily flows at the Highway 83 Gage. The flow
26 contribution from Lincoln County Drain no. 1, which delivers flows about 1 mile upstream from the
27 Highway 83 gage, was accounted for using measured mean daily flows from DNR Gage no. 6692500. As
28 such, the upstream inflow to the model was computed as the difference between the mean daily flow at
29 the Highway 83 Gage and the flow from the drain. It should also be noted that because no thalweg
30 survey was available for the North Platte model reach (as was available in the Central Platte model
31 reaches), the simulation period included a “warm-up” period that preceded the measured flow period.
32 This warm-up period was developed to allow the assumed model geometry to adjust prior to the
33 measured flow period, and included a 50 day hydrograph with flows ranging from 400 cfs to 1,000 cfs.

34 *Boundary Conditions*

35 Boundary conditions for the sediment-transport model include the downstream hydraulic boundary
36 condition and the upstream sediment supply.

37 *Downstream Boundary Condition*

38 The downstream boundary conditions for the two models between Lexington and Chapman were input
39 using stage-discharge rating curves that were developed from the steady-state hydraulic model. For the
40 North Platte model, the stage upstream from the Tri-County Diversion Structure is generally maintained
41 at an elevation equal to the top of the Ogee Spillway (pers. comm., Cory Steinke/CNPPID), so a constant
42 stage of 2770.0 feet was used over the range of modeled flows.

43 *Upstream Boundary Condition*

44 Upstream sediment load rating curves and the gradation of the inflowing load were developed for each
45 model. The gradation and sediment load rating curve for the upstream (Lexington to Odessa) model



1 was developed from the results of the Sediment Augmentation HEC-RAS model, which assumed
2 equilibrium load conditions at the upstream boundary. These results were reported on a daily basis, so
3 an inflowing sediment rating curve was developed by fitting a line through this information. Similarly,
4 results from the upstream (Lexington to Odessa) HEC-6T model at the downstream limit (Anchor Point
5 27; RM 222) were used to develop the gradation and sediment load rating curve for the sediment inflow
6 to the downstream (Odessa to Chapman) model. For the North Platte model, a sediment rating curve
7 was developed through an iterative process that involved adjusting the inflowing sediment rating curve
8 until the predicted aggradation matched the aggradation indicated by the comparative model
9 geometries (discussed in the calibration section, below). The gradation of the inflowing sediment load
10 was determined by computing the average gradation of the transported load as predicted by the model
11 over a range of discharges in the upstream mile-long reach of the model.

12 **Sediment-transport Function**

13 The Yang (1973) equation was used for the Sediment Augmentation HEC-RAS model. It appeared to
14 produce results that matched the measured data reasonably well. This equation was, therefore,
15 selected for use in each of the three models.

16 **Computational Time Steps**

17 HEC-6T performs the sediment-transport calculations for the prescribed computational time steps. As
18 discussed in the HEC-RAS User's Manual (USACE, 2010), "...smaller computation increments will increase
19 (model) run time, re-computing geometry and hydraulics too infrequently (e.g., computation increments
20 that are too large) is the most common source of model instability." For this study, the computation
21 interval was determined using procedures outlined in the Corps' Guidelines for the Calibration and
22 Application of Computer Program HEC-6 (USACE, 1992). The resulting time steps are identical to those
23 used in the Sediment Augmentation Feasibility Study (Tetra Tech, 2010), and range from 6 minutes
24 when the flow at Overton is greater than 10,000 cfs to 12 hours when the flow at Overton is less than
25 1,000 cfs (Table 4.1).

26
27 Table 4.1: Summary of computational time steps used in the HEC-6T models.

Discharge Range (cfs)		Computation Time Step (hrs)
Minimum (cfs)	Maximum (cfs)	
0.0	1,000.0	12
1,000.1	2,500.0	6
2,500.1	5,000.0	4
5,000.1	7,500.0	1
7,500.1	10,000.0	0.5
10,000.1	20,000.0	0.1

28 **Model Calibration**

29 The sediment-transport model was calibrated, to the extent possible, by comparing the predicted
30 aggradation/degradation trends to observed data along the project reach. It should be noted that
31 because the models include the existing channel geometry and the existing gradation of the bed
32 material (and not the geometry and bed material at the beginning of the measurement process), a
33 direct comparison of the magnitude of the predicted and observed changes may not be appropriate, but
34 the predicted trends in aggradation/degradation should be similar to the observed trends.



1 *Lexington to Chapman Models*

2 The data used to calibrate the Lexington to Chapman models were obtained from repeat cross-sectional
3 surveys conducted by the BOR between 1985 and 2005 (BOR, 2006). This information was used to
4 compute the mean bed elevation at the time of each survey and the resulting change in mean bed
5 elevation during the various periods between the surveys. For this study, the change in mean bed
6 elevation was computed for only the active channel as defined by the portion of the cross section where
7 aggradation or degradation was indicated by the surveys. The limits for the active channel were then
8 used to define the bank stations in the calibration runs so that the change in mean bed elevation as
9 reported by HEC-6T could be directly compared to the observed changes. Since most of the mean bed
10 elevation data represent the period between October 1, 1989, and April 1, 2002 (including the datasets
11 from 1989 to 1998 and from 1989 to 2002), the Lexington to Chapman models were executed over this
12 period.

13
14 Results from the upstream (Lexington to Odessa) model indicate that the predicted changes in mean
15 bed elevation match the observed changes reasonably well in the primary channel (Figure 4.8). Changes
16 in mean bed elevation predicted by the downstream (Odessa to Chapman) model also match the
17 observed changes reasonably well (Figure 4.9). Note the observed changes during the period between
18 1985 and 2001 were also included in Figure 4.9, since the observed trends are more useful to the
19 calibration effort than the actual magnitude of the changes.

20 *North Platte Model*

21 No repeat survey information was available to compute changes in mean bed elevation that could be
22 used to calibrate the model. However, available gage measurements at the U.S. Highway 83 gage (DNR
23 Gage no. 06693000) indicate that during the period between December, 1999 and January, 2004,
24 approximately 0.4 feet of aggradation occurred in the vicinity of the gage during this period (Figure
25 4.10). The geometry from the steady state model that was developed for this study includes surveyed
26 cross-section information at 4 locations and assumed bathymetry that was developed to calibrate the
27 steady-state model. This model geometry was compared to the geometry of a model developed by SEH
28 in 2007, which included a range of geometric conditions between 2002 and 2007. Because the
29 geometry in the SEH model is either based on 2-foot contour mapping or is based on an unknown
30 source, it is not appropriate to compare the magnitudes of the differences between the two model
31 geometries; however, a comparison of the geometries in the two models at least provides some
32 indication of trends in aggradation or degradation. The comparison indicates that the majority of the
33 model reach has been aggradational during the period between 2002 and 2010 (Figure 4.11).

34
35 The change in mean bed elevation that is predicted by the HEC-6T model matches the “observed”
36 change that is indicated by the HEC-RAS model geometry comparison reasonably well (Figure 4.11).
37 Upstream from the Highway 83 Bridge, the observed change is somewhat larger than the predicted
38 change, which is less than 0.5 feet over the approximately 3-mile long reach upstream from the bridge.
39 The predicted aggradation of about 0.6 feet at the bridge (0.09 feet/year), however, is very similar to
40 the aggradation (0.1 feet/year) that is indicated by the gage measurements in Figure 4.10. Excluding the
41 aggradation that is indicated near the upstream boundary condition, the most significant aggradation
42 occurs upstream from the Union Pacific Railroad Bridge. In general, areas with the least amount of
43 aggradation are more constricted and have higher in-channel velocities than areas with large amounts
44 of aggradation.



1 Upstream Sediment Supply Sensitivity Analyses

2 A number of sensitivity analyses could be performed on the various model inputs. Because the
3 Program's bed material samples (collected by Ayers at the Anchor Points) appear to be among the most
4 reliable data sources in the models, and because the samples were screened to eliminate potentially
5 anomalous samples during the compositing procedure that was used to develop the model input, a
6 sensitivity analysis on the bed material size was not carried out. A more significant uncertainty
7 associated with the sediment-transport model input is associated with the magnitude and gradation of
8 the sediment supply at the upstream boundary condition. In the Lexington to Odessa model, this supply
9 was estimated using the results from the HEC-RAS Sediment Augmentation model, which assumed
10 equilibrium sediment supply conditions. In the Odessa to Chapman model, the upstream sediment
11 supply was based on the results at the downstream limit of the Lexington to Odessa model. The
12 sediment supply to the North Platte model was developed to match the "observed" aggradation near
13 the upstream model limit. A sensitivity analysis was carried out to evaluate the effects of the upstream
14 sediment supply. This analysis involved increasing or decreasing the magnitude of the "best estimate"
15 sediment supply by 25 percent, and coarsening or fining the gradation of the "best estimate" sediment
16 supply by 25 percent. The analysis was carried out by comparing the predicted change in mean bed
17 elevation from the four additional model runs with the results from the calibrated model runs discussed
18 above.

19
20 In the Lexington to Odessa model, the effects of increasing the sediment supply by 25 percent are most
21 significant at the upstream model limit, where more aggradation or less degradation is indicated than
22 with the "best-estimate" loads (Figure 4.12). The effects dampen in the downstream direction to less
23 than 0.1 over a distance of about 5 miles. Interestingly, the very minor but identifiable effects of
24 increasing the upstream sediment load persist down through the Kearney Diversion Structure at a
25 limited number of locations. The effects of decreasing the upstream sediment supply are more uniform
26 (about 0.4 feet less aggradation or more degradation) through the upstream 5 miles of the model
27 (Figure 4.12). The effects of coarsening or fining the gradation of the upstream sediment supply also
28 generally limited to the upstream 5 miles, with minor differences indicated at a few locations upstream
29 from the Kearney Diversion Structure (Figure 4.13). Because varying the magnitude and gradation of the
30 upstream sediment supply do not appear to have an effect on the sediment-transport conditions in the
31 downstream reaches of the Lexington to Odessa model, the sensitivity analysis was not performed for
32 the Odessa to Chapman model.

33
34 The sensitivity analysis of the sediment supply to the North Platte model indicates the most significant
35 effects of increasing or decreasing the magnitude of the sediment supply occur in the 5.5-mile long
36 reach upstream from the Highway 83 Bridge (Figure 4.14). The model with increased sediment supply
37 shows a moderate increase in aggradation in this reach with essentially no change downstream from the
38 bridge, while the model with reduced sediment supply indicates the reach above the bridge is in balance
39 to slightly degradational and is slightly less aggradational in the reach between the Highway 83 and
40 Union Pacific Railroad Bridges. Coarsening or fining the gradation of the sediment supply also has the
41 largest impact in the reach upstream from the Highway 83 Bridge (Figure 4.15). The model with the
42 coarse gradation shows increased aggradation in this reach and significant sediment trapping just
43 upstream from the bridge, which translates to slightly less aggradation from the Highway 83 Bridge to
44 below the Highway 30 Bridge. If the gradation of the sediment supply were finer than the best estimate,
45 the reach upstream from the Highway 83 Bridge would be in balance, while the predicted aggradation
46 downstream from the bridge would be essentially the same as with the best-estimate gradation.



1 **Model Application and Use**

2 The sediment-transport models that were developed for this study have been calibrated, to the extent
3 practical, and are intended to be used as a tool in evaluating changes to sediment-transport conditions
4 that could occur as a result of different flow-related or physical changes (e.g., vegetation clearing, island
5 shaving, flow consolidation) imposed on the system. While the magnitude of the predicted results may
6 not identically match the actual response, the models can be used to evaluate changes relative to a
7 baseline condition. The input files for the three models that resulted from the calibration effort are
8 presented in Appendix C.

9
10 It should be noted that HEC-6T will compute zero flow in the side channels of closed loops when the
11 energy balancing process indicates all flow is conveyed through only one channel around an island.
12 When this occurs, no sediment-transport occurs in the dry channel and a flat water-surface profile is
13 indicated. The model results will include a warning message (Warning Message 27201) indicating there
14 is a “severe problem” because the bed is above the water-surface elevation; this is obviously not a
15 “severe problem”, since the model predicts a dry channel reach at this point of the simulation.

16
17 Utility programs are available with the MBH HEC-6T software package and are designed to simplify
18 model development and viewing the model results. In addition to the MBH utility programs, a number
19 of programs were developed to assist the user in model development and in the post-processing of
20 model results. These utility programs are discussed in the Use and Application Memorandum included
21 in Appendix D.

23 **5. Summary and Conclusions**

24 **Steady-State Model**

25 The series of one-dimensional models representing the 154 mile section of the Platte River from the Tri-
26 Country Diversion to Chapman, NE provides a reliable method for calculating hydraulic conditions
27 (WSEL, flow depth, velocity, etc.) over a range of flows. Model geometry was based on a combination of
28 LiDAR data and ground surveys. Roughness and ineffective flow areas were based on land-use data,
29 aerial photography and field observations. Significant bridges, in-line weirs and diversion structures
30 were based on as-built design plans and field surveys. A comparison of computed WSELs with levels at
31 the time of the LiDAR survey over the entire project reach indicates an average difference of less than
32 0.1 ft and standard deviation of 0.51 ft or less in any of the modeled segments. Rating curve calibrations
33 indicate reasonable agreement in main channel areas. Ground survey comparisons show that at a
34 majority of the locations, predicted WSELs were within the range of observed and rated WSELs. The
35 computed results of these models can be used to predict reach-averaged hydraulics.

36 **Unsteady Model**

37 An unsteady hydraulic model was produced based on the calibrated steady-state model. Some
38 adjustments to channel geometry, roughness, blocked and ineffective flow areas and cross section
39 configuration were necessary to improve model stability and performance. The model predicted
40 hydrograph timing, shape and peak reasonably well for long-duration natural high-flow events.
41 However, predicting short-duration high flow event required accounting for bank storage. The HEC-RAS
42 groundwater interflow module does not accurately represent the dynamic nature of bank storage in the
43 Platte River. Using 2009 event data, an empirical bank storage relationship based on hydrograph
44 characteristics was developed. A template for users to predict the appropriate bank storage
45 relationship hydrograph for each reach in between gages has been provided. As more data become



1 available, the user should compare predicted to observed data to refine the empirical parameters to
2 better the understanding of the effects of bank storage on short-duration high flow events.

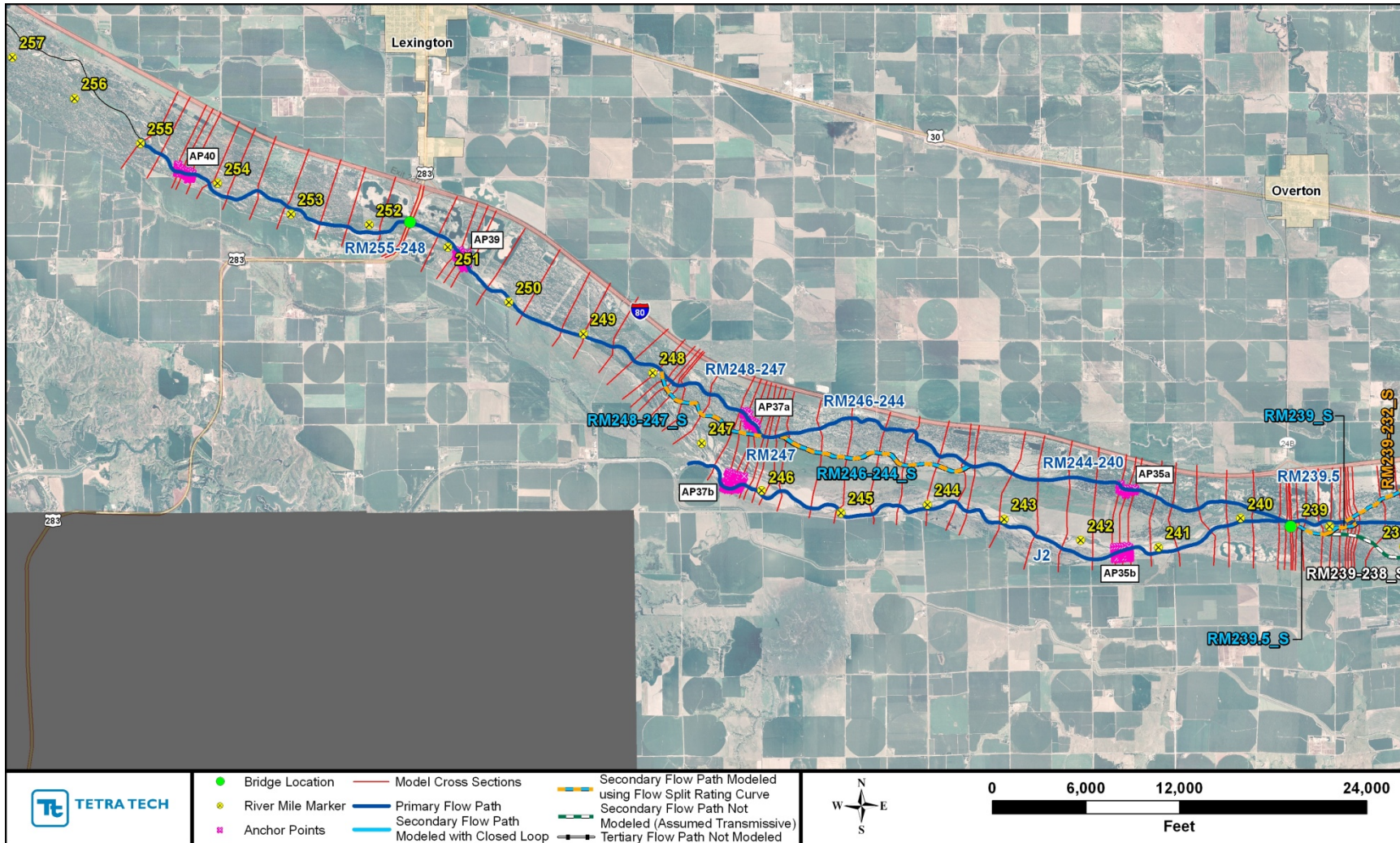
3 **Sediment-Transport Model**

4 The sediment-transport models that were developed for this study have been calibrated, to the extent
5 practical, and are intended to be used as a tool in evaluating changes to sediment-transport conditions
6 that could occur as a result of different flow-related or physical changes (e.g., vegetation clearing, island
7 shaving, flow consolidation) imposed on the system. While the magnitude of the predicted results may
8 not identically match the actual response, the models can be used to evaluate changes relative to a
9 baseline condition.

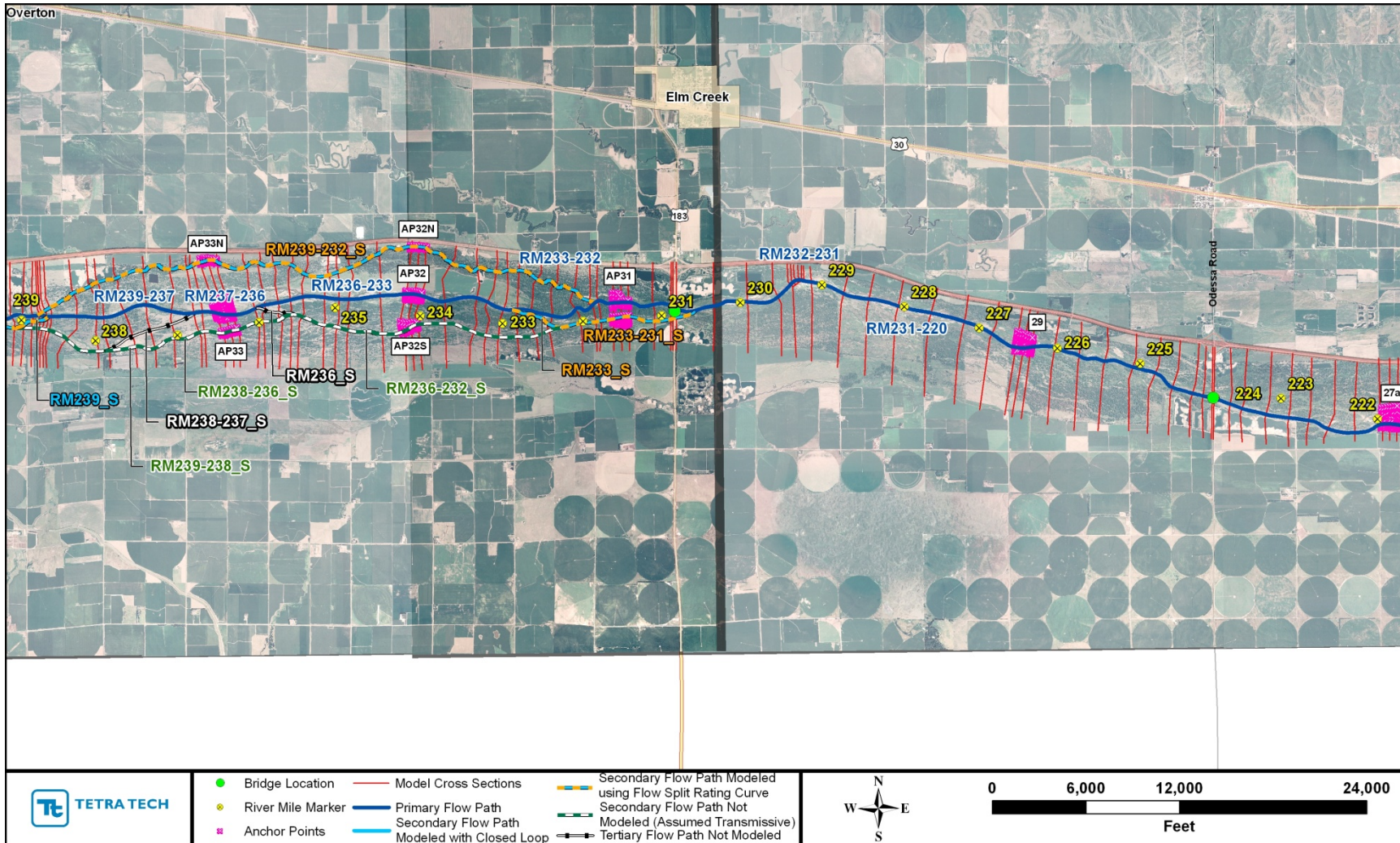
10 **Overall**

11 In considering the quality of the model calibration, it is important to understand that this is a very large
12 model for a very complex reach of river. The model will provide a valuable tool for evaluation of
13 Program activities at the reach-scale (i.e., many channel widths in length), and it provides a solid basis
14 for preparing local, higher-resolution models for evaluation at a finer spatial scale. Because the model is
15 one-dimensional and flow patterns and sediment-transport processes are fundamentally three-
16 dimensional, among a host of other factors, it is not capable of precisely describing all of the processes
17 that will control the water-surface elevations, pulse attenuation, bank storage, or sediment-transport
18 longitudinally and laterally across the channel at any specific location in the reach. The calibration
19 represents an optimization of all of the relevant input values that can reasonably be adjusted to obtain
20 the best overall agreement between measured and computed water-surface elevations throughout the
21 model domain and over the range of modeled flows. It is possible to make local empirical adjustments
22 to the input variables to more closely match the measured data. While the resulting model would
23 predict observed data more accurately than the current model for the specific conditions when the data
24 were collected, it is unlikely that results obtained from versions of the model that are modified to
25 represent other conditions for which specific calibration data are not available would be more accurate
26 than those from a similarly modified version of the current model. As noted above, the current version
27 of the model should be used to answer questions at the coarser reach scale. If the model is to be used
28 to answer questions at a finer spatial scale, submodels should be developed by extracting the relevant
29 segment from the current model, increasing the spatial resolution as appropriate, and performing a
30 local re-calibration of the smaller model using the available data.

31
32
33

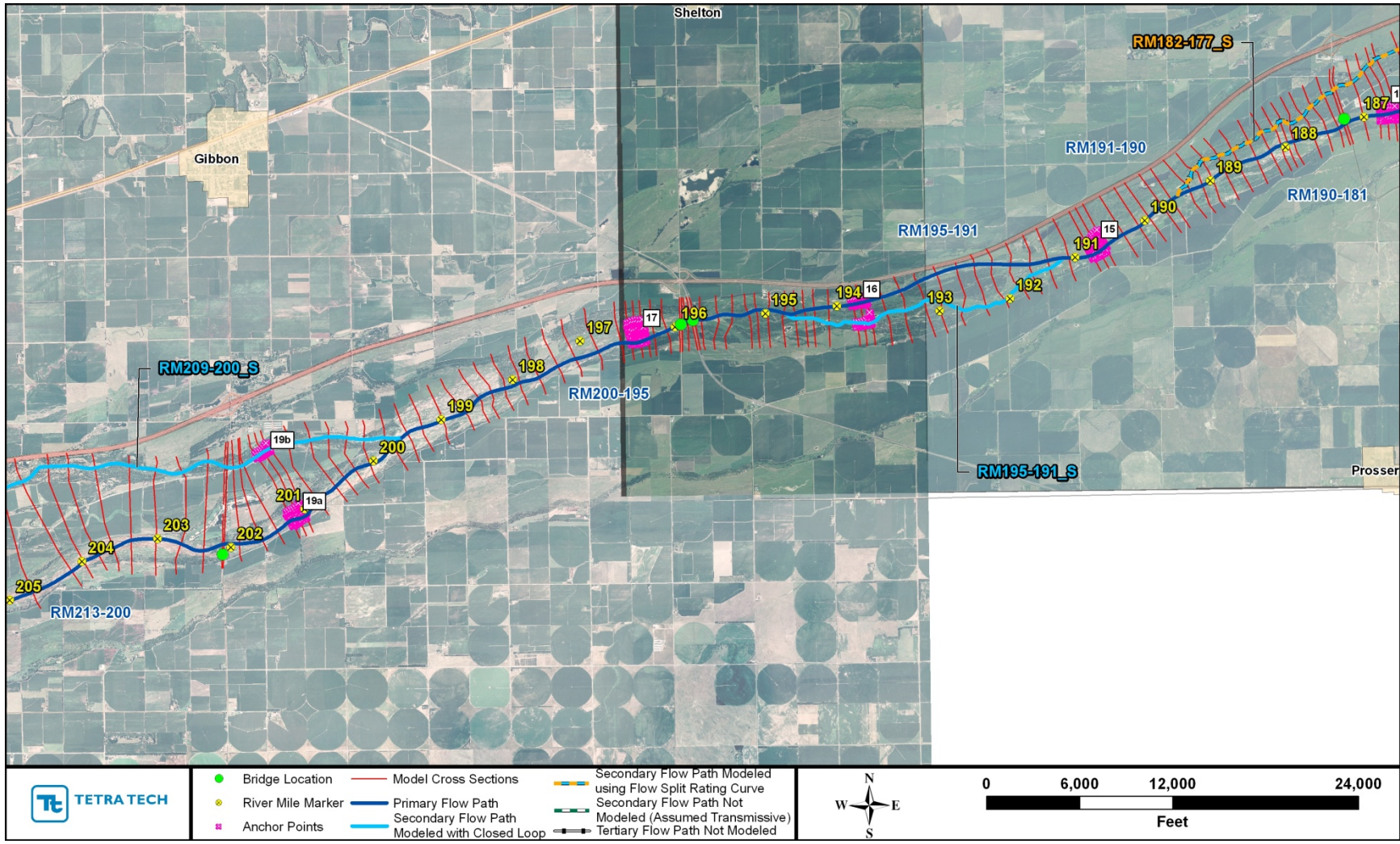


1
2 Figure 4.1a: Key features (cross sections, reaches and reach types) of the upstream sediment-transport model from RM 255 to RM 238. Also shown are
3 the locations of the Program's Anchor Point monitoring sections.

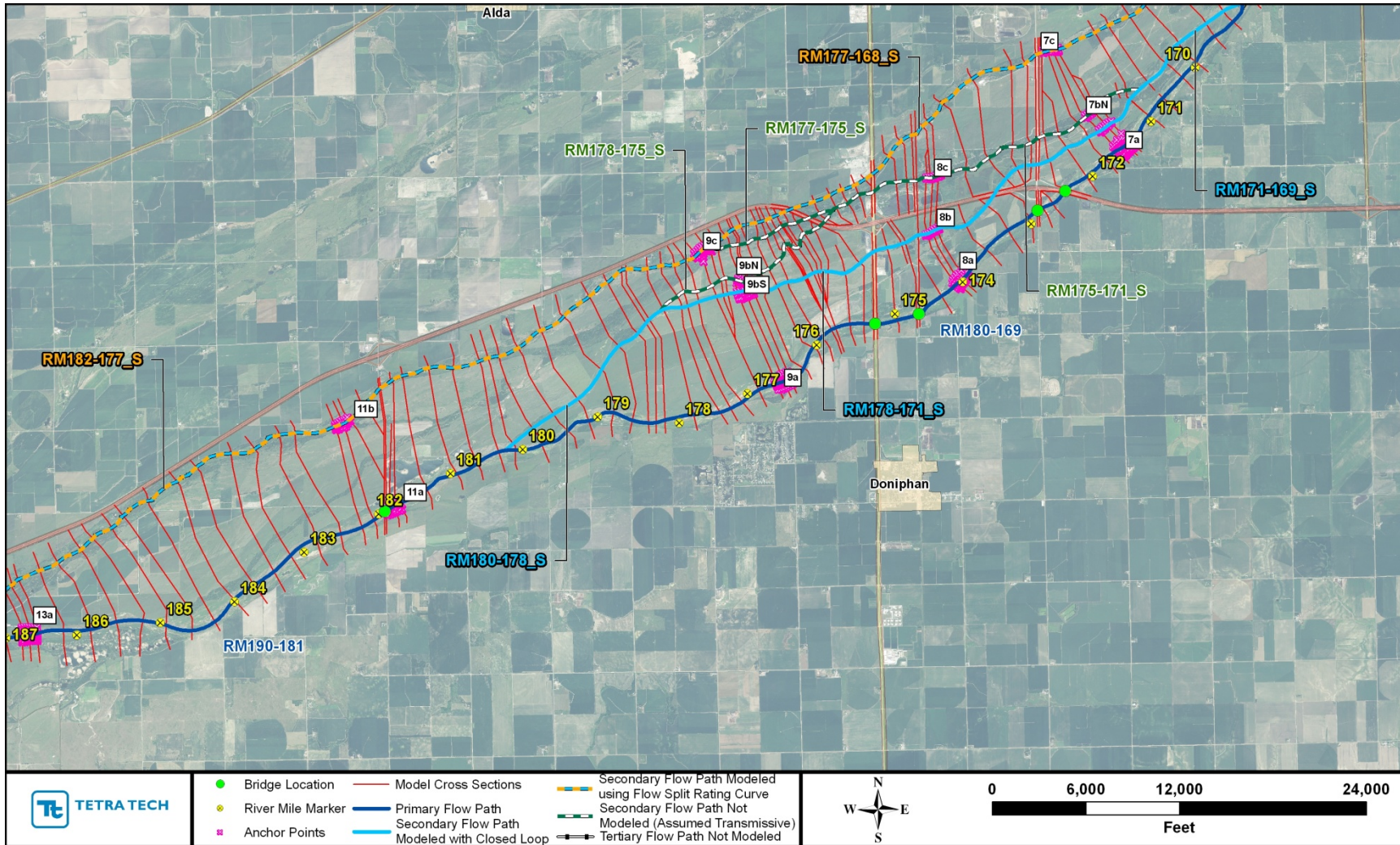


1
2
3
4

Figure 4.1b: Key features (cross sections, reaches and reach types) of the upstream sediment-transport model from RM 239 to RM 222. Also shown are the locations of the Program’s Anchor Point monitoring sections.

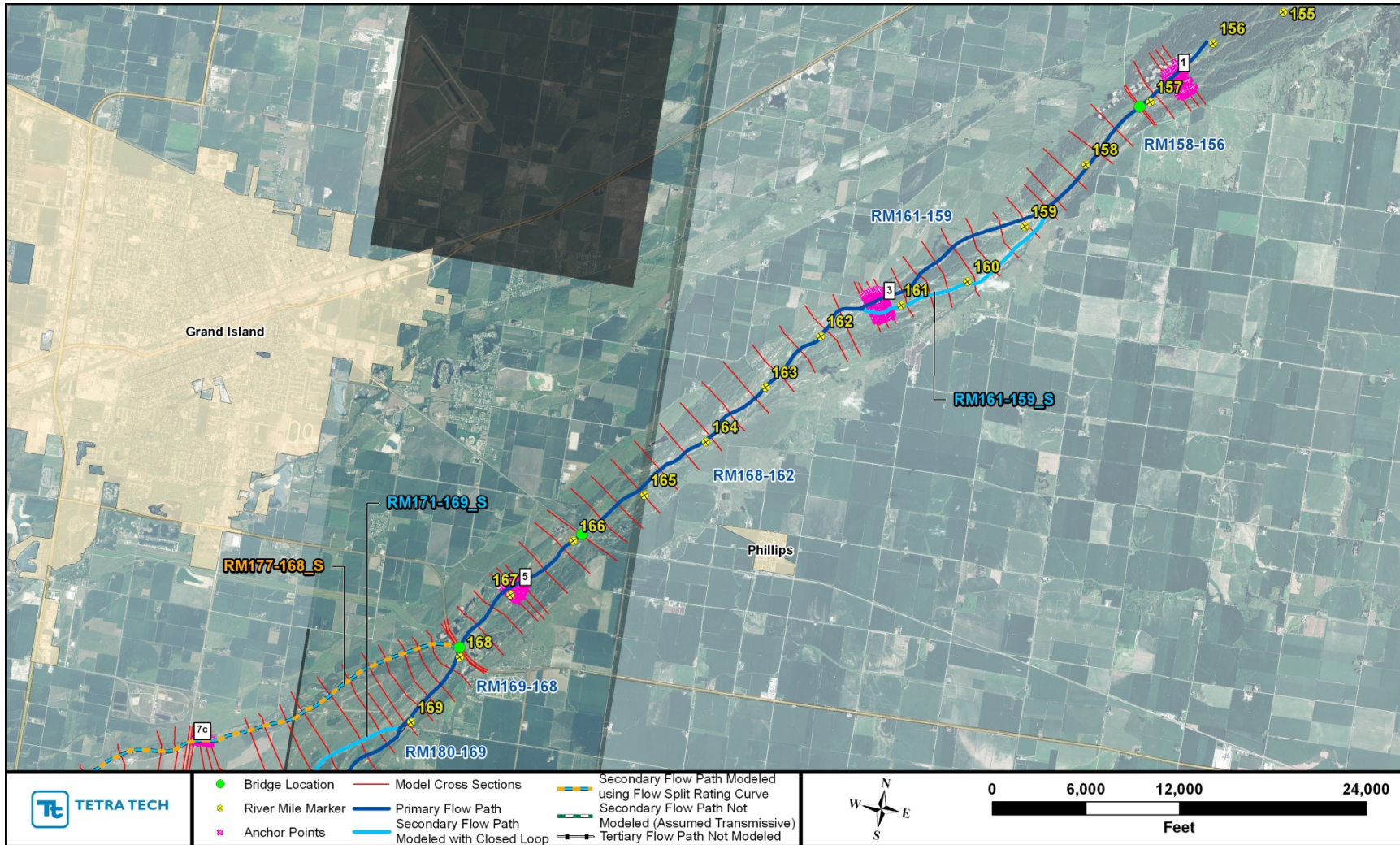


1
 2 Figure 4.1d: Key features (cross sections, reaches and reach types) of the downstream sediment-transport model from RM 205 to RM 187. Also shown
 3 are the locations of the Program's Anchor Point monitoring sections.
 4



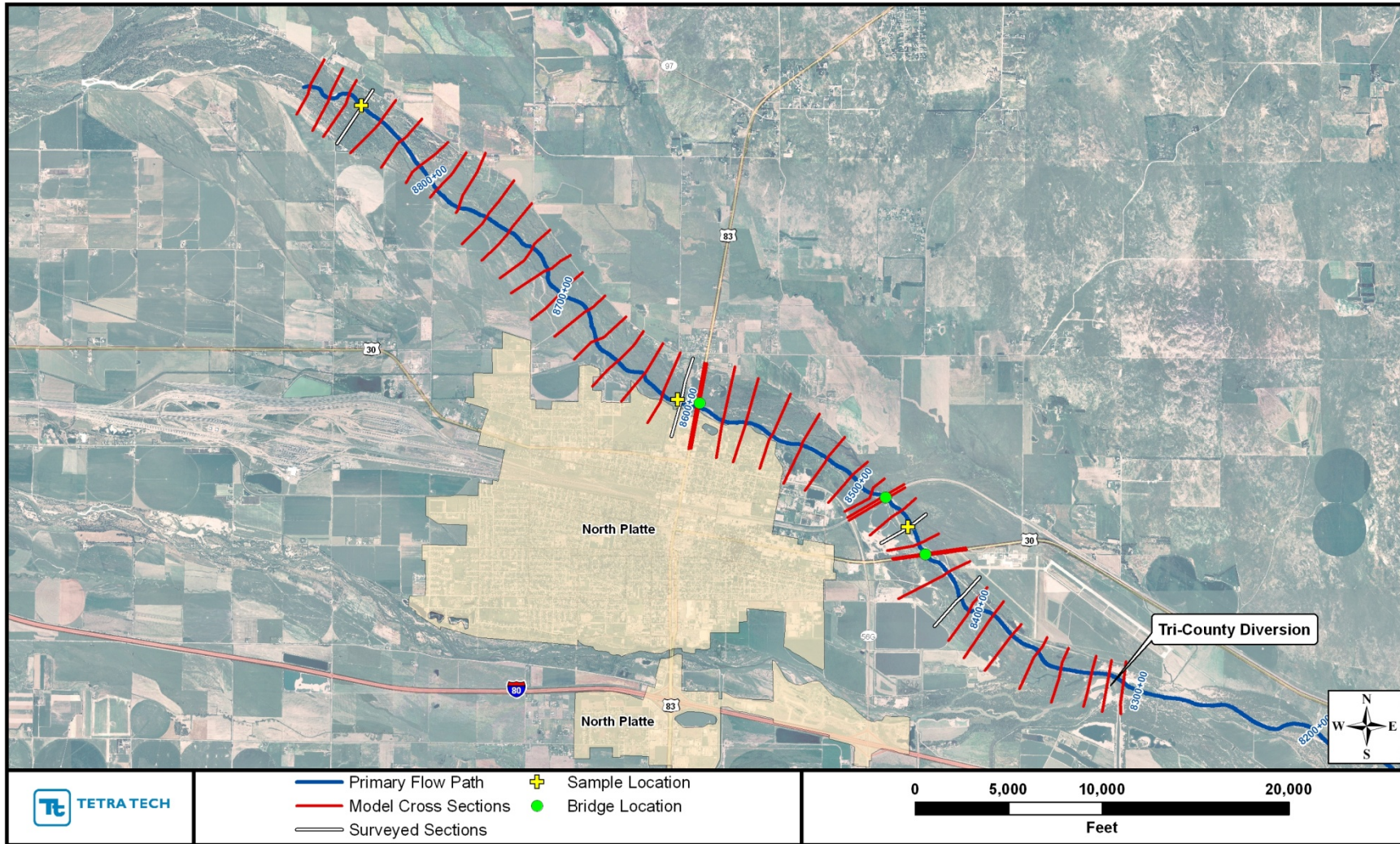
1
2
3
4

Figure 4.1e: Key features (cross sections, reaches and reach types) of the downstream sediment-transport model from RM 187 to RM 169. Also shown are the locations of the Program’s Anchor Point monitoring sections.

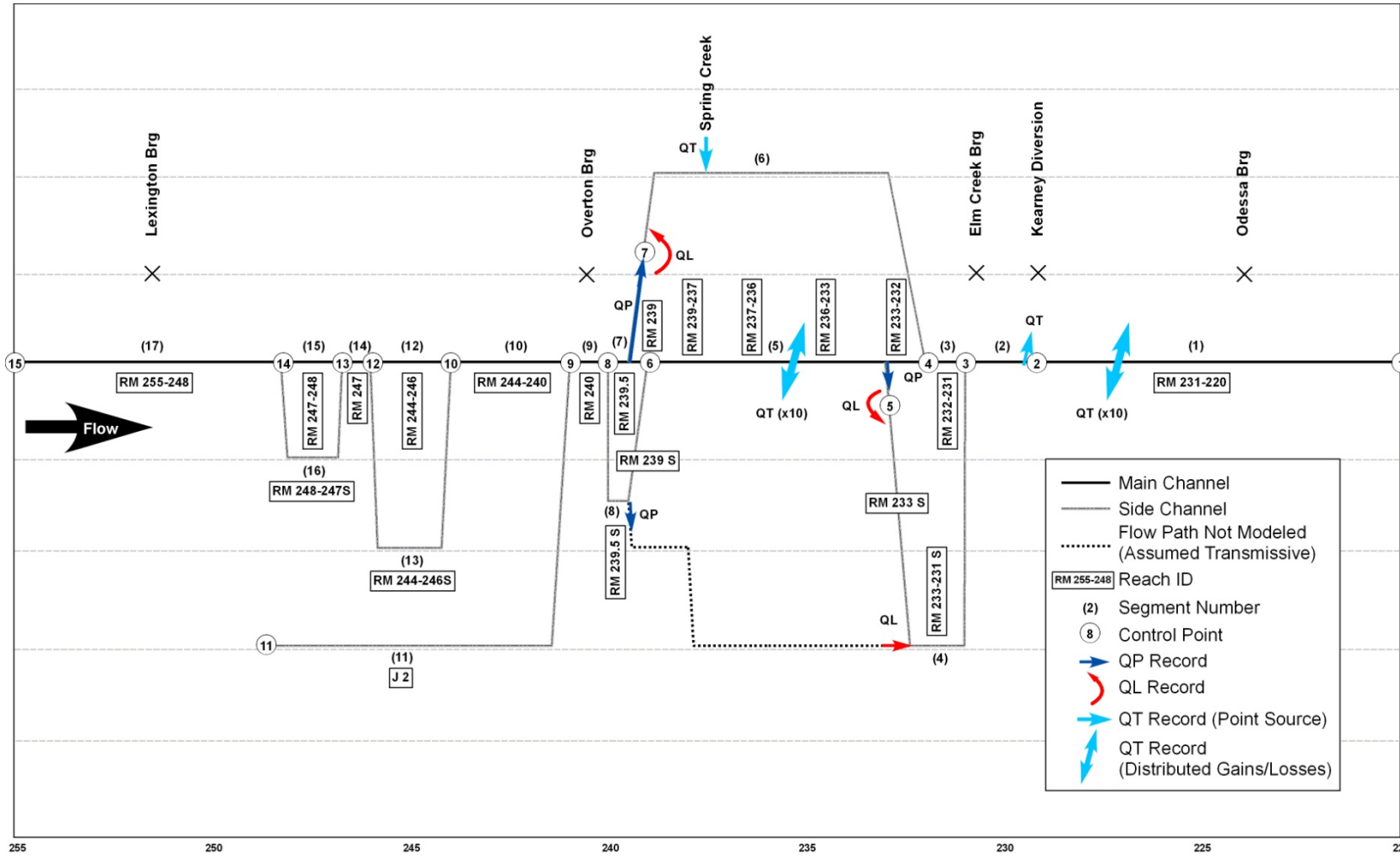


1
2
3
4

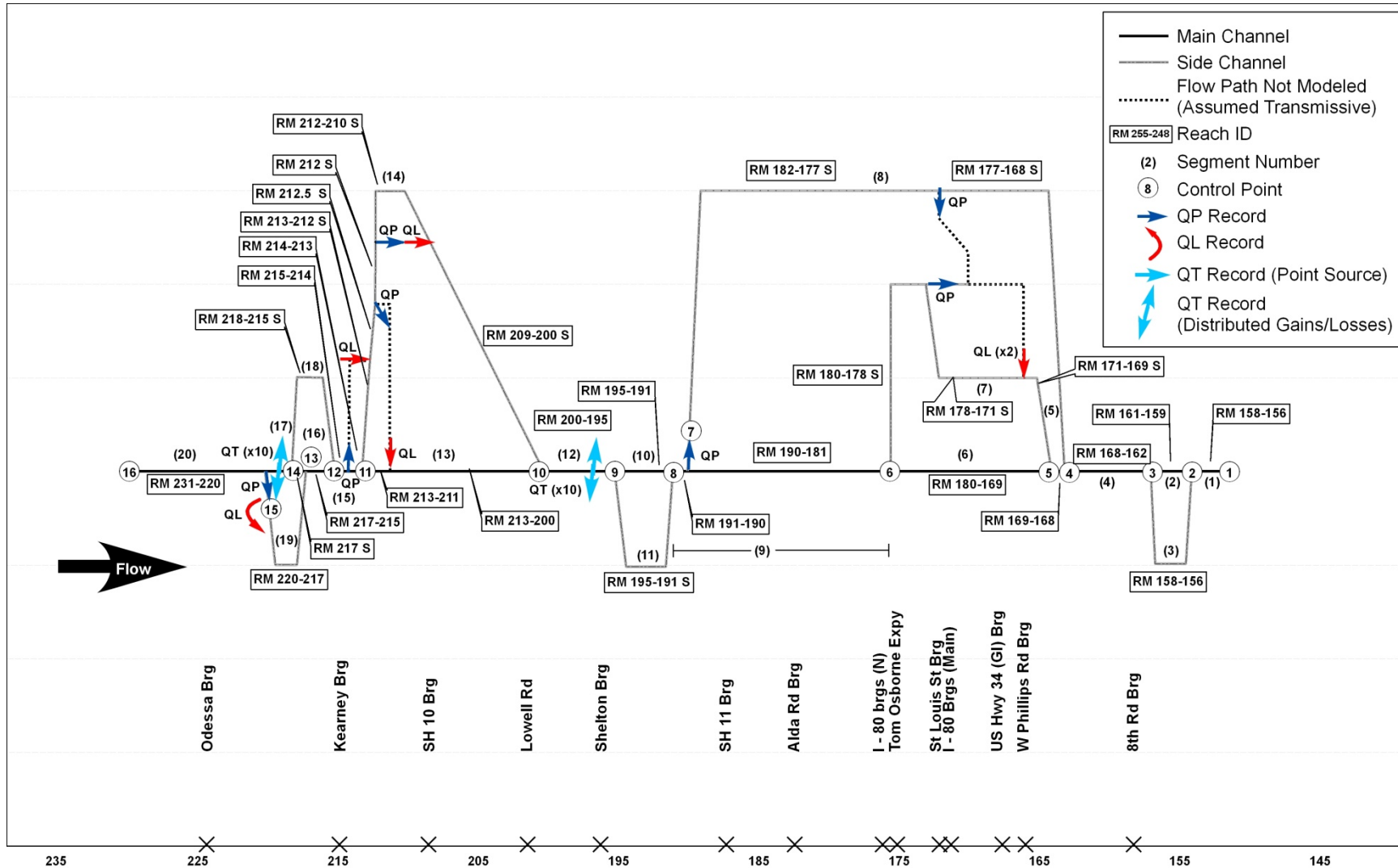
Figure 4.1f: Key features (cross sections, reaches and reach types) of the downstream sediment-transport model from RM 169 to RM 156. Also shown are the locations of the Program’s Anchor Point monitoring sections.



1 4.1g: Key features (cross sections and station line) of the North Platte sediment-transport model. Also shown are the locations of the surveyed cross
 2 sections and sediment samples collected for this study
 3

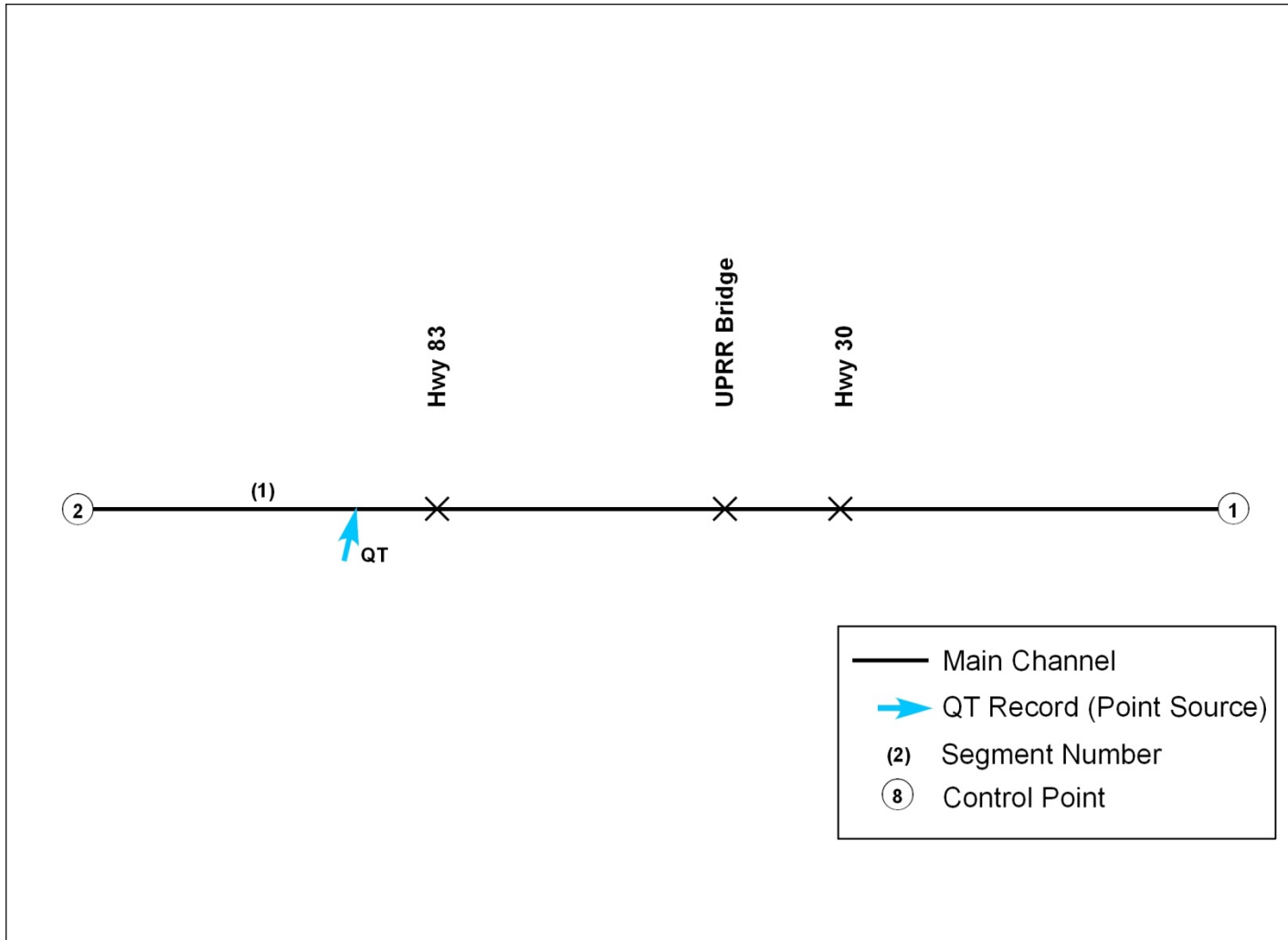


1
2 Figure 4.2a: Schematic diagram of the model segments, control points, in discharge (QP, QL, and QT Records) in the Lexington to Odessa Model
3



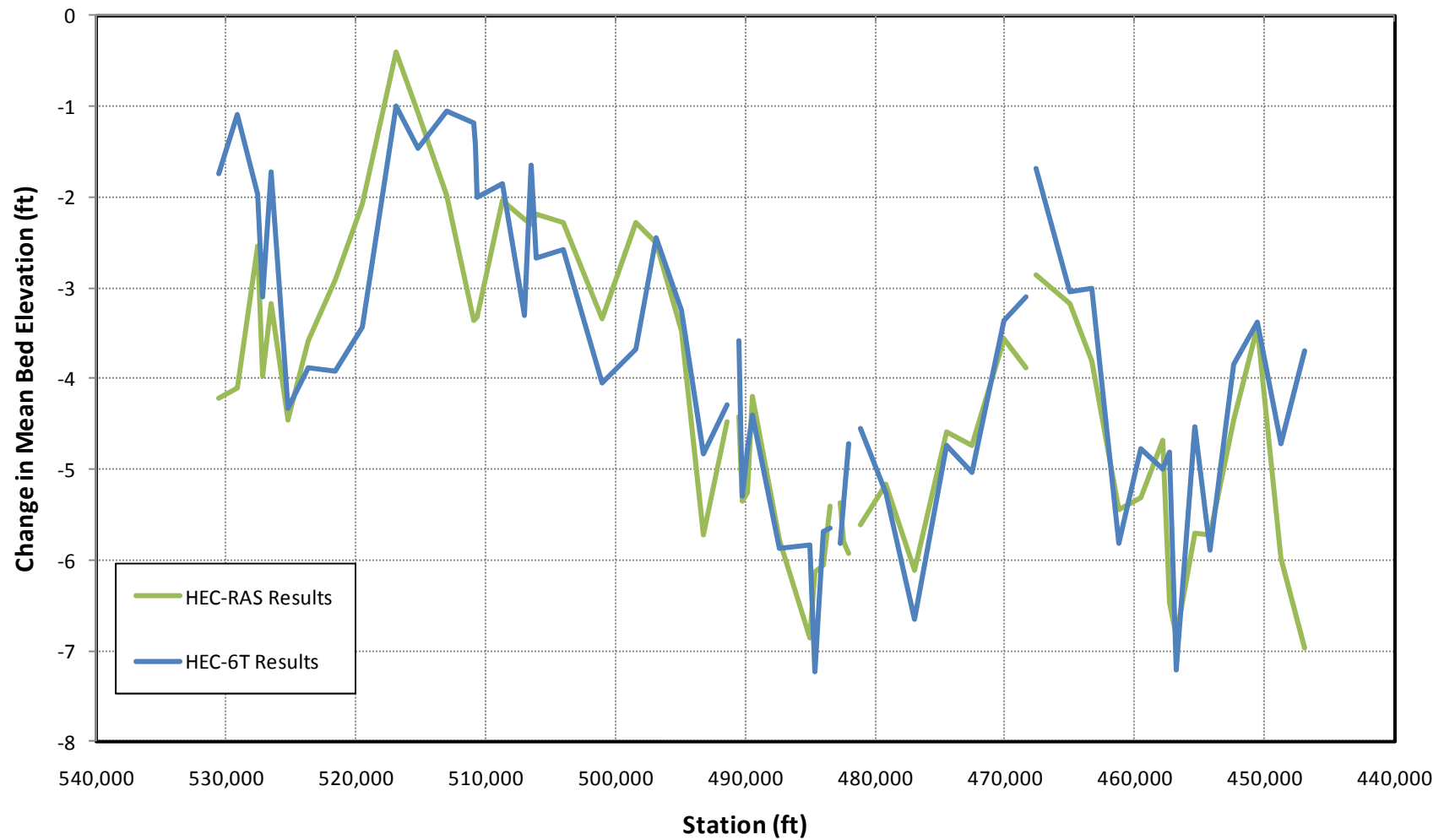
1
2
3

Figure 4.2b: Schematic diagram of the model segments, control points, in discharge (QP, QL, and QT Records) in the Odessa to Chapman Model.

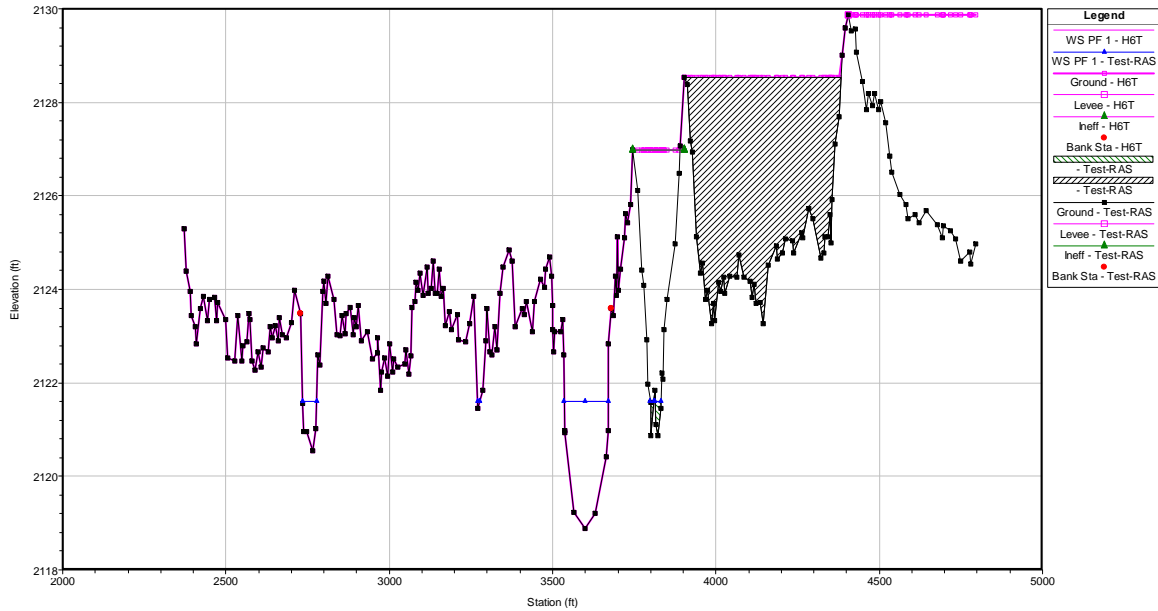


1
2
3

Figure 4.2c: Schematic diagram of the model segments, control points, in discharge (QP, QL, and QT Records) in the North Platte Model.

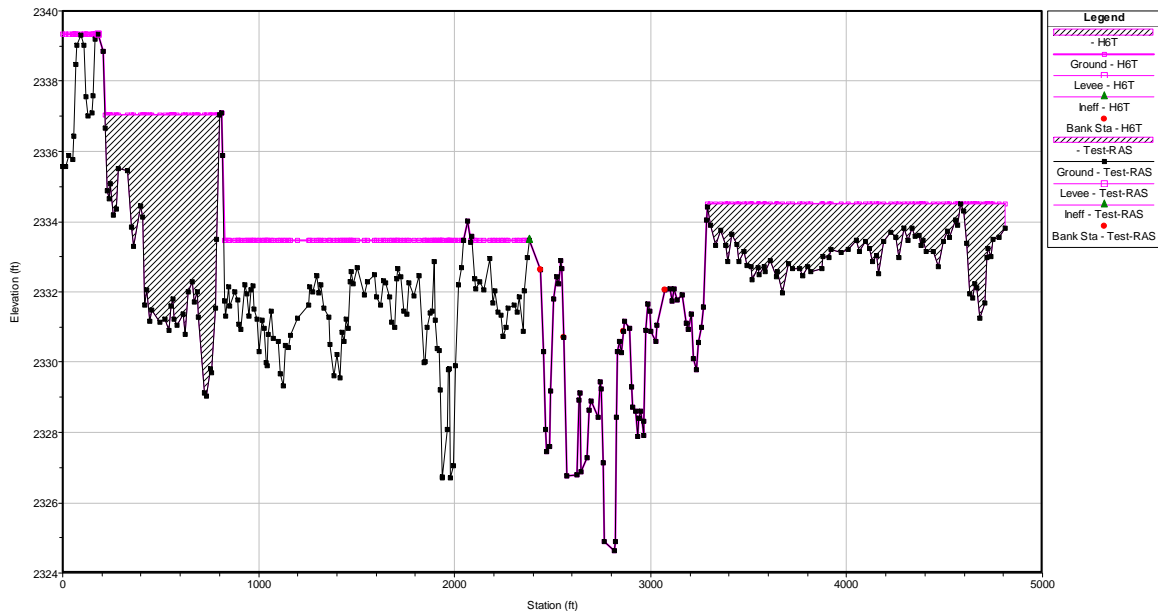


1
 2 Figure 4.3: Comparison of the mean bed change predicted by the HEC-RAS (beta version 4.2) and HEC-6T models for the North Channel of Jeffries Island
 3 at a time near the simulation instability in the HEC-RAS model.

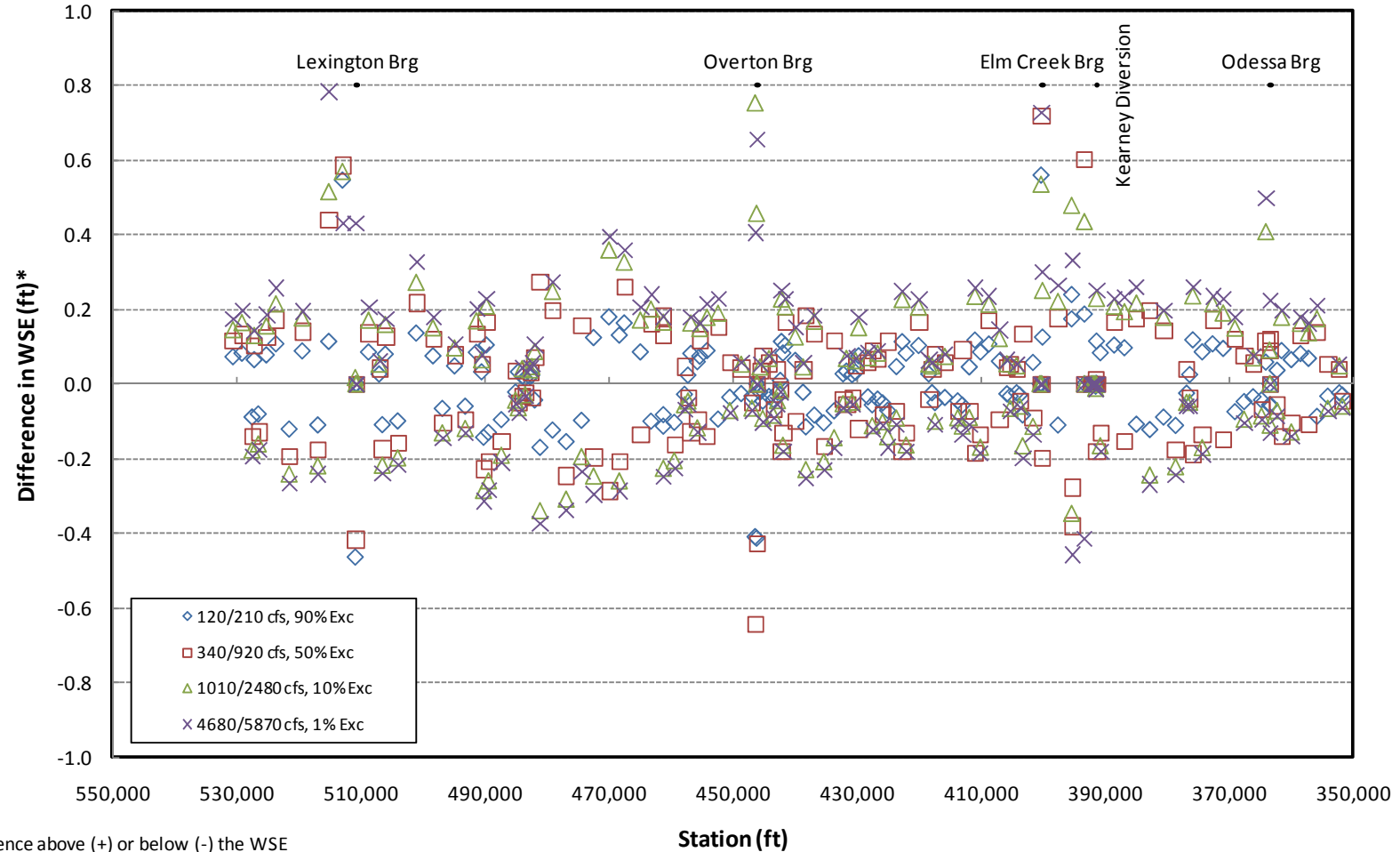


1
2 Figure 4.4a: Example of the sediment-transport model geometry modified for the HEC-6T model (Pink
3 Geometry; Cross Section 300536 in RM 213- RM 211) and the original HEC-RAS geometry from the
4 steady state model (Black Geometry).

5

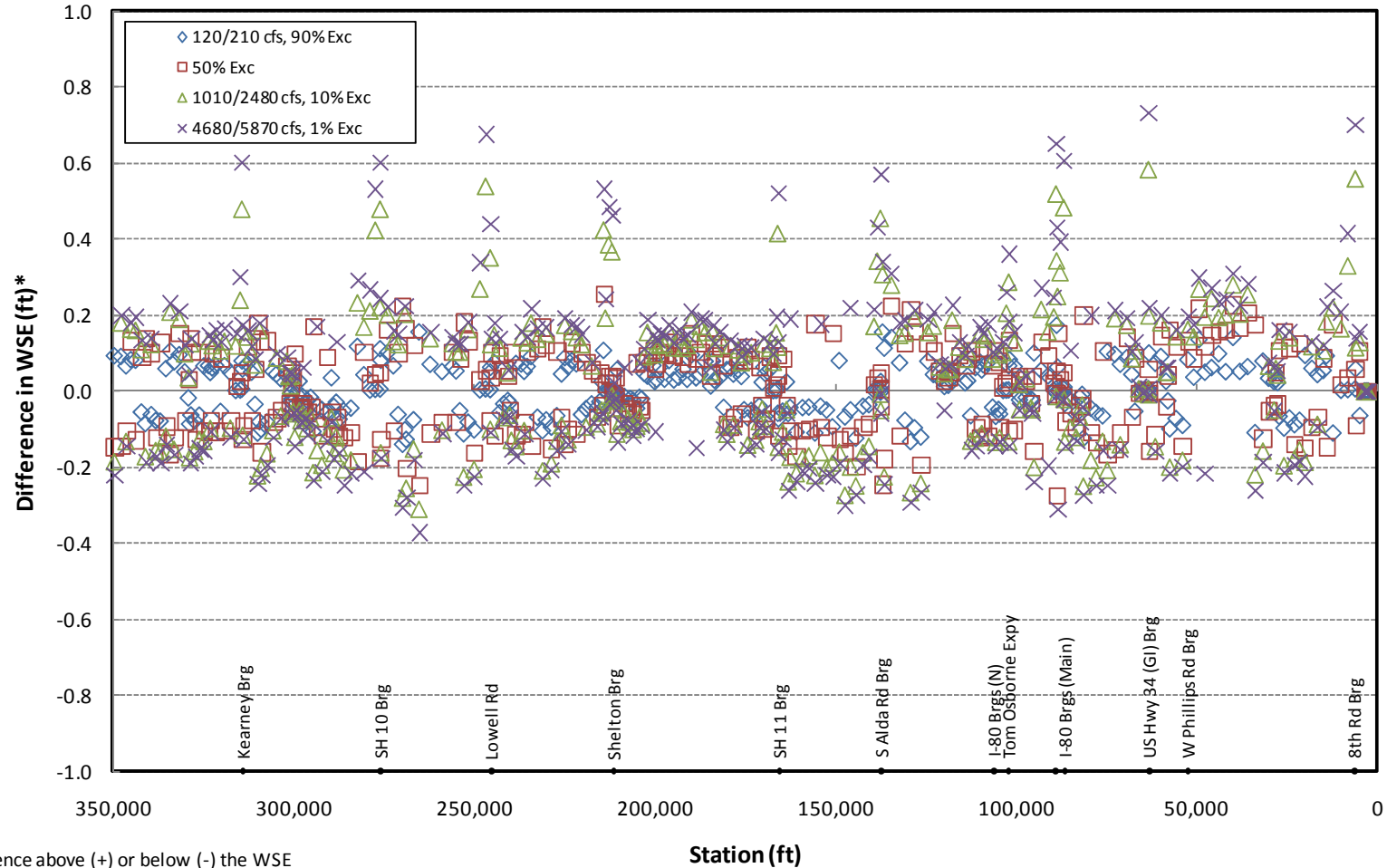


6
7 Figure 4.4b: Example of the sediment-transport model geometry modified for the HEC-6T model (Pink
8 Geometry; Cross Section 467447 in RM 244-RM 240) and the original HEC-RAS geometry from the
9 steady state model (Black Geometry)



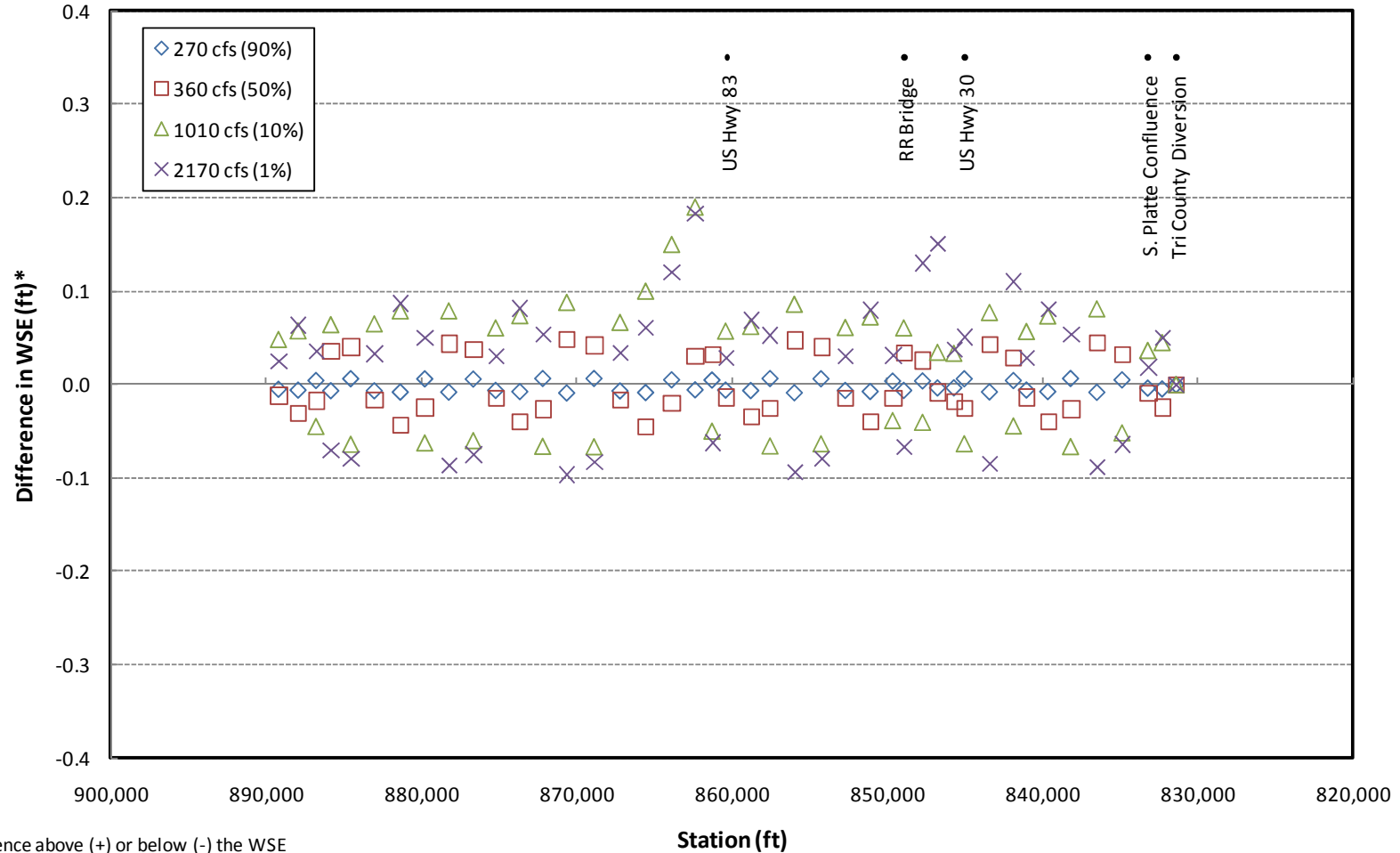
*Difference above (+) or below (-) the WSE computed using calibrated HEC-RAS geometry.

- 1
- 2 Figure 4.5a: Difference between water-surface elevations computed by the rigid boundary HEC-6T model and the calibrated, steady state HEC-
- 3 RAS model for the 90-, 50-, 10-, and 1-percent mean daily flow exceedance levels in the Lexington to Odessa model reach. Positive values
- 4 indicate over-prediction by the HEC-6T model, and negative values indicate under-prediction by the HEC-6T model
- 5



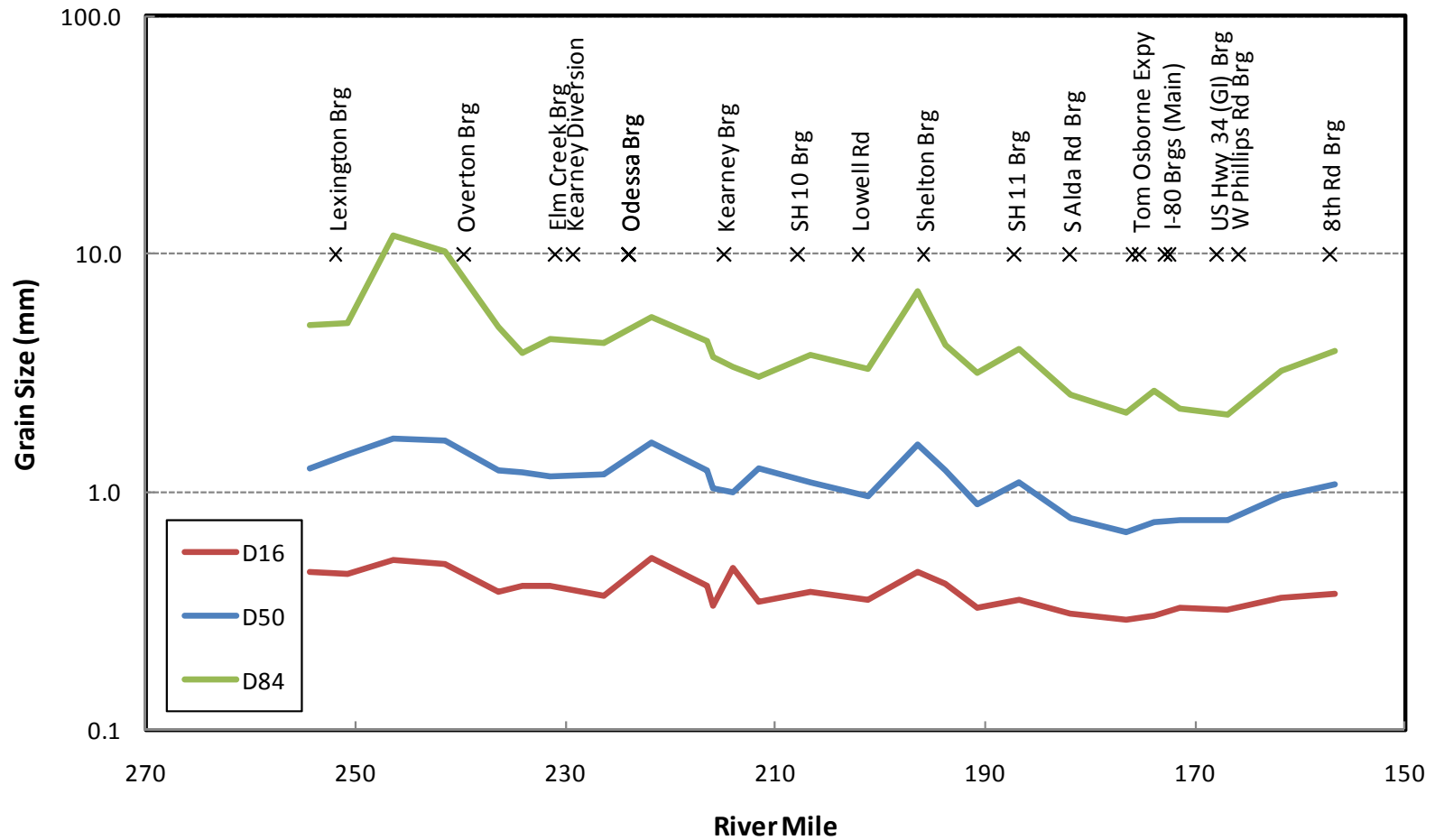
*Difference above (+) or below (-) the WSE computed using calibrated HEC-RAS geometry.

- 1
- 2 Figure 4.5b: Difference between water-surface elevations computed by the rigid boundary HEC-6T model and the calibrated, steady state HEC-
- 3 RAS model for the 90-, 50-, 10-, and 1-percent mean daily flow exceedance levels in the Odessa to Chapman model reach. Positive values
- 4 indicate over-prediction by the HEC-6T model, and negative values indicate under-prediction by the HEC-6T model
- 5

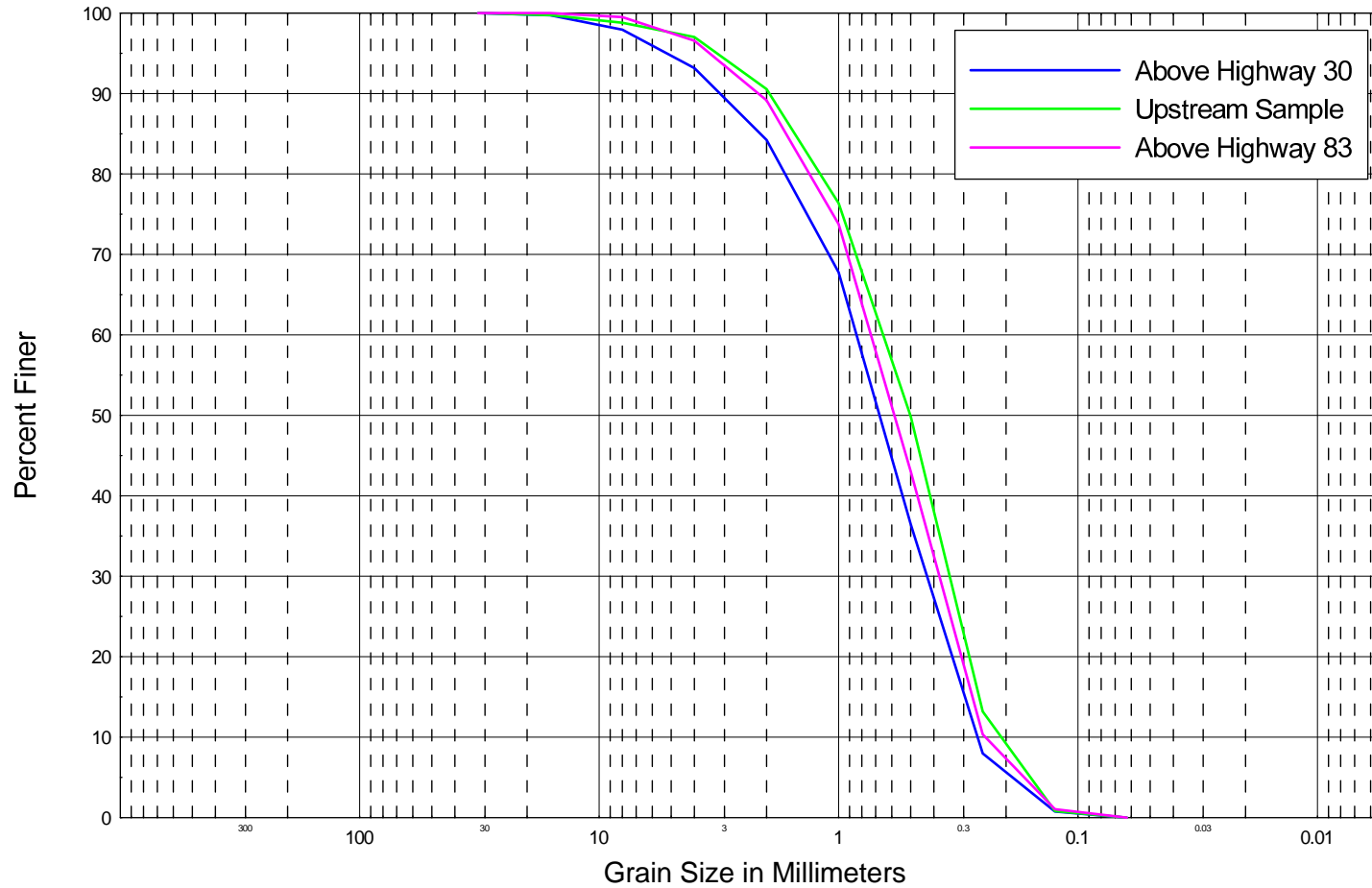


*Difference above (+) or below (-) the WSE computed using calibrated HEC-RAS geometry.

- 1
- 2 Figure 4.5c: Difference between water-surface elevations computed by the rigid boundary HEC-6T model and the calibrated, steady state HEC-
- 3 RAS model for the 90-, 50-, 10-, and 1-percent mean daily flow exceedance levels in the North Platte “Choke Point” reach. Positive values
- 4 indicate over-prediction by the HEC-6T model, and negative values indicate under-prediction by the HEC-6T model.
- 5

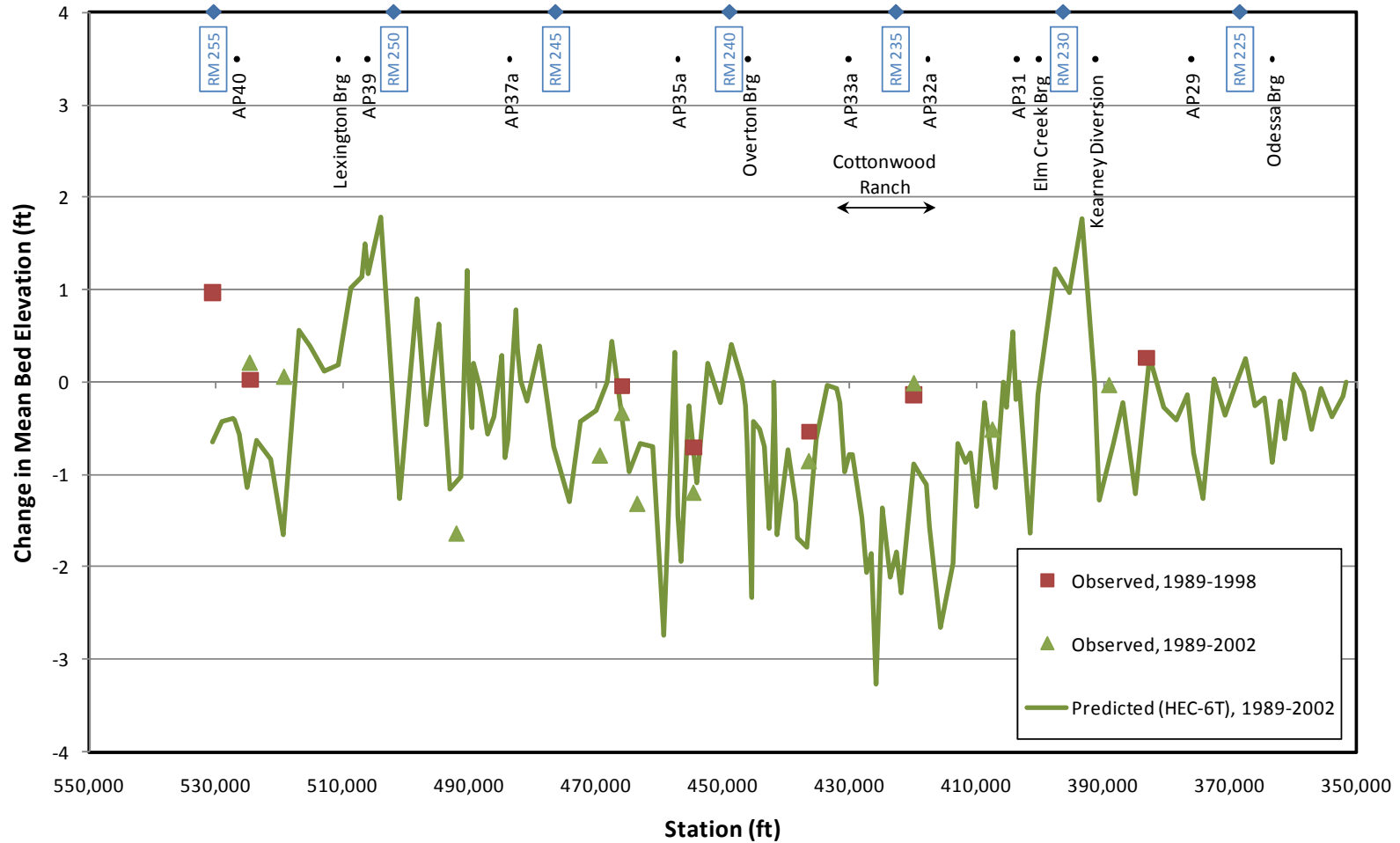


1
 2 Figure 4.6: Representative composite gradations from the Programs Anchor Point bed material samples that were used as input for the
 3 sediment-transport model.
 4

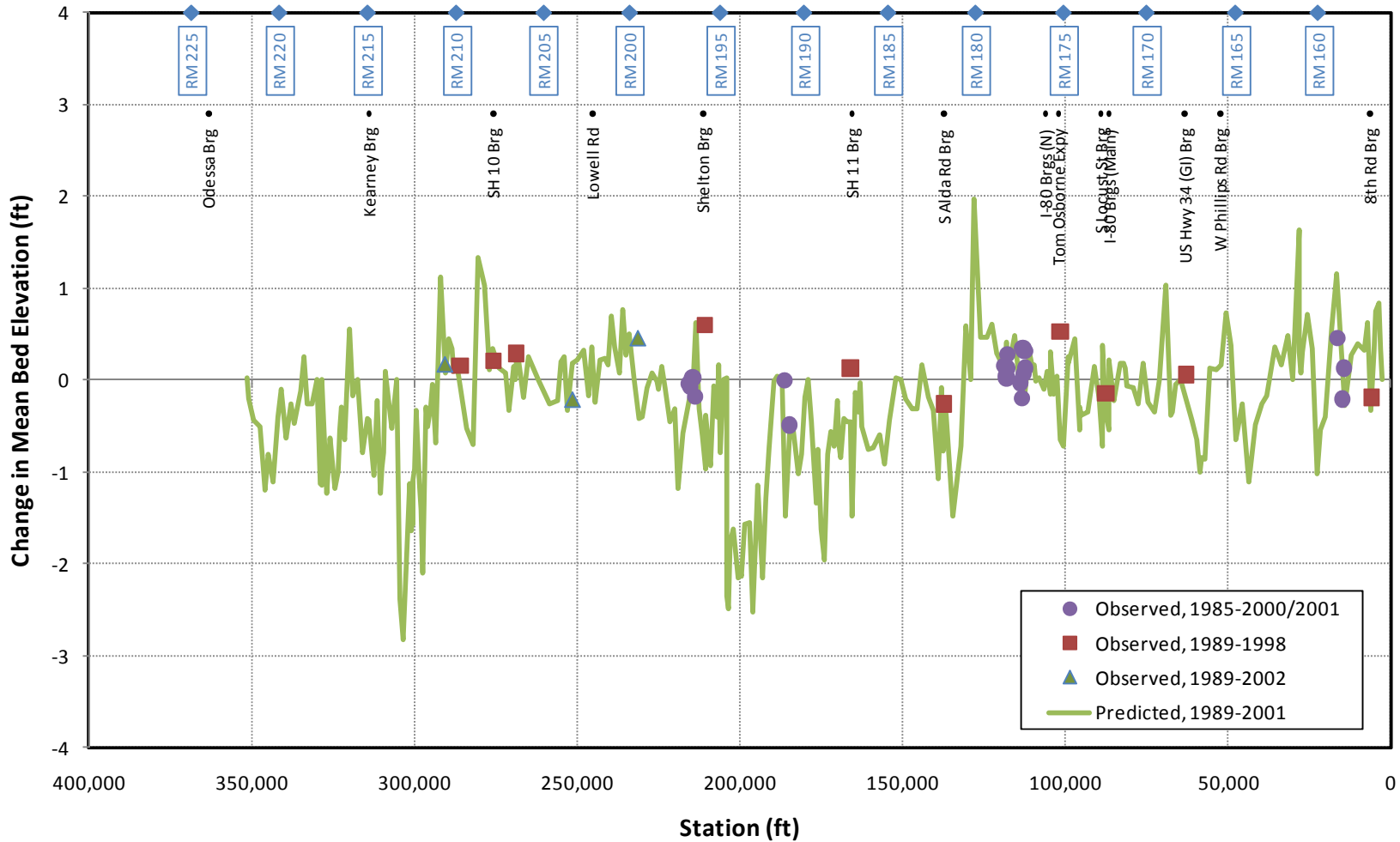


BOULDERS	COBBLES	GRAVEL					SAND					SILT or CLAY
		VC	C	M	F	VF	VC	C	M	F	VF	

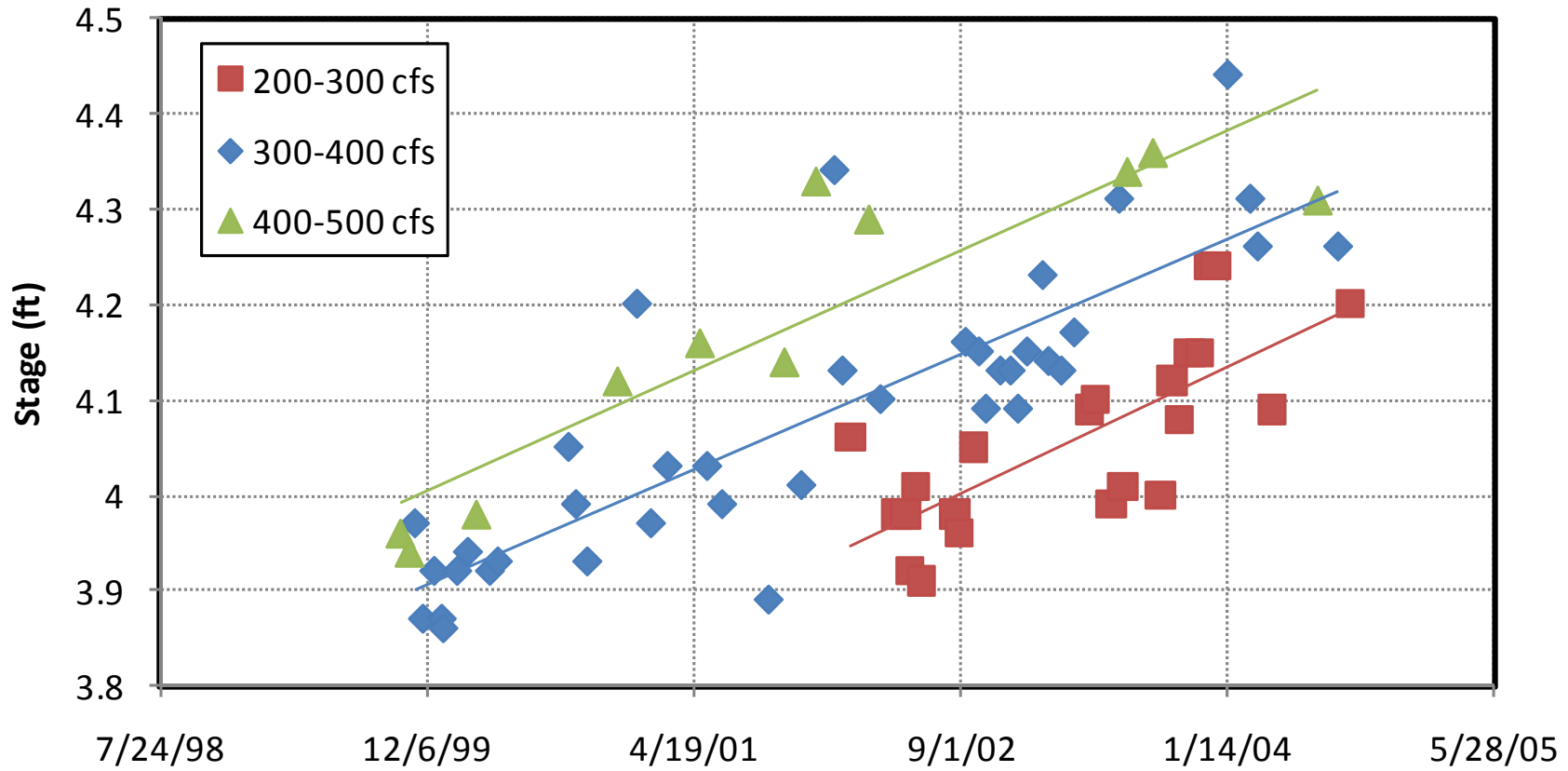
1
2 Figure 4.7: Gradation curves for the composite bed material samples collected for the North Platte “choke point” model
3



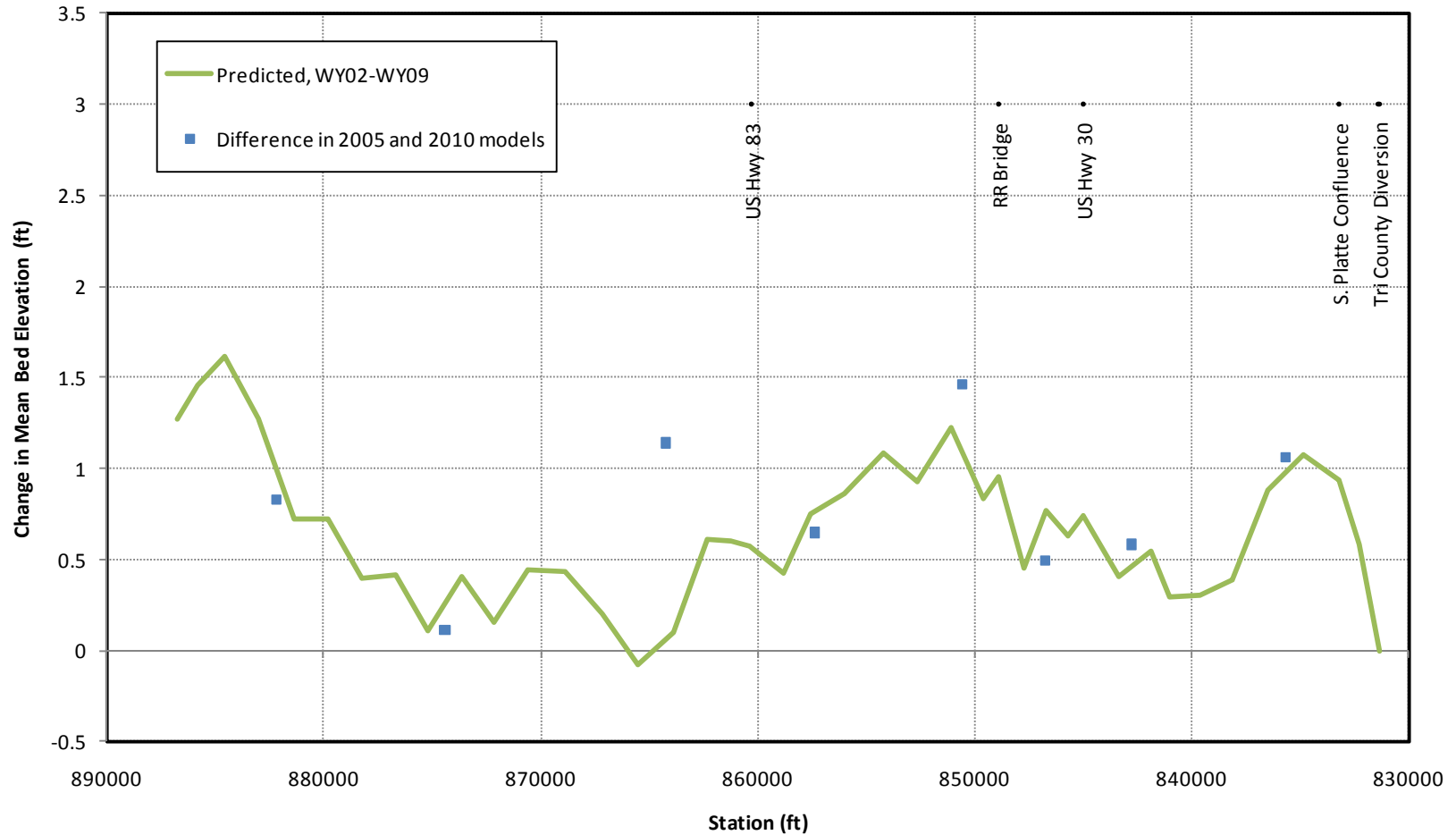
1
 2 Figure 4.8: Comparison of observed and predicted changes in mean bed elevation for the primary flow path between RM256 and RM222
 3 (Lexington to Odessa).
 4



1
 2 Figure 4.9: Comparison of observed and predicted changes in mean bed elevation for the primary flow path between RM222 and RM156
 3 (Odessa to Chapman).
 4



1
 2 Figure 4.10: Measured stages at the North Platte River (U.S. Highway 83) gage over a range of discharge classes for the period between
 3 December, 1999 and January, 2004.
 4



1
 2 Figure 4.11: Predicted change in mean bed elevation from the North Platte model for the simulation between Water Year (WY) 2002 and
 3 WY2009.



6. References

- 1 Arcement, G.K. and Schneider, V.R., 1989. Guide for Selecting Manning's Roughness Coefficients for
2 Natural Channels and Floodplains. U.S. Geological Survey Water Supply Paper 2339.
3
- 4 Barnes, H.H., 1967. Roughness characteristics of natural channels. U.S. Geological Survey Water-Supply
5 Paper 1849.
- 6 Bureau of Reclamation, 2006. Trends of Aggradation and Degradation Along the Central Platte River:
7 1985-2005. Report prepared by Holburn, E.R, Fotherby, L.M., Randle, T.J., Carlson, D.E. and
8 reviewed by Ferrari, R.L., February, 180 p.
- 9 Hicks, D.M. and Mason, P.D., 1991. Roughness Characteristics of New Zealand Rivers. Water Resources
10 Survey, DSIR Marine and Freshwater, Wellington, New Zealand.
- 11 Mobile Boundary Hydraulics, 2010. Sedimentation in Stream Networks (HEC-6T), User Manual, March
12 16.
- 13 Randle, T.J. and Samad, M.A., 2008. Platte River in Central Nebraska; Modeling of Pulse-Flow Release.
14 Bureau of Reclamation Technical Report No. SRH-2008-2.67p.
- 15 SEH, 2008. Project Update Report, Platte River Restoration and Enhancement Project (SEH A-
16 PRRIP0701.00), February 20.
- 17 Tetra Tech, 2010. Hydraulic and Sediment-transport Modeling for the Platte River Sediment
18 Augmentation Feasibility Study, Nebraska. Prepared for The Flatwater Group, September 7, 92
19 p.
- 20 U.S. Army Corps of Engineers, 1992. Guidelines for the Calibration and Application of Computer Program
21 HEC-6. Technical Document 13, October, 36 p.
- 22 U.S. Army Corps of Engineers, 2009. HEC-GeoRAS, GIS Tools for Support of HEC-RAS using ArcGIS, Users
23 Manual, Version 4.2.93, Hydrologic Engineering Center, Davis, California
- 24 U.S. Army Corps of Engineers, 2010. HEC-RAS, River Analysis System, Users Manual, Version 4.1.0,
25 Hydrologic Engineering Center, Davis, California.
- 26 U.S. Army Corps of Engineers, 2010. HEC-RAS, River Analysis System, Hydraulic Reference Manual,
27 Version 4.1.0, Hydrologic Engineering Center, Davis, California.
- 28 Yang, C.T., 1973. Incipient motion and sediment transport. Proc. Am. Soc. Civil Engineers, Journal of
29 Hydraulic Division, v. 99, no. HY10, pp. 1679-1704.

Appendix A

Appendix B

Appendix C

Appendix D